

UNIVERSIDAD DE VIGO
DEPARTAMENTO DE FÍSICA APLICADA
EPHYSLAB

UniversidadeVigo

PhD Thesis

**Improving circulation weather type
classifications using a 3D framework:
relationship with climate variability and
projections for future climates**

Memoria presentada por
Alexandre Miguel Urbano da Fonseca Ramos
para optar al título de "DOCTOR INTERNACIONAL"
por la Universidade de Vigo.
Marzo, 2012

Dr. Luis Gimeno Presa catedrático del Departamento de Física Aplicada de la Universidad de Vigo y **Dra. María de las Nieves Lorenzo González** profesora del Departamento de Física Aplicada de la Universidad de Vigo:

CERTIFICAN

Que la presente memoria titulada "Improving circulation weather type classifications using a 3D framework: relationship with climate variability and projections for future climates", ha sido realizada bajo su dirección por Alexandre Miguel Urbano da Fonseca Ramos en el Departamento de Física Aplicada en el programa de doctorado de Ciencias del Clima: Meteorología, Oceanografía Física y Cambio Climático de la Facultad de Ciencias de Ourense para optar al título de "DOCTOR INTERNACIONAL" por la Universidad de Vigo.

Y para que así conste firman la presente en Ourense a 23 de Marzo del 2012.



Dr. Luis Gimeno Presa



Dra. María de las Nieves Lorenzo González

Acknowledgements

Several are the years that one dedicates to a PhD thesis. During this time, I have not been alone; I have rather had the support of many people. Some have been there from the beginning while others have been found along the way. In the following lines, I want to express my gratitude to all of them.

First and foremost, a dedicated gratitude to my PhD supervisors, Luis and Nieves, that continually defy the pursuit of excellency in scientific knowledge, for all the hours that we spent discussing and developing this thesis.

To all the professors of the Ephyslab group, thank you for your assistance and invaluable help. You always made me feel as part of the group.

A very special thanks to my current laboratory colleagues, Isabel, Alex, Fran, Anxo, José, Ana Maria and Orland, for all the hours of fun and support which always made me feel like home. Without them, the days spent in Ourense would have been less joyful.

I cannot forget my former and present colleagues, in Lisbon, Madrid and in Zurich. From these colleagues, a special reference to Emanuel and Paulo (for the good times in Zurich), and to David (for all the friendship and the late hour discussions).

I also would like to thank my Swiss colleagues, Heini Wernli and Michael Sprenger, for all the support during my 3-month stay in Zurich and for all their help in improving this thesis.

My biggest gratitude goes to my family, but especially my mother and sister, for all the support and for always believing in me. To

my father, that started this journey with me but unfortunately could not make it to the end. I know you have always been proud of me.

To Ana, for always being there in the good and in the bad moments. I am sorry for all the days we could not spend together and simply not being there, but I hope it will be worthwhile. In any case, thank you for the so many adventures during this journey, most of which still to come...

To all my friends in Lisbon, especially Pedro, Ricardo, Tomás, Jorge, Diogo and Hugo, for all of the good moments (and they were a lot) but particularly for being there. To them, I want to say “Aos que lá ficaram”.

A special word to Ricardo Trigo, for the opportunities he gave me for the progress of my scientific work, since my time as an undergraduate student but also for the scientific stimulation and friendship.

A warm thank you to my colleagues at the Instituto de Meteorologia.

A final word: thank you for everything.

The author would like to thank the Portuguese Science and Technology Foundation (FCT) for a research grant (SFRH/BD/46000/2008).

This work was also supported by the Xunta de Galicia under Research Grants No. a) 10PXIB383169PR and b) PGIDIT06PXIB383288PR co-financed by European Regional Development Fund (FEDER).

Resumen

La siguiente tesis presenta dos bloques principales de estudio: (1) por un lado se han analizado detalladamente las aplicaciones de los patrones de circulación o weather types obtenidos a partir de datos de presión en superficie. (2) Por otro se ha realizado un ensayo metodológico donde se presenta una nueva clasificación de patrones de circulación basada en trayectorias Lagrangianas.

Los objetivos de este trabajo fueron divididos en tres partes.

- a. En la primera parte, se estudian las relaciones entre las variables climáticas de superficie y los patrones de circulación.
- b. En la segunda parte, se analizan las relaciones entre dichos patrones de circulación y la variabilidad del clima.
- c. En la tercera parte y última parte, se introduce un nuevo tipo de clasificación de patrones de circulación basado en trayectorias Lagrangianas.

El trabajo fue desarrollado para el noroeste de la Península Ibérica pero todos los procedimientos y metodologías se pueden aplicar fácilmente a otras regiones del mundo.

La organización de este trabajo se describe a continuación:

- en el **capítulo 1** se presenta una pequeña introducción sobre el sistema climático y la variabilidad del clima;
- en el **capítulo 2** se presenta una descripción de las diversas metodologías utilizadas para el cálculo de patrones de circulación y sus aplicaciones;
- en el **capítulo 3** se caracteriza el clima del noroeste de la Península Ibérica;
- en el **capítulo 4** se indican los objetivos principales de este trabajo;
- en el **capítulo 5** se describen las distintas bases de datos que se utilizan para la realización del trabajo;
- en el **capítulo 6** se estudian las relaciones entre distintas variables climáticas y los distintos patrones de circulación para la región de estudio;
- en el **capítulo 7** se estudia la relación entre los patrones de circulación y los modos de variabilidad de baja frecuencia;
- en el **capítulo 8** se estudian los cambios en la frecuencia de los patrones de circulación tanto para el clima presente como para el clima futuro;
- en el **capítulo 9** se presenta un nuevo método de clasificación de patrones de tiempo considerando una estructura 3-D de la atmósfera;
- en el **capítulo 10** se presentan las conclusiones.

Observaciones recientes sobre el norte del sector Atlántico-Europeo han destacado el hecho de que las tendencias significativas del clima son evidentes en diversas escalas temporales (IPCC, 2007; Trigo et al., 2008). La variabilidad en la circulación atmosférica es la cuestión más importante en términos de cambios en la distribución espacial, no sólo de la temperatura o la precipitación, sino también de otras variables climatológicas.

La región seleccionada para este estudio, el noroeste de la Península Ibérica, es una región caracterizada por el paso de los frentes fríos asociados al “storm track” del Atlántico norte (Trigo, 2006). Estudios anteriores han mostrado que la variabilidad de la precipitación y de la temperatura es influenciada por los modos principales de variabilidad de baja frecuencia del Atlántico Norte, Oscilación del Atlántico Norte, índice escandinavo, los índices atlánticos/occidentales o del este de Rusia (Lorenzo and Taboada, 2005; de Castro et al., 2006).

Uno de los métodos más utilizados para estudiar el efecto de los cambios en los patrones de circulación sobre el clima regional es estudiar en detalle cambios en la frecuencia de estos patrones y sus consecuencias para el clima de una región. Los patrones de circulación son específicos para una región dada y son resultado del análisis de los datos sinópticos meteorológicos generalmente sobre una celda regular, obtenida utilizando gran variedad de metodologías (Huth et al., 2008). La climatología sinóptica ayuda a identificar las configuraciones claves de los patrones de circulación y las causas que modifican el comportamiento de los diversos fenómenos que ocurren en superficie. Estos esquemas de clasificación traen orden y simplicidad al sistema climático, proporcionando una gran cantidad de información de forma codificada.

Resumen

Una clasificación de patrones de circulación es en general un método algorítmico que distingue entre situaciones meteorológicas describiéndolas a través de parámetros de circulación (por ejemplo, zonalidad, carácter ciclónico, posición de sistemas de altas y bajas presiones etc.) o por elementos de tiempo local como temperatura o precipitación. Los parámetros de circulación son usados frecuentemente ya que tales parámetros pueden ser usados muy fácilmente para relacionar ciertas características de la circulación atmosférica con el tiempo local a través de métodos estadísticos.

Estos patrones de circulación fueron calculados utilizando la presión a nivel del mar diaria de los datos del reanálisis de NCEP/NCAR (Kalnay et al., 1996). Las condiciones de circulación fueron determinadas usando parámetros físicos o geométricos, tales como la dirección y la fuerza de flujo de aire, y el grado de ciclonicidad calculados a partir de 16 puntos separados entre sí 2.5° y centrados sobre el área de estudio (Fig. R I).

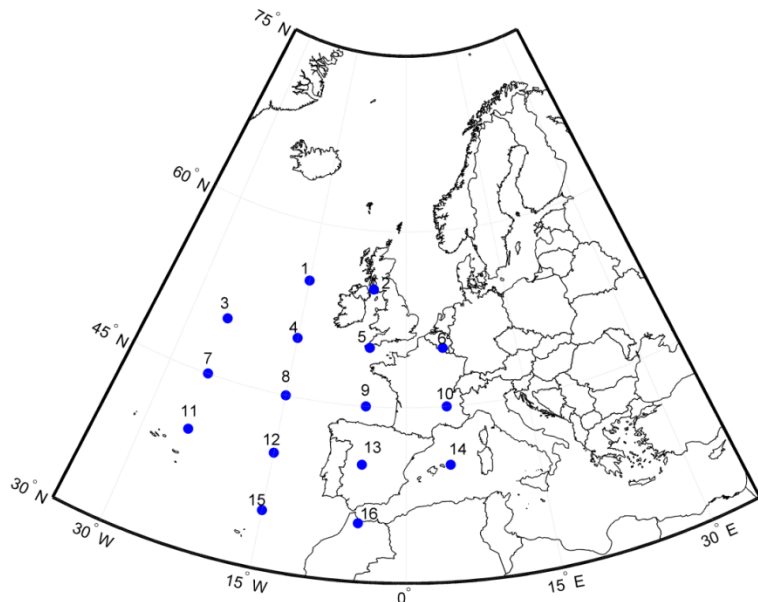
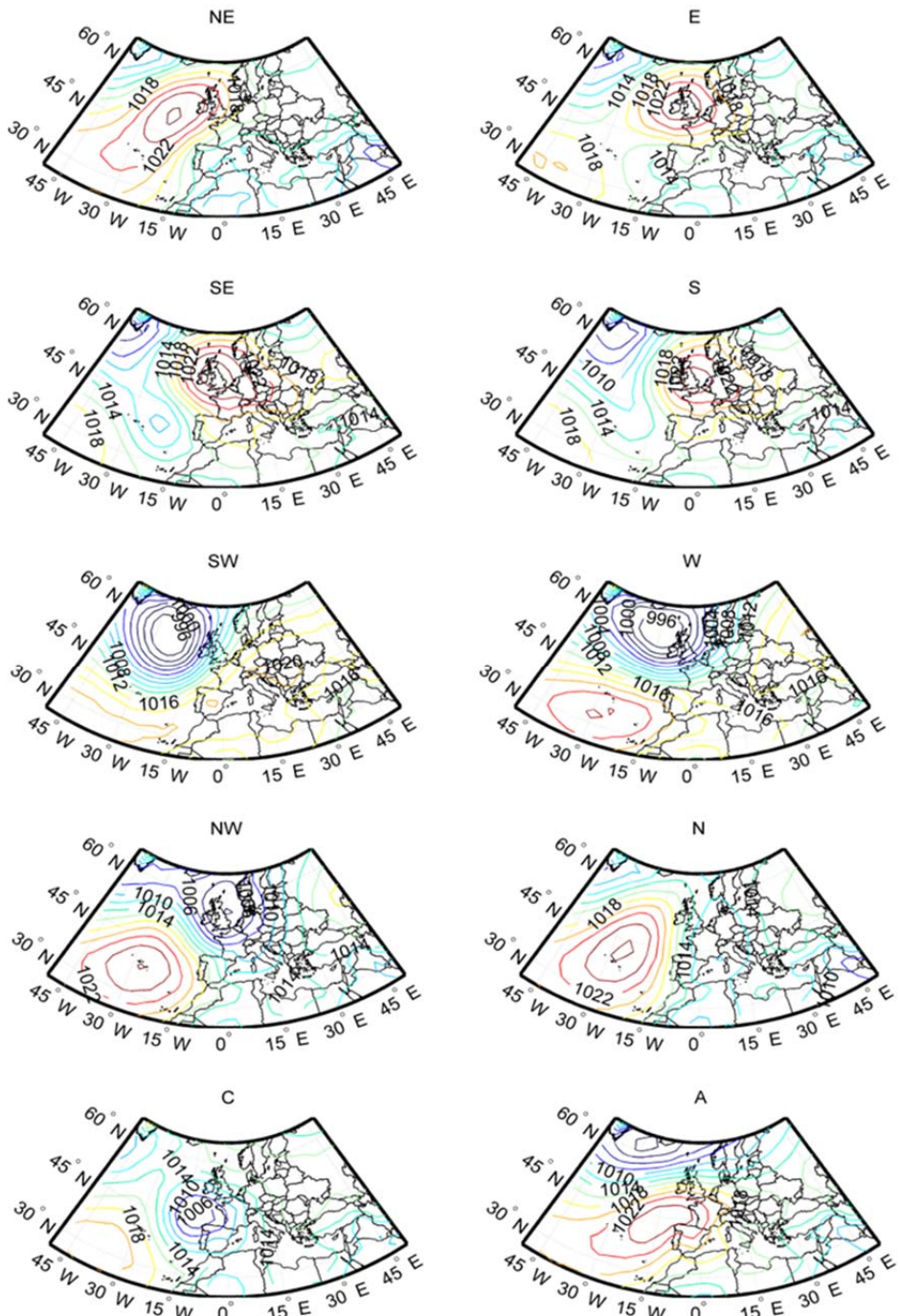


Figura R I. Sector euro-Atlántico con la localización de los 16 puntos utilizados para el cálculo de los patrones de circulación sobre el noroeste de la Península Ibérica.



La clasificación usada en este trabajo es una versión automatizada del procedimiento (Jones et al. 1993) de los “Circulation weather types” (patrones de circulación) de Lamb. En estos últimos años, este método se ha aplicado con éxito a otras regiones europeas (Goodess y Palutikof, 1998; Trigo and DaCamara, 2000; Lorenzo et al., 2008; Ramos et al., 2010; Ramos et al., 2011).

Esta versión automatizada del cálculo de patrones de circulación (Fig. R II) fue utilizada para estudiar la conexión entre modelos atmosféricos y el clima en superficie (precipitación, temperatura y descargas eléctricas (rayos)) para el noroeste de la Península Ibérica. Esto permite distinguir para cada patrón de circulación (Fig. R III) las condiciones meteorológicas más comunes. Los resultados muestran que cada patrón de circulación posee una relación particular con la precipitación y la temperatura del área de estudio.

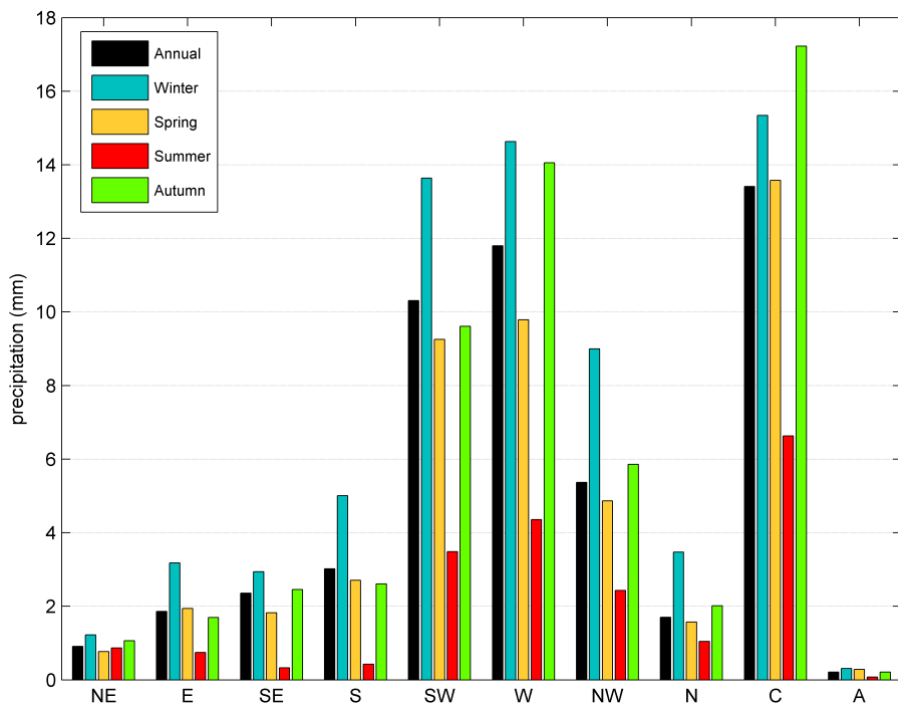


Figura R III. Precipitación media explicada por cada patrón de circulación a las escalas anual y estacional.

Además, la relación entre los patrones de circulación y las descargas eléctricas permitió que distinguiéramos qué tipos de patrones se asocian con frecuencia a los episodios de rayos, y también cuales son los más favorables a episodios severos de relámpagos.

Los modos de variabilidad de baja frecuencia tienen una influencia importante en la variabilidad del sistema climático en diversas escalas temporales y espaciales. Aunque el Oscilación del Atlántico Norte explique una porción substancial de la variabilidad del clima en Europa, es también necesario considerar otros modos de variabilidad de baja frecuencia, tales como el índice escandinavo, los índices atlánticos/occidentales o del este de Rusia. Por otro lado, la relación entre los modos de variabilidad de baja frecuencia y el clima en Europa no se puede considerar estacionaria sino que cambia con el tiempo. En esta tesis, se ha descrito la compatibilidad entre los modos hemisféricos y los modos en el sector Europeo/Atlántico Norte (Fig. R IV), utilizando los regímenes de patrones de circulación en el área de estudio (noroeste de la Península Ibérica) durante los meses invernales (Enero, Febrero, Marzo (EFM)).

Además, este estudio ha proporcionado la evidencia de que los modos calculados usando la presión media en superficie o el campo de geopotencial a 500hPa son muy semejantes en esta ventana espacial. Los resultados muestran que existe un alto nivel de coherencia entre los modos derivados de un acercamiento estadístico (usando el análisis de componentes principales) y los tipos de circulaciones físicas verdaderas (según lo representado por los patrones de circulación - Lamb circulation weather types).

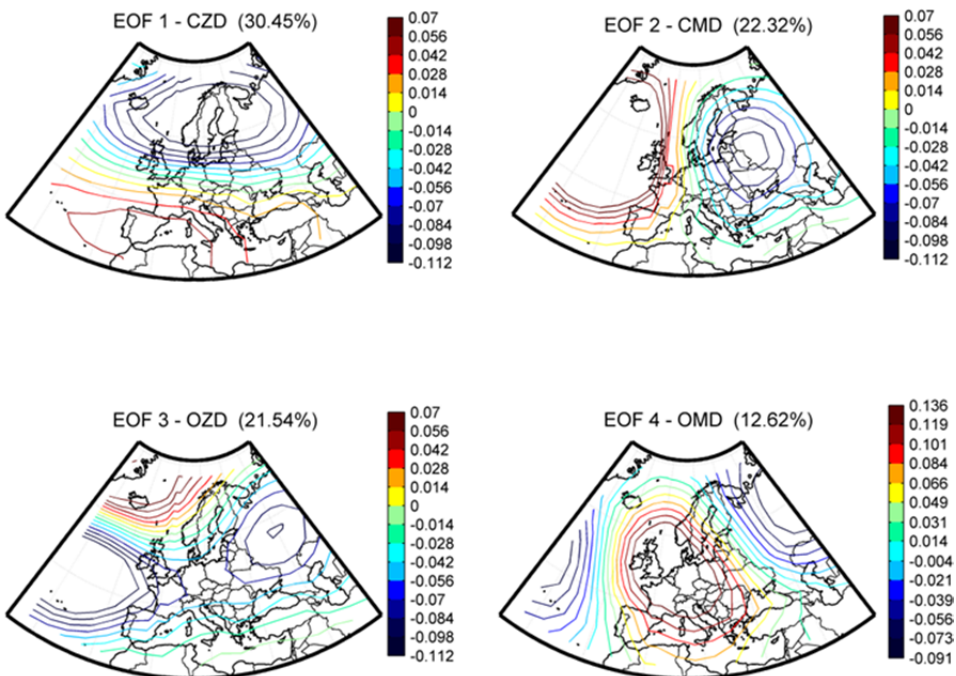


Figura R IV. Las cuatro primeras funciones empíricas ortogonales para los meses invernales (EFM) para el campo de geopotencial en 500 hPa junto con la respectiva varianza (%) explicada por cada una.

El uso de un estudio de análisis de componentes principales con ventanas continuas temporales ha permitido evaluar si los cambios en la intensidad o en la posición de estos modos pueden afectar a la circulación local (Fig. R V). Los resultados confirman que dichos cambios tienden a favorecer la ocurrencia de algunos tipos de circulación sobre otros.

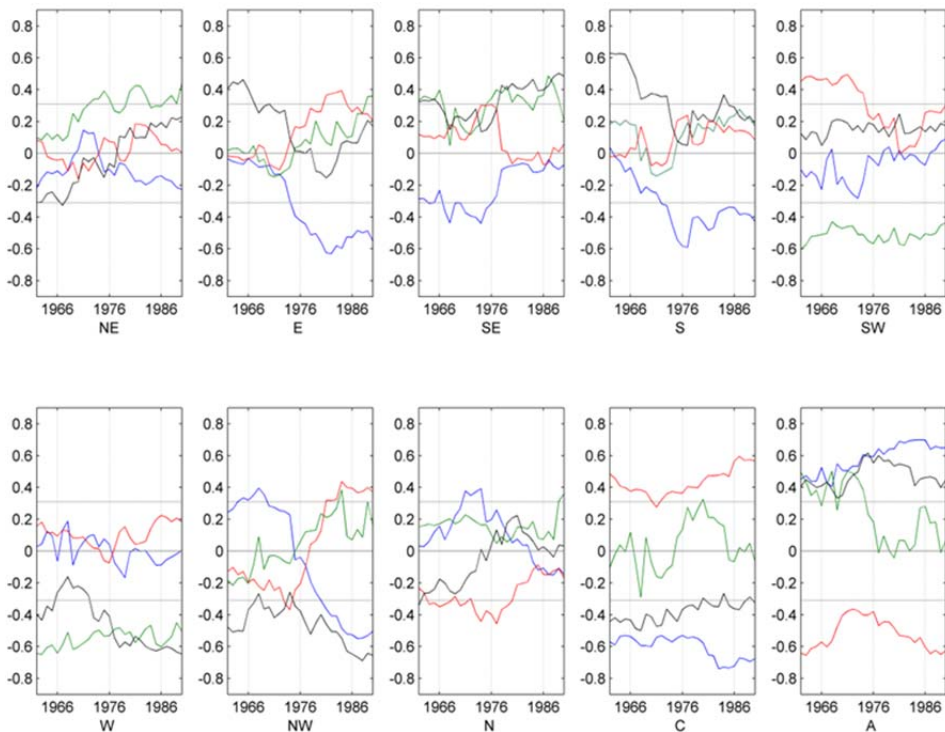


Figura R V. Correlación entre las cuatro primeras componentes principales y la frecuencia de invierno de los patrones de circulación. Se muestra la significancia al 95% en líneas punteadas. La primera ventana de análisis es 1948-1977 (centrada en 1962) y la última es 1976-2005 (centrada en 1990). Los tipos de circulación ciclónicos y anticiclónicos se representan por C y A respectivamente. El dipolo continental zonal, el dipolo continental meridional, el dipolo oceánico zonal y el dipolo oceánico meridional se representan por las líneas azul, verde, roja y negra respectivamente.

A la luz del debate sobre cambio climático y su impacto en ecosistemas, la clasificación de patrones de circulación ha ganado interés ya que cambios en las estructuras de la circulación atmosférica podría ser una de las claves para comprender el cambio climático. Todas las variaciones observadas han de estar de uno u otro modo vinculadas a alteraciones que han experimentado los patrones de circulación de las diversas regiones del planeta. Así pues, fueron analizados diferentes escenarios del IPCC con 3 modelos climáticos globales para estudiar los cambios en la frecuencia de ocurrencia de los patrones de circulación

esperados en el noroeste de la Península Ibérica para el siglo XXI. Para ello primeramente se evaluó la capacidad de los modelos para reproducir el clima actual y la frecuencia estacional actual de los patrones de circulación comparando la simulación de control para la última mitad del siglo XX con los resultados obtenidos a partir del reanálisis de NCEP/NCAR.

En este estudio, se siguió el procedimiento de Demuzere et al. (2008a) esto es, extrayendo del campo de presión a nivel del mar los errores estacionales sistemáticos de cada modelo. Los resultados obtenidos presentan una mejora importante cuando los errores sistemáticos se quitan de los campos de presión a nivel del mar (Fig. R VI). Las diferencias en las frecuencias estacionales de los diversos tipos de circulación entre los datos de los modelos y los del re-análisis son más bajas que cuando comparamos los resultados sin las correcciones en el campo de presión a nivel del mar. Por lo tanto, fue encontrado que en la mayoría de los casos las discrepancias en la frecuencia de los tipos de circulación entre los modelos y la re-análisis se pueden explicar debido al “bias” estacional que presentan los modelos globales del clima.

Los cambios en la frecuencia de los patrones de circulación para el siglo XXI también fueron analizados. Pequeños cambios (la mayor parte de ellos menos de 6% y no-significativos) en la frecuencia de los patrones de circulación fueron encontrados para el período 2046-2065, mientras que las diferencias en la segunda parte (2081-2100) son más grandes. Para la segunda mitad del siglo XXI, hay una disminución del patrón ciclónico, oeste, y sudoeste en primavera y en verano. Para el otoño, hay una disminución proyectada del patrón de oeste y ciclónico y un aumento en la frecuencia del patrón anticiclónico (Fig. R VII).

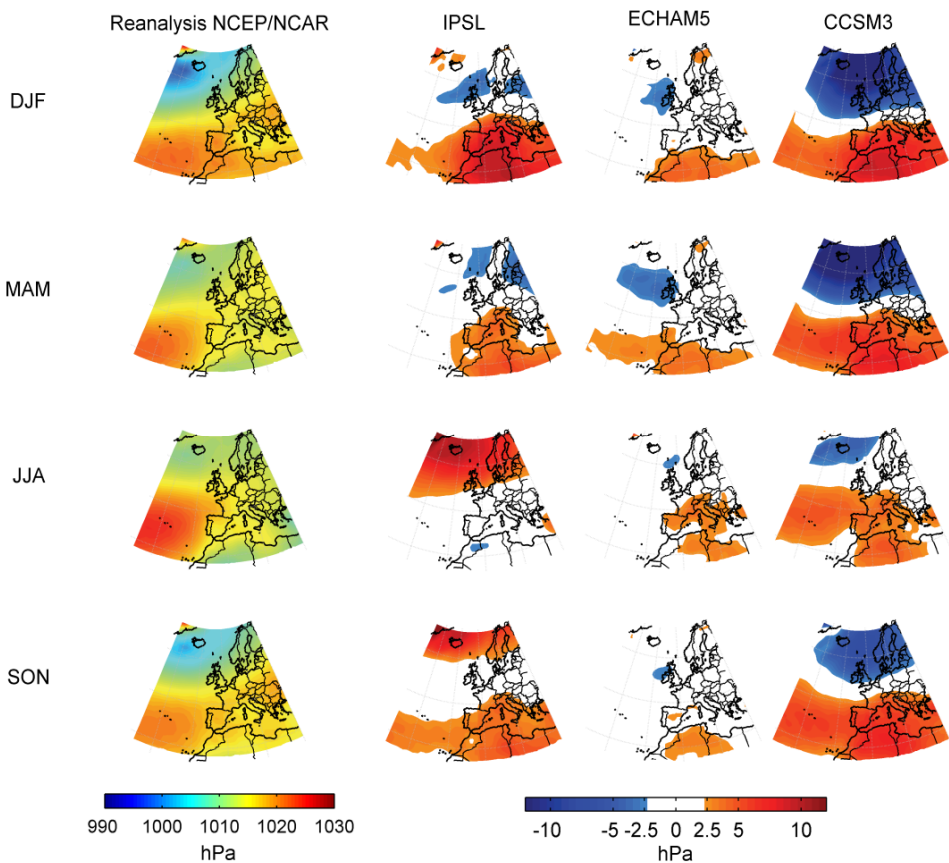


Figura R VI. Diferencias estacionales en la presión a nivel del mar para el período 1961-1999. La primera columna muestra la presión a nivel del mar durante el período 1961-1999 utilizando los datos del reanálisis NCEP/NCAR. Las columnas siguientes muestran la diferencia entre la presión a nivel del mar en los tres modelos. Las estaciones fueron definidas como sigue: invierno (DEF), primavera (MAM), verano (JJA) y otoño (SON).

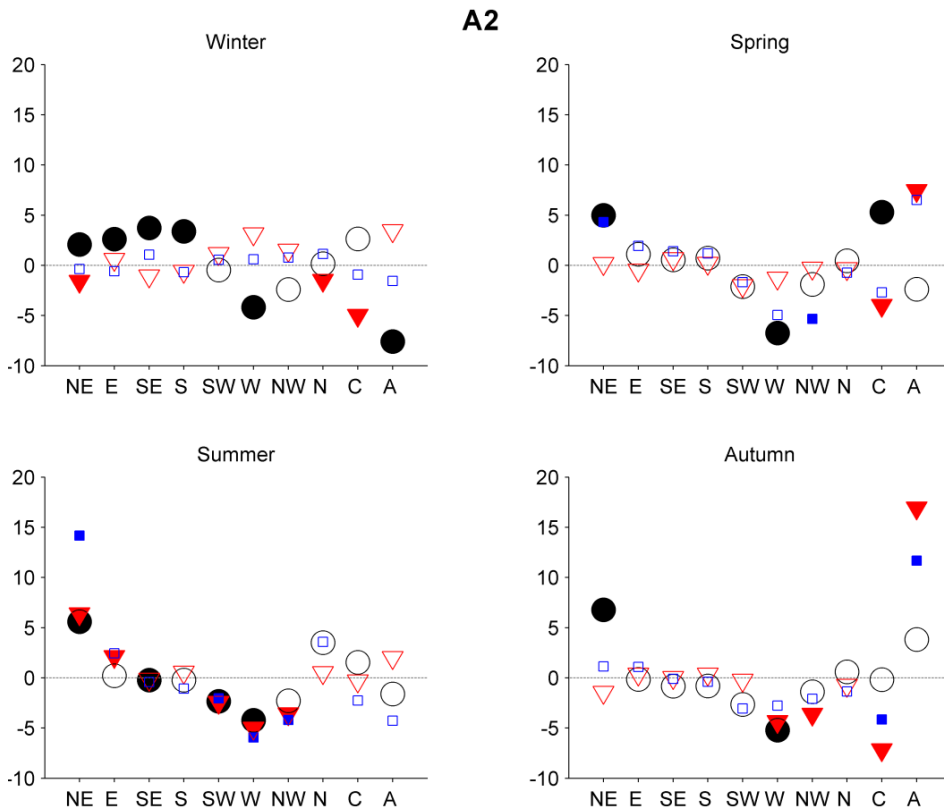


Figura R VII. Cambios esperados en la frecuencia estacional de aparición de los patrones de circulación para el periodo 2081-2100 en el escenario A2 con referencia al periodo 1961-1999 en (%). (IPSL, círculo negro, ECHAM5, triángulo rojo y CCSM3, cuadrado azul). Los símbolos llenos muestran las diferencias significativas al nivel 0.05.

En la tercera y última parte de esta tesis, se presenta un nuevo método de clasificación de tipos de circulación para el área de estudio (noroeste de la Península Ibérica), basado en el análisis de las trayectorias hasta 90 horas hacia atrás que llegan en esta área, según lo calculado con el modelo de dispersión tridimensional Lagrangiano de partículas FLEXPART. Los datos del modelo FLEXPART contienen 1 398 800 posiciones de partículas con su estado meteorológico grabadas cada 6 horas y durante un período de 5 años (2000-2004). Para conseguir una

retrotrayectoria de 5 días representativa, cada 6 h se realizará un análisis de clústeres para cada grupo de retrotrayectorias de 5 días (Fig. VIII).

Este análisis de clústeres se aplica para separar las retrotrayectorias y tener las masas y flujos de aire representativos para cada día. Además de la posición (latitud y longitud) de las partículas, en el análisis de clústeres, se definieron y calcularon varias medidas de análisis a partir de las características de cada trayectoria obtenida del FLEXPART, curvatura de la trayectoria, flujo ciclónico o anticiclónico, evolución de la humedad, origen y distancia recorrida de la trayectoria.

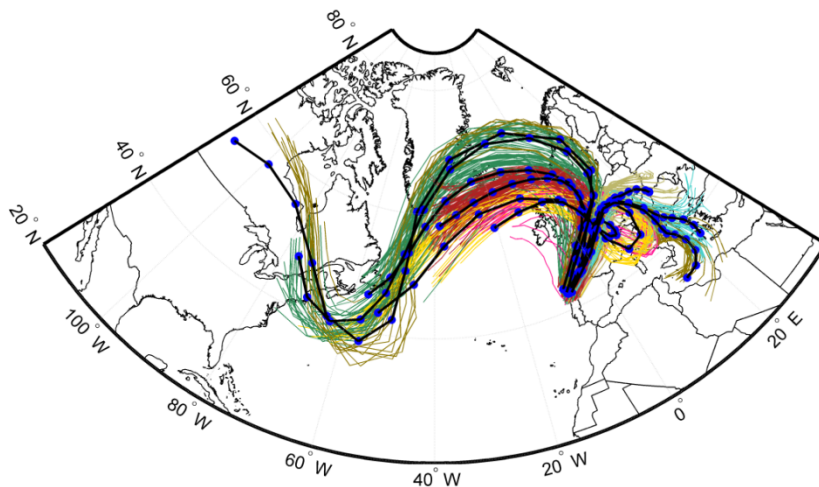


Figura R VIII. Retrotrayectorias (90h) que llegan al noroeste de la Península Ibérica (41°N - 44.5°N y 10°W - 6°W) en un día determinado (11/11/1999 - UTC 12). Las líneas de color corresponden a las distintas trayectorias que llegan al dominio y las líneas negras corresponden a los centroides calculados por el método de Dorling.

El catálogo final obtenido tiene para cada día un máximo de cinco secuencias de aire, cada una caracterizada por las cinco características descritas arriba (altura de la trayectoria, evolución de la humedad, distancia recorrida) (Fig. R IX). Este método supone una simplificación de la gran cantidad de información que proporciona el conjunto inicial de datos del modelo de partículas FLEXPART ya que al final nos quedamos solo con las trayectorias que son representativas

(centroides salidos del análisis de clústeres) de las distintas masas de aire que llegan al noroeste de la Península Ibérica, capturando así lo esencial de la dinámica de la circulación atmosférica.

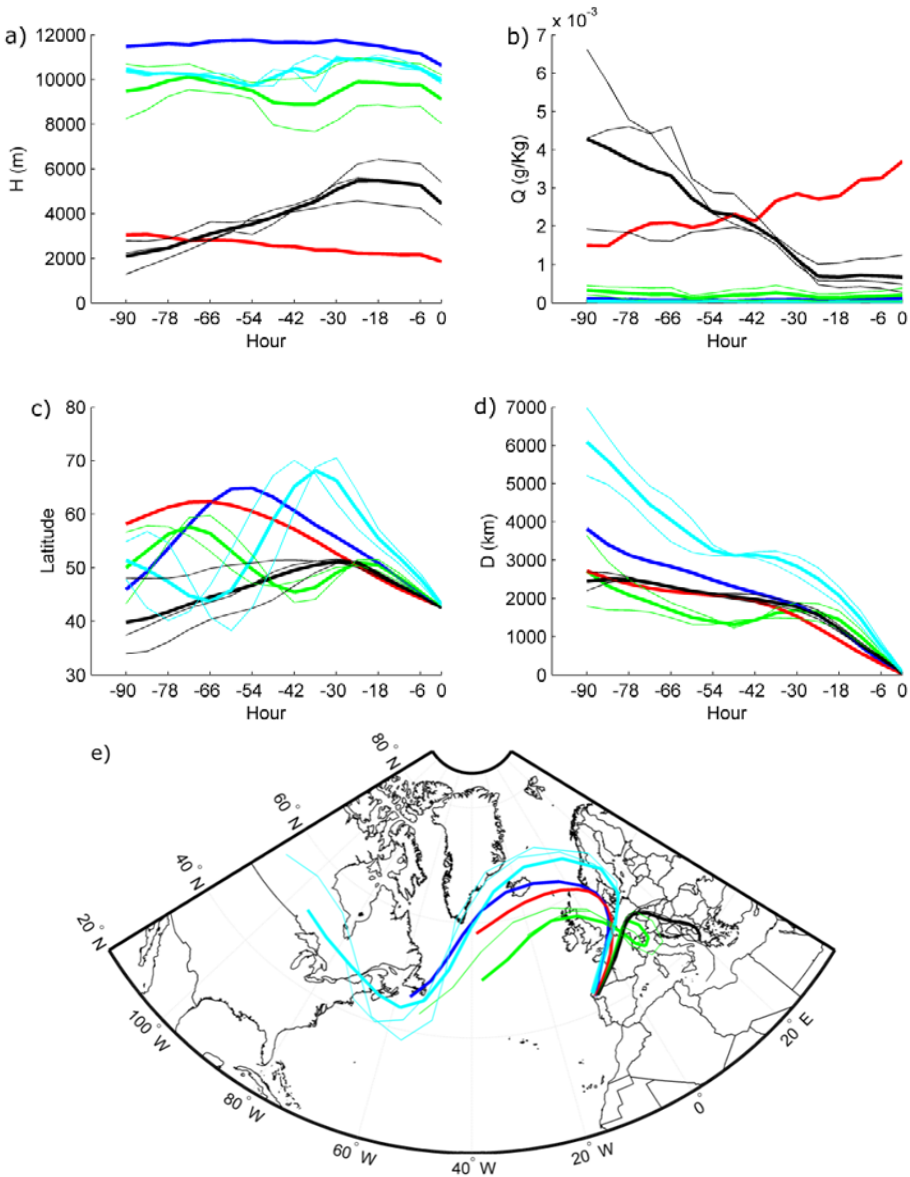


Figura R IX. Evolución temporal de las características de las retrotrayectorias para a) la altura de la trayectoria, b) la humedad específica, c) latitud y d) distancia al centro (e) para el día representado en la Fig. VIII. Las líneas finas de colores corresponden a las trayectorias calculadas en la Fig. VIII (computadas con el método de Dorling) mientras que las líneas gruesas de colores corresponden a las cinco secuencias de aire finales que caracterizan el día.

El nuevo método aquí propuesto considera parte de la complejidad tridimensional de la circulación atmosférica (Fig. R X). Por otra parte proporciona información meteorológica integrada en el tiempo que también puede ayudar a comprender el desarrollo de sistemas meteorológicos (perspectiva Lagrangiana), que va más allá de la descripción tradicional de la situación sinóptica instantánea (perspectiva Euleriana). La nueva clasificación Lagrangiana de tipos de circulación permite capturar cambios en humedad a lo largo del flujo debido a la evaporación y a la precipitación.

La contribución climatológica de esta nueva clasificación indica que el método puede capturar con exactitud las características principales de la estacionalidad del clima regional. Permite una distinción apropiada de procesos en las diferentes estaciones y ayuda a determinar aspectos de la variabilidad intra-estacional de la región.

Además de caracterizar los aspectos del ciclo anual, el método puede identificar estructuras dinámicas meteorológicas distintas tal y como se demuestra en los diferentes casos de estudio analizados (eventos intensos y/o extremos) como precipitación intensa, ola de calor, ola de frío, bloqueos, DANAS) tanto en términos de tipos de circulación clásicos (Eulerianos) como con el nuevo método aquí desarrollado (Lagrangiano). El nuevo método de clasificación Lagrangiano agrega información valiosa sobre las condiciones meteorológicas pertinentes, no observada en la clasificación Euleriana.

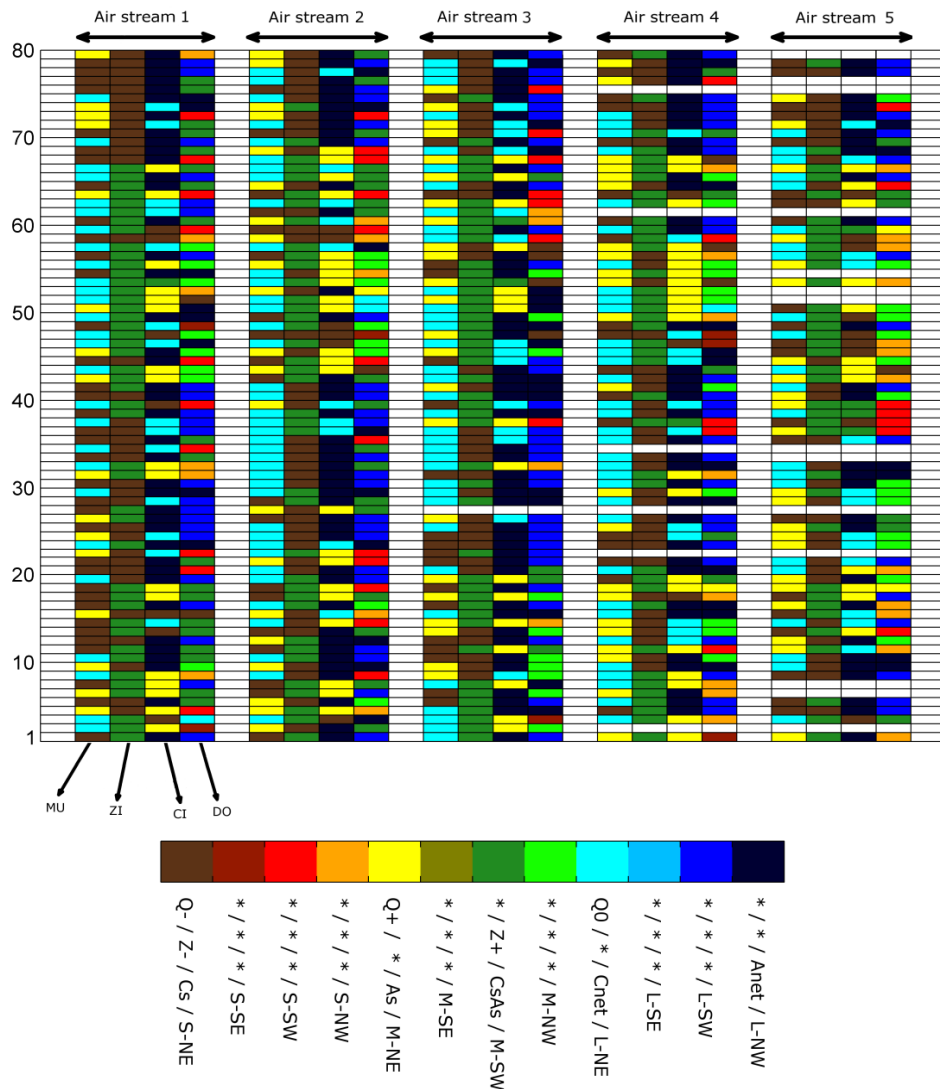


Figura R X. Catálogo final con los 80 primeros días de la nueva clasificación (desde el 01/12/1999 al 18/02/2000). Cada día es caracterizado por un máximo de cinco masas de aire y cada una de ellas se puede describir por cuatro características del flujo.

Así, por ejemplo, para la ola de calor 2003 en la Península Ibérica, el método captura el transporte de corto alcance asociado a la baja térmica en el centro de la Península, y el transporte de medio y largo alcance asociado a la circulación global anticiclónica. También, los sistemas de DANAS con señal en muchos casos sólo en altitud son

detectados por el nuevo método Lagrangiano, mientras que la clasificación clásica de tipos de circulación (Euleriana) solamente puede recoger las características superficiales del flujo. En esto sentido, esta clasificación de patrones de circulación es más robusta que los métodos clásicos porque por un lado se tiene en cuenta los patrones de flujo que llegan a una región en concreto y por el otro permiten mostrar los efectos locales de una determinada situación meteorológica y tener un mejor entendimiento de la física que hay detrás de ese sistema. De esta forma se complementa la información proporcionada por la clasificación Euleriana de los patrones de circulación.

Esta nueva clasificación, aquí desarrollada para el noroeste de la Península Ibérica, es fácilmente aplicable a otras regiones del globo.

Las conclusiones principales de esta tesis se pueden resumir en los siguientes puntos:

- 1) Los patrones ciclónico, oeste y sudoeste son los que producen más precipitación, mientras que el patrón anticlónico se asocia a no precipitación en el noroeste de la Península Ibérica. Además, para la temperatura máxima, los valores más altos se asocian generalmente a los patrones de sureste, sur y sudoeste mientras que los valores más bajos se dan con los tipos de oeste, noroeste y norte.
- 2) Fue observado, para las diferentes estaciones del año, que existen diversos mecanismos asociados a la actividad de rayos en el noroeste de la Península Ibérica. Estos mecanismos se relacionan mayoritariamente con características atmosféricas que no tienen una signatura clara en los niveles atmosféricos más bajos, (ej. presión a nivel del

mar), por lo que los patrones de circulación no son suficientes para explicar completamente los mecanismos presentes en todos los casos.

- 3) Los cambios en la posición e intensidad de los modos de variabilidad de baja frecuencia en el sector Atlántico-Europeo tienden a favorecer la ocurrencia de algunos patrones de circulación frente a otros. El aumento en la variación explicada del dipolo zonal continental y la correlación (positiva) negativa cada vez mayor entre este modo y el tipo (anticiclónico) ciclónico pueden ayudar a explicar la disminución de la precipitación en el invierno.
- 4) El estudio de la circulación local atmosférica por medio de patrones de circulación puede dar información valiosa para evaluar los escenarios futuros del cambio climático. Por otra parte, son fáciles de calcular, por lo que son ventajosos frente a otros métodos (ej. métodos downscaling).
- 5) De acuerdo con las relaciones entre los patrones de circulación y precipitación en el noroeste de la Península Ibérica para el clima actual, uno puede hacer la suposición de que se favorecen las condiciones de sequía en verano y primavera. También para el otoño se pueden asumir condiciones más secas, basadas en la disminución prevista de los patrones de oeste y ciclónicos y un aumento de los patrones anticiclónicos. Este comportamiento está de acuerdo con el aumento esperado en el índice de la Oscilación del Atlántico Norte para el final del siglo XXI.
- 6) La nueva clasificación de patrones de circulación basado en trayectorias y que fue desarrollada en esta tesis puede

describir la complejidad tridimensional de la circulación atmosférica. Por otra parte, proporciona una información física integrada del desarrollo de los sistemas (perspectiva Lagrangiana), que va más allá de la descripción tradicional de la situación sinóptica instantánea (perspectiva Euleriana).

- 7) Además, la nueva clasificación captura aspectos de la estructura tridimensional de la atmósfera permitiendo establecer claramente situaciones sinópticas, como las DANAS, que pueden no tener una signatura clara en niveles atmosféricos más bajos y que por lo tanto no son detectados por la clasificación basada solamente en el campo de presión a nivel del mar.

Synopsis

The following thesis has two central concepts that were the main motivations for this work: gathering and studying in detail examples of applications of circulation weather types; and a pure methodological essay, where a new circulation weather types classification based on lagrangian air trajectories is presented.

The objectives of this work were divided into three parts:

- a. In the first part, the relationship between surface climate variables and circulation weather types is studied.
- b. In the second part, the relationship between circulation weather types and climate variability is analyzed.
- c. In the third part, a new circulation weather type classification scheme based on lagrangian air trajectories is introduced.

The work was developed for the northwestern Iberia Peninsula but all the procedures and methodologies can be applied easily to other regions of the World.

This thesis is organized as follows:

- **chapter 1** presents a brief introduction about the climate system and climate variability;
- **chapter 2** presents an overview of the different weather types methodologies and its applications;
- **chapter 3** characterizes the climate in the northwest Iberia Peninsula;
- **chapter 4** states the main objectives of the present work;
- **chapter 5** describes the different datasets that are used;
- **chapter 6** studies the relationship between surface climate variables and circulation weather types for the northwest Iberia Peninsula;
- **chapter 7** relates the circulation weather types and the modes of low frequency variability;
- **chapter 8** studies changes in the frequency of circulation weather types in present and future climate;
- **chapter 9** presents a new method of circulation weather types taking into account a 3D structure of the atmosphere;
- **chapter 10** concludes.

Recent observations have highlighted the fact that significant climate trends are evident at different time scales over the North Atlantic-European (NAE) sector (IPCC, 2007; Trigo et al., 2008).

The variability in atmospheric circulation is the most important issue in terms of the changes in the spatial distribution, not only of temperature or precipitation, but also of other climatological variables.

The region selected for this study is Galicia, in the northwest Iberian Peninsula. It is characterized by the passage of cold fronts associated with the storm track in the North Atlantic Ocean (Trigo, 2006). Previous studies have shown that the precipitation and temperature variability is linked to the main North Atlantic modes of low-frequency variability, i.e., not only the North Atlantic Oscillation, but also the Scandinavian index and the eastern Atlantic/western Russia (Lorenzo and Taboada, 2005; deCastro et al., 2006). This region has undergone a significant decrease in precipitation over the last 40 years, especially during winter (e.g., Paredes et al., 2006; Trigo et al., 2008).

Circulation patterns are specific to a given region and result from the examination of synoptic weather data, usually on a regular grid, obtained using a wide variety of methodologies (Huth et al., 2008). Circulation types are usually defined for each day and tend to reflect the local circulation that actually occurs in a simple way. The complexity of the continuum of atmospheric circulation is the main motivation for researchers to find an easier manner of categorizing it. Classifications of atmospheric circulation intend to summarize this complexity into a reasonable and manageable number of discrete classes (types). There are different ways to classify climates into similar classes.

The usage of classifications, in order to state the weather, has become more in use in recent decades since the advance of computers

Synopsis

which made it possible to develop fast and objective methods in order to process large amounts of data. Furthermore, many climatological studies and applications need to have the data as simplified as possible. This is achieved by analyzing gridded dataset (usually sea level pressure or geopotential height at different levels) and grouped them into a relatively small number of distinct categories.

In the study reported herein, an automated version of synoptic circulation types (Lamb circulation weather types) that was initially developed for the British Isles (Jones et al., 1993) is used, which describes the local circulation in terms of the circulation parameters, in this case. The circulation conditions were determined using physical or geometrical parameters, such as the direction and strength of airflow, and degree of cyclonicity based on 16 grid points centered in the domain, using the sea level pressure field of the NCEP/NCAR reanalysis (Fig. S I).

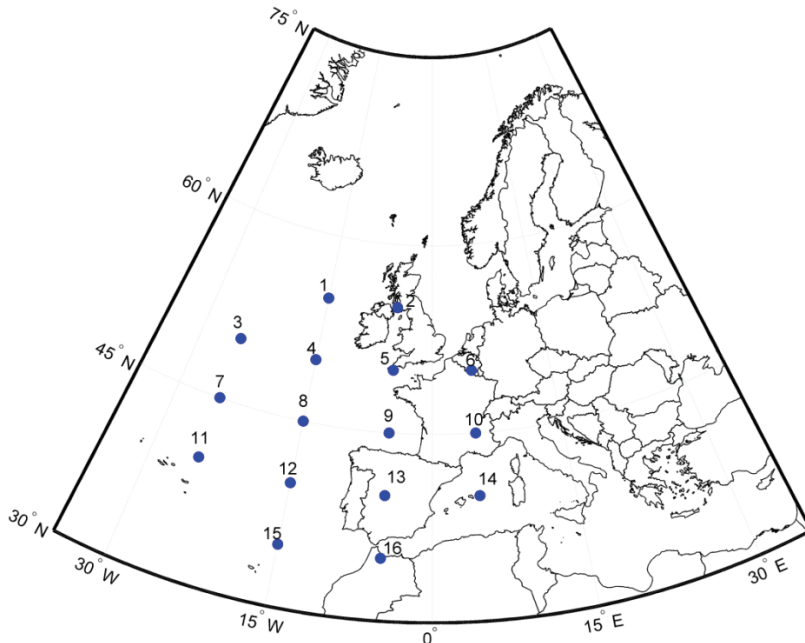


Figure S I. Pressure grid points used to compute the Lamb weather types for the NW Iberia Peninsula.

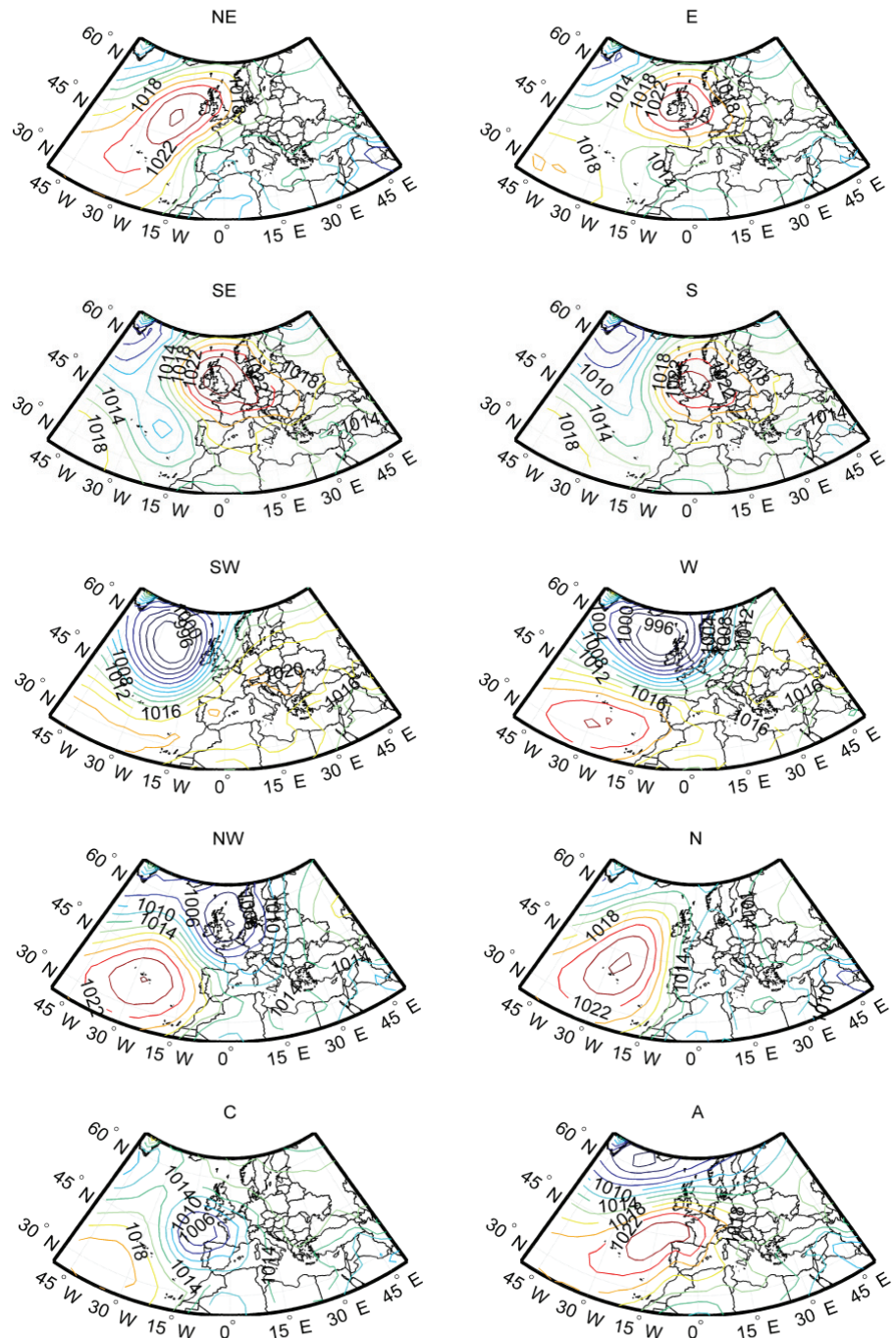


Figure S II. Annual average composite sea level pressure field of the 10 pure circulation weather types for the 1948-2008 period.

Synopsis

Additionally, the circulation type methodology used here has been applied successfully to the Iberian Peninsula in several other studies, especially those relating to precipitation, e.g., those of Trigo and DaCamara, (2000) and Lorenzo et al., (2008).

This automated version of the Lamb circulation weather type classification scheme (Fig. S II) was used to study the relationship between atmospheric circulation patterns and surface climate (precipitation, temperature and lightning discharges) in the northwestern Iberian Peninsula. This allows differentiating each circulation weather type (Fig. S III) in terms of meteorological variables, increasing the knowledge of the effects of atmospheric circulation in the region. Results show that there is a clear difference between each circulation weather type and the average precipitation and temperature.

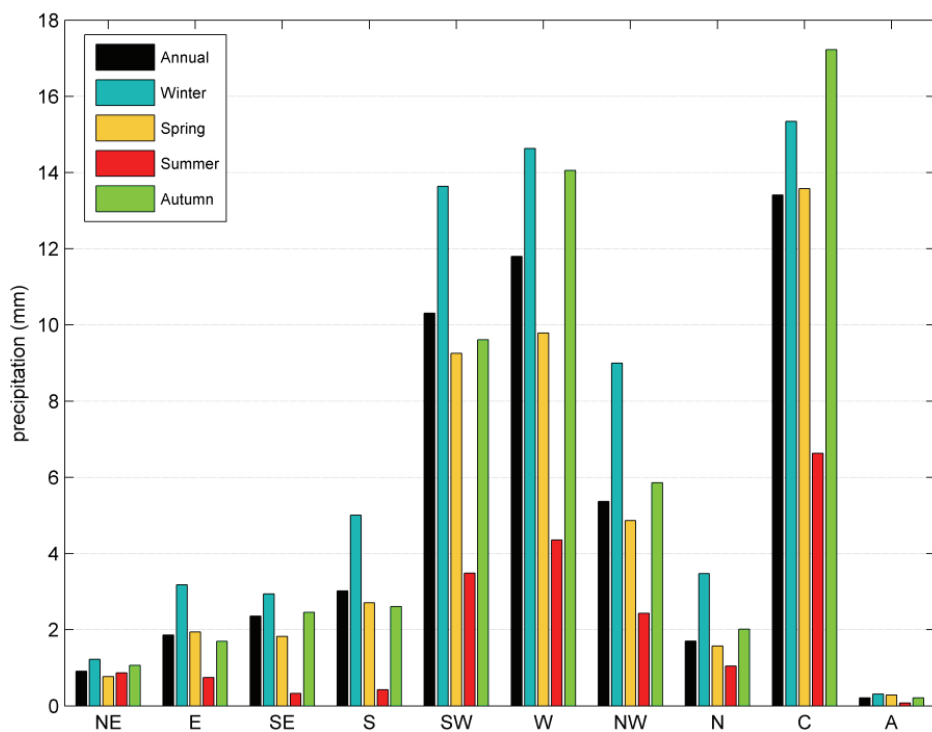


Figure S III. Average precipitation explained by each weather types at annual and seasonal scales.

In addition, the relationship between the circulation weather types and lightning discharges allowed us to distinguish which types are frequently associated with lightning episodes, and also the ones that are favorable to severe lightning episodes.

Modes of low-frequency variability have a major influence on the variability of the climate system at different temporal and spatial scales. Although the North Atlantic Oscillation explains a substantial portion of the climate variability in Europe, it is also necessary to consider other modes of low-frequency variability, such as the Scandinavian index, the eastern Atlantic or the eastern Atlantic/western Russia indices.

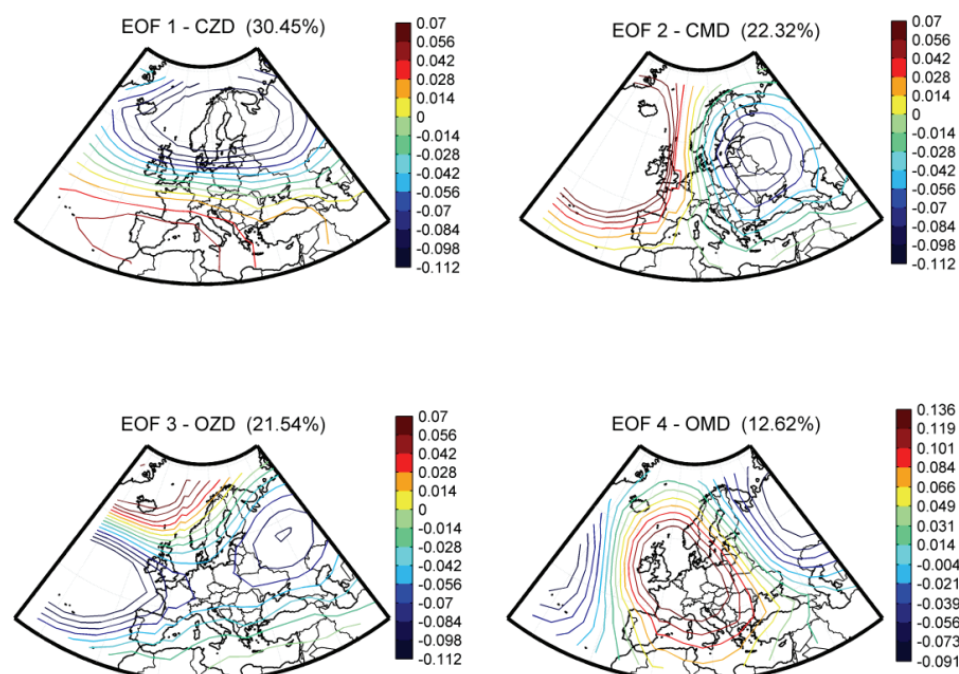


Figure S IV. The first four leading empirical orthogonal function patterns for the winter months (JFM) for the sea level pressure field together with the respective variance (%) explained by each.

Furthermore, the relationship between the modes of low-frequency variability and the climate in Europe cannot be considered to be stable over time. In this thesis, an assessment of the compatibility between the modes of low-frequency variability in Europe and local circulation regimes (the Lamb circulation weather type) was made, in order to observe how shifts in the positions of the modes of low-frequency variability in Europe (Fig. S IV), can affect local circulation.

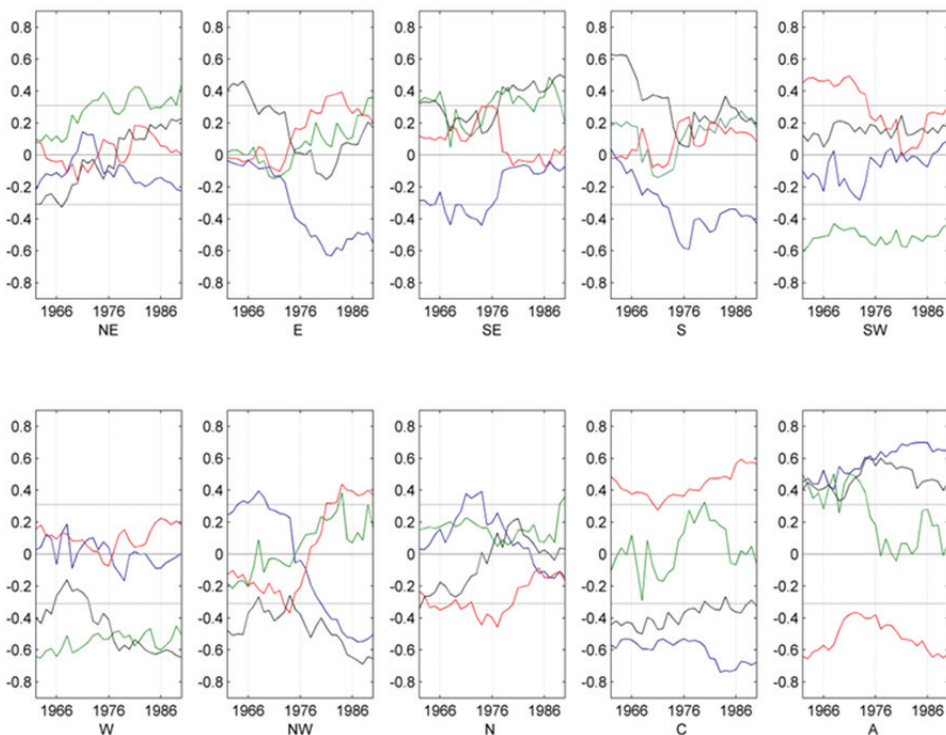


Figure S V. Correlation between the four principal loading factors and the winter frequency of the circulation weather types. The significance at the 95% level is also shown (dotted lines). The first analysis window is set as 1948-1977 (centred on 1962) and the last window is 1976-2005 (centred on 1990). Cyclonic and anticyclonic are denoted by C and A, respectively. The continental zonal dipole, continental meridional dipole, ocean zonal dipole, and ocean meridional dipole are represented by blue, green, red, and black lines respectively.

Evidence shows that the modes computed using the sea level pressure field or the geopotential height at 500hPa field are very alike in this spatial window. The results show that there is a high degree of coherence between the modes derived from a statistical approach (using Principal Component Analysis) and the real physical circulations (as represented by the circulation weather types). The use of a Principal Component Analysis approach using continuous time windows allowed assessing whether changes in the intensity or position of these modes can influence the local circulation (Fig. S V). The results confirm that changes in both the position and the intensity of the modes tend to favor the occurrence of some circulation types in preference to others.

Moreover, projected climate scenarios simulated by different global coupled climate models were studied in order to assess changes in the synoptic variability of the northwestern Iberian Peninsula in the 21st century. To this end, changes in the frequency of the different circulation weather types computed for the study area using three different models included in the IPCC 4th assessment report were investigated. The control simulation for the late 20th century was also evaluated objectively from the results obtained using data from the NCEP/NCAR reanalysis, as to evaluate the ability of the model to reproduce the present climate (Fig. S VI). Comparisons embrace not only seasonal mean sea level pressure fields but also the mean seasonal frequency of circulation types.

The procedure of Demuzere et al. (2008a) to compute the circulation weather types for each coupled global climate models was used, that is, without the corresponding systematic seasonal errors that are observed in the sea level pressure field of each model for the present climate.

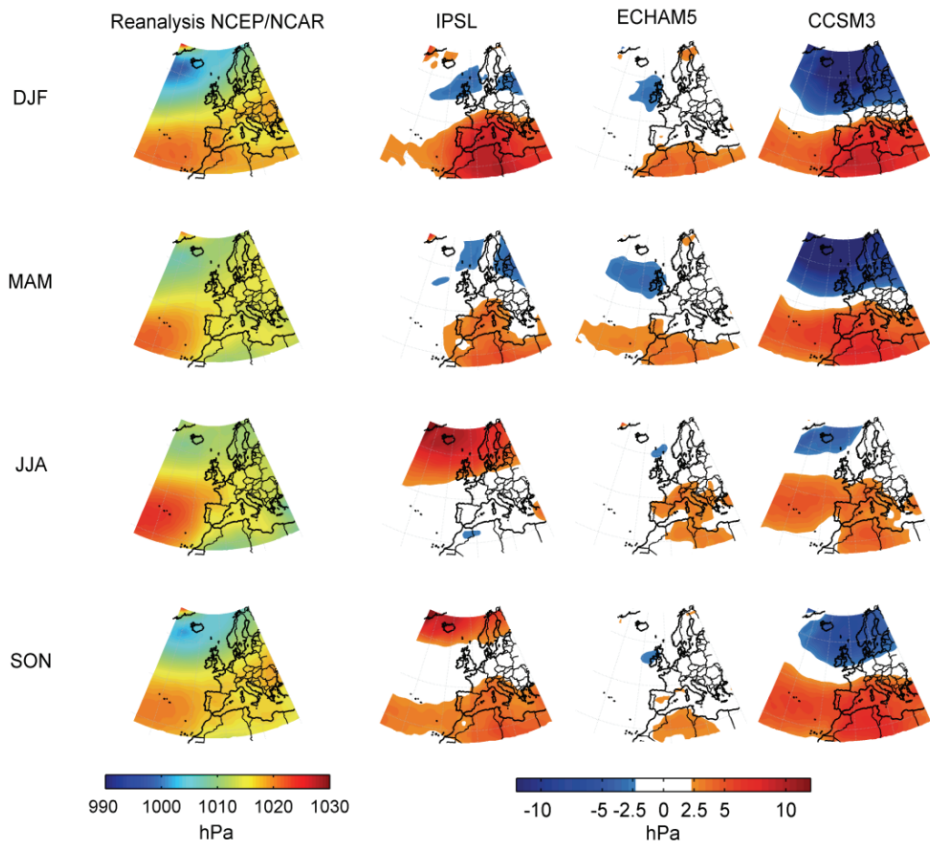


Figure S VI. Mean seasonal sea level pressure differences for the 1961-1999 period. First column shows the seasonal mean sea level pressure during the 1961-1999 period using the NCEP/NCAR reanalysis data. The next columns show the difference between the mean sea level pressure from the three models. Seasons were defined as follow: winter (DJF), spring (MAM), summer (JJA), and autumn (SON).

The obtained results present an important improvement when the systematic errors are removed from the sea level pressure fields, since the differences in the circulation weather type frequency between the models and the reanalysis are lower when compared to the results without the sea level pressure corrections. Therefore, it was found that in most cases the discrepancies in the circulation weather types between the models and the reanalysis can be explained by the seasonal mean bias.

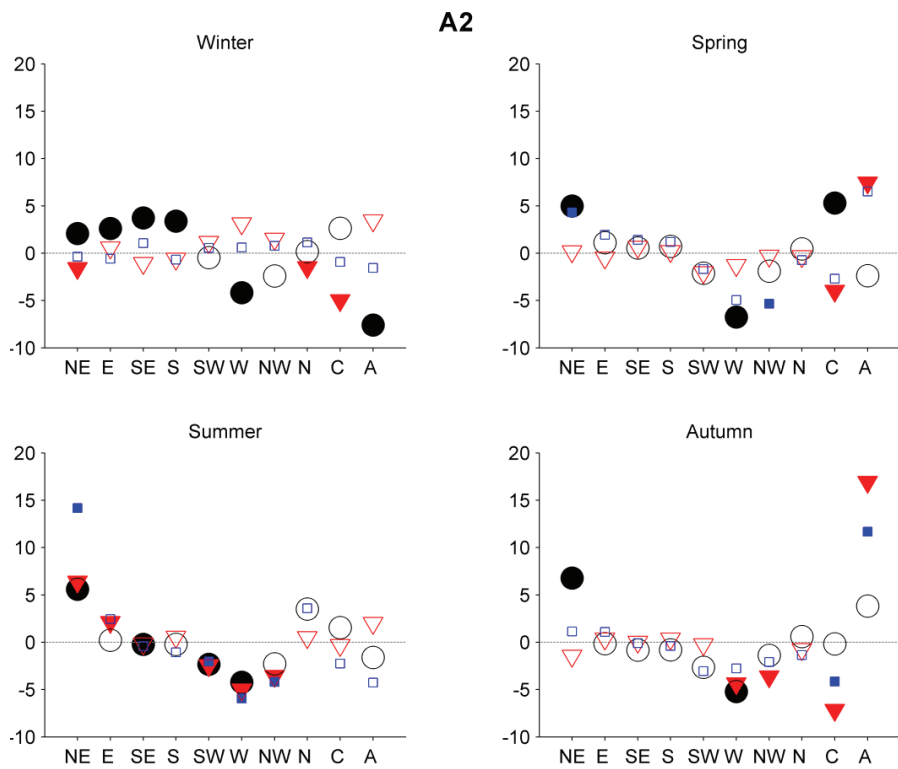


Figure S VII. Projected seasonal mean frequency of the circulation weather types changes (%) for the late 21st century (2081-2100) in the scenario A2. The mean frequency of the circulation weather types are relative to the 1961-1999 period (IPSL, black circle, ECHAM5, red triangle and CCSM3, blue square). The filled symbols show the significant differences at level 0.05.

On the other hand, the frequency of different circulation weather types in a given area gives valuable information as to assess climate change. The changes in the mean circulation types frequency for the 21st century were also analyzed. Small changes (most of them less than 6% significant) in the frequency of the types were found for the 2046-2065 period, while the differences in the second period (2081-2100) are larger. Results show that, for the second period, in all scenarios there is a decrease for cyclonic, western, and southwestern types in spring and summer (Fig. S VII). This change is larger for A2 scenario.

In the last part of the thesis, a new classification method for the large-scale circulation characteristic of a specific target area (northwestern Iberian Peninsula) is presented, based on the analysis of 90-h backward trajectories arriving in this area, as calculated with the 3-D Lagrangian particle dispersion model FLEXPART. A cluster analysis is applied in order to separate the backward trajectories into up to five representative air streams for each day (Fig. S VIII).

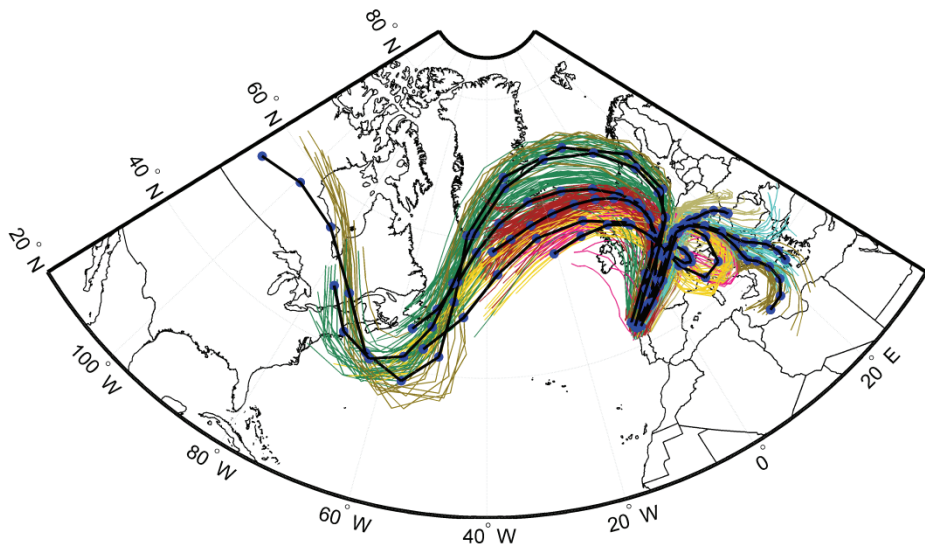


Figure S VIII. Backward trajectories (90h) arriving to the northwest Iberia Peninsula (41°N – 44.5°N and 10°W – 6°W) on a particular day (11/11/1999 - 12 UTC) in color lines and the respective clusters position (blue dots) computed by the Dorling method (dark lines).

This cluster analysis is applied to separate and have the representative back trajectories (air masses) for each day. In addition to the position (latitude and longitude) of the particles, in the cluster analysis were also defined and computed several measures to analyze the characteristics of each trajectory obtained from FLEXPART, (height of the trajectory, evolution of moisture source trajectory, distance traveled) (Fig. IX).

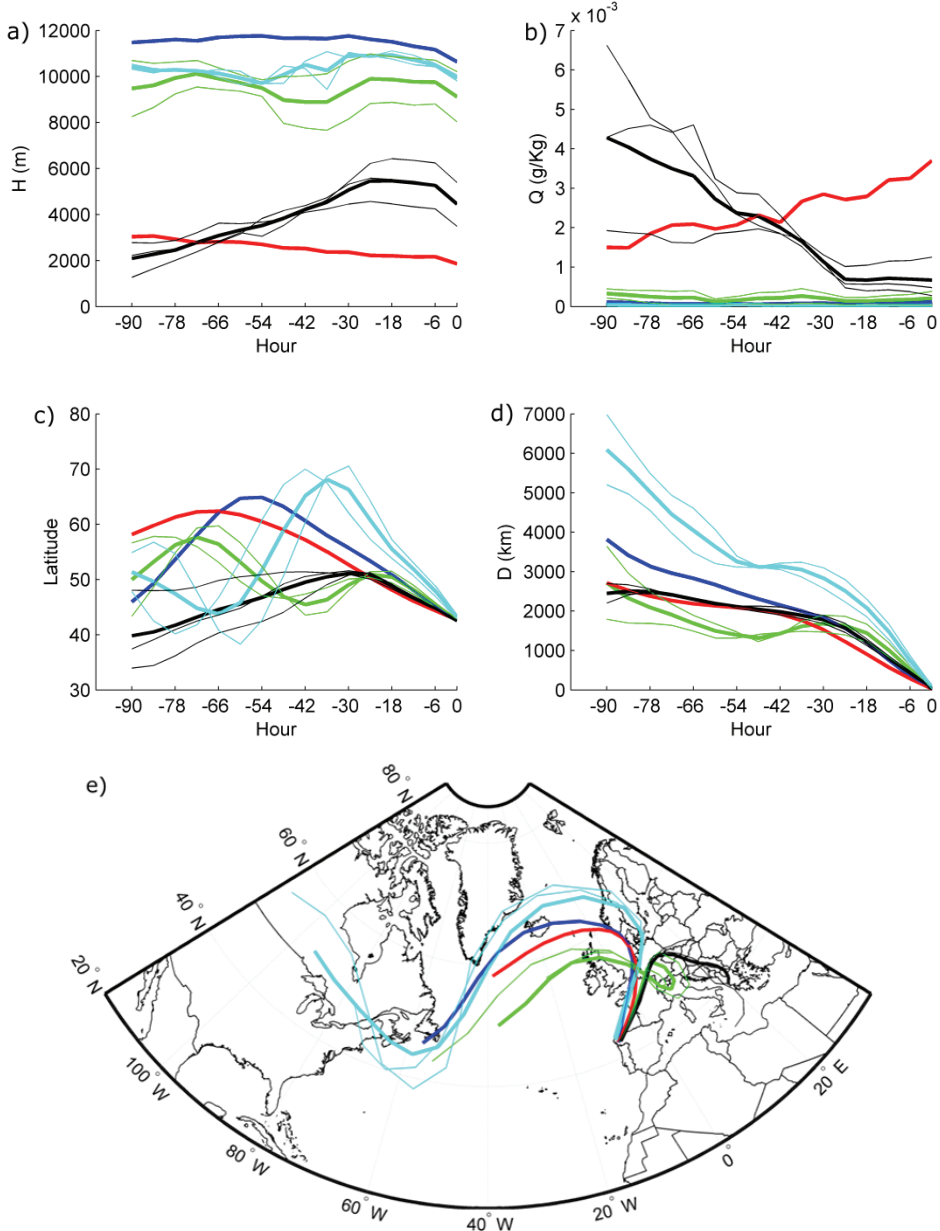


Figure S IX. Time evolution of the back-trajectory properties for a) height of trajectory (H), b) specific humidity (Q), c) latitude and d) distance to the center (D) shown in Fig. VIII. The colored thin line corresponds to the centroid trajectories (previous computed with the Dorling method) while the colored thick lines correspond to the final five air streams characterizing the day (see text for details). In e) the final air streams are shown. The color code is the same as in a) to d).

Synopsis

The final catalogue has for each time step a maximum of five air streams, each characterized by the five characteristics described in chapter 9 (integrated change in specific humidity; curvature of the path; cyclonicity of the flow; and distance and origin) (Fig. S X). This method is able to reduce the large amount of information in a comprehensive trajectory data set into a small number of distinct air streams, which capture the essential dynamics of the meso- and synoptic-scale flow situation.

This new method describes the three-dimensional complexity of the atmospheric circulation. Moreover, it provides time-integrated physical information on the development of the systems (Lagrangian perspective), which goes beyond the traditional description of the instantaneous synoptic situation (Eulerian perspective). For example, the Lagrangian classification allows capturing changes in moisture along the flow due to evaporation and precipitation.

The climatological assessment of this new classification indicates that the method is able to capture with good accuracy the main features of the seasonality of regional climate. It allows a proper distinction of processes between seasons and helps determining aspects of the intra-seasonal variability.

Besides characterizing aspects of the annual cycle, the method is able to identify distinct dynamical structures. Case studies of an intense precipitation event, namely heat wave, cold wave, blocking system, cut-off low and an extra-tropical cyclone are analyzed in terms of the new and the Lamb classification. It is shown that the new classification method adds valuable information about the pertinent meteorological conditions which are missing in an Eulerian approach.

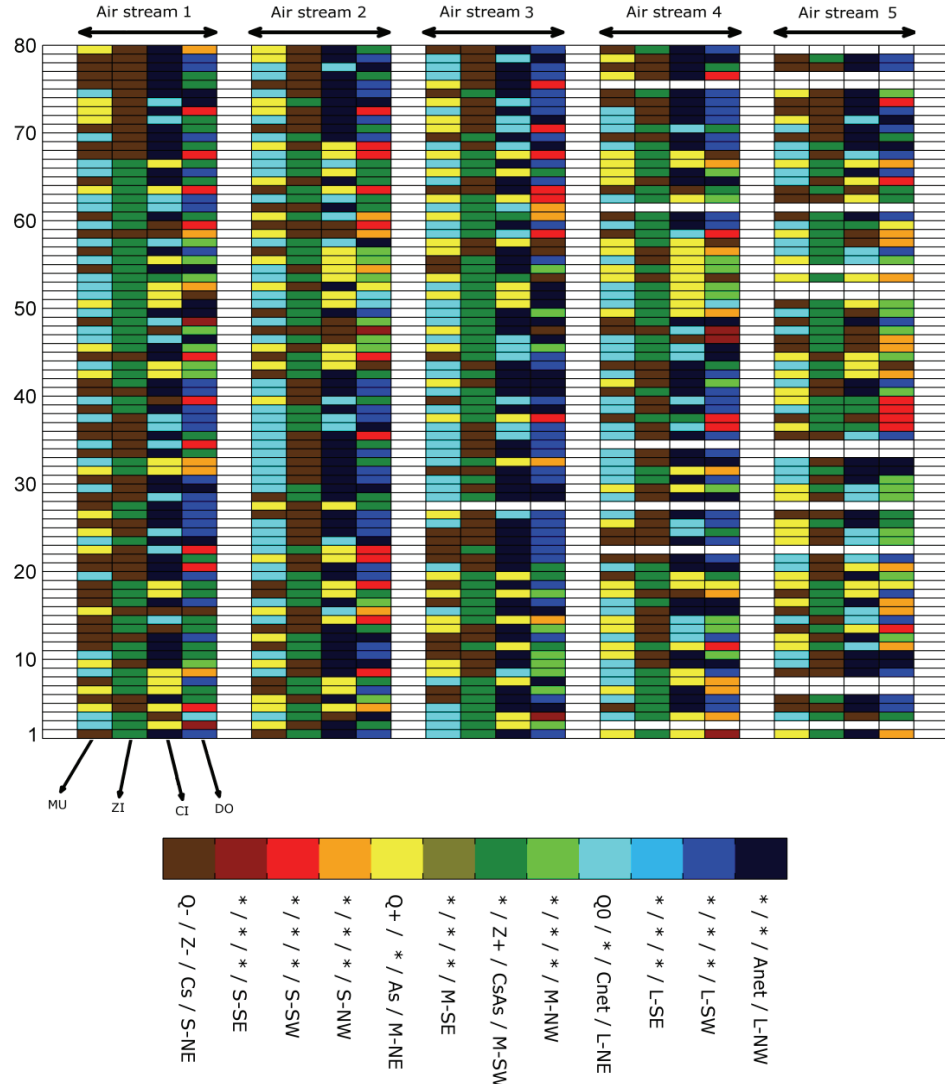


Figure S X. Representation of the final catalog for 80 first days (from 01/12/1999 to 18/02/2000). Each day is characterized by at most five air streams and each air stream can be described by four flow properties (Moisture uptake, zonality index, cyclonicity index and distance-origin).

For example, for the 2003 heatwave in the Iberian Peninsula, the method captures the short range transport associated with the thermal low, and respective advection of African air streams, and the medium and long range transport associated with the anticyclonic circulation. As a further example, the cut-off low systems with its high-altitude

depression are picked up by the new method, whereas the Eulerian Lamb classification is only able to pick up surface characteristics of the flow. In this sense, the method goes a step further in adding valuable information to the classification of a particular atmospheric flow situation.

This novel approach, developed here for the region of the Iberian Peninsula, should be general enough to be suitable for the classification of air streams over other regions of the globe.

In the following lines the main conclusions of this PhD thesis are listed as follow:

- 1) The cyclonic, western and southwestern types were the synoptic patterns that produced the highest levels of precipitation, while on anticyclonic-type days there was virtually no precipitation in the northwestern Iberian Peninsula. Regarding the maximum temperature, the highest values were generally found for the southeast, south and southwestern types, while the lowest values were found for the western, northwestern and northern types.
- 2) It was observed that for different seasons, there were different mechanisms associated with the triggering of lightning activity in the northwestern Iberian Peninsula. These mechanisms were often related to atmospheric features that did not have a clear signature at lower atmospheric levels, (e.g. sea level pressure fields); the circulation weather types alone could not fully explain the mechanisms in all cases.

- 3) Changes in the position and the intensity of the low frequency variability modes in the North Atlantic European sector tended to favour the occurrence of some circulation weather types, in preference to others. The increase in the explained variance of the continental zonal dipole, and the increasing negative (positive) correlation between this mode and the cyclonic (anticyclonic) type, helped to explain the overall decrease in winter precipitation in the region studied.
- 4) The study of atmospheric local circulation using circulation weather types can give valuable information when assessing future climate change scenarios. Moreover, they are easy to compute, which is an advantage over other methods (e.g., downscaling methods)
- 5) Based on the relationship between different circulation weather types and the precipitation in the northwestern Iberian Peninsula for present climate, one can make the assumption that there will be dry conditions in summer and spring. For autumn we may also assume dryer conditions, based on the expected decrease in the western and cyclonic types, and an increase in the anticyclonic type. This behavior is in accordance with the increase in the NAO index that is expected to occur toward the end of the 21st century.
- 6) The novel trajectory-type method developed in this PhD thesis is able to describe the three-dimensional complexity of atmospheric circulation. Moreover, it provides time-integrated physical information on the development of the systems (from a Lagrangian perspective); this goes beyond

Synopsis

the traditional description of the instantaneous synoptic situation (Eulerian perspective).

- 7) The new trajectory types capture aspects of the three-dimensional structure of the atmosphere that allow synoptic situations to be pinpointed—for example, cut-off low pressure systems—that may not have a clear signature at lower atmospheric levels, and would be missed by classification methods based only on the sea level pressure field.

Table of contents

1. Introduction	1
1.1 Climate system	1
1.2 Climate Variability	3
1.3 Daily local weather circulation	10
2. Circulation weather type classifications	13
2.1 Methodologies	14
2.1.1 Methodologies using predefined types	15
2.1.2 Methodologies producing derived types	18
2.1.3 Lamb circulation weather types	23
2.1.4 Applications of the circulation weather type classifications	24
2.2 Air mass trajectories and their applications	27
3. Climatic characterization of the northwestern Iberian Peninsula	31
3.1 Surface characterization	33
3.2 Large-scale influence	42
4. Objectives	51
5. Data	55
5.1 Large-scale meteorological fields	55
5.2 Hemispheric modes of low-frequency variability	56
5.3 Coupled general circulation model simulations	57
5.4 Lightning data	58
5.5 Weather observation station data	61
5.6 Trajectory Datasets	62
5.7 Case studies	64

6. Relationship between surface climate variables and circulation weather types	67
6.1 Introduction	67
6.2 Methodology	69
6.3 Circulation weather types for the NW Iberian Peninsula	71
6.4 Relationship between circulation weather types and precipitation	75
6.5 Relationship between circulation weather types and temperature	81
6.6 Relationship between circulation weather types and lightning activity	83
6.7 Summary	91
7. Compatibility between modes of low-frequency and circulation weather types	93
7.1 Introduction	93
7.2 Methodology	97
7.3 Circulation weather types for NW Iberia Peninsula	100
7.4 Stationary variability	101
7.5 Non-stationary variability	109
7.6 Summary	117
8. Trends in present and future circulation weather type frequency in the northwest Iberian Peninsula	121
8.1 Introduction	121
8.2 Methodology	123
8.3 Trends in circulation weather types in the 20th century	126
8.4 Evaluation of the CGCM models	127
8.4.1 Evaluation using SLP fields	127
8.4.2 Evaluation using circulation weather types	129
8.5 Changes in the frequency of circulation weather types in the 21st century	132
8.6 Summary	136
9. A new circulation weather type classification based upon Lagrangian air trajectories	139
9.1 Introduction	139
9.2 New classification based upon Lagrangian Backward Trajectories	141
9.2.1 Clustering of trajectories	141

9.2.2 New characteristics and dynamical classification	144
9.3 Trajectories types for selected case studies synoptic patterns	150
9.3.1 Cold front - 12/11/2002	152
9.3.2 Cut off low system - 10/10/2001 to 12/10/2001	153
9.3.3 5-day averaged highest precipitation period - 17/10/2001 to 21/10/2001	155
9.3.4 Coldwave - 15/12/2001 to 22/12/2001	157
9.3.5 Heatwave - 01/08/2003 to 15/08/2003	159
9.3.6 Blocking episode - 14/01/2000 to 29/01/2000	162
9.4 Comparison between Lamb circulation weather types and trajectory types	164
9.5 Climatological assessment of Lagrangian circulation type classification	170
9.5.1 Intra-seasonal variability of individual characteristics	170
9.5.2 Combined characteristics	176
9.5.3 Precipitation associated with trajectory weather types	179
9.6 Summary	183
10. Summary, concluding remarks and future work	187
Bibliography	195
List of Acronyms	219
List of Figures	223
List of Tables	231
List of Publications	235

Preface

This thesis is written on work developed from 2008-2012 in the Ephyslab (Environmental Physics Laboratory) group at the University of Vigo, under the supervision of Dr. Nieves Lorenzo and Professor Luis Gimeno. Part of my project was carried out at the Swiss Federal Institute of Technology Zurich (ETH), in the Institute for Atmospheric and Climate Science (IACETH), in collaboration with Professor Heini Wernli, and Dr. Michael Sprenger.

The remainder of the thesis is organized as follows:

- Chapter 1 presents a brief introduction about the climate system and climate variability;
- Chapter 2 presents an overview of the different weather type methodologies and their applications;
- Chapter 3 characterizes the climate in the northwest of the Iberian Peninsula;
- Chapter 4 states the main objectives of the present work;
- Chapter 5 describes the different datasets that were used;
- Chapter 6 studies the relationship between surface climate variables and circulation weather types for the northwest of the Iberian Peninsula;

- Chapter 7 relates the weather circulation types and the modes of low frequency variability;
- Chapter 8 studies changes in the frequency of weather circulation types in the present and future climate;
- Chapter 9 presents a new method for weather circulation types, taking into account the 3D structure of the atmosphere;
- Chapter 10 gives the conclusions of this work.

The funding for the work was obtained (in the first year) through “Xunta de Galicia”, under project PGIDIT06PXIB383288PR. After this, the funding was obtained through Portuguese Science Foundation (FCT) PhD grant BD/46000/2008.

1. Introduction

1.1. Climate system

The climate can be defined as a set of averaged quantities completed with higher moment statistics (such as variances, covariances, correlations, etc) that characterize the structure and behaviour of the atmosphere, hydrosphere and cryosphere over a period of time (Peixoto and Oort, 1992). The climate system is a complex, interactive system controlled by five non-isolated systems (Fig. 1.1); these are the atmosphere, the land surface, the cryosphere, the hydrosphere and the biosphere.

The climate system changes with time under the effects of its own internal dynamics, and due to changes in external factors; these external factors include natural phenomena such as volcanic eruptions and solar variations, as well as human-induced changes in the composition of the atmosphere.

The temperature of the Earth depends largely on solar radiation. In simple terms—and over long periods—the quantity of incoming shortwave solar radiation absorbed by the Earth and atmosphere is balanced by the Earth and atmosphere releasing the same amount of outgoing longwave radiation. Nearly half of the incoming shortwave solar radiation is absorbed by the Earth's surface, where it is transferred

to the atmosphere via the warming of air in contact with the surface, via evapotranspiration, and via longwave radiation that is absorbed by clouds and greenhouse gases. The atmosphere emits longwave radiation back to Earth, as well as out to space. A detailed estimate of the Earth's annual and global mean energy balance is shown in Fig. 1.2.

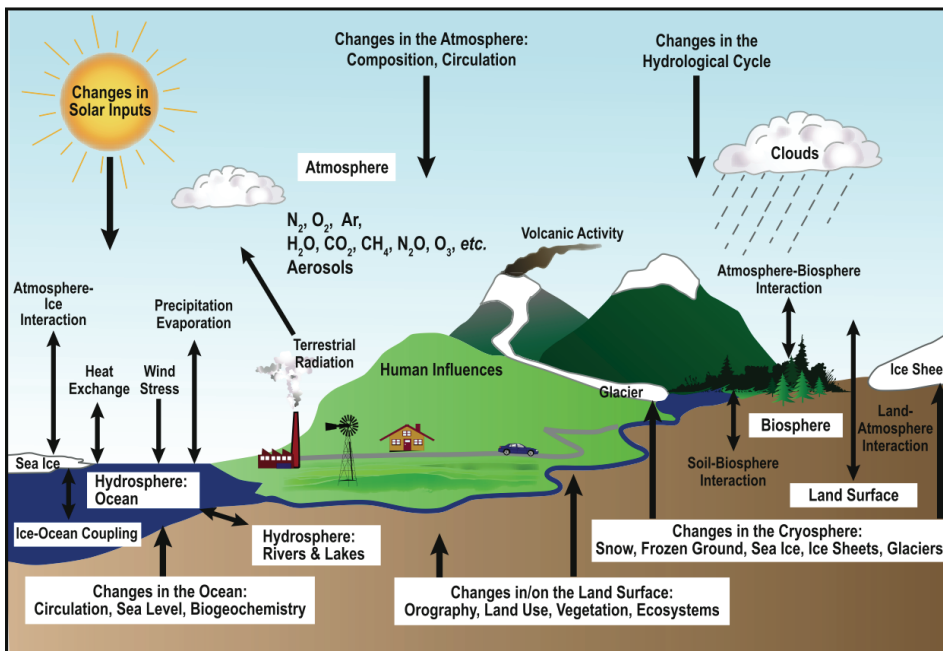


Figure 1.1. Schematic view of the components of the climate system, and their processes and interactions. Source: IPCC, 2007.

There are three main ways to change the radiation balance of the Earth. These are; a) changing the incoming shortwave solar radiation (e.g. changes in Earth's orbit or in the solar activity), b) varying the fraction of solar radiation that is reflected (e.g. changes in cloud cover, atmospheric particles or vegetation) and c) altering the outgoing longwave radiation from Earth (e.g., changes in the concentrations of greenhouse gases). The climate system responds directly to such changes (as well as indirectly) through a variety of feedback mechanisms.

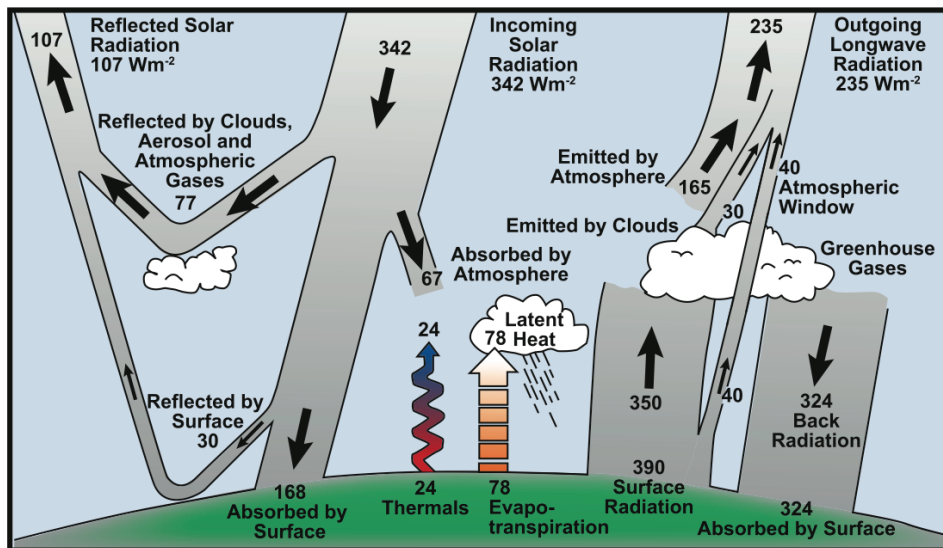


Figure 1.2. Estimate of the Earth's annual and global mean energy balance. Source: Kiehl and Trenberth, 1997.

1.2. Climate Variability

The natural variability of the global climate system depends not only on the variations in external solar forcing, but also on two features of the system itself; namely, feedback and non-linear behaviour. Additionally, in the last century, anthropogenic forcing has played an increasingly important role in climate variability (IPCC, 2007).

There are several ways to name the patterns of atmospheric variability (Quadrelli and Wallace, 2004). Teleconnection patterns or oscillations refer to the preferential modes of low frequency (temporal large-scale) variability. They can be defined as recurrent and persistent synoptic patterns of pressure and circulation anomalies that typically extend over large geographic areas and have a great influence on the climate (Hurrel, 1995).

The idea that the low frequency variability modes of the general circulation in the Northern Hemisphere can be characterized by a small number of preferred circulation patterns, or regimes, comes from the

pioneering work of Baur (1931) and Namias (1950) in the first half of the last century (see Pandolfo, 1993 and Monahan et al., 2003, for a comprehensive review).

The existence of multiple atmospheric circulation regimes was first observed by Sutera (1986), who demonstrated the bimodality of the probability density function (PDF) of an index measuring the amplitude of wavenumbers 2-4 of the mid-latitude 500 hPa height field.

Additional observational evidence for the existence of regimes was given by Kimoto and Ghil (1993), who, in an estimate of the joint PDF of the leading two modes from a principal component analysis (PCA) of the 700 hPa geopotential height field, showed the existence of distinct departures from multi-normality, which corresponded to four distinct hemispheric circulation regimes. In the same year, Cheng and Wallace (1993) used a hierarchical cluster analysis technique (at 500 hPa) to recognize three preferred circulation regimes in the Northern Hemisphere. The clusters identified by Cheng and Wallace were in close agreement with those identified by Kimoto and Ghil. More recently, Smyth et al. (1999) and Corti et al. (1999) confirmed Cheng and Wallace's results using distinct statistical methods (specifically, mixture model clustering and visual inspection of the joint PDF of the leading two PCA modes).

Parallel with the nonlinear statistical studies described above, it is also possible to use linear statistical approaches to study extratropical atmospheric low frequency variability. The statistical techniques used include correlation analysis and PCA (e.g., Wallace and Gutzler, 1981), rotated PCA (e.g., Barnston and Livezey, 1987), singular value decomposition (e.g., Wallace et al., 1992) and canonical correlation analysis (e.g., Perlitz and Graf, 1995). The results of these analyses

described a number of characteristic variability structures—such as the North Atlantic Oscillation (NAO) and the East Atlantic Pattern (EA)—each of which consists of a spatial pattern modulated by a time series that fluctuates in amplitude and sign.

These patterns have large spatial dimensions, and their time scales range from several weeks to months or even years. Furthermore, consecutive years are not independent of each another. Relationships that arise between two meteorological phenomena that are apparently independent, due to their geographical distance and time discrepancies can be described as teleconnections. Teleconnections are therefore intrinsic phenomena of the climate system, and are present as recurrent circulation fluctuations in the atmosphere and ocean that occur at distant locations, but are nevertheless correlated. They reflect important aspects of the internal variability of the climate system and the interaction between the atmosphere and other components such as the oceans.

The low frequency variability modes in the atmosphere are of paramount importance for the study of regional climate. The first major studies to refer to low frequency variability modes were those of Wallace and Gutzler (1981) for the winter period, and Barnston and Livezey (1987) for all seasons. For the North Atlantic European sector (NAE), the most prominent patterns (Fig. 1.3) are the North Atlantic Oscillation (NAO), the East Atlantic Pattern (EA), Euroasian pattern 1 (also referred as East Atlantic/Western Russia pattern (EA/WR)) and Euroasian pattern 2 (also referred as the Scandinavian pattern (SCA)), according to Barnston and Livezey (1987).

1. Introduction

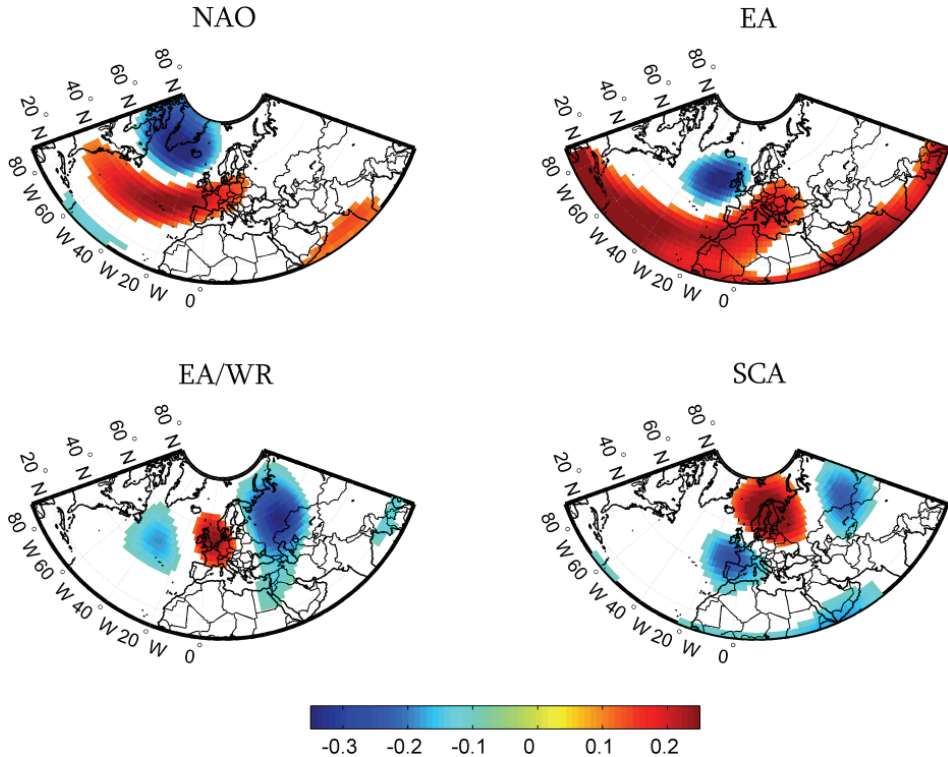


Figure 1.3. Spatial patterns of the main teleconnections over the Atlantic Northern Hemisphere. The figures represent the temporal correlation between monthly standardized height anomalies at each grid point, and the monthly teleconnection pattern time series from 1950-2005. (Adapted from Lorenzo et al., 2008).

North Atlantic Oscillation

The most important mode of variability in the North Atlantic area is the NAO (e.g. Trigo et al., 2002). NAO is a large-scale fluctuation in atmospheric pressure in the Atlantic Ocean, between the high pressure region near the Azores and the low pressure region near Iceland. This mode of variability exerts a dominant influence on climate over many parts of Europe (e.g. Hurrell, 1995), mainly in the winter months.

The NAO consists of a north-south dipole of anomalies, with one centre located over Greenland, and the other centre of the opposite sign spanning the central latitudes of the North Atlantic between 35°N and

40°N (Azores high). It has two main phases; NAO positive and NAO negative, which influence the climate differently in the NAE sector. These differences are mainly related to changes in the location and intensity of the jet stream.

In the positive phase of the NAO, the pressure gradient between the Azores and Iceland is enhanced, with a positive pressure anomaly over the Azores, and a negative anomaly over Iceland. In this case, the stormtrack is more active than normal, and is further north than normal; this typically produces colder and drier winters in the Mediterranean Basin, and warmer and wetter winters in northeastern Europe.

In the negative phase of the NAO, the pressure gradient between the Azores and Iceland is weaker than normal, with a negative anomaly in the Azores and a positive anomaly over Iceland. The stormtrack is weaker and is located to the south, producing warmer and wetter conditions in the Mediterranean basin.

East Atlantic Pattern

The EA is the second most important low frequency mode of variability over the North Atlantic, and it is present throughout the year. It has a very similar structure to that of the NAO, because it is likewise based on a north-south anomaly dipole that extends over the entire North Atlantic. Its centres are located further southeast than those of the NAO; one over the high latitudes of the North Atlantic and Scandinavia, and the other over northern Africa and the Mediterranean Sea. For this reason, the EA pattern is often interpreted as a “southward shifted” NAO pattern. However, the lower-latitude centre contains a strong subtropical link associated with modulations in the subtropical ridge intensity and location. This subtropical link makes the EA pattern distinct from its NAO counterpart.

1. Introduction

During the positive phase, the high-pressure center in the North Atlantic presents negative anomalies, whereas the low-pressure center presents positive anomalies; this results in surface temperatures that are above average in Europe, particularly in the Iberian Peninsula. This phase intensifies the westerly winds over the mid-latitudes of the eastern North Atlantic and the majority of Europe. During the negative phase, this change with the occurrence of an anticyclonic blocking located west of the United Kingdom. This pattern presents interdecadal variability.

The EA explains a significant part of the variability in the precipitation and temperature over the western Iberian Peninsula (Lorenzo and Taboada, 2005; Lorenzo et al., 2008; Rodrigo and Trigo, 2007; Rodríguez-Fonseca and Serrano, 2002; Saenz et al., 2001; Serrano et al., 1999; Vicente-Serrano and López-Moreno, 2006). Observations have demonstrated this to be strongly related to episodes of ocean upwelling at the northwestern coast of the Iberian Peninsula (deCastro et al., 2008a and b). On the other hand, the observed extreme temperature tendencies over the Iberian Peninsula have also been associated with this pattern (Rodríguez-Puebla et al., 2009).

East Atlantic/Western Russia Pattern

The EA/WR is the third pattern affecting Eurasia the most throughout the year. During wintertime, it has two main anomaly centres over the Caspian Sea and western Europe, and another two centres of opposite sign located over western and northwestern Russia, and northwestern Europe. In spring, a third anomaly centre appears over the Portuguese coast; this centre is of the same sign as the one over Russia. In autumn, this centre appears further west, since it experiences a pronounced shift towards Greenland.

This pattern is also characterized by two phases. During the positive phase, the centre over western Europe and northwestern China presents positive anomalies, whereas the centre over the North Atlantic and northern Caspian Sea shows negative anomalies (Barnston and Livezey, 1987; Wallace and Gutzler, 1981). The most pronounced and persistent negative phases tend to occur in winter and early spring.

The main anomalies in surface temperature are associated with the positive phase of this pattern, and are above average in eastern Asia and below average in eastern Russia and northwestern Africa. Precipitation is below average in central Europe.

Scandinavian Pattern

The SCA presents a primary centre of anomalies that encompasses Scandinavia and large portions of the Arctic Ocean and northern Siberia, and it is present throughout the year. It has two additional, though weaker, centres of opposite sign located over western Europe, and Mongolia and western China.

During the positive phase, positive anomalies are observed over Scandinavia and western Russia, whereas negative anomalies are observed in the other centres. Its negative phase is associated with negative anomalies over Scandinavia and western Russia, and positive anomalies in the other centers. The positive anomalies of this phase block anticyclones. Thus, temperatures are below average over central Russia and western Europe, and precipitation is above average in central and southern Europe and below average in Scandinavia. Its variability is seasonal, interannual and interdecadal.

This pattern influences the variability in precipitation and temperature over the Iberian Peninsula (Lorenzo and Taboada, 2005;

Lorenzo et al., 2008; Rodríguez-Fonseca and Serrano, 2002; Serrano et al., 1999).

As previously stated, the European region is strongly influenced by the patterns over the North Atlantic. However, it is also under the influence of patterns or oscillation modes in other regions of the world. The El Niño-Southern Oscillation (ENSO) phenomenon is a clear example of this (Rasmusson et al., 1983, Garcia-Serrano et al., 2010; Rodríguez-Fonseca and Rodríguez-Puebla, 2010).

1.3. Daily local weather circulation

Daily local weather circulation is influenced by many factors. Simplistically, one can state that the main driver of local circulation is the presence of high- or low-pressure systems, and the corresponding ridges and troughs at height levels above sea level. The presence of mountains and air-sea interactions should also be taken into account when considering local weather circulation. In addition, as stated before, seasonal variations in the amount of solar radiation that reaches a region generate intra-annual variability.

Meteorological systems such as extra-tropical depressions, blocking patterns, cut off lows, Azores high or thermal lows are the most important features characterizing the daily local weather circulation in the Iberian Peninsula. A detailed characterization of the climate in the Northwest (NW) Iberian Peninsula is given in chapter 3. The annual variability of these meteorological systems is often related to low frequency variability modes (e.g. Barriopedro et al., 2006; Nieto et al., 2007a).

The complexity of the continuum of atmospheric circulation is the main motivation for researchers attempting to find a simpler method

of categorization. Classifications of atmospheric circulation are intended to reduce this complexity; they achieve this by summarizing the data into a reasonable and manageable number of discrete classes (types). There are different ways to classify climates into similar classes. In ancient Greece, climes were defined to describe the weather depending upon latitude.

Over the last century, researchers have attempted to explain and understand the relations between the larger-scale atmospheric behavior and local weather and the climate response, leading to numerous weather and circulation type classifications (as will be described in chapter 2). The classifications were used mainly for weather forecasting purposes, while in recent decades the applications of circulation classifications have widened. Circulation weather types (CWT) are used to describe and understand the physical links between low frequency variability modes, synoptic features, and surface weather at various scales and locations. They are typically based on a single level of the atmosphere, as will be shown in chapter 2.

2. Circulation weather type classifications

In general, classification can be seen as the assignment of objects to groups (cases) so that common features are shared within each class, and there are dissimilarities between the classes. In the case of circulation classifications, this process provides a method for categorizing the continuum of atmospheric circulation into a reasonable and manageable number of discrete classes (types).

Classifications have had a long history in meteorology and climatology. Since the beginning of meteorology, until a few decades ago, classifications (generally called “catalogs of synoptic types”) were used mainly in weather forecasting (e.g. Hess and Brezowsky, 1952; Lamb, 1972). The use of classifications to describe the weather has grown in the decades since the advent of computers, which made it possible to develop fast and objective methods to process large amounts of data. Furthermore, many climatological studies and applications require that the data be as simplified as possible; this is achieved by analyzing a gridded dataset (usually sea level pressure or geopotential height at different levels), and grouping the data into a relatively small number of distinct categories. As a consequence, several classification

2. Circulation weather type classifications

methods have been developed, and are currently used in a large wide range of applications. In addition, in 2002, Sheridan stated that the “Synoptic weather-typing, or the classification of weather conditions or patterns into categories, continues to be popular, and numerous methods have been developed over the past century”. Recent applications of these classifications can be found in climate studies (for past, present and future climates), and in innovative applications in ensemble forecasting, increasing the variety of synoptic-climatological studies (Huth et al., 2008). Due to the wide range of classification methods in meteorology and climatology, this overview will focus on the classification of atmospheric circulation patterns, and classification based on air mass trajectories.

This overview is divided into two parts. The first section describes the most common methodologies for the classification of atmospheric circulation patterns, and their applications. In the second section, a description is made of the applications of air mass trajectories.

2.1. Methodologies

Different methods exist for the classification of circulation weather types (CWTs), as was shown by Huth et al., 2008, and Phillip et al., 2010. These different methodological approaches can be categorized by the kind of type definition they use. Two main strategies can be discerned concerning the relation between type definition and the assignment of objects. The first strategy is to establish a set of types prior to the process of assignment (predefined types), while the second is to arrange the entities to be classified (daily patterns in this case) following a certain algorithm, such that the types are—together with the assignment—the result of the process (derived types). The use of

predefined types is valid for a deductive, top-down approach, where it is already known what the relevant types look like; the generation of derived types is useful for an inductive, bottom-up approach, where more or less no knowledge of the structure of the dataset or the effects of certain types is assumed, but is obtained using data mining.

Methods using predefined types include those with subjectively chosen weather situations, and those where the allocation of days to one type depends on thresholds or rules (Table 2.1). The Lamb circulation type, which will be used several times in the following chapters, is highlighted in bold in Table 2.1.

In contrast, methods using derived types are based on the idea of identifying types that are indicated by any structure existing in the dataset itself. In particular, three main strategies can be discerned (PCA, leader algorithm, and optimization methods); these will be discussed later in the manuscript.

2.1.1. Methodologies using predefined types

Two different approaches can be defined within these classification methods. Some methods attempt to reproduce CWTs that have previously been defined subjectively, and others use quantitative thresholds or rules to determine the allocation of each day to one class. These approaches have in common a presumed concept of the relation between circulation and surface weather variables such as temperature and precipitation, although this is rarely formulated explicitly. Especially for European surface weather it is, for example, important whether the large scale flow is organized zonally or meridionally. Predefined types are therefore preferentially defined to clearly discern between these two configurations.

2. Circulation weather type classifications

Table 2.1. Overview of the different circulation weather type classification methods. The Lamb circulation weather type is highlighted in bold. The abbreviations are defined as follows: variables used for classification (SLP: sea level pressure; H: geopotential height; U/V: zonal and meridional wind; PW: precipitable water).

	Classification Methods	Variables	References
predefined types	<i>Subjective</i>		
	Hess-Brezowsky*	Not specified	Hess and Brezowsky, 1952.
	ZMAG*	Not specified	Lauscher, 1985.
	<i>Threshold</i>		
	Objectivized Lamb (Jenkinson-Collison)	SLP	Lamb, 1972; Jones et al., 1993.
	Litynski	SLP	Litynski, 1969.
	WLKC733	U/V700,H925/ 500, PW	Dittman et al., 1995; Philip et al., 2010.
	<i>PCA algorithm</i>		
derived types	P27	H500	Kruizinga, 1979.
	TPCA	SLP	Huth, 1993.
	PACXTR	SLP	Esteban et al., 2006
	<i>Leader algorithm</i>		
	Lund	SLP	Lund, 1963.
	Kirchhofer original types	H500	Kirchhofer, 1974.
	<i>Optimization algorithm</i>		
	CKMEANS	SLP	Enke and Spekat, 1997
	SANDRA /SANDRAS	SLP	Philipp et al., 2007; Philipp et al., 2008.
	NNW (original)	H500	Michaelides, 2007.
	NNW (COST733)	SLP	Philipp et al., 2010.

* Not adaptable domain

Subjective classifications are based on expert knowledge of the effects of certain CWTs on various surface climate parameters, i.e., they attempt to discern between typical synoptic situations. Since they are subjective, the definition of the typical situation is not straightforward. This increasing spread of possibilities for different situations results in the characteristically high number of types of subjective classifications, ranging from 29 for the Hess and Brezowsky, 1952, to 43 for the ZAMG-classification (Lauscher, 1985). An objectivized version of the Hess and Brezowsky catalogue was designed by James, 2007; an example is given from this in Fig. 2.1, where it is shown the sea level pressure (SLP) and the 500 hPa geopotential height (H500) mean composites for the half-year winter, and for the objectivized Hess and Brezowsky types 1 to 15 (out of 29) for the winter half-year.

Threshold-based methods, such as the objectivized Lamb (Jones et al., 1993), Litynski (Litynski, 1969), or WLKC733 (Philipp et al., 2010), define their types each day by setting a limit between types, or predefined rules of assignment. For example, a distinction can be made between days with a westerly main flow over the domain, and those with a northerly, easterly, or southerly direction, where the angles used to delimit the sectors represent the thresholds between the types. The objectivized Lamb and Litynski catalogue uses the SLP as a classification variable, while the WLKC733 uses a combination of the U and V components of the 700 hPa wind fields, and the geopotential height at 950 hPa (H950) and 500 hPa (H500) with the integrated precipitable water (PW) content.

More detailed descriptions of the objectivized Lamb CWT will be given in section 2.1.3 and chapter 6.

2. Circulation weather type classifications

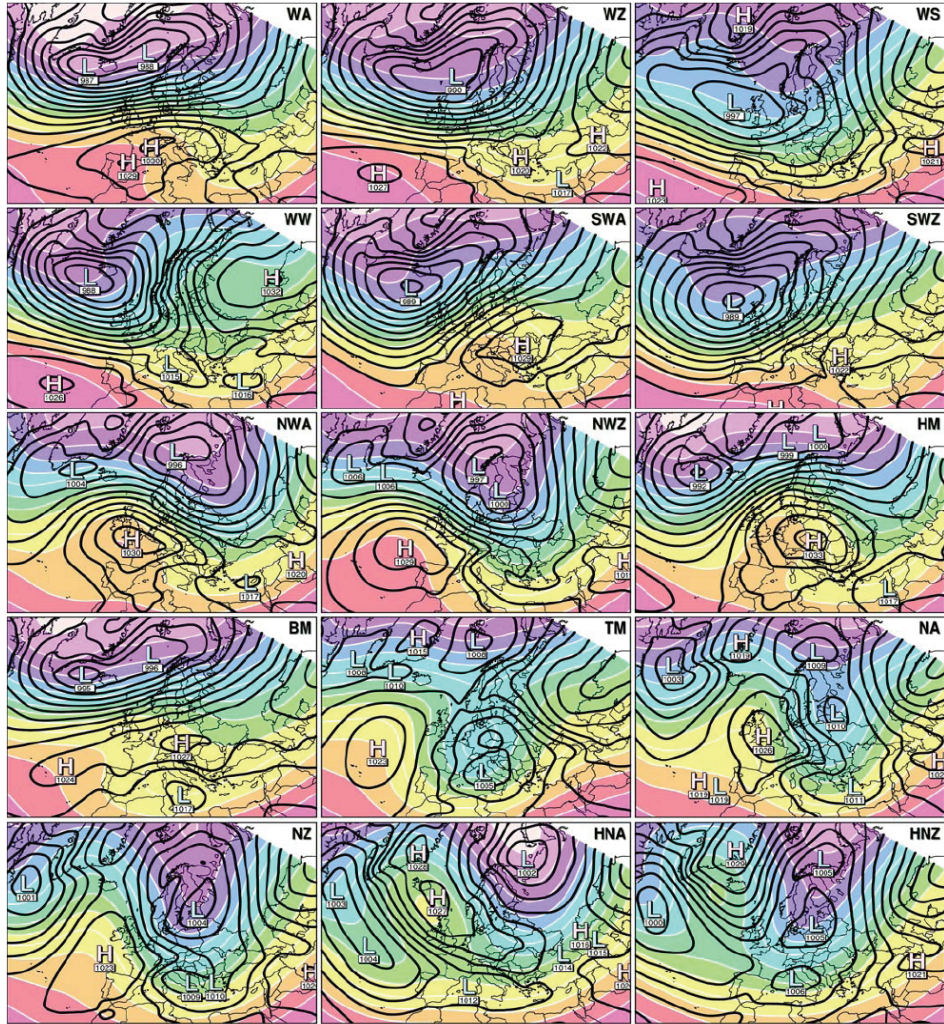


Figure 2.1. Example of the objectivized Hess and Brezowsky (GWLs). Climatological composites of GWLs 1–15 (out of 29) for the winter half-year, showing H500 (color-filled field) and SLP (black contours) (source: James, 2007).

2.1.2. Methodologies producing derived types

In contrast to methods that use predefined types, all of the methods producing derived types are centred on the idea of identifying types that are intrinsic in the dataset. Three main strategies in particular are used. The first group uses principal component analysis (PCA) to determine the principal components (PCs) explaining the major

fractions of the variance of the input data, while the patterns to be classified are assigned to classes according to some measure of relation to the PCs. The second strategy is to find leading patterns according to the number of patterns similar to them within a certain distance; this is called a leader algorithm (Hartigan, 1975). The third strategy uses a combinatorial approach to optimize a partition according to a function; typically, this involves the minimization of the within-type variability.

The main objective of PCA is to provide a compact description of the spatial and temporal variability of a data series in terms of orthogonal functions or statistical modes. Typically, most of the variance in the spatially distributed time series is in the first few orthogonal functions, whose patterns may then be linked to possible dynamical mechanisms. The potential of PCA to be used as a classification tool was suggested by Richman, 1981, and discussed by Gong and Richman, 1995. The basic process for using PCA as a classification tool consists of assigning each case to a PC according to some rule. However, several different modes of PCA exist, which differ fundamentally from each other (Richman, 1981), and serve different purposes as they can act as a data preprocessing tool prior to cluster analysis.

The potential use of PCA as a classification tool was discussed by Richman in 1981. The two most common PCA modes used for classification are: a) the s-mode, in which the eigenvectors describe the spatial pattern of variability, and the principal components describe the time variations (an example of its application can be found in the P27 (Kruizinga, 1979) or the PACXTR method (Esteban et al., 2006), and b) the t-mode, where the principal components describe the importance of a spatial pattern, and the loadings reflect the extent of their time variant realization (an example of its application can be found in the T mode

2. Circulation weather type classifications

PCA (Huth, 1993 or Huth, 2000)). An example of a T mode analysis is given in Fig. 2.2, where a comparison is made between the T mode PCA types found for an observed dataset, and those found for a control global climate model.

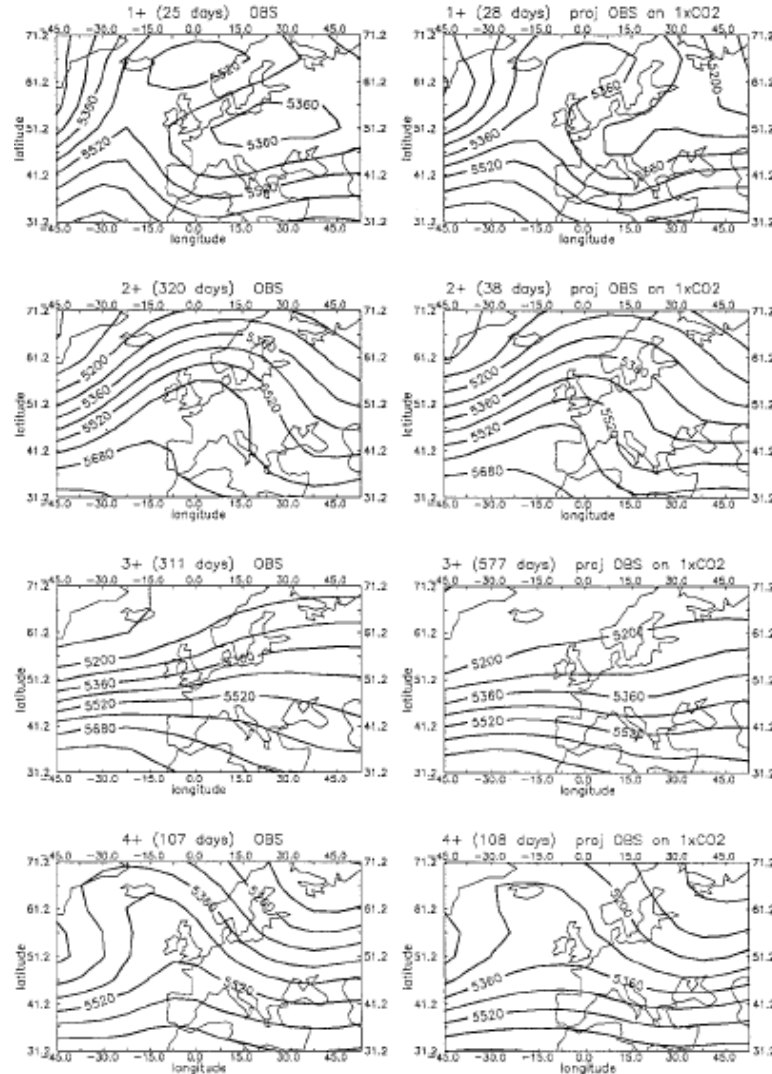


Figure 2.2. An example of circulation weather types generated using T-mode PCA. Mean H500 patterns of circulation weather types over Europe, found for the observed data (left column), and their projections onto the UKHI global climate model (right column). Each type is represented by its number, and its frequency of occurrence (adapted from: Huth, 2008).

Classification methods based on the leader algorithm (Hartigan, 1975) can be found in the Lund (Lund, 1963) and Kirchhofer original types (Kirchhofer, 1974) method. These methods search for key (or leader) patterns in the original data, which are located in the centre of high-density clouds of entities (days) within the multidimensional phase space spawned by the variables, i.e. grid-point values. The leader algorithm is a simple and quick clustering that searches for a key pattern in the sampled maps.

The last family of classifications consists of the so-called optimization algorithms, in which several approaches are used to organize a set of days into groups in a certain way, such that a chosen function is optimized. The CKMEANS method (Enke and Spekat, 1997) is based on the k-means algorithm. In the CKMEANS, the initialization is performed by randomly selecting one object (SLP daily fields). The seed for the second cluster is then determined as the object most different from the first, while the seed for the third cluster is the object with the highest sum of distances from the first two seed-patterns, and so on, until every cluster has one seed-pattern. In a stepwise procedure, the starting partition, initially consisting of the k seed-patterns is gradually identified: all remaining days are assigned to their most similar class. After the initial assignment of all days has been performed, the iterative k-means clustering process is launched. The centroids converge towards a final configuration, which has no similarities with the starting partition. An example of CWTs generated using the CKMEANS method (Enke and Spekat, 1997) for Central and Western Europe, for summer, is shown in Fig. 2.3.

The SANDRA /SANDRAS methods (Philipp et al., 2007; Philipp et al., 2008) are based on a heuristic simulated annealing algorithm. The

2. Circulation weather type classifications

difference between SANDRA and SANDRAS is that in the latter, instead of single day patterns, three-days-sequences are used. The only differences in the k-means are so called wrong re-assignments, i.e., objects may be removed from their nearest cluster, depending on a probability which is high at the beginning, but slowly decreases during the optimization process.

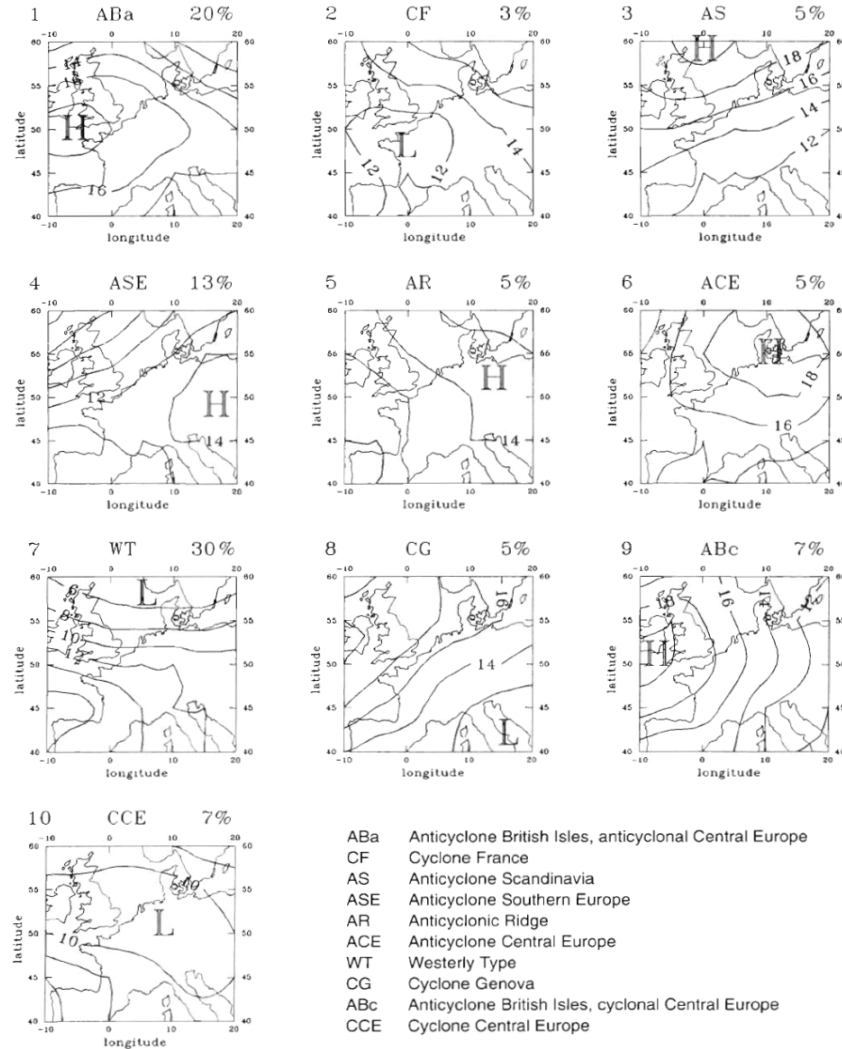


Figure 2.3. An example of circulation weather types in Central and Western Europe, generated using CKMEANS (source: Enke and Spekat, 1997). Composite images of 1000 hPa geopotential height charts for summer (JJA) in Central and Western Europe are shown. The percentage values at the top right of each graph indicate the frequency of the respective circulation weather type.

The self-organized map technique (SOM or SOFM) employs a neural network algorithm that uses unsupervised learning to determine generalized patterns in data (Kohonen, 1982). This technique reduces the dimensions of large datasets by grouping similar data records together and organizing them in a two dimensional array, which is referred to as a map. The NNW (original) and the NNW (COST733) are examples of two catalogues that use the SOM technique; they differ only in the classification variable used, namely H500 (Michaelides, 2007) or SLP (Philipp et al., 2010).

2.1.3. Lamb circulation weather types

Since the use of the Lamb circulation type's methodology will be recurrent in the next chapters, a detailed overview will be given here, and the computational procedures will be described in chapter 6.

This classification of atmospheric circulation into weather types was carried out for the British Isles by Lamb, 1972. This was a manual classification, and was based on the analysis of daily SLP fields for the British Isles. In his work, Lamb defined seven principal types:

- West (W); • South (S);
- Northwest (NW); • Anticyclonic (A);
- North (N); • Cyclonic (C).
- East (E);

In addition, a set of hybrid classes was created; these correspond to days with a mixture of characteristics from the seven principal classes (for example, the class AW corresponds to cases where there is atmospheric circulation with anticyclonic vorticity that is associated with a flux mainly from the W sector). The days that cannot be included

2. Circulation weather type classifications

in any of the above classes are also taken into account. These are days that show: a) inconstant and/or extremely intense flow (whether weak or very strong); b) changes of atmospheric circulation during the day; c) incompatible hybrid types. However, the analysis of the charts in this procedure requires not only a very experienced meteorologist, but also large amounts of time.

The manual Lamb classification was adapted by Jenkinson and Collinson (1977) for an objective automated classification for the British Isles, which was later evaluated by Jones et al., 1993. This automated classification is based on the use of a set of indices associated with the direction and vorticity of geostrophic flow. This automated method was recently adapted for different areas in the Iberian Peninsula; for the SE Iberian Peninsula (Goodess and Palutikof, 1998), for Portugal (Trigo and DaCamara, 2000), and for the NW corner of the Iberian Peninsula (Lorenzo et al., 2008). Several applications of the Lamb CWT will be discussed in section 2.1.4, while in section 6.2 a detailed description of the automated classification method will be presented.

2.1.4. Applications of the circulation weather type classifications

In recent years, the usefulness of CWT classifications has been investigated for a wide range of applications, in scientific domains from climate, to environmental areas such as air quality and forest fires, to extreme events such as flood, drought, avalanches. A large number of studies in the literature describe the application of circulation weather type classifications and some examples of such applications are given below.

Europe

Regarding the climate in Europe, several studies focus on the assessment of long-term changes (trends or regime shifts) in the frequency and persistence of CWTs, for both past and future climates (e.g., Huth, 2001; Demuzere, 2008a). In addition, studies quantifying the links between circulation changes and observed climatic trends are also common (e.g., Hope et al., 2006; Cahynová and Huth, 2009). There are also studies pointing out other applications for synoptic CWTs. Some studies relate these large-scale synoptic patterns to mean levels of surface O₃ (e.g., Demuzere et al., 2008b; Leśniok et al., 2010), while others study the mechanism that characterizes the triggers for extreme events, e.g., floods (Prudhomme and Genevier, 2011), or wildfires around the Mediterranean region (Kassomenos, 2010). In addition, James, 2008, attempt to use the synoptic CWT in medium-and extended-range ensemble forecasting.

Iberian Peninsula

The following gives a description of the different classification methods that are used in the Iberian Peninsula, and their application (note that this is not an exhaustive description).

The first studies to use automated classifications of the atmospheric circulation affecting the Iberia Peninsula were developed on both monthly (Corte-Real et al., 1995) and daily (Zhang et al., 1997; Corte-Real et al., 1998; Romero et al., 1999) timescales, and were computed using principal component analysis, followed by a k-means cluster analysis. In the years since, several studies using an automated version of the Lamb CWT have been published (e.g. Goodess and Palutikof, 1998; Trigo and DaCamara, 2000; Spellman, 2000; Goodess and Jones, 2002). These works studied the relationship between

2. Circulation weather type classifications

precipitation in different regions of the Iberian Peninsula, for different purposes; e.g., to explain precipitation trends, or to construct precipitation scenarios for future climate or precipitation prediction. The application of CWT classifications in the Iberian Peninsula has been restricted largely to studies of precipitation; these classifications have not typically been applied in temperature studies.

In the last decade, the use of different classification methods in the Iberian Peninsula has increased; this is due to reductions in computation time, but also because new climate weather-related datasets have become available. Studies of the Iberian Peninsula that use other classification methods are shown in Table 2.2.

Table 2.2. Example of studies of the Iberian Peninsula that use classification methods other than the Lamb circulation weather type.

Relationship with:	References
Precipitation	Rodriguez-Fonseca and Serrano, 2002; Santos et al., 2005; Fragoso and Gomes, 2008; Casado et al., 2010
Temperature	Serra et al., 1999; Bermejo and Ancell, 2009; Esteban et al., 2009
Snow	Esteban et al., 2005
Wild fires	Pereira et al., 2005; Rasilla et al., 2010
Dimming/Brightening	Sanchez-Lorenzo et al., 2009
Hail events	Aran et al., 2011
Lightning activity	Pineda et al., 2010
Wave height	Rasilla and Codrán, 2010
Aerosols	Alonso-Perrez et al., 2011

Despite this, the automated version of the Lamb circulation is still a very popular method in fields like climatology, atmospheric sciences, or in studies of weather-related health impacts. Examples of this can be found in:

- precipitation (Spellman, 2000; Martin-Vide, 2002; Paredes et al., 2006; Vicente-Serrano et al., 2006; Garcia-Herrera et al., 2007; Lorenzo et al., 2008; Vicente-Serrano et al., 2011);

- maximum and minimum temperature (chapter 6);
- wind (Rasilla et al., 2002; Azorín et al., 2009).
- association with lightning activity (Tomas et al., 2004; Ramos et al., 2011);
- snow pack variability (López-Moreno and Vicente-Serrano, 2007)
- hospital admissions (de Pablo et al., 2009);
- relationship with modes of low frequency variability (Lorenzo et al., 2008; Ramos et al., 2010);
- future atmospheric circulation scenarios (Lorenzo et al., 2011).

2.2. Air mass trajectories and their applications

Trajectory paths are a useful tool for describing air mass motions, and are applied in several fields in the atmospheric sciences (Stohl, 1998). For such applications, the problem of dividing the atmosphere into a set of air parcels—which are forced to move by three-dimensional winds—under certain physical conditions can be solved using Lagrangian models (Stohl, 1998; Stohl et al., 2001). A comparison between three frequently used trajectory models (TRAJKS, LAGRANTO and FLEXTRA) was given by Stohl et al., 2001.

Trajectories have been used not only to interpret individual flow situations, but also to study the history of air masses, both backward and forward, with large sets of trajectories. Trajectory analyses are commonly used in air quality studies, and are based on the cluster analysis of large sets of trajectories. The main idea is to have a multivariate statistical technique that splits a data set into a number of groups. Dorling et al., 1992a gives a detailed description of their clustering technique, which allows distinct flow patterns and large scaling circulation features to be discriminated (Dorling et al., 1992b;

2. Circulation weather type classifications

Stohl and Scheifinger, 1994). Fig. 2.4 presents an example of results from a cluster analysis by Dorling et al., 1992a for the trajectories arriving at Eskdalemuir (south Scotland) in the period February-July, 1981-1984.

The analysis of trajectories approaching a chosen target region provides an alternative to studying CWT classifications (e.g., Stohl and Scheifinger, 1994; Jorba et al., 2004; Nyanganyura et al., 2008).

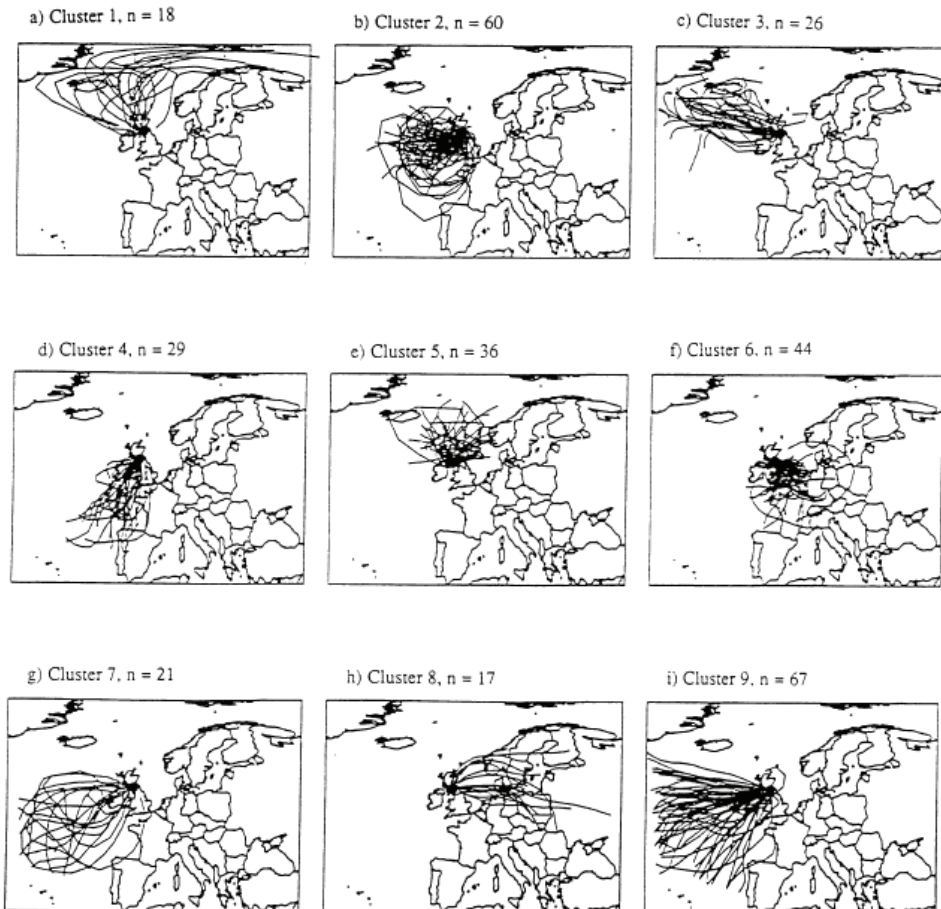


Figure 2.4. Results of a trajectory cluster analysis showing nine clusters that were identified with their trajectory members (originally presented by Dorling et al., 1992a). The work is based on trajectories arriving at Eskdalemuir (south Scotland) in the period February-July, 1981-1984.

Trajectory analysis can also be used to study moisture supply regions—by tracking air parcels moving in a given area (James et al., 2004; Nieto et al., 2006; Gimeno et al., 2010)—or precipitation at different timescales (Sodemann et al., 2008). Most of these studies use only information on the position (latitude, longitude and height) of the air parcels; in the case of moisture sources studies, information on the specific humidity of the air parcels is also used

Knowledge of how the properties of an air parcel change with time allows a better estimation of the evolution of meteorological phenomena. Once the additional thermodynamic conditions of air parcels are known, the development of particular structures can be easily followed. Backward trajectory analysis can also be performed in the examination of meteorological structures (e.g. Stohl, 2001; Eckhardt et al., 2004; Wernli and Davies, 1997; Knippertz and Wernli, 2010).

3. Climatic characterization of the northwestern Iberian Peninsula

The area under scope in this work—that is, the NW Iberian Peninsula—corresponds to the Spanish region of Galicia and the north of Portugal. The area extends between approximately 40°N and 44°N , and 9.5°W and 6°W (see Fig. 3.1, red rectangle).

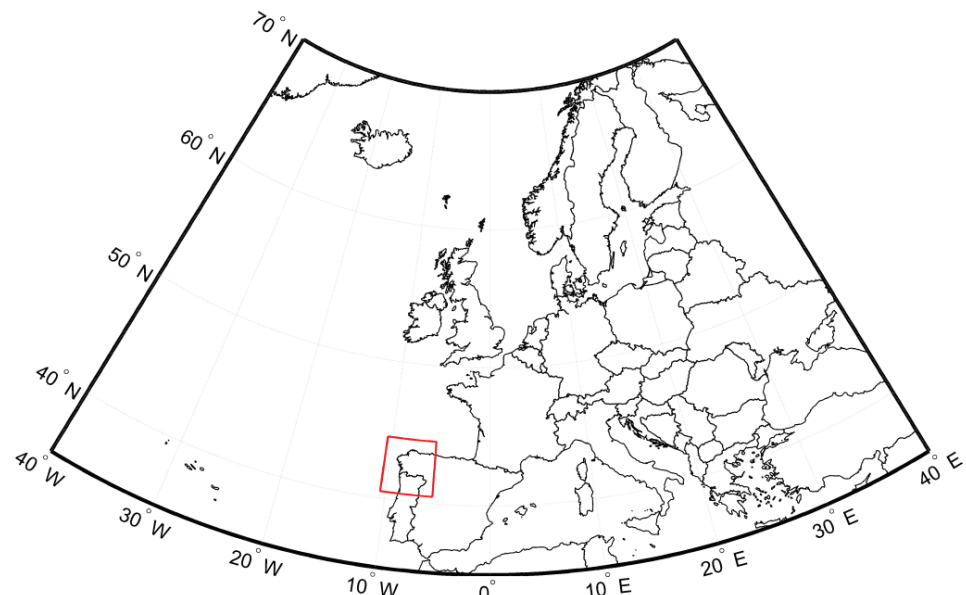


Figure 3.1. Location of the area studied, enclosed by the red rectangle.

Regarding altitude (Fig. 3.2), the highest values in the NW Iberian Peninsula are between 1000m and 1500m, with the exception of Serra da Estrela (SET), in Portugal, which peaks just below 2000 m, and Manzaneda (M), in Galicia, which peaks just below 1800 m. The northern landscape of the domain becomes mountainous towards the interior, with several plateaus indented by river valleys. Continentally, the regions farthest from the Atlantic Ocean are approximately 220 km away. The orography of Portugal and Galicia also affects the domain. In the north, the Cantabrian Mountains border Galicia, while in the northern/central part of Portugal, the Spanish Meseta (Inner Plateau) borders the region.

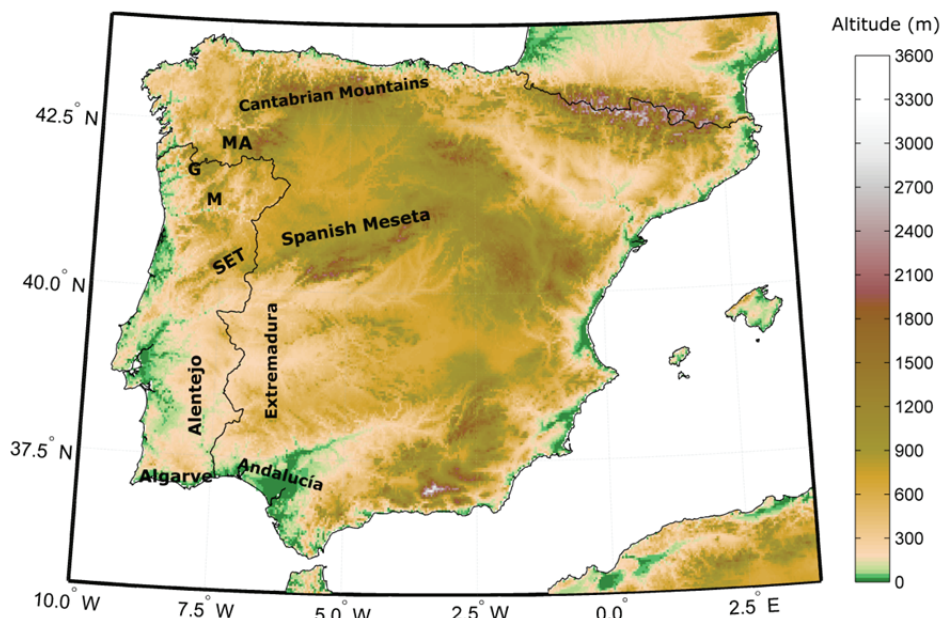


Figure 3.2. Orography of the Iberian Peninsula. The topologic names mentioned throughout the chapter are also included in the figure.

Although the variations in the climactic factors are rather small, they are enough to produce significant variations in air temperature and, most significantly, in precipitation, as will be described in more detail later. The northern areas of the domain represent one of the

wettest areas in Europe, while the southern part of the domain is characterized by a mild Mediterranean climate, but with well-known vulnerabilities; namely, droughts and desertification (SIAM, 2002; SIAM, 2006).

Climate is a complex mixture of many elements, including temperature, humidity, wind, precipitation, pressure and cloudiness; these factors combine to define the physical and chemical environment at the surface of Earth.

3.1. Surface characterization

To put the NW Iberia Peninsula into a climactic context, the spatial distribution of the mean annual maximum air temperature in the Iberian Peninsula is shown in Fig. 3.3a. As shown, the mean annual maximum air temperature values in the W Iberia Peninsula vary between 24°C in the southern part of Portugal and 18°C in Galicia. The mean annual minimum air temperature values (see Fig. 3.3b) range from 12°C in southern Portugal to 6°C in Galicia. Microclimates produced by valleys and mountains are also present in the domain. In general, the coastal regions of Galicia and Portugal tend to have a milder climate than the interior regions.

The mean annual accumulated precipitation (Fig. 3.4) also shows a high degree of spatial variability. The highest values are found in the North of Portugal and Galicia, with values higher than 1500 mm, while the lowest values are found in the southern regions of Portugal, with values below 400 mm.

3. Climatic characterization of the northwestern Iberian Peninsula

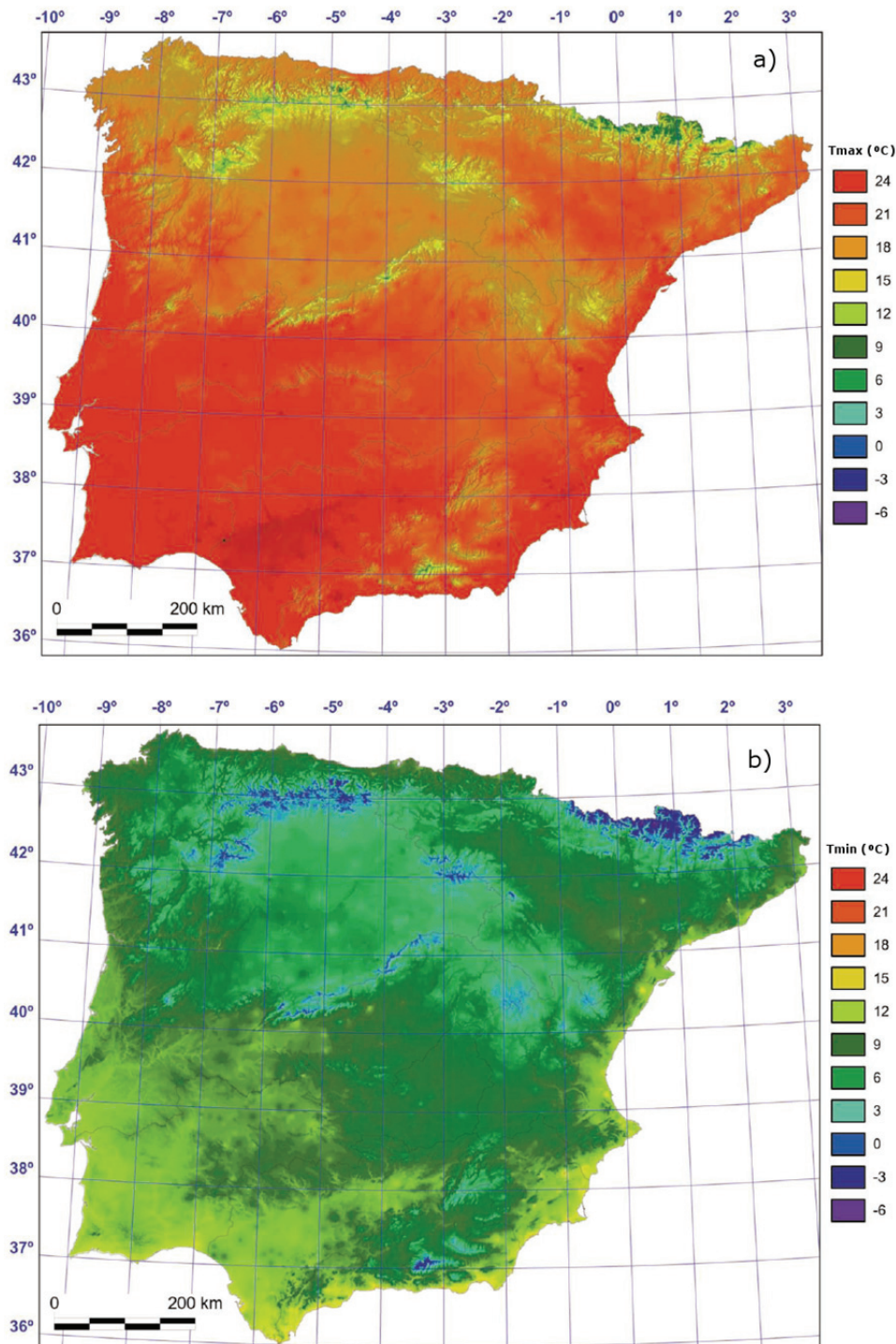


Figure 3.3. Spatial distribution of (a) the mean annual maximum air temperature (b) the mean annual minimum air temperature in the Iberian Peninsula, during the 1951-1999 period (source: Ninyerola et al., 2005).

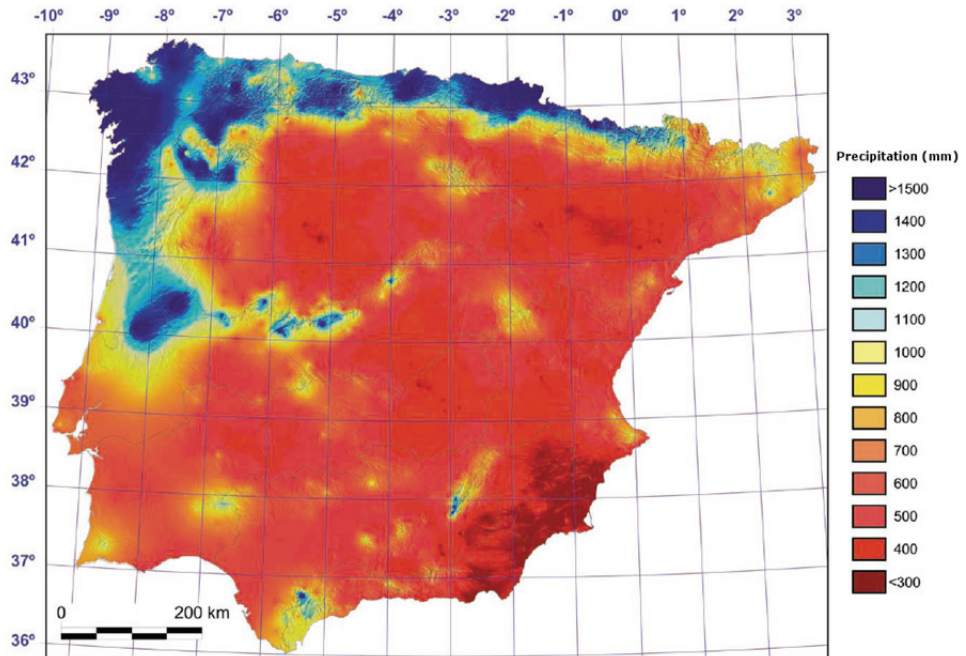


Figure 3.4. Spatial distribution of the mean annual accumulated precipitation, during the 1951-1999 period (source: Ninyerola et al., 2005).

Since the results presented in this work focus on the NW Iberian Peninsula, a detailed description of the seasonal maximum and minimum air temperature, and the variability in precipitation, is made for the Euroregion Galicia-North Portugal, based on the characterization of the region made by Gomez-Gesteira et al., 2011.

The maximum seasonal air temperature on land is represented in Fig. 3.5. Although the data shown in the maps follow expected trends closely, with the highest temperatures being recorded in summer and the lowest temperatures being recorded in winter, a few points merit discussion. A marked difference between coastal and continental temperatures can be observed in summer in Galicia, when at the same latitude maximum continental temperatures are of the order of 2°C higher. In contrast, in the northern region of Portugal, the highest temperatures are found inland. In winter, this effect is even more

3. Climatic characterization of the northwestern Iberian Peninsula

pronounced, with continental temperatures of the order of 5°C lower than coastal temperatures. Deviations from this general pattern are mainly due to orographic effects (see Fig. 3.2). The presence of orographic barriers along the coastline is also responsible for the rapid transition from a maritime climate at the coast to a continental climate at distances less than 100 km from the coast.

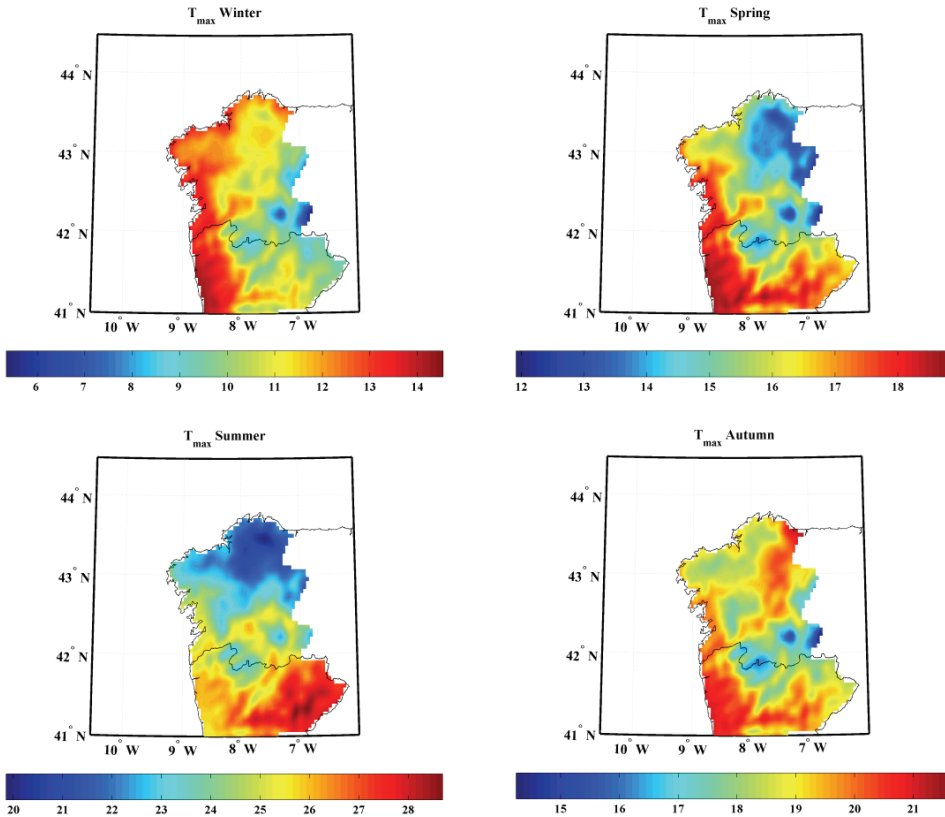


Figure 3.5. Seasonal spatial distribution of the mean maximum air temperature (°C) for the 1961-2006 period, in winter (DJF), spring (MAM), summer (JJA) and autumn (SON) (source: Gómez-Gesteira et al., 2011).

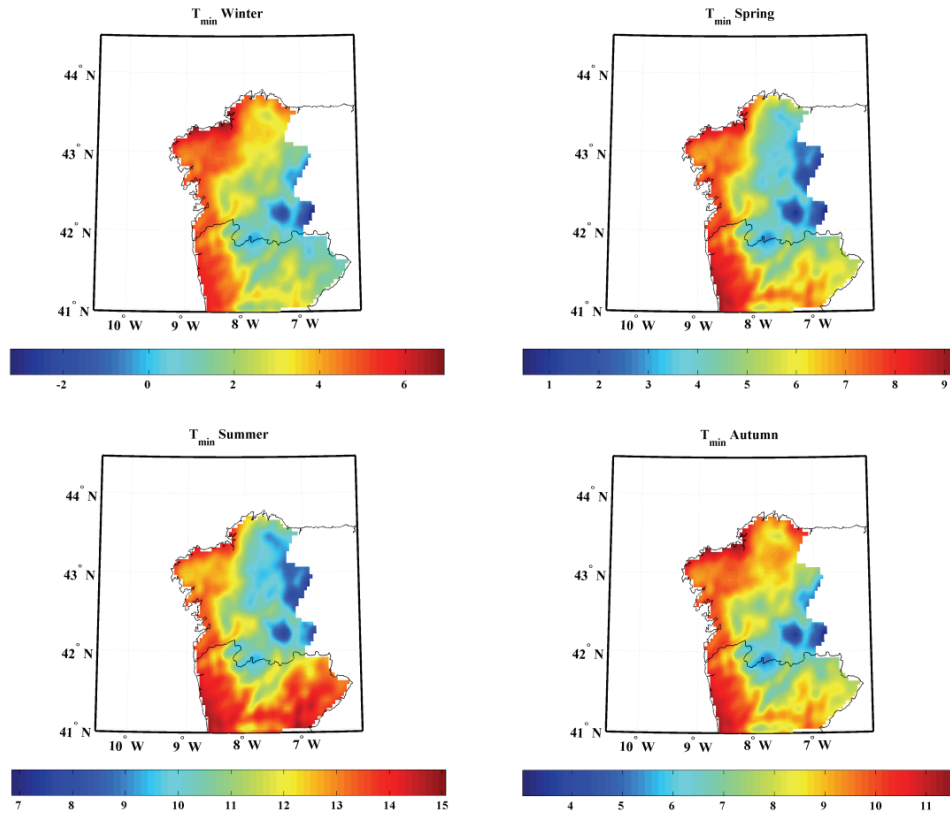


Figure 3.6. Seasonal spatial distribution of the mean minimum air temperature ($^{\circ}\text{C}$) for the 1961-2006 period, in winter (DJF), spring (MAM), summer (JJA) and autumn (SON) (source: Gomez-Gesteira et al., 2011).

Similar patterns can be observed for minimum air temperatures (Fig. 3.6). The lowest temperatures in Galicia always correspond to the continental region, where the highest mountains are located. For northern Portugal, the highest minimum temperatures are found in the interior region, while for other seasons the highest minimum temperatures are generally found in the coastal regions.

The seasonal mean accumulated precipitation is shown in Fig. 3.7. In general, moderate precipitation values are observed at coastal locations, and low values are observed in the interior regions. The maximum values are observed along the Galician ridge in the northern part of the area, and along the Xures/Geres (G) and Marão (M)

3. Climatic characterization of the northwestern Iberian Peninsula

mountain ranges in the southern part. Seasonally, the highest precipitation values are observed in autumn and winter, reaching values close to 1000 and 1200 mm per season, respectively. Minimum values of under 300 mm were observed in summer.

The intensity of winter precipitation is influenced by the orography. Incoming fronts from the Atlantic Ocean are affected by the presence of mountains near the coastline, which act as barriers that hinder the movement of the fronts towards the interior. For this reason, the precipitation in these mountain regions is enhanced (Foehn effect). In general, the coastal and adjacent areas are characterized by a maritime climate, with mild summers and rainy winters. In contrast, the interior of the region is characterized by a continental climate, with dry summers and cold winters.

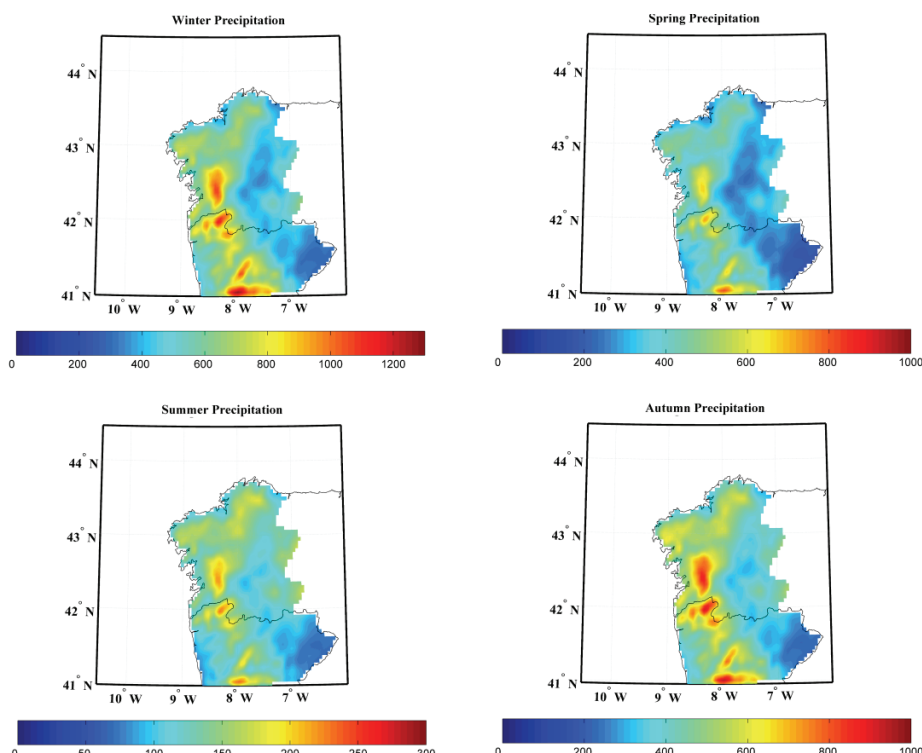


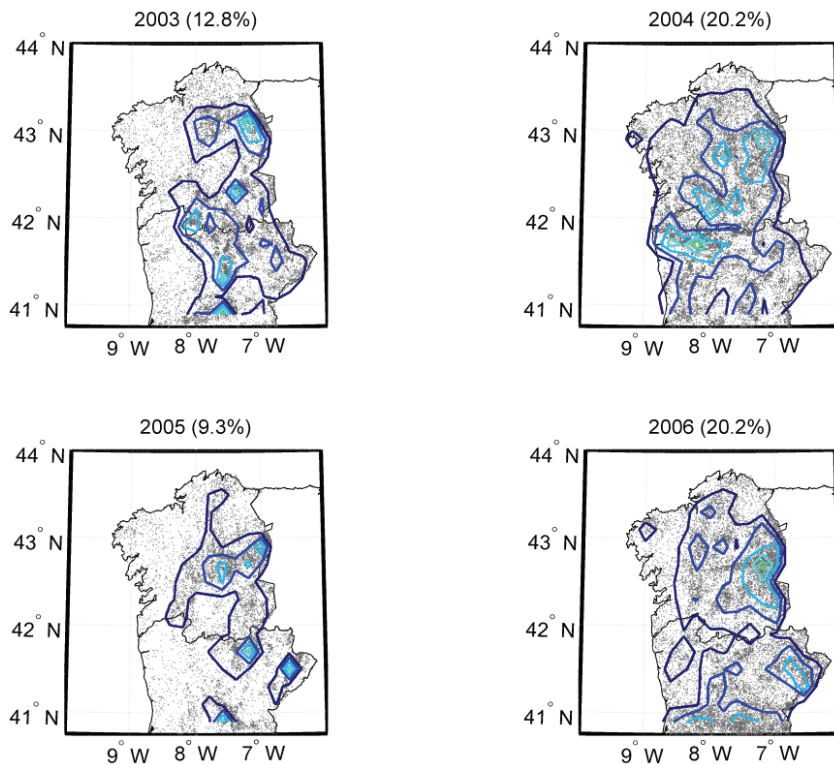
Figure 3.7. Seasonal spatial distribution of the mean accumulated precipitation (mm) for the 1961-2006 period, in winter (DJF), spring (MAM), summer (JJA) and autumn (SON) (source: Gomez-Gesteira et al., 2011).

The lightning observation dataset was characterized by a large temporal and spatial variability in the number of occurrences, and a large geographical distribution of cloud-ground (CG) discharges. The same methodology as that used by Ramos et al., 2011 (for Portugal) was used, but in this case the domain was extended towards the Galicia region. The inter-annual variability of the spatial density distribution (given by the number of flashes/km²) is shown in Fig. 3.8; the data shown is given relative to all CG discharges, incorporates data from 2003 to 2009, and was measured on a 0.2° x 0.2° grid. The existence of a high inter-annual variability in the CG discharges was immediately noticeable, with low-activity years in 2005 and 2008, while maximum counts were achieved in 2004 and 2006. Moreover (as noted earlier), there were clear spatial inhomogeneities, particularly for the maximum CG discharge occurrences, which were non-uniform throughout the years. Some years appeared to be dominated by a meridional gradient (e.g., 2008 and 2009), while others presented a more zonal configuration (e.g., 2003, 2005 and 2007). Despite this high variability in space, some regions had a higher probability of showing high-density CG discharge values; specifically, these were the mountain ranges (Geres and Manzaneda). In contrast, Atlantic coastal areas presented very low densities of CG discharges. Nevertheless, when compared with other regions in the eastern and northern sectors of the Iberian Peninsula (especially the Pyrenees and the Mediterranean coastal sector), these values could be considered as relatively low (Pineda et al., 2010; Rivas Soriano et al., 2005).

It has been shown before that the monthly Iberian Peninsula CG discharge regime varies considerably throughout the year, on both seasonal and monthly timescales (Rivas Soriano et al., 2005). The

3. Climatic characterization of the northwestern Iberian Peninsula

seasonal distribution of all individual CG discharges is shown in Fig. 3.9; the corresponding density distribution is also represented. The first obvious result was the large seasonal variability in the density of the flash distributions, with winter months presenting much smaller numbers of CG discharges when compared with spring, but particularly with summer and autumn. Interestingly, there were appreciable differences between the spatial distributions of CG discharges in different seasons. During the winter months (DJF), the highest numbers of CG discharges were found in coastal areas. The main factor responsible for this spatial pattern is the frequent travelling lows that cross the Atlantic in winter. In spring (MAM), the spatial distribution was more homogenous throughout the entire domain, with the highest density being found in inland areas.



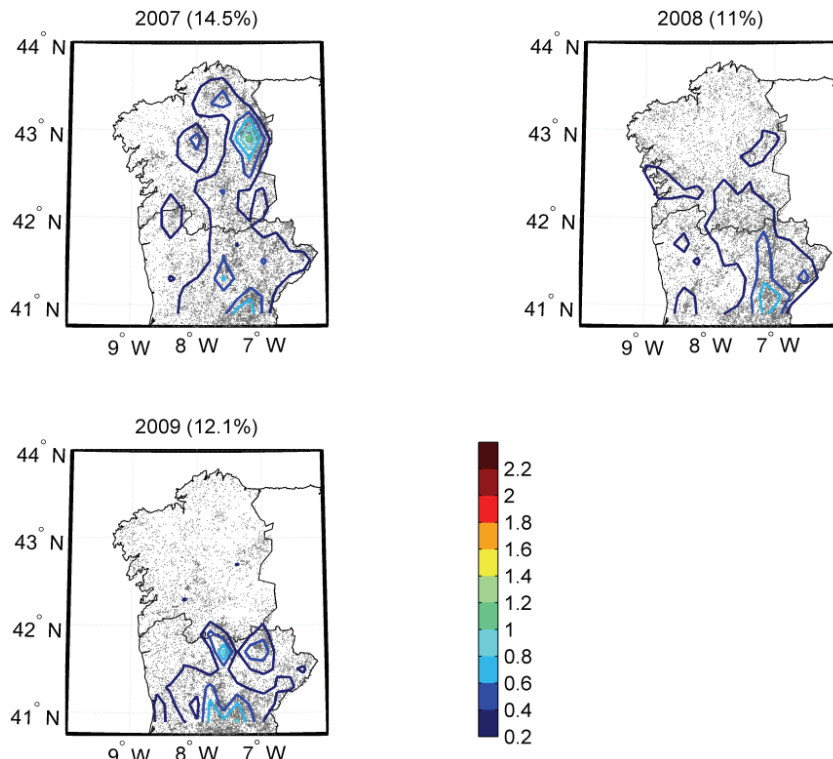


Figure 3.8. Annual spatial density distribution of CG discharges (colored contours). Values are given as number of discharges/km² per year, over a regular 0.2° x 0.2° grid. All CG discharges for each year are represented by grey dots. The percentage of CGs per year is also shown.

In summer months (JJA), the highest CG density values were found in the eastern sector of the domain, with lower values in the coastal regions. The northeastern part of North Portugal and Galicia are characterized by complex terrain with orographic systems, which are favorable for the generation of uphill currents during hot weather, thus allowing the creation of cumulonimbus clouds (Ćurić et al., 2003). Finally, during autumn (SON), the atmosphere is often characterized by colder and moister air masses advected from the Atlantic ocean, which can interact with the still reasonably warm Iberian continental mass (Martín et al., 2004; Valero et al., 2009). This situation can foster instabilities that favour thunderstorms, increasing the number of CG discharges throughout the region.

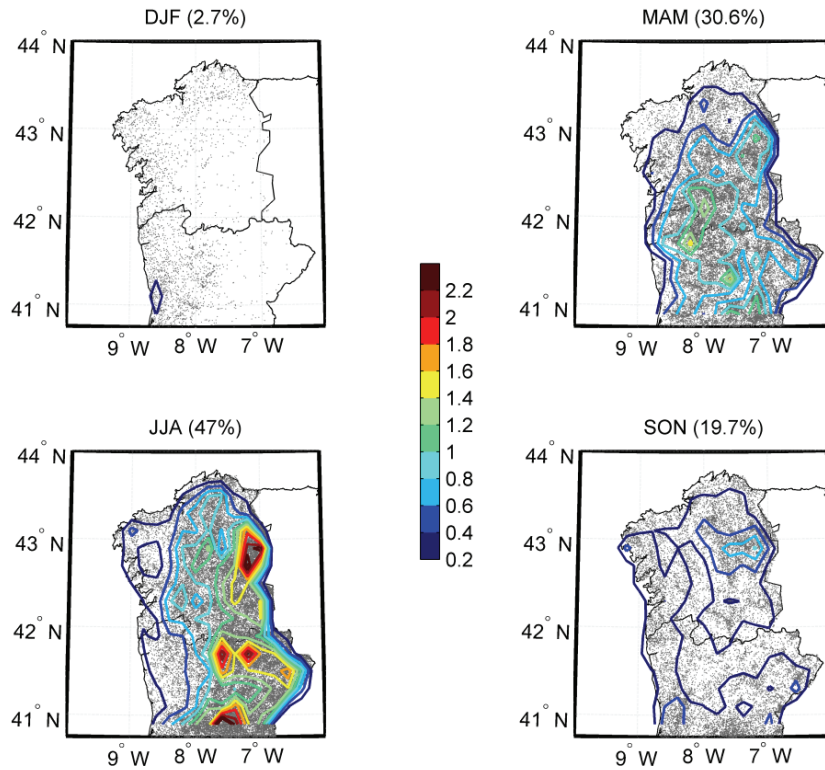


Figure 3.9. Seasonal spatial density distribution of CG discharges (colored contours). Values are given as the number of discharges/km² per season, over a regular 0.2° x 0.2° grid. All CG discharges for each season are represented by grey dots. The percentage of CGs per season is also shown.

3.2. Large-scale influence

The atmospheric circulation in the area (Fig. 3.10) is governed by two main centers of activity; an anticyclonic zone south of 40°N, centred near the Azores, and a low pressure area centered around 60°N, near Iceland. In summer, the Azores High moves northwestward. A thermal low develops over the IP from April to September, giving rise (Hoinka and de Castro, 2003) – in combination with the Azores High – to equatorward coastal winds. Regarding the geopotential height at 500 hPa, the pressure surfaces are lower at the poles and higher through the equator, indicating that in the summer months westerly winds at height prevail.

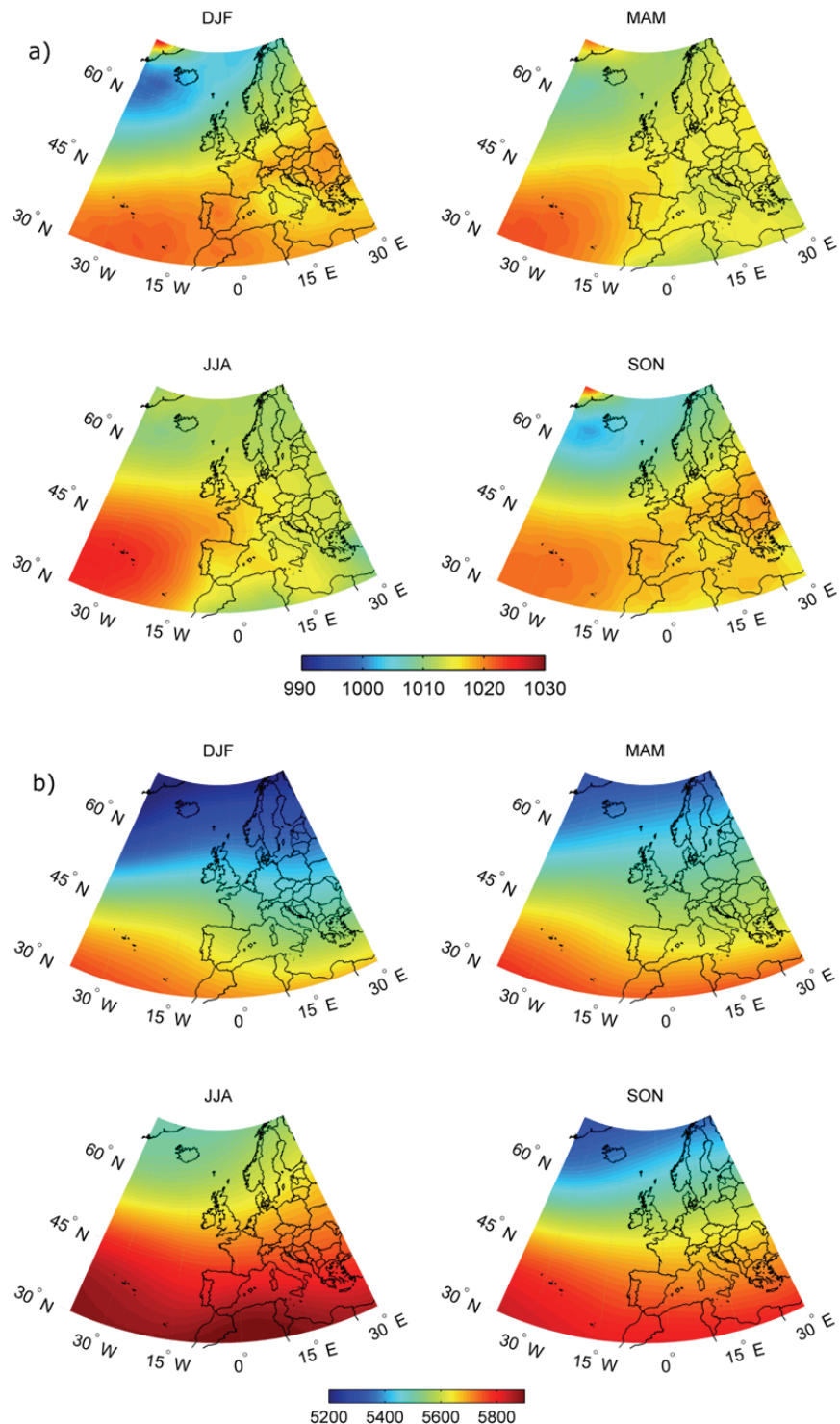


Figure 3.10. Seasonal a) mean sea level pressure (hPa) and b) geopotential height (m), during the 1961-1999 period, using the NCEP/NCAR reanalysis data.

Fronts and associated depressions tend to develop in well-defined areas. The major zones of frontal-wave development are areas that are most frequently baroclinic, a result of airstream confluence (Barry and Chorley, 2003). This is the case off eastern North America, especially in winter. At mid-latitudes, the variability of the climate is related to travelling low-pressure systems (Trigo, 2006), which are sometimes diverted from their regular path by the presence of persistent and quasi-stationary high-pressure systems (Rex, 1950; Barriopedro et al., 2010). Thus, both systems were expected to influence some of the characteristics and variability of the studied region (NW Iberia peninsula).

Extra-tropical cyclones have a strong influence on local weather, as their passage is related to strong winds, precipitation, and temperature variability. The Iberian Peninsula (Fig. 3.11) is one of the most favourable areas for the passage of minimum central pressures. The relative maximum of cyclonic activity over the Iberian Peninsula exhibits a strong annual cycle, and is mostly due to the summer activity of the Iberian thermal low (Trigo, 2006), a quasi-stationary signature that rarely brings precipitation. In winter, however, most of the cyclones travel along the northern Atlantic or, secondarily, through the Azores-Mediterranean axis.

Although the tracks delineated by the cyclone centers do not cross the region under study, it is important to note that an extra-tropical cyclone often reaches 1500 to 2000 kilometers in diameter (Longshore, 2000), and that the frontal precipitation associated with extra-tropical cyclones typically occurs south of the low pressure centre. The target region is mainly affected by low-pressure systems traveling north of the Iberia Peninsula.

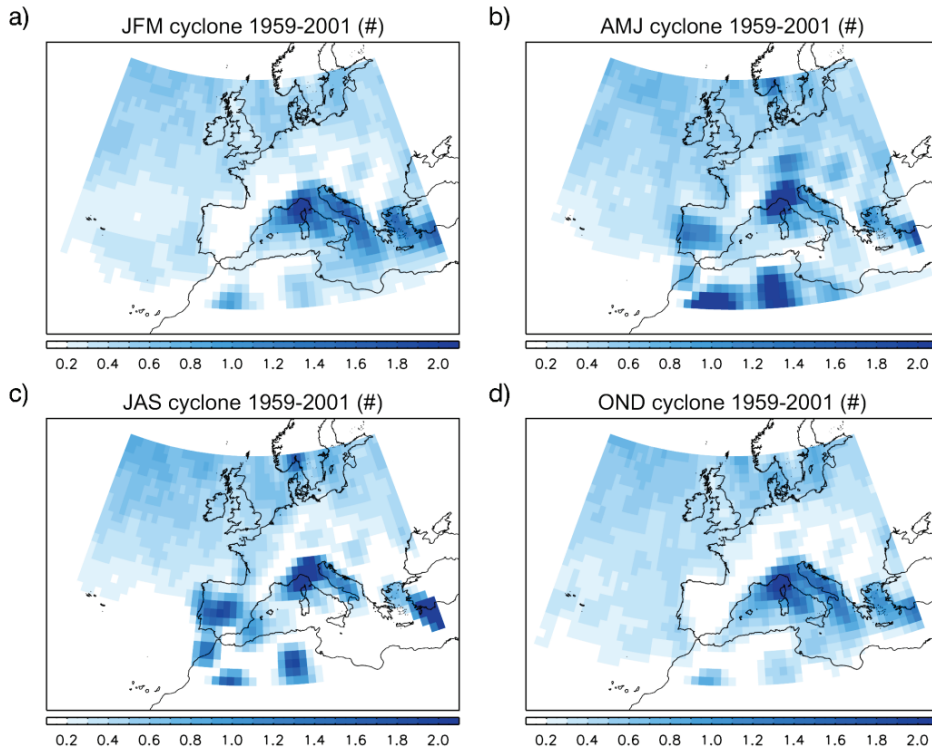


Figure 3.11. Seasonal spatial distribution of the positions where lows reach their minimum central pressure, using the 6-hourly database of the ERA-40 reanalysis and the cyclone tracking method of Trigo et al., 1999. The values correspond to the average number of events detected per $1.125^\circ \times 1.125^\circ$ grid box (source: adapted from Gomez-Gesteira et al., 2011).

On the other hand, blocking activity interrupts the normal progression of extra-tropical cyclone systems and suppresses the mid-latitude westerly winds (typically over a period of a week or two), which are replaced by meridional flows (e.g. Barriopedro et al., 2010). Therefore, persistent anomalous temperatures and a marked redistribution of precipitation over large areas of middle and high latitudes, including the NW Iberian Peninsula, are typical fingerprints of blocking patterns (Trigo et al., 2004a; García-Herrera et al., 2007). The region under study (NW Iberia Peninsula) is frequently affected by eastern Atlantic/western Europe blocking (Fig. 3.12). The region is especially affected during winter and spring, while in summer blocking

activity is rare. Several authors report a decreasing trend in Atlantic blocking activity during the second half of the 20th century; the decrease in the frequency of blocking days in the region is largely confined to winter and early spring (e.g. Barriopedro et al., 2006; Croci-Maspoli et al., 2007).

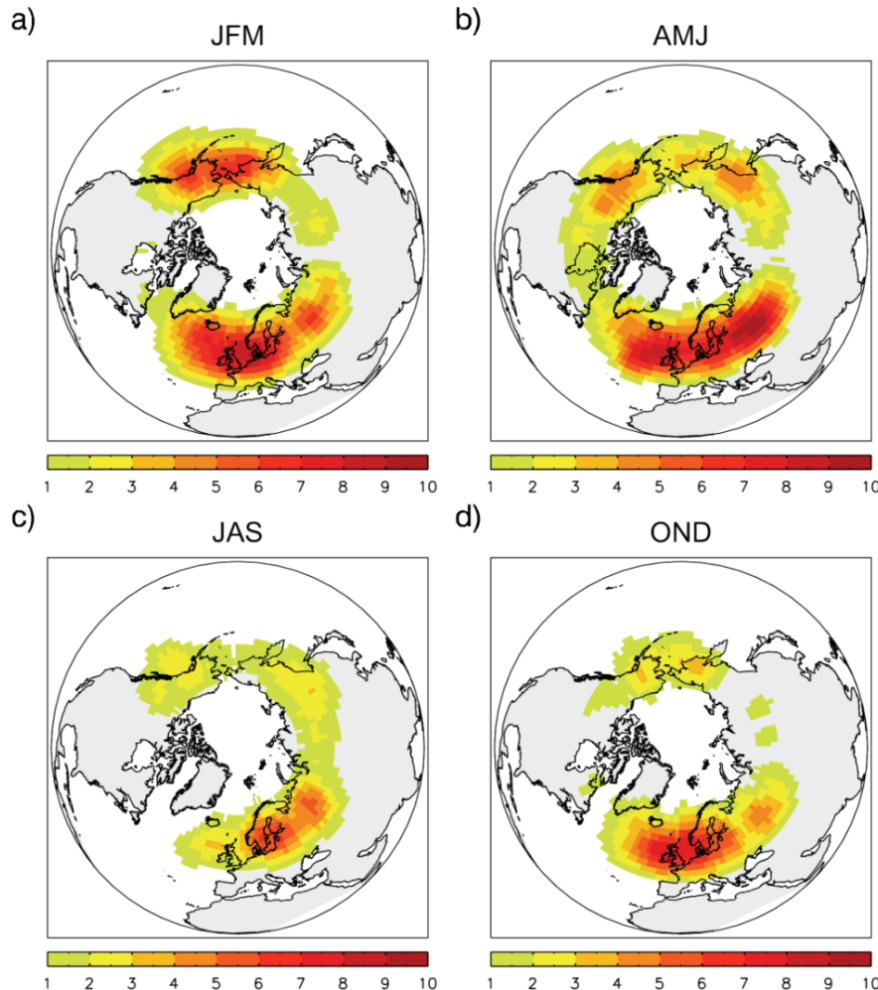


Figure 3.12. Total seasonal frequency of blocking centre positions for the 55-yr period 1948-2002; (a) spring, (b) summer, (c) autumn and (d) winter. Blocking centre positions were calculated using the NCEP/NCAR reanalysis dataset (source: adapted from Barriopedro et al., 2006).

Cut off low systems (COLSs) are common in the NW Iberian Peninsula (Nieto et al., 2005; Nieto et al., 2007a; Fig. 3.13). COLSs consist of a closed upper-level low that has become completely displaced (cut off) from the basic westerly current, and moves independently of that current. Their intensity is highest in the upper troposphere and the magnitude of the associated cyclonic circulation decreases towards the surface; it is even possible to find anticyclonic circulation at the surface. COLS systems in the vicinity of the NW Iberian Peninsula are usually associated with unstable conditions, and even with severe convective episodes (Nieto et al., 2007b; Ramos et al., 2011). In addition, Nieto et al., 2007a, found that more than half of the cut-off low systems found in the European sector are associated with blocking events, particularly in spring and winter, when these quasi stationary anticyclonic patterns are more frequent.

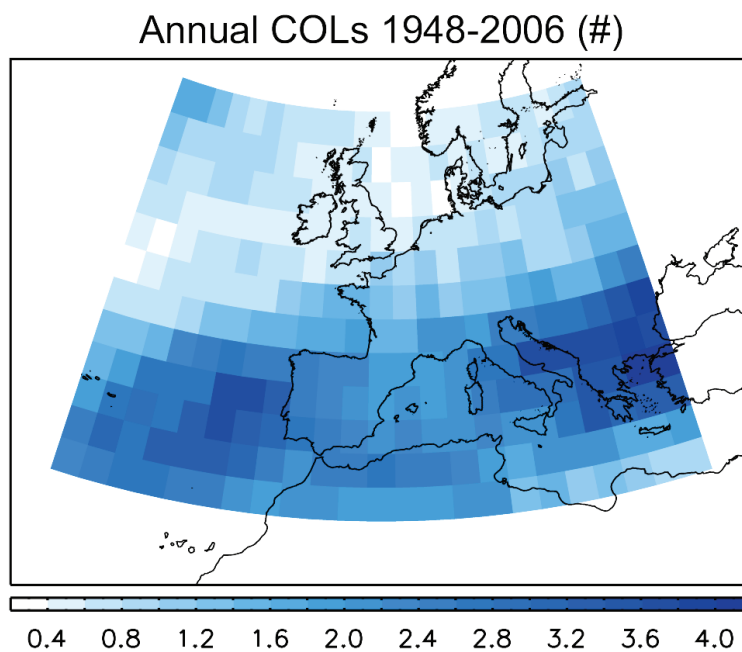


Figure 3.13. Spatial annual distribution of the cut off low systems, created using NCEP/NCAR reanalysis. The values correspond to the average number of events detected per $2.5^\circ \times 2.5^\circ$ grid box (source: adapted from Nieto et al., 2008).

As mentioned in chapter 1, modes of low frequency variability are also an important factor when studying the climate variability of the NW Iberian Peninsula. Previous studies (e.g. Rodríguez-Puebla et al., 1998; Lorenzo and Taboada, 2005; deCastro et al., 2006; Trigo et al., 2008; Ramos et al., 2010) have considered that the most representative regional patterns of atmospheric variation in the Northern Atlantic-European sector influencing the Iberia Peninsula are NAO, EA, SCAN and EA/WR. While these modes are defined throughout the year, their strength varies considerably, being more prominent in winter and less well-defined in the summer months (e.g. Barnston and Livezey 1987; Corte-Real et al., 1995; Trigo and Palutikov, 2001). The impact of these major atmospheric circulation modes upon the precipitation in Europe is also greater during the winter months (Dunkeloh and Jacobbeit, 2003; Trigo and Palutikov, 2001). Fig. 3.14 shows the relationship between monthly precipitation and the NAO index for Europe. The highest anti-correlation is observed between the NAO index and precipitation in the NW Iberian Peninsula for march.

Although the NAO is, to date, the most commonly studied mode in the Iberian Peninsula (e.g. Rodríguez-Puebla et al., 1998; Trigo et al., 2004b), several studies have demonstrated that additional modes must be considered if the variable structures of winter precipitation in the NW Iberian Peninsula—and even the variable structures of river flows—are to be explained (e.g. Lorenzo and Taboada, 2005; deCastro et al., 2006; Trigo et al., 2008). In 2010, Rodríguez-Puebla et al. studied the relationship between extreme temperature events in the Iberian Peninsula and modes of low frequency variability. In addition, several studies have indicated the influence of the main atmospheric circulation modes on circulation weather type (CWT) frequency and the occurrence

of drought in Spain (Rodó et al., 1997; Rodríguez-Puebla et al., 1998; Pozo-Vázquez et al., 2005; Ramos et al., 2010).

The climate variability in the Iberian Peninsula is therefore not straightforward; it is a complex challenge, with different synoptic systems and modes of low frequency variability playing different roles, which will be studied in this work.

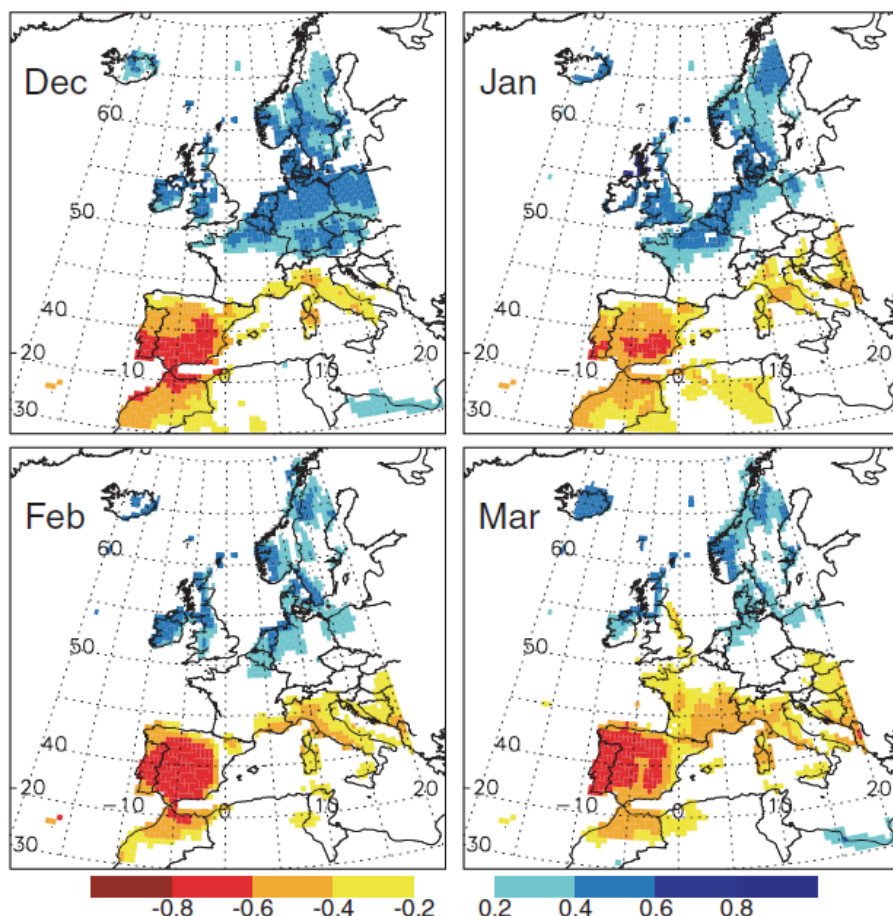


Figure 3.14. Values showing correlation between monthly European precipitation (CRU data set) and the corresponding monthly NAO index, for the 1960-2000 period (source: adapted from Trigo et al., 2008).

4. Objectives

Two central aims motivated this work; these were to gather examples of the application of circulation weather types, and study them in detail, and to perform a purely methodological essay that presented a new circulation weather type classification system based on Lagrangian air trajectories. The work was developed for the NW Iberian Peninsula, but all of the procedures and methodologies could easily be applied for other regions of the world.

The objectives of this work were divided into three parts. The first set of objectives were concerned with the study of the relationship between surface climate variables and circulation weather types. The second set were to do with the analysis of the relationship between circulation weather types and climate variability, and the third set aimed to introduce a circulation weather type classification scheme based on Lagrangian air trajectories. A short description of each objective is given below.

- In the first part (Chapter 6), two examples of the application of circulation weather types are made by relating them to climate variables. In this part the objectives were:

- 1) To study the seasonal circulation weather type-dependent relationship between temperature and precipitation for the

4. Objectives

NW Iberian Peninsula. This study should allow each circulation weather type to be differentiated in terms of meteorological variables, increasing knowledge of the effects of atmospheric circulation in the region.

- 2) To attempt an uncommon application for the circulation weather types for the NW Iberian Peninsula. The main idea here was to assess if circulation weather types can explain the variability of lightning activity, or if additional meteorological variables are needed. This extra knowledge should help to predict lightning activity over the region, minimizing the associated impact.

• In part two (Chapter 7 and Chapter 8) the objectives were twofold:

- 3) To study the compatibility of the circulation weather types in the NW Iberian Peninsula and the modes of low frequency variability in the North Atlantic-European sector. The modes of low frequency variability were computed using an Empirical Orthogonal Function (EOF) analysis of the daily SLP and H500 fields. An objective comparison was made taking into account the principal component loading patterns and the daily local circulation weather types, to show if any circulation weather type presented any preferable modes of low frequency variability. This would increase knowledge of this field, if changes in the positions and intensities of the low frequency variability modes had an impact on the local circulation weather types in the region.

4) To study future climate scenarios for the NW Iberian Peninsula, by studying circulation weather types. To achieve this, the ability of the control simulations of the different coupled general circulation models (CGCMs) to reproduce the present climate was evaluated in a primary analysis. Secondly, the frequency of circulation weather types in the future climate was computed for different CGCMs, and for forcing simulations corresponding to three SRES emission scenarios, representing low, medium and high greenhouse gas concentration scenarios. This objective could help to prove that the use of circulation weather types can be a useful tool in validating the control simulations of CGCMs; it could also help in assessing the accuracy of CGCMs, and in studying changes in atmospheric circulation under future climate change scenarios.

- In part III (Chapter 9) a new circulation weather type classification scheme based on Lagrangian air trajectories is presented:
- 5) A new classification method using a 3-D framework was proposed, where the objective was to analyze the backward trajectories of the particles arriving in the northwestern Iberian Peninsula. This purpose was achieved by using the successful 3-D Lagrangian particle dispersion model FLEXPART. The data from the model consist of 1,398,800 particle positions and their meteorological state properties, recorded every six hours over a five-year period (2000-2004). We therefore had a daily catalogue containing information about the air masses before they arrived at the target area

4. Objectives

(trajectory types). This classification is intended to be more robust than the classical circulation weather type methods, since it takes into account not only the flow patterns arriving at a certain area, but also allows the local effects of a certain meteorological system to be shown, and allows a better understanding of the physics behind that system.

5. Data

5.1. Large-scale meteorological fields

Some of the objectives of this investigation required that the selected data had global or regional cover, with sufficient spatial and temporal resolution. All large-scale meteorological fields used in this work were obtained from the National Center for Environmental Prediction (NCEP) database. Consequently, two reanalysis datasets were used. The first set used contained the daily mean fields retrieved from the NCEP/NCAR reanalysis data (Kalnay et al., 1996), with a 2.5° grid data resolution. The variables retrieved are summarized in Table 5.1.

Table 5.1. Variables for the NCEP/NCAR reanalysis data used in this work.

Variable	acronym	unit	levels
Sea level pressure	SLP	hPa	surface
Geopotential height	H	hPa	1000; 500
Relative humidity	RH	%	925; 850; 700

To satisfy the requirement that data of a higher spatial resolution should be used, additional meteorological fields (Table 5.2) from the NCEP Final Analyses of the Global Tropospheric Analyses (NCEP FNL data; FNLDODC/NOAA/NWS/NCEP, 2000) at 1° grid resolution were

5. Data

retrieved. The original data is available from the RDA (<http://dss.ucar.edu>) in dataset number ds083.2.

Table 5.2. Variables for the NCEP Final Analyses of the Global Tropospheric Analyses reanalysis data used in this work.

Variable	acronym	unit
Convective Available Potential Energy	CAPE	J/kg
Lifted Index	LI	K

The Convective Available Potential Energy (CAPE) and the Lifted Index (LI) are instability indices (Wallace and Hobbs, 2006) that give information about the stability of the troposphere and about whether convection can be enhanced or inhibit.

Monthly mean precipitation data (from a 2.5° latitude \times 2.5° longitude grid) taken from the Global Precipitation Climatology Project (GPCP) of the Global Energy and Water Cycle Experiment (<http://cics.umd.edu/~yin/GPCP/main.html>) between December 1979 and December of 2004 was also retrieved.

5.2. Hemispheric modes of low-frequency variability

The standard NAO, EA, EA/WR and SCA low frequency variability mode indices were obtained from the Climate Prediction Center (CPC) of the National Oceanic and Atmospheric Administration (NOAA), for the years 1950-2008. These low frequency variability mode indices were computed for the entire Northern Hemisphere, using Rotated Principal Component analysis (RPCA) (Barnston and Livezey, 1987). This procedure isolates the primary teleconnection patterns for all months and allows time series of the patterns to be constructed. The RPCA technique was applied to monthly mean standardized 500 hPa height anomalies for the entire Northern Hemisphere (20°N - 90°N),

between January 1950 and December 2008. The anomalies were standardized by the 1950-2008 base period monthly means and standard deviations.

For each of the twelve calendar months, the ten leading unrotated EOFs were first determined from the standardized monthly height anomaly fields in the three-month period centred on that month; that is, the July patterns were calculated based on the June through August monthly standardized anomaly fields. A Varimax rotation was then applied to these ten leading un-rotated modes, yielding the ten leading rotated modes and their time series for that calendar month.

The standard annual NAO, EA, EA/WR, and SCA low frequency variability modes (also referred to as teleconnection patterns) are shown in Fig. 1.3. It is important to note that hereafter, the hemispheric low-frequency variability modes (NAO, EA, EA/WR and SCA) will be referred to as hemispheric modes.

5.3. Coupled general circulation model simulations

The use of coupled general circulation model simulations (CGCMs) allows the study of future climate scenarios. Data from three models studied in the IPCC, 2007 were retrieved. The choice of models was determined mainly by the availability of daily data. In addition, the use of other CGCM simulations made the quantification of uncertainties more reliable.

The three models used were:

- 1) The IPSL climate system model IPSL-CM4 from Institut Pierre Simon Laplace des Sciences de l'Environnement Global (IPSL), France, with a spatial resolution of 2.5° by 3.75°;

5. Data

- 2) The 5th generation of the ECHAM general circulation model (ECHAM5/MPI-OM) from the Max Planck Institute for Meteorology, Hamburg, Germany, with a spatial resolution of $\sim 1.9^\circ$ by 1.9° ;
- 3) The CCSM3, NCAR Community Climate System Model 3.0 from the USA, with a spatial resolution of 1.4° by 1.4° .

Additional information about the salient features of these CGCMs is shown in Table 8.1 of IPCC, 2007.

Data for the daily mean sea level pressure of the three climate models, and from four different forcing simulations, were obtained from the WCRP CMIP3 multi-model database (<https://esg.llnl.gov>). These simulations corresponded to a control simulation and three emission scenarios from the special report on emission scenarios (SRES) for low (B1), medium (A1B) and high (A2) concentrations of greenhouse gases (Nakicenovic and Intergovernmental Panel on Climate Change, Working group III, 2000).

The climatological control simulation period used in the 20th century was defined as the 1961-1999 period. For the 21st century, the coincidental temporal resolution availability of daily data for the 3 models allowed us to analyse two periods, the first between 2046 and 2065, and the second between 2081 and 2100.

5.4. Lightning data

The Portuguese Lightning Location System (LLS) has been in service since June of 2002, and is operated by the national weather service, the Instituto de Meteorologia (IM). It is composed of 4 IMPACT 141T-ESP detectors, which are installed throughout Portugal, in Braga,

Castelo Branco, Alverca and Olhão (Fig. 5.1). Since 2005, the IM has received data from the Agencia Estatal de Meteorología (AEMET), from the five sensors located nearest to the border (Jerez de la Frontera, Armilla, Getafe, Matacán and Santiago – Fig. 5.1), thus improving the accuracy of the network.

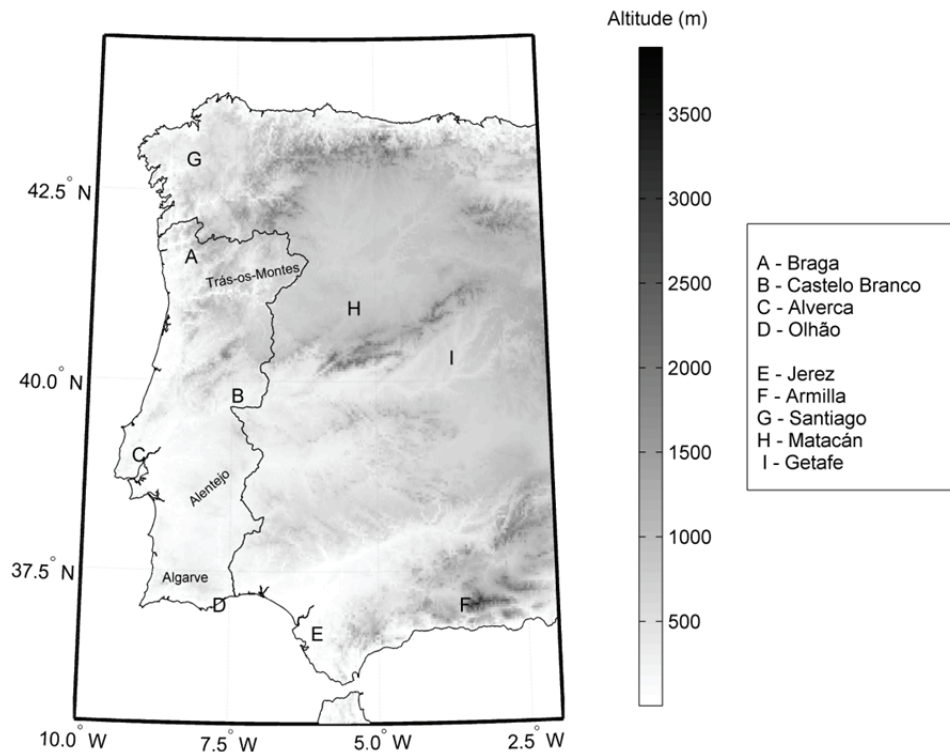


Figure 5.1. The locations of the nine (four in Portugal and five in Spain) Lightning Location System detectors are indicated with capital letters. The Portuguese regions referred to in the text are also identified in the figure.

According to Rodrigues et al. (2008), the software manufacturer indicates an error in spatial location over the continental area of Portugal, which varies between 500 m and 1 km for the semi-major axis of a 50% probability ellipse. The manufacturer also assures—for the same area—an efficiency higher than 90% for strokes with peak current greater than 5 kA. These values were found using the detection

5. Data

efficiency of each sensor (based on the threshold value and gain sensor), which was supposed to be the same for all sensors. In addition, detection efficiency varies over the continental area of Portugal. Consequently, and following the work of (Soriano et al., 2005), we also did not attempt to correct the data for detection efficiency, but evaluated the lightning data using the measured values. The annual and spatial variations may therefore have been slightly biased by changes in the lightning detection network, and its characteristics.

The network uses a combination of time-of-arrival (TOA) and magnetic-direction-finding (MDF) to locate lightning. The system also estimates several other properties, including the current peak, the multiplicity (number of strokes in a flash), and the type of discharge (cloud-ground, cloud-cloud). According to Jerauld et al. (Jerauld et al., 2005), current peaks are underestimated by lightning locating systems.

This work focused on cloud-ground (CG) discharges that strike the Portugal mainland, i.e., all other discharges were disregarded. Information about the semi-major axis (a measure of the location error) was also available in the dataset. An initial quality control process was performed to ensure that CG discharges with an error larger (semi major axis) than 25 km were excluded from the analysis (which corresponded to 4% of all data). At the synoptic scale employed in this work, the 25 km threshold was considered sufficient. If we had been analysing a finer scale (e.g., CG discharges striking transmission electric systems), a smaller threshold would have been appropriate.

5.5. Weather observation station data

Data from different daily weather observation stations were used in this work. The station data sources used were the Agencia Estatal de Meteorología (AEMET), and Meteogalicia. Table 5.3 summarizes the different variables and periods for each weather station. Fig. 5.2 shows the location of each weather station.

Table 5.3. Characteristics of the weather stations used in this work. Additionally, the type of climate variable used, the climate variables (temperature (Temp) or/and precipitation (Prec)), the period and the respective source are shown.

ID	Station	Temp	Prec	Period	Source
1	As Pontes	X		1961-2006	AEMET
2	Santiago	X		1961-2006	AEMET
3	Sarria	X		1961-2006	AEMET
4	Lourizán	X	X	1950-2005	Meteogalicia
5	Vigo	X		1961-2006	AEMET

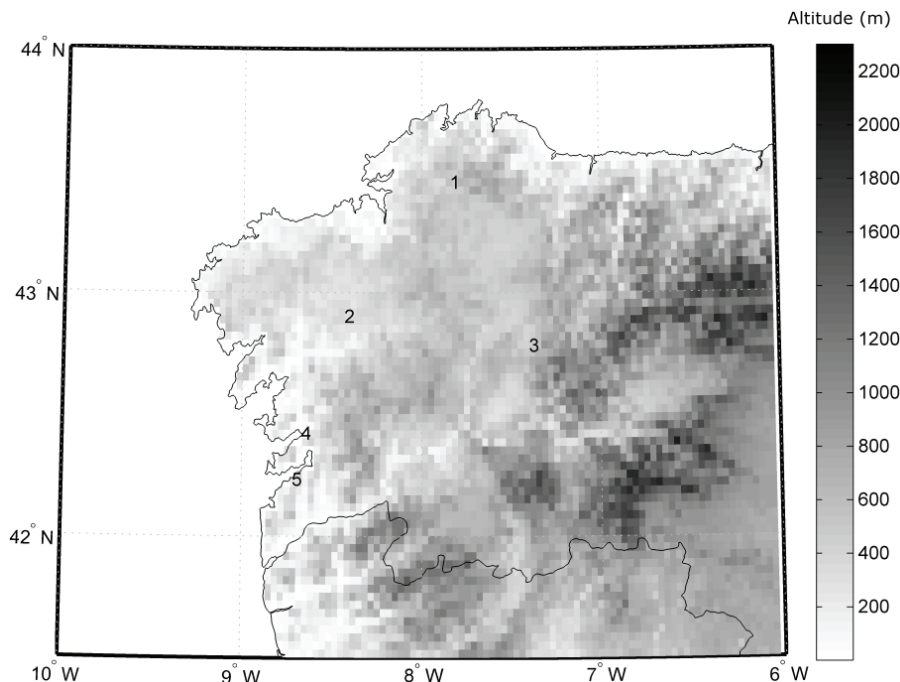


Figure 5.2. Location of each weather station. The ID numbers correspond to the ones in Table 5.3.

5. Data

Climatic time series typically exhibit spurious (non-climatic) jumps and/or gradual shifts due to changes in station location, instrumentation, environment or observing practices (Aguilar et al., 2003). In daily resolution climatic time series, there are often also some observation days missing, making data quality control an important consideration.

The weather station data presented here were checked in advance, using quality control procedures. These procedures aimed to identify errors in data processing, including errors in manual input data such as the daily maximum temperature being lower than the daily minimum temperature, non-existent dates and erroneous outliers. Although the data series underwent routine quality control procedures at the respective weather services (AEMET, Meteogalicia), another step using the procedure in RClimate gave greater assurance of the quality of the data, where the main purpose was to identify errors in data (<http://ccma.seos.uvic.ca/ETCCDMI/>). Outliers in the daily maximum, minimum and mean temperatures were identified if they fell outside a given pre-defined range. In this case, the range was defined as lying within three standard deviations (std) of the climatological mean of the value for the day, i.e., $\text{mean} \pm 3 \text{ std}$. Daily maximum and minimum temperature values outside this range were checked manually, and edited on a case-by-case basis when needed.

5.6. Trajectory Datasets

Backward trajectories were generated using the Lagrangian dispersion model FLEXPART (Stohl et al., 2005). This model has been applied in a variety of fields of study, including, among many others, atmospheric transport (James et al., 2008; Stohl and Sodemann, 2010),

convection and pollution (Palau et al., 2009), biomass burning studies (Cammas et al., 2009) and source-receptor relationships (Paris et al., 2010). In this study, 6-hourly ECMWF meteorological analysis data was used as input data for the FLEXPART model, for the period from 1/11/1999 to 30/11/2004. The positions of each particle (latitude, longitude and height) as well as their physical and thermal properties (specific humidity, density and temperature) were recorded at each time-step.

The atmosphere was divided into a set of homogeneous air parcels (also referred to as particles). This simulation used a total of 1,398,800 particles homogeneously distributed over the entire globe. Three-dimensional winds from ECMWF were used to advect the particles, and a set of parameterisations described the subgrid-scale physical processes. For details on the parameterisation schemes see the FLEXPART technical note (Stohl et al., 2005). At each time-step, the particles within the target region (NW IP) - i.e., a subset of the 1,398,800 particles - were selected for more detailed study of their backward trajectories.

The analysis period (1/12/1999 to 30/11/2004) can be considered as a relatively neutral period with regard to climate variability, given that no extremely active El Niño Southern Oscillation (ENSO) episode occurred within the period, according to the multivariate ENSO Index as defined by Wolter and Timlin, (1998). Simultaneously, the signal from the North Atlantic Oscillation (NAO), which is of eminent importance for the climate variability of IP, was weak, as derived from the NAO index of the Climate Diagnostics Centre (Hurrel, 1995).

5.7. Case studies

Because of its location, the NW Iberian Peninsula is affected by different synoptic features (Gomez-Gesteira et al., 2011). Several case studies (chapter 9.3) were analysed to validate the trajectory method with different synoptic conceptual models, and to compare it with the Lamb circulation weather types (CWT) for a given case. The events retained here are known to affect the region, and were obtained from different datasets. Table 5.4 summarizes the different case studies.

Table 5.4. *Different case studies analyzed to validate the trajectory method.*

Case Study	Period	Dataset
Cold front	12/11/2002	Trigo, 2006
Cut off low	10/10/2001 - 12/10/2001	Nieto et al., 2005
High precipitation	17/10/2001 - 21/10/2001	Lourizán weather station
Coldwave	15/12/2001 - 22/12/2001	Lourizán weather station
Heatwave	01/08/2003 - 15/08/2003	Trigo et al., 2009
Blocking event	14/1/2000 - 29/1/2000	Barriopedro et al., 2006

Since the NW Iberian Peninsula is characterized by the passage of cold fronts associated with the storm track in the North Atlantic Ocean and the passage of cyclones that strike directly the region (Trigo, 2006), a cold front system was studied. The cold front studied corresponded with the day on which the 'Prestige' vessel began to have problems (12/11/2002); it sank later in the same week (Lechuga, 2006). This case was retrieved from the cyclone database of Trigo, (2006).

Cut off low systems (COLSs) are very common in the Mediterranean region of the Iberian Peninsula, but are not as common in the NW Iberian Peninsula (Nieto et al., 2005). In any case, COLSs are an important synoptic feature to be analysed, since most of the time they bring instability to the region, and they do not have any signature in the

SLP field. The 10/10/2001 to 12/10/2001 COLSs were selected from the database of Nieto et al., (2005).

Given that the NW Iberian Peninsula is the region with the highest annual precipitation in the IP (Herrera et al., 2010; SIAM, 2002), the case study also focused on the highest precipitation period, averaged over 5 days for the region (17/10/2001 to 21/10/2001).

A coldwave case was also analysed. The 15/12/2001-22/12/2001 period was chosen because it corresponded to the highest minimum temperature anomalies found at the Lourizán weather station. According to the NOAA Climate Watch in December 2001, in this period "heavy snowfalls have caused traffic chaos in Italy, southern France and Spain (mainly Catalonia, in northern and north-east Spain). In addition, the AEMET recorded the lowest temperature (-10.5°C) for Barajas Madrid Airport on 16/12/2001.

The heatwave event of 2003 (01/08/2003 to 15/08/2003) that struck not only central Europe (García-Herrera et al., 2010), but also the NW Iberian Peninsula (Trigo et al., 2009; deCastro et al., 2011), was also selected as a case study.

Blocking events are characterised by a large-scale high pressure system with an anticyclonic circulation dominating the troposphere (Rex, 1950). In the target region, the blocking events located over the North Atlantic Ocean are known to have more influence on the local weather (Barriopedro et al., 2006). Taking this into account, an event was selected from the 14/1/2000 to 29/1/2000 blocking database of Barriopedro et al., (2010). The selected event was the most persistent blocking that occurred in the 12/1999 to 11/2004 period in the North Atlantic Ocean.

6. Relationship between surface climate variables and circulation weather types

6.1. Introduction

The study of surface climate variables (especially precipitation and temperature) and their variability is one of the most important fields of study in climate sciences, due to its social and economic impact (e.g., Collier and Krysztofowicz, 2000; Garcia-Herrera et al., 2010 and references therein).

The inter-annual variability of precipitation and temperature in the NW Iberian Peninsula was studied in detail by Gomez-Gesteira et al., (2011). It was shown that both the maximum and minimum land temperature have increased annually since 1974, at a mean rate on the order of $0.5^{\circ}\text{C dec}^{-1}$. This behavior is especially marked for the maximum temperature in spring and summer, and for the minimum temperature in spring, summer and autumn. For precipitation, the results showed decreases in winter, and increases in autumn since 1974. No clear annual trend was observed during the other seasons.

The aim of this chapter is to study the relationships between atmospheric circulation weather types (CWT) and precipitation, temperature and lightning discharges in the NW Iberian Peninsula, and the seasonal variability of these relationships. An automated version of the Lamb circulation weather type classification scheme was used for this purpose.

Studies quantifying the links between weather circulation types (defined using different methodologies) and the observed surface climatic variables can be found not only for the Iberian Peninsula (e.g. Corte-Real et al., 1998; Trigo and DaCamara, 2000; Santos et al., 2005; Paredes et al., 2006; Lorenzo et al., 2008; Casado et al., 2010; Bermejo and Ancell, 2009; Ramos et al., 2011), but also for other regions of Europe (e.g. Sepp and Jaagus, 2002; Tveito, 2010; Cahynová and Huth, 2009; Hanssen-Bauer and Førland, 2000; Chen, 2000). Several other studies have considered other regions of the world (e.g. Cassano et al., 2011; Frias et al., 2009; Cavazos, 1997; Sheridan, 2002).

The remainder of this chapter is organized as follows: In section 6.2, a comprehensive description of the methodology is given. In section 6.3, a description of the different CWTs is given. Sections 6.4, 6.5 and 6.6 show the relationship between CWTs and precipitation, temperature and lightning discharges, respectively. Finally, section 6.7 presents the conclusions.

6.2. Methodology

In this work, adaptations of the Lamb CWT were used for the NW Iberian Peninsula (Lorenzo et al., 2008). As mentioned in section 2.1.3., the CWTs were computed taking into account physical or geometrical considerations such as the direction and strength of airflow and the degree of cyclonicity. The indices used in this case—namely, southerly flow (SF), westerly flow (WF), total flow (F), southerly shear vorticity (ZS), westerly shear vorticity (ZW) and total shear vorticity (Z)—were computed using SLP values obtained for the 16 grid points (p_1-p_{16}), shown in Fig. 6.1. These points were moved 5° to the north compared with the study of Trigo and DaCamara, 2000, to centre the study area in the grid. Reanalysis data for the SLP field were obtained from the National Center for Atmospheric Research. The daily CWTs for the 1948–2008 period were considered. The following expressions were used to calculate the indices:

$$\begin{aligned} \mathbf{SF} &= 1.305[0.25(p_5 + 2p_9 + p_{13}) - 0.25(p_4 + 2p_8 + p_{12})]; \\ \mathbf{WF} &= [0.5(p_{12} + p_{13}) - 0.5(p_4 + p_5)]; \\ \mathbf{ZS} &= 0.85[0.25(p_6 + 2p_{10} + p_{14}) - 0.25(p_5 + 2p_9 + p_{13}) - \\ &\quad - 0.25(p_4 + 2p_8 + p_{12}) + 0.25(p_3 + 2p_7 + p_{11})]; \\ \mathbf{ZW} &= 1.12[0.5(p_{15} + p_{16}) - 0.5(p_8 + p_9)] - 0.91[0.5(p_8 + p_9) - 0.5(p_1 + p_2)]; \\ \mathbf{F} &= (\mathbf{SF}^2 + \mathbf{WF}^2)^{1/2}; \\ \mathbf{Z} &= \mathbf{ZS} + \mathbf{ZW}; \end{aligned}$$

The conditions established to define the different CWTs were the same as in Trigo and DaCamara, (2000), and the following set rules were used:

- (1) The direction of flow was given by $\tan^{-1}(WF/SF)$, with 180° being added if WF was positive. The appropriate direction was computed using an eight-point compass, allowing 45° per sector.

6. Relationship between surface climate variables and circulation weather types

(2) If $|Z| < F$, the flow is essentially straight and was considered to be of a pure directional type (eight different cases, according to the directions of the compass).

(3) If $|Z| > 2F$, the pattern was considered to be of a pure cyclonic type if $Z > 0$, or of a pure anticyclonic type if $Z < 0$.

(4) If $F < |Z| < 2F$, the flow was considered to be of a hybrid type and was therefore characterized by both the direction and the circulation (8×2 different types)

These rules allowed 26 different weather types; 10 pure types (NE, E, SE, S, SW, W, NW, N, C, and A), and 16 hybrid types (8 for each C or A hybrid).

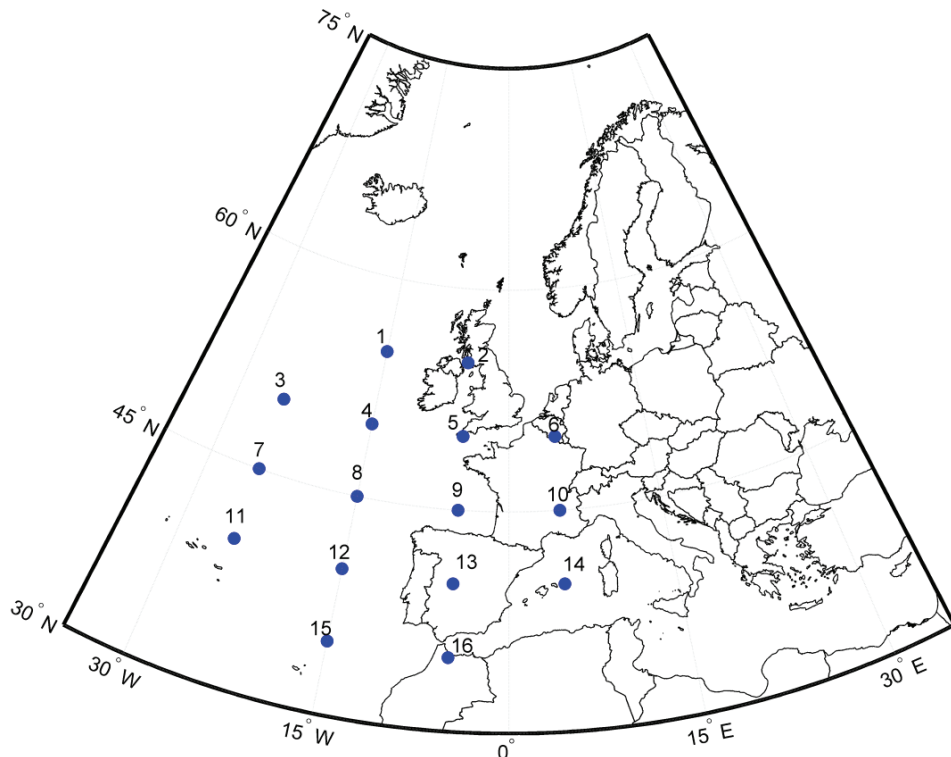


Figure 6.1. Pressure grid points used to compute the Lamb weather types for the NW Iberian Peninsula.

To achieve a practical, statically reliable analysis, the 26 CWTs were regrouped into ten basic types. This was done using the same approach as that used by Jones et al., (1993) and Trigo and DaCamara, (2000). Each of the 16 hybrid types was categorized in the relevant purely directional or cyclonic/anticyclonic-type group, with a weight of 0.5 (e.g., a day with AN types was included as 0.5 in A type and 0.5 in N type). Therefore only ten CWTs were retained (NE, E, SE, S, SW, W, NW, N, C and A).

The surface climate variables that were related with the CWTs were precipitation and temperature. For precipitation, data from Lourizán were used, and for temperature, data from As Pontes, Santiago, Sarria and Vigo were used (Table 5.3 and section 5.5.). Large-scale monthly mean precipitation data (for the period between December 1979 and December of 2004) from the Global Precipitation Climatology Project (GPCP) was also used (see section 5.1.).

6.3. Circulation weather types for the NW Iberian Peninsula

The computation of CWTs for the NW Iberian Peninsula over the 1948-2008 period allowed us to create a comprehensive daily catalogue; this catalogue will be used not only in this chapter, but also in the chapters following. To obtain a better knowledge of the catalogue, the annual composite of each CWT was computed. The relative seasonal frequency of each CWT was also determined.

Fig. 6.2 shows the annual composites for the period January 1948–December 2008, for the 10 pure CWTs (NE, E, SE, S, SW, W, NW, N, C and A). The main features of each CWT are:

- **NE** (northeasterly) represents days characterized by an extended high pressure settled over the west of Ireland and low pressure in the Mediterranean Sea;
- **E** (easterly) represents synoptic situations characterized by high pressure over the British Isles and low pressure dominating in North Africa;
- **SE** (southeasterly) types are characterized by low pressure extending towards Madeira and high pressure over Northern Europe;
- **S** (south) represents situations characterized by high pressure over the British Isles and low pressure established in the North Atlantic (Azores region);
- **SW** (southwesterly) represents days characterized by a low-pressure system to the west of Ireland with a large anticyclone over the Mediterranean region;
- **W** (west) represents synoptic situations characterized by a low-pressure system over the North Atlantic, with a high-pressure system over the Azores;
- **NW** (northwesterly) represents days characterized by a low-pressure system over the British Islands and an anticyclone system located over Azores;
- **N** (north) represents days characterized by the presence of the Azores high pressure near the Azores Islands and a low pressure over southern Europe and the Mediterranean basin;
- **C** (cyclonic) represents synoptic situations characterized by a low-pressure centre over the NW Iberian Peninsula;
- **A** (anticyclonic) represents days characterized by an extended high-pressure centre between the Iberian Peninsula and the Azores Islands.

6. Relationship between surface climate variables and circulation weather types

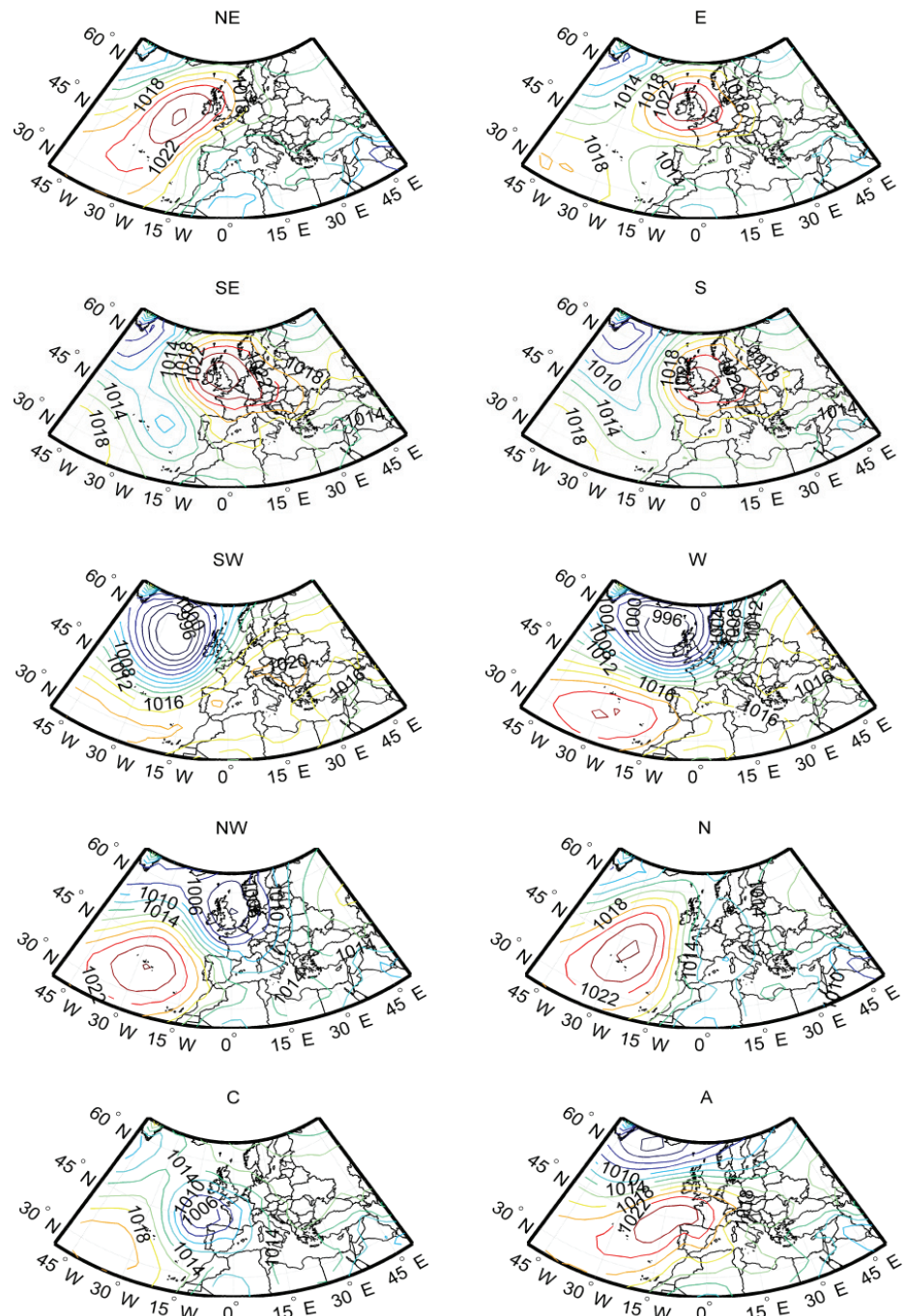


Figure 6.2. Annual average composite SLP field of the 10 pure circulation weather types, for the period 1948-2008.

The relative seasonal frequency of each CWT is shown in Fig. 6.3, for the period 1948-2008. The A types dominated in all seasons, with frequencies ranging from 43.7% in summer to 31.0% in spring. This result was with line with Fig. 3.10, which shows the mean state of the atmosphere in terms of the SLP. It is also interesting to note the changes in the direction of the flow between winter and summer.

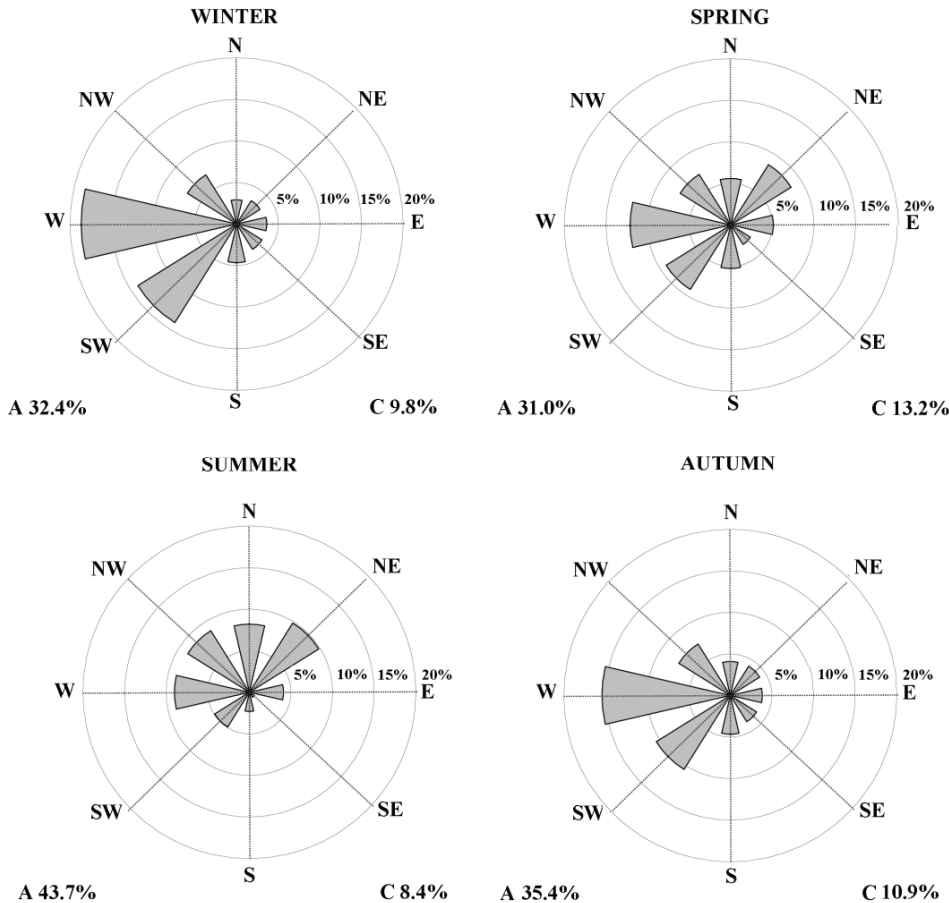


Figure 6.3. Mean frequency (%) of circulation weather types in winter (DJF), spring (MAM), summer (JJA) and autumn (SON). These frequencies were computed using the NCEP/NCAR reanalysis SLP fields for the period 1948-2008.

In winter, the flow comes mainly from the western quadrants NW, W and SW, with a large proportion of type A (32%) and type C (10%) circulation. The W and SW types, as shown in Fig. 6.2, are associated with the high frequency of winter Atlantic lows travelling north of the Iberian Peninsula (Trigo, 2006).

In contrast, in summer the flow comes mainly from the Northern regions (NW, N and NE), but also from the W (8%), with a large proportion of type A circulation (44%). Moreover, the NW, N and NE types are associated with an anticyclone located west of the Iberian Peninsula; the Azores anticyclone therefore dominates the circulation in the summer.

Regarding the other seasons, in autumn the CWT frequencies were very similar to the ones found in the winter months, whereas the spring months appeared to be characterized by a mixture between the CWT frequencies found in the summer and winter seasons.

In chapter 8, changes in the frequency of the CWTs will be analyzed for the NW Iberian Peninsula, for the period under study.

6.4. Relationship between circulation weather types and precipitation

The relationship between precipitation and the CWTs was studied by calculating the mean precipitation for each CWT over the period studied. Knowledge of the relationship with the CWTs can be used to predict, for example, daily precipitation (e.g. Conway et al., 1996) and monthly precipitation (e.g. Trigo and DaCamara, 2000). It can also be used to downscale precipitation regimes from GCM simulations (e.g. Goodess and Palutikof, 1998).

Data from the Lourizán climatological weather station was used for the daily precipitation data (for the period between 1950 and 2005). First, to determine whether the Lourizán could be assumed to be a representative point for the precipitation in NW Iberian Peninsula, the correlation between the monthly precipitation variability from this station and the monthly precipitation from the GPCP between December 1979 and December of 2004 was computed, and is shown in Fig. 6.4. There was a very high correlation (above 0.8) between the two datasets from the NW Iberian Peninsula. Therefore, it was assumed that the precipitation data from the Lourizán station was representative of the precipitation within the area under study.

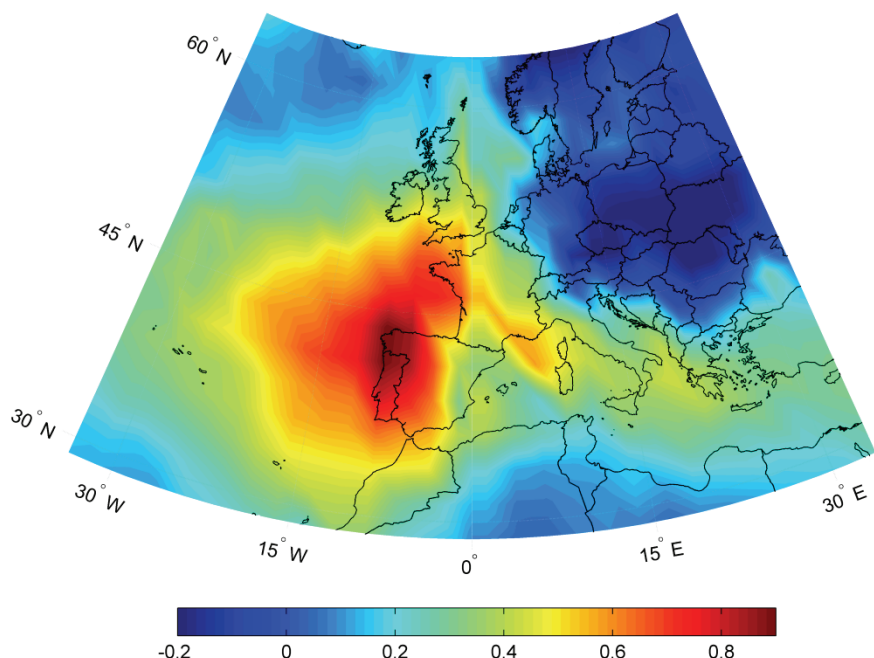


Figure 6.4. Values for the correlation between the monthly precipitation data of the Lourizán station in Galicia and the monthly precipitation data of the GPCP, during the 1979-2004 period.

The average rainfall associated with each CWT on an annual and seasonal basis (Fig. 6.5) for the 1950-2005 period was computed. The same approach as that used for the frequency of the CWT was applied here (section 6.2). That is, for a hybrid type, the precipitation for that day was included with a weighting of 0.5 into the corresponding pure directional and cyclonic/anticyclonic types.

An analysis of Fig. 6.5 showed clear evidence of the correspondence between the synoptic characteristics of each CWT and the average precipitation explained by each. The cyclonic type was the synoptic situation that produced the highest average annual precipitation (13.41 mm), followed by the W (11.80 mm) and SW (10.31 mm) types. In contrast, the NE (0.91 mm) and N (1.70 mm) types produced less precipitation, while on A-type days there was virtually no precipitation (0.21 mm). At a seasonal scale, weather types that produce higher and lower precipitation were maintained. As shown in Fig. 3.7 (seasonal average precipitation in the NW Iberian Peninsula), there was a high seasonal variability in the precipitation in the region. This seasonal variability was also present here, since for winter there were generally higher levels of precipitation associated with the CWT than with other seasons. The C type, again, was the one that was associated with more precipitation, especially in autumn and winter. This was in agreement with recent results from Santos et al., (2005) that relate large-scale atmospheric flow to wintertime precipitation. These authors show that over northern Portugal the C regime is particularly expressive in terms of precipitation.

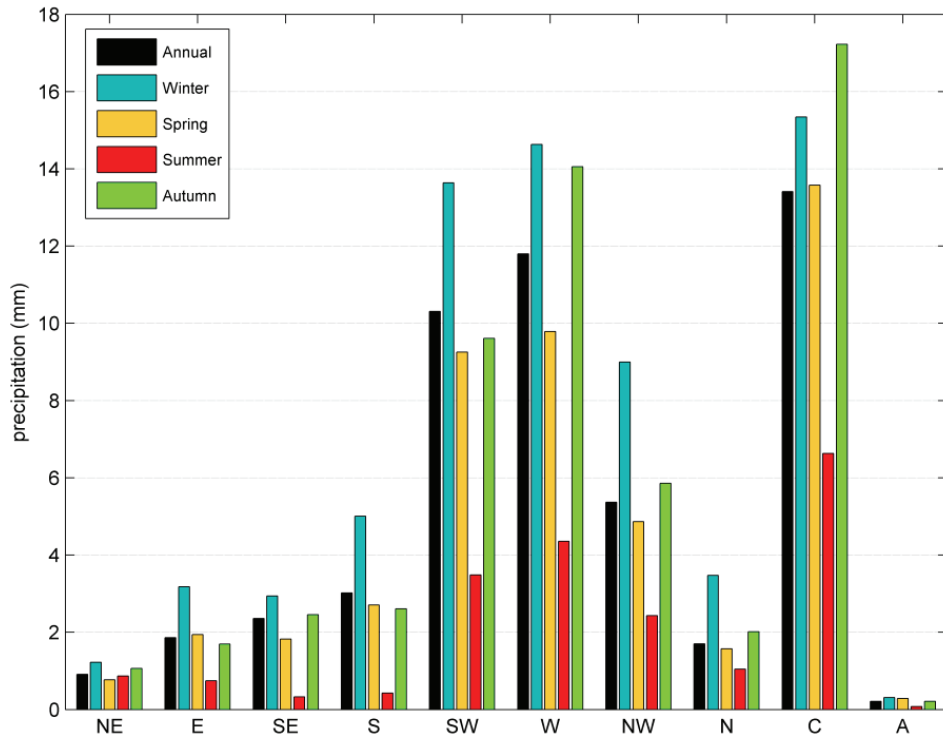


Figure 6.5. Average precipitation explained by each weather type, at annual and seasonal scales. The seasonal division is the same as that used in Fig. 6.3.

The intensity of daily precipitation and its relationship with the CWTs were also studied. To achieve this, five categories of precipitation magnitude were constructed following a method adopted in previous studies (Osborn et al., 2000; Osborn and Hulme, 2002; Gallego et al., 2006); these were no rain, light rain, moderate rain, intense rain and very intense rain. These categories were again computed for both annual and seasonal scales. The definitions of each category are presented in Table 6.1.

Using this classification, the contribution of each CWT to the different categories of precipitation was analyzed. As we can see from Fig. 6.6, at an annual scale, C, W and SW types were responsible for the vast majority of intense and very intense precipitation events, with smaller contributions from the NW and S types. In addition, for nearly

80% of the days when a C, W or SW type occurred, precipitation was present in the region. In contrast, for more than 90% of A-type days there was no precipitation. In general, the types responsible for producing less daily mean precipitation (Fig. 6.5) were also the ones (NE, E, SE and S) that had no precipitation, for more than 50% of the times that these CWTs occurred.

Table 6.1 Definition of each category of precipitation (P) in mm for winter (DJF), spring (MAM), summer (JJA) and autumn (SON) seasons, and for annual cycles.

Season	Light	Moderate	Intense	Very intense
Winter	$0 < P \leq 3$	$3 < P \leq 9$	$9 < P \leq 21$	$P > 21$
Spring	$0 < P \leq 2$	$2 < P \leq 6$	$6 < P \leq 15$	$P > 15$
Summer	$0 < P \leq 1.5$	$1.5 < P \leq 4$	$4 < P \leq 10$	$P > 10$
Autumn	$0 < P \leq 2$	$2 < P \leq 8$	$8 < P \leq 19$	$P > 19$
Annual	$0 < P \leq 2$	$2 < P \leq 7$	$7 < P \leq 17$	$P > 17$

Considering the seasonal data shown in Fig. 6.7, the results were very similar in autumn and winter, where the intense and very intense episodes occurred frequently, and mainly for the C, W and SW types, with a significant number of cases occurring in spring (but less frequently). In summer, A-type situations were the predominant weather type; these were again related to the days with no precipitation (more than 90%). However, even in summer, more than 40% of the C and W-type days had at least light precipitation, in contrast with the results for winter (where this was true for more than 10% of the days).

6. Relationship between surface climate variables and circulation weather types

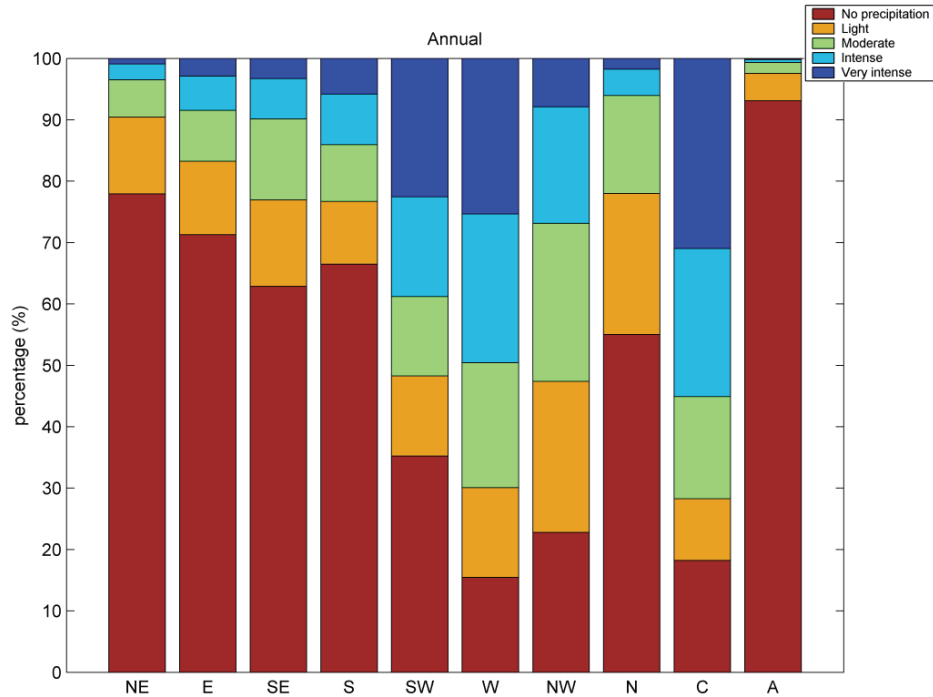


Figure 6.6. Contribution of the CWT to the different categories of annual precipitation.

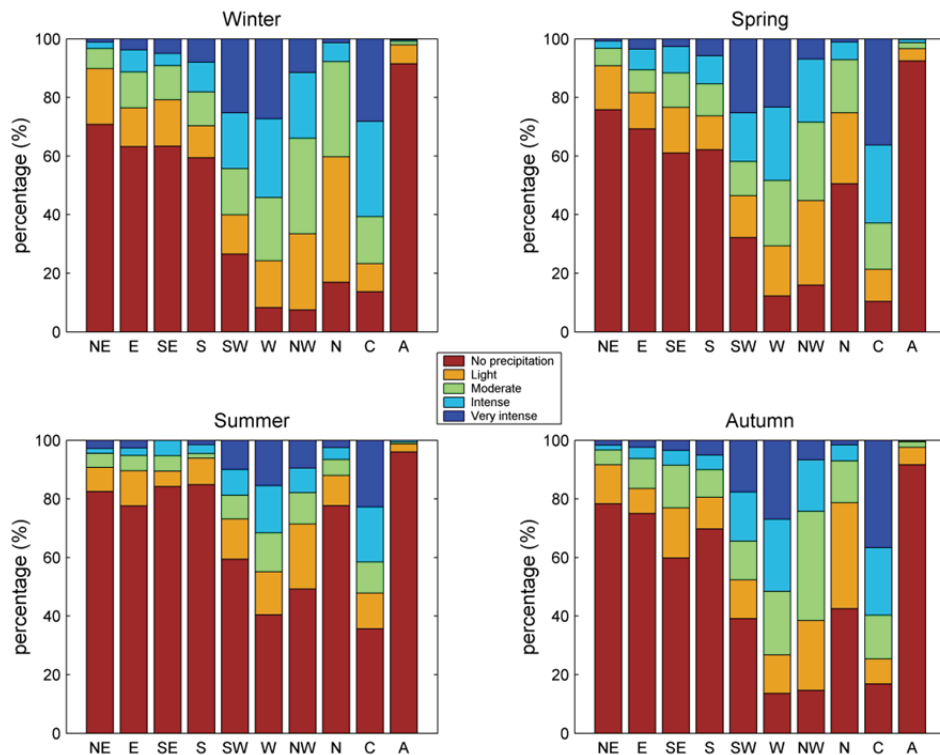


Figure 6.7. Same as Fig. 6.6, but showing seasonal data.

6.5. Relationship between circulation weather types and temperature

Few studies exist that relate CWTs and the temperature for the Iberian Peninsula. However, examples of this can be found in studies by Bermejo and Ancell, (2009) and Fernández-Montes et al., (2010).

Similarly as for precipitation, the relationship between the maximum and minimum temperature and the CWTs was also studied. This was achieved by computing the mean values for the maximum and minimum temperature for the days where a particular CWT occurred. The temperature data was taken from the As Pontes, Santiago, Sarria and Vigo weather stations for the 1961-2006 period. In the case of the temperature, only the ten pure types were retained (NE, E, SE, S, SW, W, NW, N, C and A), since the procedure applied for precipitation could not be applied here.

The computation of the average values was done individually for each weather station, for annual and seasonal scales. At first sight, the temperature variability for the different CWTs showed similar results for all 4 weather stations. The main difference was in the magnitude of the mean temperature values, which was closely related to the spatial seasonal variability in the maximum and minimum temperatures in the NW Iberian Peninsula (Fig. 3.5 and Fig. 3.6). The correlation between the mean temperature series for the 10 CWTs (annual and seasonal) was computed for the 4 weather stations. The results showed that a higher level of correlation was found for the maximum temperature than for the minimum temperature. In any case, the correlations for the minimum temperature were also significant, at a 5% level. Therefore, to avoid repetition, the results presented in this

section corresponded to the mean values (which was considered to be representative of the NW Iberian Peninsula) for the 4 weather stations.

The variability of the annual and seasonal maximum and minimum temperature is shown in Fig. 6.8 for each CWT. A clear difference was observed in the temperatures for different CWTs; this was especially true for the maximum temperature. For the maximum temperature, the highest values were generally found for the SE, S and SW types, while lowest values were found for the W, NW and N types. In addition, for the maximum temperature, the largest differences within types were found for the spring months (8.7°C), while the smallest differences were found for the winter months (5.0°C). For the minimum temperatures, the largest differences were found in the winter months (4.2°C), with the smallest differences in the summer months (1.9°C).

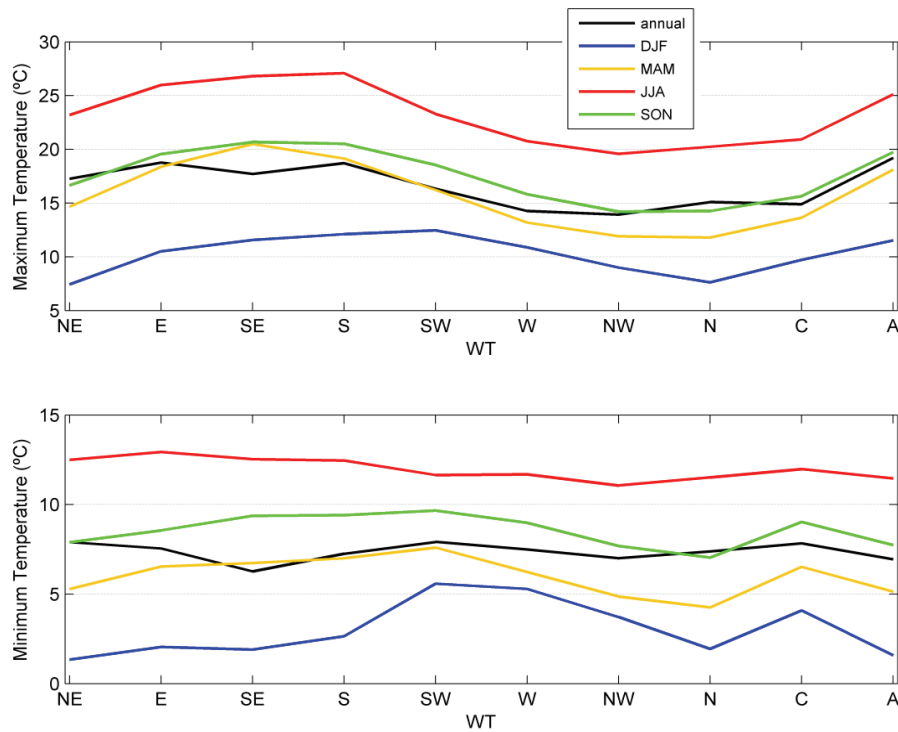


Figure 6.8. Average annual and seasonal maximum and minimum temperature for each pure circulation weather type.

This temperature variability can be explained by taking into account the climate variability in the Iberian Peninsula, and the particular location of the NW Iberian Peninsula. In summer, a thermal low develops over the Iberian Peninsula (Hoinka and de Castro, 2003), so the high mean maximum temperature values associated with the E, SE and S types were connected to the advection of hot air from the interior regions of the Iberian Peninsula. The SW, W, NW, and N types were associated with the more humid and colder air that comes from the Atlantic Ocean, and therefore presented lower mean maximum temperature values. In winter, the CWTs that usually account for the lower levels of precipitation in this domain (E, SE, S, N and A) showed a higher mean maximum temperature and a lower minimum temperature. These types are usually associated with clear-skies days, in which the daytime temperatures are enhanced by solar short waves, while at night the strong clear-sky emission of long wave radiation cools the lower troposphere.

Spring and autumn showed very similar behavior, especially for the maximum temperature, with higher temperatures being found for the E and SE, while lower temperatures were found for the NW, N and C types.

6.6. Relationship between circulation weather types and lightning activity

An analysis of lightning events per CWT for the period 2003-2009 is shown for both annual (Table 6.1) and seasonal (Table 6.2) scales. The first column (WT) represents the percentage of total days with each specific WT; the second column represents the ratio of lightning days (rLD) for each specific CWT frequency; the third column simply shows

the total number of lightning days (LD) for each CWT; the last column shows the contribution (CG) of each CWT to the total CG discharges (in percentage). The last line of each table corresponds to the sum of all CWT lines, except for the rLD column, where it corresponds to the absolute lightning days ratio. Note that the rLD, LD and CG that occurred during days characterized by an hybrid CWT (see section 6.2) were redistributed with a weight of 0.5 into the corresponding pure directional and cyclonic/anticyclonic types, following the same approach adopted for the WT (see section 6.2).

The classification from columns rLD, LD and CG allowed us to distinguish between CWTs frequently associated with lightning episodes (regardless of whether these episodes were severe or not), and CWTs favourable for severe lightning episodes (in which there were a very high number of CG discharges per episode), whether these events were rare or not. To be completely clear about the meaning of each number, we can look in detail at the two CWTs dominated by either anticyclonic (A) or cyclonic (C) vorticity, at the annual scale (Table 6.2). The A type corresponded to 38% of all days, while the C type represented only 10%; however, the vast majority of A days were not related to CG discharges (with a ratio of only 7.5%), while most C type days were indeed characterized by some level of CG activity (ratio of 53%). In any case, the large number of A-type days was responsible for the total number of CG discharges (27.3%), while the percentage of C-type days contributed to 15% of the total discharges. The NE and E also showed high rLD values (near 34% for both types).

Table 6.2. Circulation weather type frequency, lightning days ratio (rLD), total lightning days (LD) and cloud-ground discharge (CG) frequency, on an annual basis. (Bold values represent the three dominant situations).

	CWT (%)	rLD (%)	LD (days)	CG (%)
NE	5,7	33,9	49	17,4
E	4,1	34,1	36	16,0
SE	2,6	16,5	11	4,2
S	4,2	13,6	15	1,2
SW	9,5	14,8	36	4,4
W	14,2	16,5	60	3,7
NW	6,6	16,6	28	1,9
N	4,8	31,1	38	8,9
C	10,3	53,1	140	15,0
A	38,2	7,5	74	27,3
<i>Total</i>	<i>100,0</i>	<i>23,8</i>	<i>485</i>	<i>100,0</i>

In a closer look at the seasonal data (Table 6.3), the C type was evenly distributed over the four seasons, and was frequently associated with lightning activity, although the ratios diminished in the summer. Episodes associated with the NE type were rare in winter months, but were the most important in other seasons. The relation between the NE type and very active thunderstorms in warm months was evident. The C and W types were responsible for the highest percentage of CGs in winter (50% and 22%, respectively). As seen before (chapter 3), the number of strikes in winter was much smaller than during the warmer seasons. In winter, convection is essentially forced synoptically; it is not forced by afternoon radiation-induced convection, so thunderstorms can form in the Atlantic, and then advected towards the studied region.

In spring, the most important types were C, NE and E. The NE type was related to the thunderstorms with the largest number of discharges (21.7%), followed by the E type (20.5%). In addition, when a C-type day occurred, the probability of lightning activity on these days was near 60%.

Table 6.3. Same as Table 6.2, but for seasonal data.

	Winter				Spring			
	CWT (%)	rLD (%)	LD (days)	CG (%)	CWT (%)	rLD (%)	LD (days)	CG (%)
NE	4,2	24,5	7	5,5	6,7	33,7	15	21,7
E	4,4	0,0	0	0,1	5,0	52,3	17	20,6
SE	3,5	0,0	0	0,2	3,2	22,0	5	5,9
S	3,6	4,4	1	0,5	3,6	26,1	6	2,1
SW	9,5	8,3	5	7,7	9,8	15,9	10	2,9
W	17,9	12,4	14	22,0	13,6	13,1	12	1,9
NW	6,0	17,1	7	8,0	7,0	13,3	6	3,7
N	3,6	26,1	6	5,2	4,8	30,6	10	12,9
C	7,9	46,0	23	49,9	14,1	56,9	52	14,2
A	39,5	0,4	1	0,9	32,3	7,5	16	14,1
Total	100,0	13,9	63	100,0	100,0	27,1	146	100,0

	Summer				Autumn			
	CWT (%)	rLD (%)	LD (days)	CG (%)	CWT (%)	rLD (%)	LD (days)	CG (%)
NE	5,8	45,7	16	16,2	5,9	33,3	13	15,3
E	2,5	9,0	9	13,4	4,4	33,9	10	17,3
SE	1,2	0,3	3	4,3	2,6	21,2	4	2,0
S	4,0	1,1	7	1,1	5,7	2,8	1	0,4
SW	8,4	1,6	10	3,1	10,4	17,4	12	9,4
W	11,2	2,9	8	1,8	14,3	29,7	27	8,3
NW	7,0	1,3	7	0,7	6,4	22,2	9	1,0
N	6,5	7,6	12	8,1	4,1	34,6	9	4,9
C	9,2	23,6	27	7,3	9,8	60,8	38	29,7
A	44,3	7,1	44	44,0	36,6	5,2	12	11,7
Total	100,0	10,0	140	100,0	100,0	26,1	133	100,0

We should once again stress that in summer, the NE type was by far the most prominent pattern associated with thunderstorms over the NW Iberian Peninsula, with high rLD values (45.7%). Other WTs such as the A-type presented lower rLD values (7.1), but high CG discharge values. A closer look at Fig. 6.2 indicated that the A-type days were characterized by a NE/E flow in the Galicia region, which explained the

higher CG discharge values. Although it was responsible for only 9 thunderstorm days, the E type was third in terms of CG percentages, which meant that summer storms under this type of circulation were not very frequent, but rather strong.

In contrast to the winter months, most of the CG discharges in the other seasons developed inland (see chapter 3), far from inhibitive sea breezes. Inland, solar radiation during the day promotes soil heating, and makes energy available for convection. On the contrary, close to coastal areas this heating cycle is damped considerably, reducing the amount of energy available for thunderstorm development. Even thunderstorms formed inland and advected to coastal areas tend to be dissipated, as the sea breezes cut the energy supply for convection and the organization of convective cells. This heat source is very important for afternoon spring thunderstorms, but there is another important factor in this season. Although at low levels we may already have important heat content, frequently in early spring we still find very cold air masses at higher levels producing large lapse rate values that are favourable for deep convection (Pineda et al., 2010). Furthermore, in summer, the small low-pressure system over Iberia, frequently forced by long periods of very warm weather (thermal lows), induces a cyclonic circulation over Iberia (Hoinka and De Castro, 2003), increasing the probability of lightning.

The CWTs responsible for most lightning episodes in autumn were somewhat similar to those found in summer (NE and E), with a large contribution from C types; they were responsible for most important events (30% of total autumn CG discharges, with a rLD of 61%). The CG values indicated that thunderstorm activity over the NW Iberian Peninsula is almost guaranteed when these three synoptic

conditions occur in autumn. In this season, the sea surface temperatures (SSTs) are higher than in spring, a fact that compensates for the lack of very cold air at altitude, enabling once again the steep lapse rates that are favourable for deep convection.

In the context of the Iberian Peninsula, it must be stressed that the total number of CGs over the NW Iberian Peninsula is relatively low when compared with other areas (Pineda et al., 2010; Rivas Soriano et al., 2005). Rivas Soriano et al., (2005) concluded that the spatial distribution pattern of CG discharges in central and east Iberia is clearly related to the orography, and that the maximum lightning activity is related not only to the Pyrenees and the Sistema Ibérico mountain range, but also to the Mediterranean sea. In addition, Tomas et al., (2004), studied the relationship between CWTs (centred in the Iberian Peninsula) and CG discharges between 1992 and 1994, and found that on an annual scale, the C type presented the greatest flash frequency, and days with an easterly component (NE, E, SE) generated 30.7% of the total CG discharges in that period. We must of course carefully bear in mind that most of the CG discharges considered by Tomas et al., (2004) were located in northern and eastern Spain.

Additionally, composites were computed for each WT, for two separate situations; 1) days with more than five CG discharges, and 2) days with no CG discharges. The maps of the two instability indices CAPE and LI (not shown since they were very similar to the CAPE maps) were analysed. The geopotentials near the surface (H1000) level and at high levels (H500) are shown, to allow an evaluation of large-scale circulation forcing; the mean relative humidity (RH) for the 925-700 hPa layer is also shown in Fig. 6.9.

6. Relationship between surface climate variables and circulation weather types

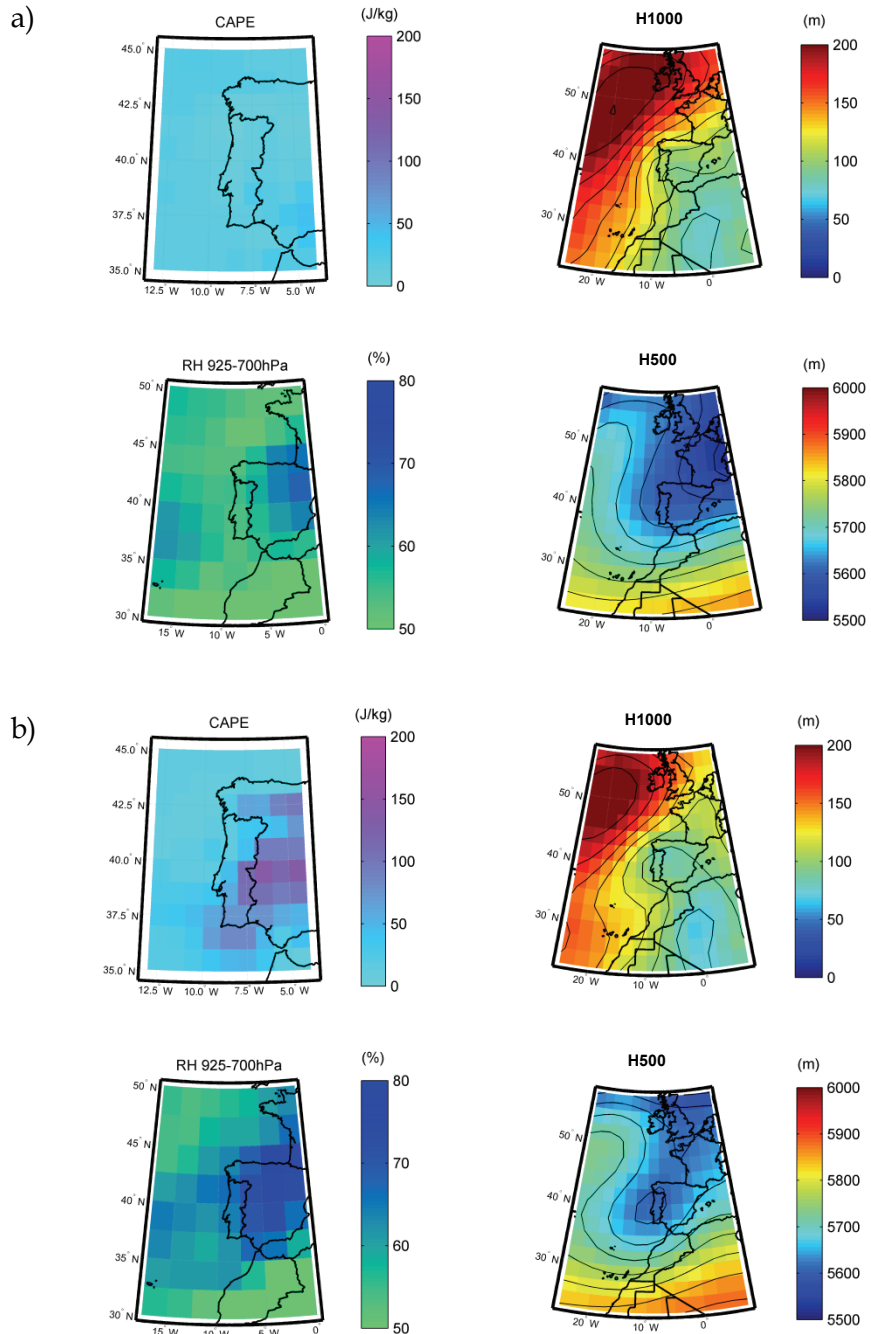


Figure 6.9. Composites of days in winter with the NE circulation weather type, for a) stable days and b) unstable days, for mean daily fields of CAPE (J/kg), H1000 (m), and RH (%) and H500 (m).

Since a large number of composites were computed, for both stable and unstable situations, for all climatic seasons, for the sake of simplicity only an example for the NE type in spring is discussed here.

As mentioned before for spring and summer, the inland solar radiation during the day promotes soil heating, and increases the amount of energy available for convection. This heat source is very important for afternoon spring thunderstorms, but there is another important factor in this season. Although at low levels we may already have important heat content, frequently in early spring we still find very cold air masses at higher levels producing large lapse rate values that are favourable for deep convection (Pineda et al., 2010). Thus one can say that in this season, synoptic scale patterns still play a major role, particularly when allied with the triggering mechanism enabled by high solar radiation. This description fits well with the NE types, which were responsible for the highest CG values in this season. In Fig. 6.9 (composites for the NE type) we can see a cold air mass over the NW Iberian Peninsula (in the form of a cut-off low or a pronounced trough) when we analyze the 500hPa geopotential height composites.

Nieto et al., (2007a) found that more than half of the cut-off low systems found in the European sector are associated with blocking events, particularly in spring and winter, when these quasi stationary anticyclonic patterns are more frequent. Comparing stable (Fig. 6.9a) and unstable days (Fig. 6.9b) for the NE type in spring, the impact (on the CAPE values and humidity) of the trough positioned over the NW Iberian Peninsula – and a visible cut-off low system centered in western Iberian Peninsula – is clear.

6.7. Summary

In this chapter the relationships between the atmospheric circulation (given by the CWT) and the precipitation, temperature and lightning activity in the NW Iberian Peninsula were studied, as well as the seasonal variability of these relationships. To achieve this, an adaptation of the Lamb CWT was computed for the NW Iberian Peninsula. In addition, meteorological weather station data (for both temperature and precipitation) was used.

The most important results were as follows:

- The A weather type was the most frequent pattern throughout the year. W and SW types were also frequent, especially in autumn and winter;
- There was a clear difference between each CWT and the corresponding average precipitation. The C, W and SW types were the synoptic patterns that produced higher levels of precipitation, while on A-type days there was virtually no precipitation;
- For the different CWTs there was a clear temperature variability, especially for the maximum temperature. For the maximum temperature, the highest values were generally found for the SE, S and SW types, while lowest values were found for the W, NW and N types.
- The highest differences in the maximum temperature within the types were found for the spring months, with the lowest differences being found for the winter months. Regarding the minimum temperature, the highest differences were found in the winter months, with the lowest differences being found in the summer months.
- The relationship between the CWTs and CG discharges (annually and seasonally) allowed us to distinguish which types were

6. Relationship between surface climate variables and circulation weather types

most frequently associated with lightning episodes, and also which ones were favourable for severe lightning episodes (in which a very high number of CG discharges per event occurred).

- The mechanisms associated with lightning activity are often related to atmospheric features that do not have a clear signature at lower atmospheric levels, (e.g. sea level pressure fields), so their associated WT alone cannot fully explain mechanisms in all cases. In that situation, additional upper level meteorological fields may be needed for a deeper knowledge.

7. Compatibility between modes of low-frequency and circulation weather types

7.1. Introduction

Recent observations have highlighted the fact that significant climate trends are evident at different time scales over the North Atlantic European (NAE) sector (IPCC, 2007; Trigo et al., 2008). The variability in atmospheric circulation is the most important issue in terms of the changes in the spatial distribution, not only of temperature or precipitation, but also of other climatological variables.

A distinctive characteristic of the interannual variability of large-scale circulation patterns is the degree to which they are organized spatially, as represented by their modes of low frequency variability. These patterns, which are considered by many authors to be the preferred modes of low frequency variability of atmospheric circulation, consist of in-phase or out-of-phase variations of geopotential or sea level pressure in areas normally termed 'centres of action'. Modes of low frequency variability are concepts for understanding the complex

relationship between planetary-scale circulation and regional climate, including the occurrence of extreme events.

The first major studies to refer to modes of low frequency variability were those of Wallace and Gutzler, (1981) for the winter period and Barnston and Livezey, (1987) for all seasons. For the NAE sector, the most prominent patterns according to Barnston and Livezey, (1987) are the North Atlantic Oscillation (NAO), East Atlantic Pattern (EA), Euroasian pattern 1 (also referred as East Atlantic/Western Russia pattern (EA/WR)) and Euroasian pattern 2 (also referred as the Scandinavian pattern (SCA)). Over the last two decades, several studies have assessed the impact of these modes on the European climate (in particular on temperature and precipitation). The NAO is the main mode of low frequency variability in the NAE sector and is correlated with the surface climate in most of the European region (Hurrell and van Loon, 1997; Lu and Greatbatch, 2002; Trigo et al., 2002; Jones et al., 2003; Bojariu and Gimeno, 2003). For example, positive NAO index during winters are associated with a northward shift in the Atlantic storm activity, with enhanced activity from southern Greenland across Iceland into northern Europe and a modest decrease in activity to the south, which cause drier conditions to Southern Europe (Hurrell et al., 2003).

However, this relationship between the NAO and the climate in Europe cannot be considered to be fully stable. Chen and Hellström, (1999) pioneered the study of the non-stationarity of circulation-to-weather links in Europe. A number of other studies also note the non-stationary nature of this relationship, in terms of not only surface temperature (Slonosky et al., 2001; Gimeno et al., 2003,) or sea surface temperature (Walter and Graf, 2002), but also precipitation (Zveryaev, 2006; Beranová and Huth, 2007). Jung et al. in 2003 were the first to

suggest that the reason for the non-stationarity of the relationship between the variability modes and surface weather was in the changing positions of the action centres of the NAO. In a recent study, Vicente-Serrano and López-Moreno, (2008) emphasized that the non-stationary relationship between the NAO and precipitation is linked to inter-decadal variability in the position of the NAO pressure centres. Moreover, the spatial configuration of the NAO changes substantially prior to the occurrence of clear shifts in the magnitude and spatial distribution of its influence on precipitation patterns in Europe.

Although the NAO is known to be the main modes of low frequency variability of the Northern Hemisphere that influences the European Climate, some studies have also focused on the influence of other modes of low frequency variability on the NAE sector. The reports include those on precipitation (eg., Rodríguez-Puebla et al., 1998; Wibig, 1999; Blackburn and Hoskins, 2001), on the impact on river flow (Lorenzo and Taboada, 2005) and on the upwelling intensity (deCastro et al., 2008). Relationships between other modes of low frequency variability over the NAE and temperature may also be found in Sáenz et al., (2001) and Beranová and Huth, (2008).

Studies of the temporal variability of the effects of other modes of low frequency variability also conclude that the relationship between these other modes of low frequency variability (apart from the NAO) and temperature and precipitation also varies in time and space (Krichak and Alpert, 2005; Beranová and Huth, 2008).

At the same time, their significance also varies seasonally, tending to be stronger during some seasons than others. For example, the NAO is more pronounced during winter and less clear during the summer months (Corte-Real et al., 1995; Trigo et al., 2001). In general,

the impact of the major modes of low frequency variability (especially those with zonal dipoles) on precipitation in Europe is higher and more pronounced during the winter months (Glowienka-Henze, 1990; Dunkeloh and Jacobbeit, 2003), when the baroclinity is higher in the extratropical latitudes than it is during the summer. Therefore the results presented in this chapter are only focus in the winter months, despite having performed analyses for other seasons as well.

One further method used for studying the effects of changes in circulation patterns on regional climate is the estimation of changes in these patterns. Circulation patterns are specific to a given region and result from the examination of synoptic weather data, usually on a regular grid, obtained using a wide variety of methodologies (Huth et al., 2008; chapter 2). Circulation weather types (CWT) are usually defined for each day and tend to reflect the local circulation that actually occurs in a simple way. In contrast, the modes of variability are estimated at a larger temporal and spatial scale than the CWT and are characterized by a recurring and persistent, large-scale pattern of pressure that covers vast geographical areas. Modes of low frequency variability reflect large-scale changes in the atmospheric wave and jet stream patterns and they are generally defined by means of principal component analysis. Therefore the circulation field at each time can be approximated by a linear combination of several modes of low frequency variability. In this way, there is no reason to suppose that the modes of low frequency variability resemble individual circulation patterns.

The aim of this chapter is to assess the compatibility between the modes of low-frequency variability in Europe (computed using a principal component analysis (PCA)) and local circulation regimes

(using an automated version of the Lamb CWT classification), thus to observe how shifts in the positions of the modes of low-frequency variability in Europe, could affect local circulation

The remainder of the paper is organized as follows. In section 7.2, we describe the methodologies used in their analysis. In section 7.3, we describe the synoptic CWT briefly. In section 7.4, we introduce the concept of modes of low frequency variability, computed using PCA for sea level pressure and 500hPa geopotential height fields, and their relationship to CWT. In section 7.5, the non-stationary nature of the modes of low frequency variability and its influence on the frequency of each CWT are discussed. Section 7.6 concludes.

7.2. Methodology

The main database that we used consists of daily Sea Level Pressure (SLP) retrieved from NCEP/NCAR reanalysis data (Kalnay et al., 1996, chapter 5). The daily winter, in this chapter refers to the months of January, February and March (JFM), SLP fields from 1948-2005 with a grid size of 2.5°. The spatial window covers the area 30°N - 76°N and 37°W - 56°E.

In this study, four different sets of data are used, in which three corresponding to different methods of quantifying atmospheric circulation variability (sections (a)-(c)) and one corresponding to the identification of the non-stationary modes of low frequency variability in the NAE sector (section (d)).

a) Daily circulation weather type classification

In this chapter, the same daily CWT database computed in chapter 6 is used. Data were obtained only for the winter season (JFM) for the years from 1948 to 2005.

b) Hemispheric modes of low frequency variability

The standard NAO, EA, EA/WR, and SCA modes of low frequency variability indices were obtained from the Climate Prediction Center (CPC) of the National Oceanic and Atmospheric Administration (NOAA) for the years 1948-2005 (chapter 5). It is important to note that hereafter the hemispheric modes of low-frequency variability ((NAO, EA, EA/WR, and SCA) are referred as hemispheric modes.

c) Stationary modes of low frequency variability in the NAE sector

The PCA technique is one of the most commonly applied to the detection of modes of low frequency variability and has been used in a variety of climatological studies, e.g. Jolliffe, 1990; Corte-Real et al., 1999; Wibig, 1999; Huth, 2006; Zveryaev, 2006.

In order to identify the modes of low frequency variability in the NAE sector, a PCA technique was carried out. Here we use the same methodology as Barnston and Livezey, (1987) but with two differences: (1) we use daily fields and (2) we only take into account the NAE sector (30°N – 76°N and 37°W – 56°E).

This technique was first applied to the daily winter (JFM) SLP field for the whole period of analysis (1948-2005) and taking into account the NAE sector (30°N – 76°N and 37°W – 56°E). The covariance matrix was created using the time values at each grid point. This

corresponds to a PCA in S-mode (using the terminology found in Richman, (1986)), which means that the eigenvector describes the spatial pattern of the modes of low frequency variability and the principal components (PCs) describe the time variations (in our case the indices of the low frequency variability modes in NAE sector). Due to the fact that our grid covers an area between 30°N and 76°N, each grid cell in the data is the same size, but each grid cell on the Earth is a different size, according to its latitude. In order to ensure the equality in the grid areas, the gridded data were weighted by the square root of the cosine of latitude (Chung and Nigam, 1999). Finally, a Varimax orthogonal rotation was also applied. The same methodology was also applied to the daily 500-hPa geopotential height field (H500).

d) Identification of the non-stationary modes of low frequency variability in the NAE sector

In order to identify changes in the modes over time for the winter months (JFM) in the NAE sector, we computed a moving window PCA (with a 30-year period) for JFM, which allowed us to study not only the changes in the spatial patterns over time but also the changes in position and intensity of the modes. The methodology and spatial domain used to compute the 30-year period PCA was the same as the one described in section 7.2 c). The first period used in the PCA was 1948-1977 (using 1962 as the central year), the next period was 1949-1978, and so on until the final period 1976-2005 (using 1990 as the central year).

In the following sections, several correlation analyses are made. In order to do so, new time series are created. These time series are seasonal (JFM) and they are averages from daily time series (in the case of the

modes and frequency of the CWT) and from monthly time series (in the case of the hemispheric modes).

7.3. Circulation weather types for NW Iberia Peninsula

The CWT for the NW Iberia Peninsula have been described extensively in chapter 6. For these reason, in this chapter, only the frequency of the CWT observed during the winter months (JFM) is shown (Fig. 7.1). The most obvious result is that on winter days, the CWT that has the greatest frequency of occurrence is anticyclonic circulation, which occurs on about one third of the days analyzed. The CWT driven by air flow from a westerly direction (i.e. NW, W and SW) have higher frequency (6.2%, 17.2%, and 13.6% respectively) than the eastern CWT (less than 5% each). Cyclonic CWT occur on about 10% of the winter days that were analyzed.

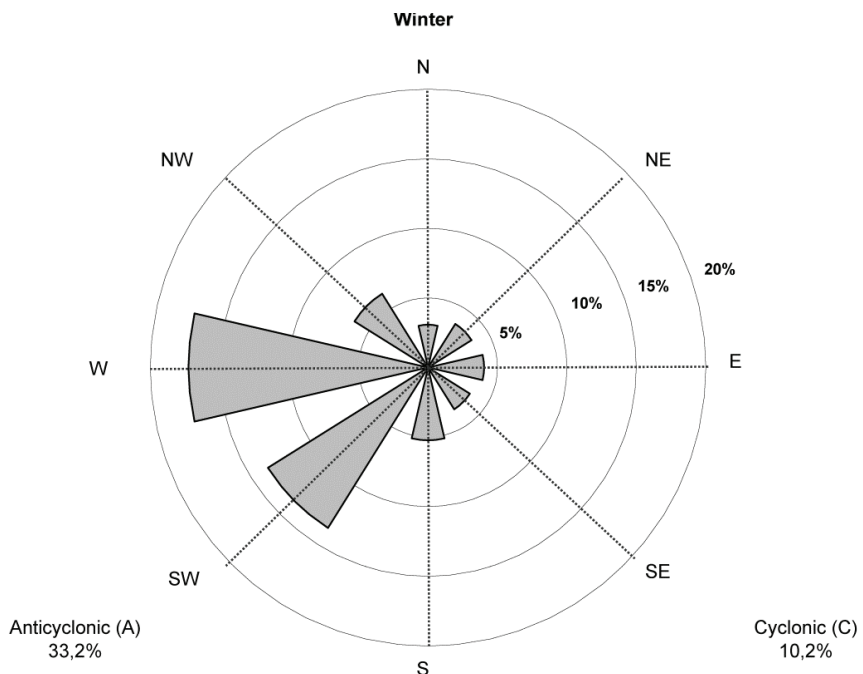


Figure 7.1. Frequency (%) of circulation weather types in winter months (JFM).

7.4. Stationary Variability

The Lamb classification of CWT is an important tool used for the study of the daily synoptic variability of a given region. However, in most cases, these daily local circulations are related to the modes of low frequency variability. In order to investigate this influence, we computed the PCA, not only for the winter (JFM) SLP field in the NAE sector, but also for the 500 hPa geopotential height field in our area of study (30°N – 76°N and 37°W – 56°E).

For both the SLP and H500 fields, the four main EOF patterns and the respective variance explained by each, in winter, are shown in Fig. 7.2 and Fig. 7.3, respectively. At first glance and on the basis of mere visual comparison, the results for both fields seem very similar. For the first two EOFs the same pattern appears for both fields, while those of EOF 3 and EOF4 are switched between them, i.e., the pattern of EOF3 in the SLP field corresponds to that of EOF4 in the H500 field and that of EOF4 in the SLP corresponds to that of EOF3 in the H500 field.

Despite the strong resemblances in the two fields, correlations between the time series of the SLP and H500 modes were computed to provide a more thorough comparison (Table 7.1). The results support the visual resemblances with high correlations (significant at a 99% level) between the first two correspondent modes. Regardless of the change in the positions of the patterns of EOF3 and EOF4 with respect to explained variance in the SLP and H500, when analyzing the cross-correlation between them, there were high correlations in both cases - more than 0.92). In order to put these modes into context, we also computed the correlations (Table 7.2 a) and b)) between the time series of the modes and the hemispheric modes (NAO, EA, EA/WR and SCA).

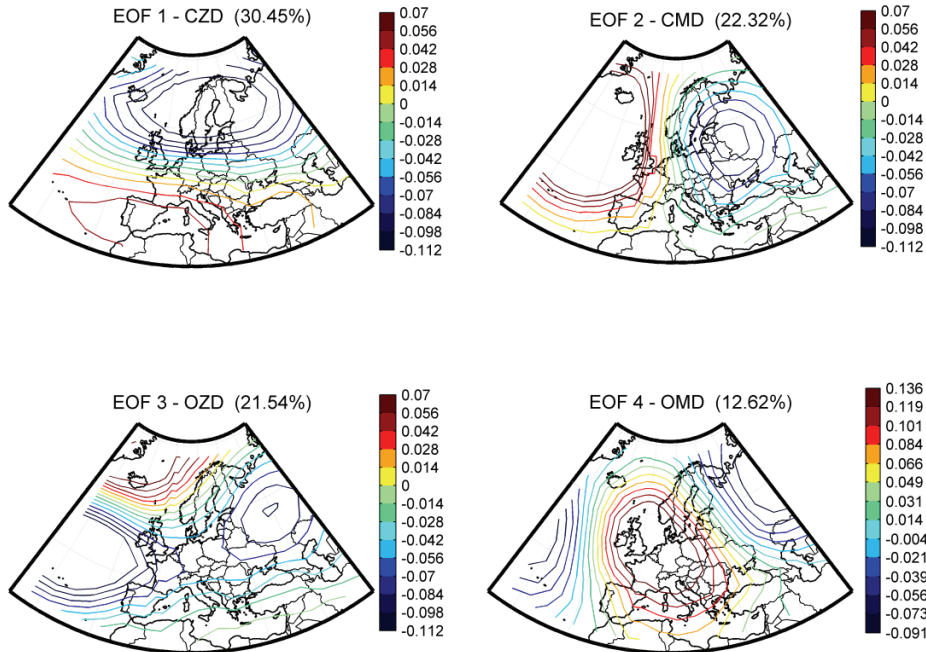


Figure 7.2. The first four leading EOF patterns for the winter months (JFM) for the SLP field together with the respective variance (%) explained by each.

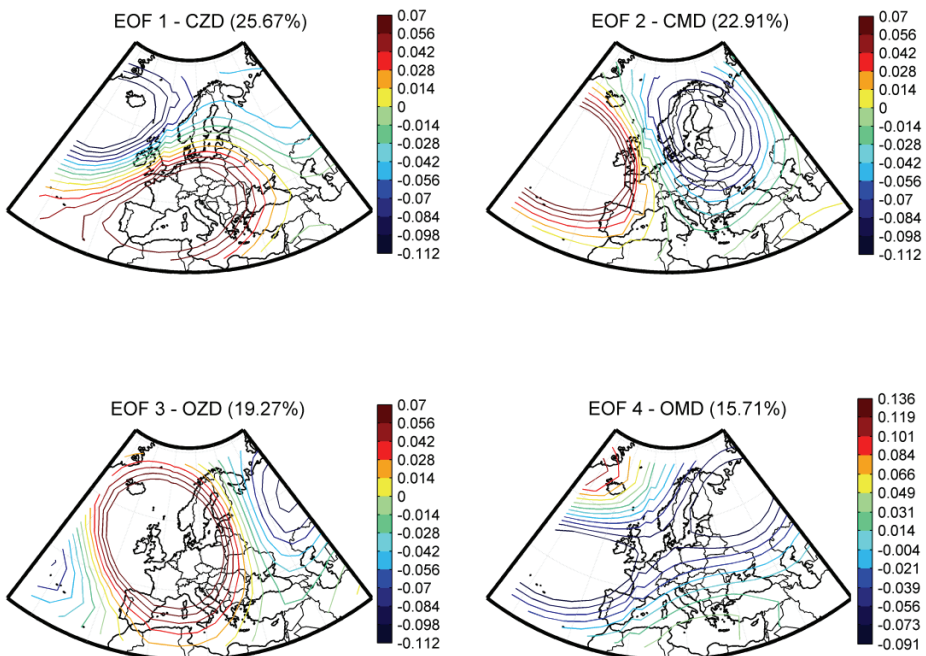


Figure 7.3. The first four leading EOF patterns for the winter months (JFM) for the H500 field together with the respective variance (%) explained by each.

Table 7.1. Correlation between the times series of both EOFs fields (SLP vs H500) computed for the region of study is shown (values in bold represent correlations that are statistically significant at the 99% level).

SLP	H500			
	PC1	PC2	PC3	PC4
PC1	0.91	0.450	0.14	-0.47
PC2	-0.18	0.87	0.16	0.03
PC3	-0.41	-0.31	-0.20	0.93
PC4	0.40	0.29	0.92	-0.24

Table 7.2. Correlation between the hemispheric modes time series and the time series of the EOF computed a) for the SLP field and b) for the H500 field (values in bold represent correlations that are statistically significant at the 99% level).

a) SLP	NAO	EA	EA/WR	SCA
PC1	0.77	0.29	0.20	-0.70
PC2	-0.15	-0.41	0.08	-0.54
PC3	-0.83	0.08	-0.08	0.04
PC4	0.30	0.28	0.72	-0.40

b) H500	NAO	EA	EA/WR	SCA
PC1	0.75	0.47	0.22	-0.55
PC2	0.23	-0.34	0.16	-0.72
PC3	0.06	0.15	0.76	-0.21
PC4	-0.79	0.04	0.01	-0.06

For both climate modes (SLP and H500 field), the first PC has the highest correlation (0.77 and 0.75) with the NAO. For the second PC, the highest correlations are with SCA for both fields. In the case of the third PC, for the SLP field it has the highest correlation with the NAO pattern and for the H500 field it has the highest correlation with EA/WR. In contrast, for the fourth PC, the SLP-PC is highly correlated with EA/WR and for the H500 field it has the highest correlation with the NAO. For the third and fourth PCs, this correlation structure was as expected, due to the change in the position of EOF3 and EOF4 with respect to the

explained variance in the SLP and H500 fields. These results show that, in general, for our spatial window, there is a one-to-one correspondence between the modes at SLP and H500. Given that the CWT that we consider in this work are based on the surface fields, from now on, we will only focus on the SLP field modes. We now describe briefly the four leading modes in the NAE sector for the SLP field (Fig. 7.3) and provide our own nomenclature for naming the modes.

The first EOF (EOF 1), a Continental Zonal Dipole (CZD), explains about 30% of the total variance and is characterized by the presence of strong centres in Scandinavia (negative) and in the Iberian Peninsula (positive), these being separated by a strong north-south gradient. This mode is similar in structure to the NAO pattern (it has a 0.77 correlation with it) but with some influence of the SCA pattern since the correlation between the PC-CZD and SCA are also important (-0.69).

EOF 2 is a Continental Meridional Dipole (CMD), which is characterized by two large-scale structures, with their main centres of action over the Atlantic region and over Western Europe. It accounts for 22% of the explained variance. This mode may be associated with the type 1 Eurasian pattern (EU1) described by Barnston and Livezy, (1987), also known as the Scandinavian pattern (SCA). From Table 1a) we can see that it presents higher correlation with the SCA (-0.54 and significant at a 95% level).

EOF 3 is an Ocean Zonal Dipole (OZD), which resembles the NAO pattern. The most important difference is that the OZD is northward shifted when comparing with the NAO. Besides that, it also extends more over Western Europe and therefore has a larger horizontal scale. It accounts for 21% of the total variance. This mode has the maximum and minimum values of the centres of action located over

Greenland and the Azores region respectively, favouring a high correlation value with the NAO (-0.83).

EOF 4 is an Ocean Meridional Dipole (OMD) and accounts for 12% of the total variance. This pattern has a main (positive) centre located between the British Isles and Denmark. It has two other centres, which are located to the northwest of the Azores Islands and over Northern Russia. This pattern bears some resemblance to the type 2 Eurasian pattern (EU2) described by Barnston and Livezey, (1987), which is also referred to as the East Atlantic/West Russia (EA/WR) pattern using the terminology of the Climate Prediction Centre of the NOAA. In fact, this mode presents the highest correlations with the EA/WR (0.72).

We provide strong evidence that the modes computed from the SLP field or the H500 field are very alike in this spatial window. Despite this, there is not an obvious one-to-one correspondence between the SLP/H500 modes and the hemispheric modes. This lack of correspondence can be explained by the different methodologies (atmospheric levels, domain, time period, rotation) used when computing the PCA and was also discussed in others studies, e.g. Beranová and Huth, (2008); Jolliffe, (2002). In our particular case, the most obvious result is that, EA is missing in the modes computed for this spatial window. The most probable explanation for this is the selection of the domain. EA is described by Barnston and Livezey, (1987) as a center near 55°N, 20°-30°W with a strong north-west-southeast gradient over western Europe and an oppositely signed anomaly band over 25°-35N, 0°-10°W. Since our domain is limited to 30°N - 76°N we believe that is why this mode is missing in our analysis. It is also interesting to note that the absence of EA pattern is compensated by

another NAO like pattern (OZD) maybe in part because of the EA pattern is also structurally similar to the NAO pattern but with the anomaly centers displaced southeastward.

Now that the characterization of the modes in our domain is made, the next evaluation will be focus on the links between the Galician CWT and the modes.

Firstly, the major hemispheric modes that affect the dominant patterns of variability of atmospheric circulation in Galicia is studied (Table 7.2). Secondly, the spatial domain will be reduced and the focus will be on the modes in the NAE sector (Fig. 7.2 and Fig. 7.3). Given that we have already demonstrated the relationship between hemispheric modes and the modes in the NAE sector, the first issue will be considered only briefly.

Table 7.2 shows the coefficients obtained from the correlation between the four large-scale hemispheric modes and the frequency of the 10 CWT during the winter months (JFM). As expected, the most significant correlations are those obtained between the NAO and the frequency of cyclonic and anticyclonic CWT. This inverse correlation with the frequency of cyclonic type is in line with the decrease in the occurrence of storm tracks in the region when the NAO is in its positive phase (Trigo, 2006). The EA index also shows a high correlations with the frequency of SW type, which the third most frequent type is occurring in winter. The EA/WR index shows a fairly high correlation with the frequency of W, NW, and SE CWT. Finally, the SCA index exhibits a pattern of behavior that is the opposite of the NAO, showing a high negative correlation with the frequency of anticyclonic type and a high positive correlation with the frequency of cyclonic type.

Table 7.3. Correlation between the hemispheric modes time series and the frequency of the synoptic circulation weather types in winter (values in bold represent correlations that are statistically significant at the 99% level). The cyclonic and anticyclonic circulation weather types are referred to as C and A, respectively.

	NE	E	SE	S	SW	W	NW	N	C	A
NAO	-0.13	-0.24	-0.38	-0.28	-0.03	0.18	-0.08	-0.06	-0.61	0.54
EA	-0.29	-0.09	-0.13	0.00	0.52	0.23	-0.27	-0.40	-0.12	-0.13
EA/ WR	-0.16	0.23	0.34	0.17	0.28	-0.49	-0.42	-0.06	-0.09	0.23
SCA	0.12	0.08	-0.15	0.02	-0.01	0.17	0.31	0.23	0.42	-0.50

Finally, we discuss the relationship between the CWT and the modes in the NAE sector, using the SLP four leading PC loading factors. For each day, we carried out an objective comparison between the four leading PC loading factors and the daily local CWT in the study area. By combining the corresponding daily CWT with the four PCs we were able to compute, for each CWT, the statistical distribution of the PCs. The results are summarized in Fig. 7.4. Here, we call the four leading PC loading factors PC-CZD, PC-CMD, PC-OZD, and PC-OMD, respectively. The boxes in the figure show the lower, median, and upper quartile values, respectively. The whisker lines are also shown and are drawn to 1.5 times of the interquartile range. For the first PC (PC-CZD), the most striking result is the difference between the cyclonic (negative index for PC-CZD) and anticyclonic type (positive index for PC-CMD), which are in line with the results for the storm track in Iberia (Trigo, 2006; Garcia-Herrera et al., 2007) and the ones presented in Table 7.3. It is interesting to note that the CWT that are driven by the direction of flow tend to occur with a negative PC-CZD index. Due to the nature of the strong north-south gradient of the CZD pattern, the indices of the W and E types are opposite in sign.

The strong west-east gradient in the CMD pattern in the Iberian Peninsula influences some of the directional CWT; especially those from NE, E, SW and W, where an opposite distribution may clearly be seen (cf. NE and E vs. SW and W). There is no apparent difference between the cyclonic and anticyclonic types in the CMD pattern.

For PC-OZD, the only very clear point to note is, once again, the difference in sign between the cyclonic (positive index for PC-CZD) and anticyclonic type (negative index for PC-OZD). Given that the CZD and OZD share some common characteristics but are opposite in sign (see the description above) it is expected that their behaviors are similar.

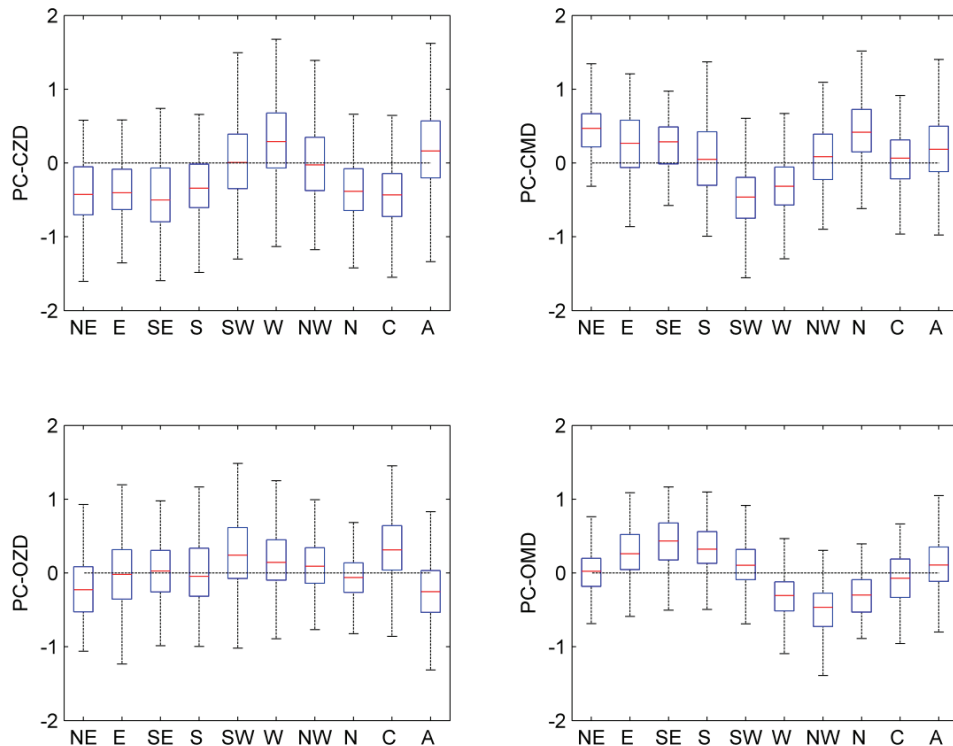


Figure 7.4. Distribution of the four corresponding PC indices for each circulation weather type. The boxes represent the lower, median, and upper quartile values. The whisker lines are drawn at a scale of 1.5 times the inter-quartile range.

Finally, the results for PC-OMD show an interesting symmetrical distribution between E, SE, S and W, NW, N, which is remarkably consistent with the meridional dipole of this pattern shown in Fig. 7.4. When the PC-OMD has a positive index the E, SE, S CWT are more common, and when PC-OMD has a negative index the W, NW, N CWT prevail.

7.5. Non-stationarity variability

In section 7.4, the four NAE sector leading modes that affect the European climate in winter were identified. Some studies have addressed the time variability of the effects of the modes. These works show that there are important changes in the relationship between atmospheric variables and these modes, in space as well as in time (Krichak and Alpert, 2005; Beranová and Huth, 2008; Vicente-Serrano and López-Moreno, 2008).

In order to identify the temporal changes in position and intensity of modes, over the whole NAE sector (30°N – 76°N and 37°W – 56°E), we used a moving window PCA technique with a 30-year period for the winter months (JFM), thus yielding 29 sub periods with 30 years long covering the years 1948-2005. Thus, the first period of analysis was 1948-1977 (centred on 1962) and the last period was 1976-2005 (centred on 1990). From each period considered, we obtained the explained variance for the four leading modes together with the EOF pattern and its corresponding PC.

The basic configuration of these modes remained the same, regardless of whether the analysis was stationary (section 7.4) or nonstationary (section 7.5). The dipoles remained the same, changing only in position or intensity (see below). We therefore use the same

terminology for the EOF patterns and the corresponding loading factors as in section 7.4.

The variance explained by each EOF over the period 1948-2004 for each 30-year window is represented in Fig. 7.5. The most striking result is an increase in the explained variance of EOF1 (the CZD) from 27% in the first window to 32% in the last, this being consistently the leading mode in each of the 30-year windows. This increase is most obvious between 1952-1981 and 1962-1991. It is also very interesting to note that at the beginning of the period of analysis the CMD represents the second largest total variance, but over time this variance reduces (accompanied by an increase in variance accounted for by the CZD). After the 1956-1985 window, there are also some changes in order of the second and third most explained variance between the CMD and the OZD. It is worth stating that after the 1962-1991 window, for the most part the OZD represents the second largest variance. The contribution of the OMD shows no significant change over the period of analysis.

Fig. 7.6 shows the four leading modes in the region represented, using six selected 30-year time windows (1951-1980, 1956-1985, 1961-1990, 1966-1995, 1971-2000 and 1976-2005). Furthermore, we also analyze changes in the intensity of these modes (Fig. 7.7). The intensity of the modes is given by doing the seasonal average (JFM) of the daily PCs of the modes. With this classical measure (time series of the PCA method) we can evaluate changes in the intensity of the modes and also the sign of the modes (Jolliffe, 2002). The most obvious result is the eastward shift in the position of the CZD, with the positive (negative) action centres being located in the Azores (Iceland) region at the beginning of the first 30-year window (1948-1977) and in southern Iberia (Scandinavia) in the last 30-year window (1976-2005).

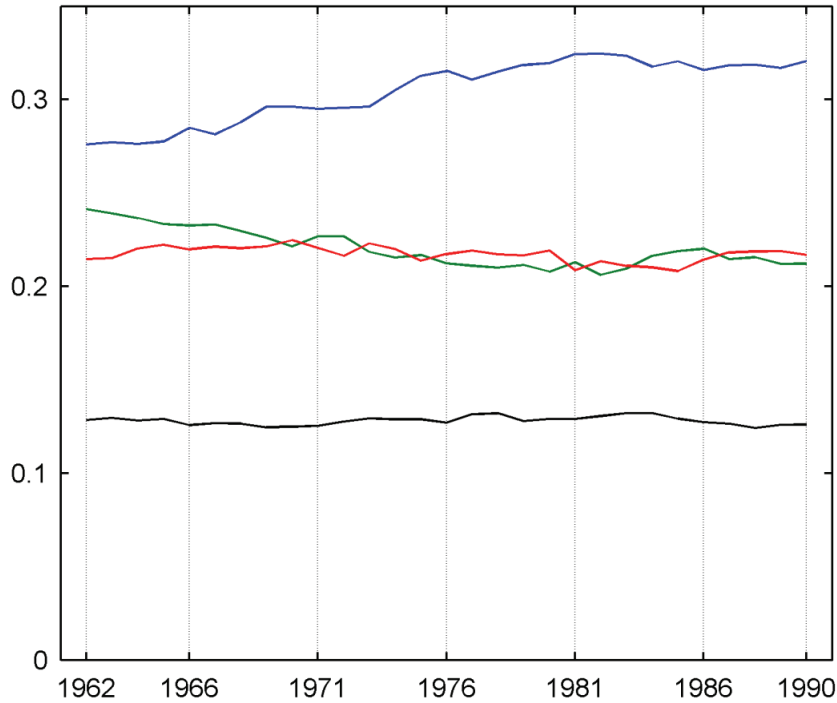


Figure 7.5. Variance explained by each EOF over time. The first analysis window is 1948-1977 (centred on 1962) and the last is 1976-2005 (centred on 1990). The CZD, CMD, OZD, and OMD are represented by the blue, green, red, and black lines, respectively.

These results are in line with those presented by Ulbrich and Christoph, (1999) and Vicente-Serrano and López-Moreno, (2008), who stated that the location of the NAO pattern undergoes multi-decadal changes. This change in the CZD is less pronounced prior to the 1966-1995 window, but more pronounced thereafter. This result seems to support the work done by Cassou et al., (2004) and Peterson et al., (2003), who stated that the NAO might experience a significant eastward displacement towards Europe when it is in its positive phase and a westward shift during its negative phase. Furthermore, alongside this pronounced shift in the position of the CZD, there is also a step increase (significant at a 95% level) in its intensity, which is pronounced in the last 20 years (Fig. 7.7).

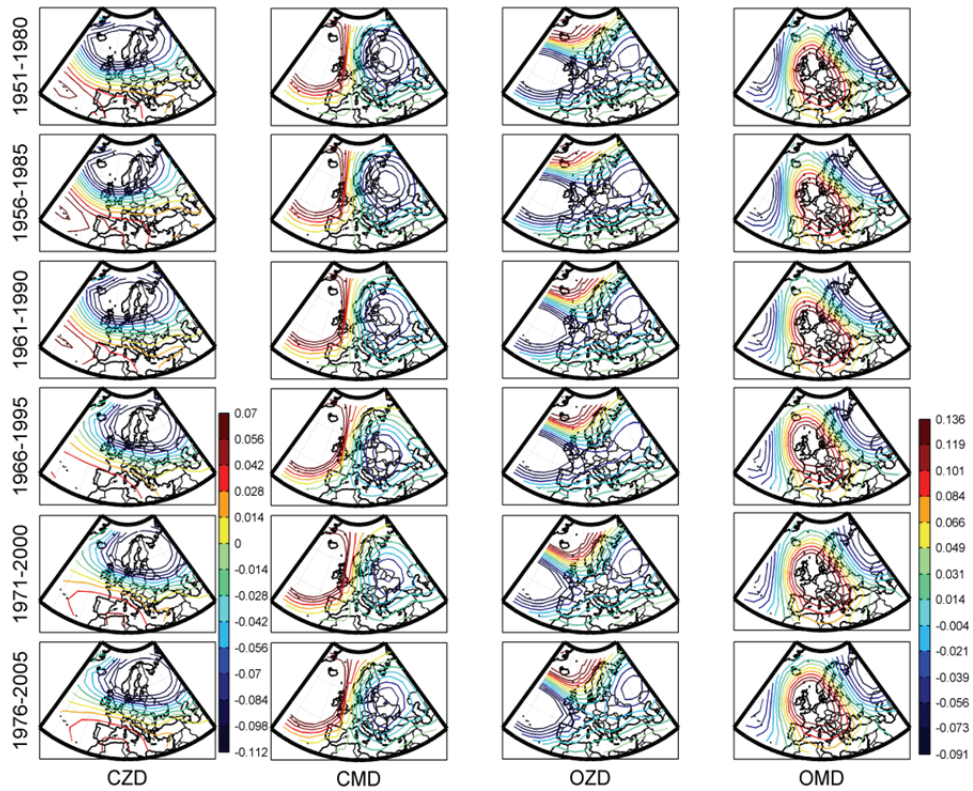


Figure 7.6. The first four leading EOF patterns for the winter months (JFM) obtained using a PCA on the SLP field using a 30-year moving window.

In the other modes (CMD, OZD, and OMD), there is no obvious shift in the positions of the dipoles. In reality, the OMD has three centres of action, with two negative centres to the west and east of central Europe, and a positive centre in central Europe, but because our area of interest is located in the western part of the region, we focus on the left side of these centres of action. In this case, it seems there is a very slight increase in the positive part of the tripole, pushing the left (negative) part of the tripole further west.

Despite the absence of any obvious shifts in the position of these modes (CMD, OZD and OMD), there are some interesting points to note in terms of the changes in their intensities (Fig. 7.7). For the intensities, we also determined whether changes described below are significant by

performing a t-student test. For all period the analysis the PC- CZD show an increase in their intensity significant at a 95% level. On the PC-CMD, there is almost any change in the intensity and signal. On the contrary, the PC-OZD shows an initial increment but in the final 3 decades there is a high decrease in the PC of this mode (significant at 95% level). Finally, the PC- OMD appears to have a very slight increase in intensity (not significant at a 95% level).

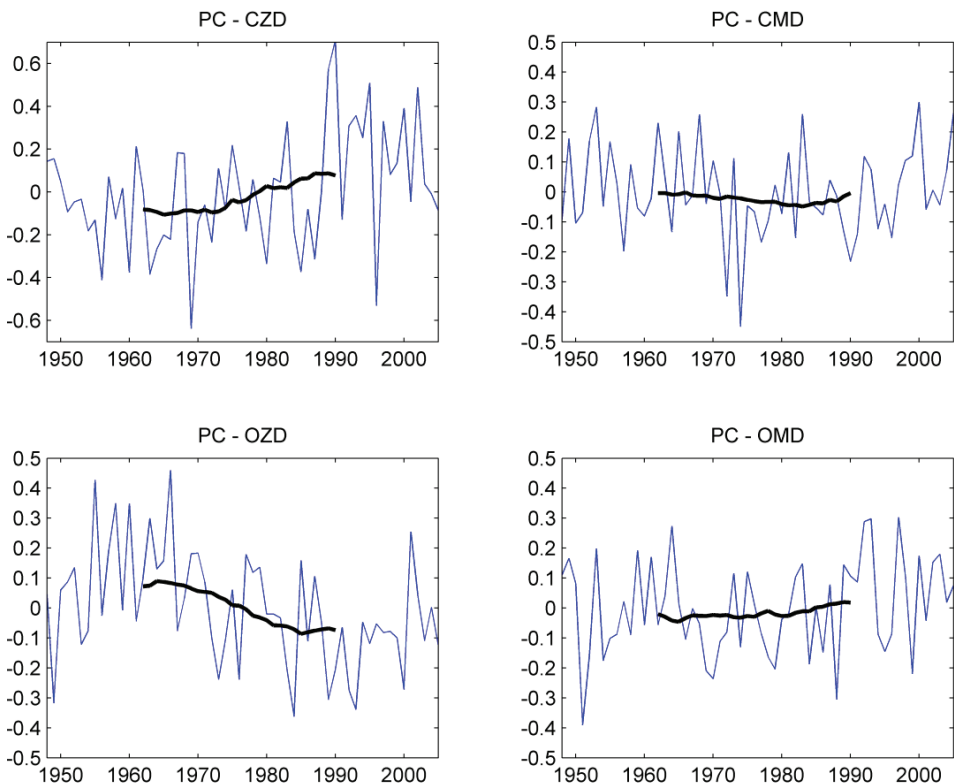


Figure 7.7. Intensity of the modes given by doing the seasonal average (JFM) of the daily PCs of the modes represented in Fig. 7.2 30-year moving average is also represented (black lines).

Having studied the changes in the position and intensity of the four NAE sector leading modes that affect Europe and our study area in particular, we wished to determine the effects of these changes on the local circulation patterns. In order to achieve this, we computed the correlation between the four leading principal components of the PCA (using the 29 30-year time windows) and the respective seasonal frequency of CWT (Fig. 7.8).

When we analyzed Fig. 7.1 the striking result was that there were CWT that in winter had low frequency, especially the ones on the 1st and 2nd quadrants (NE, E, SE, S, and N). Each of these types represents, in average, less than 5 days per winter, and so should be treated with caution, despite some significant changes being apparent. Therefore, we do not discuss them in this work. For the main changes in the correlation coefficients (SW, NW, and A types) we also computed a significance test (t-student for the linear trends and a Mann-Whitney test when a step change occurs).

The most frequent anticyclonic type (which produces virtually no rain in Galicia) and the next four most frequent CWT (SW, W, NW, and cyclonic) (which together explain almost all of the precipitation in Galicia (Lorenzo et al., 2008)), require further discussion. For the SW type, it may be seen that the correlation between the PC-OZD and the frequency of this circulation type is always positive, but starts to decrease linearly after 1970, changing over time from being significant to no significant. This change in the correlation coefficient is significant at a 95% level. Since there is no change in the position of this mode (OZD), this phenomenon may be attributed to changes in the intensity of its associated dipole. In fact, there is an increase in the intensity of this mode up to 1980 followed by a step decrease (Fig. 7.7). The OZD mode

7. Compatibility between modes of low-frequency and circulation weather types

in the Iberia Peninsula is characterized by a SW/NW flow (Fig. 7.6), depending of the signal of the intensity (positive/negative) of the mode. Therefore, it is expectable that the correlation between PC-OZD and the frequency of SW type decreases when the intensity of the OZD mode tends to negative values. For the other modes (CZD, CMD, and OMD), there are no obvious changes in the correlation.

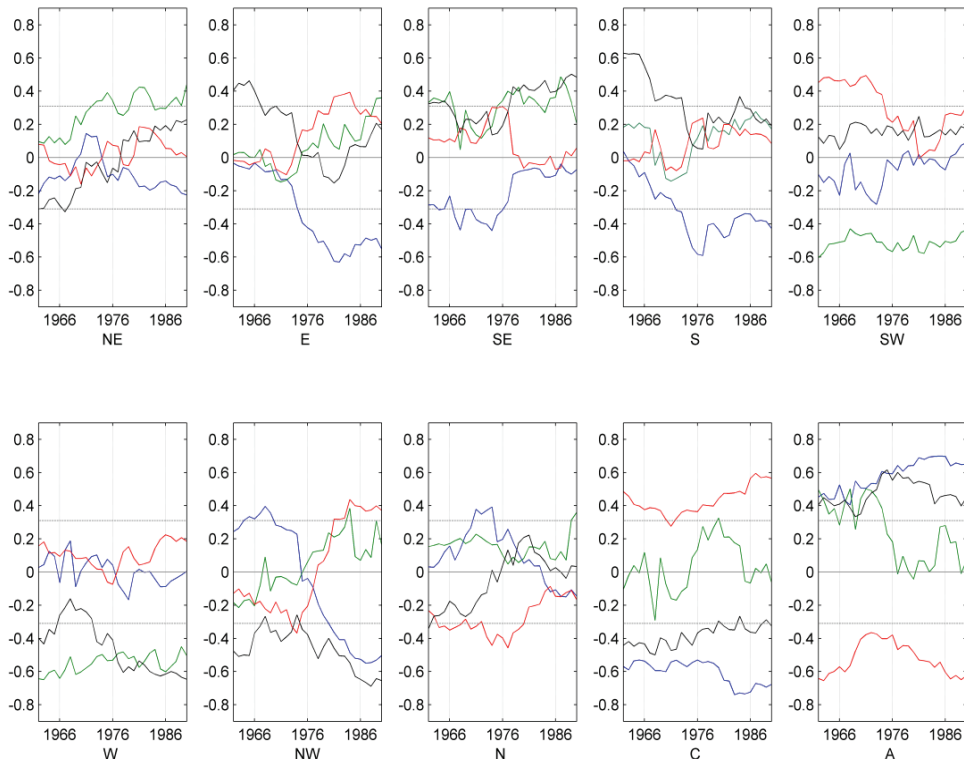


Figure 7.8. Correlation between the four principal loading factors and the winter frequency of the circulation weather types. The significance at the 95% level is also shown (dotted lines). The first analysis window is set as 1948-1977 (centred on 1962) and the last window is 1976-2005 (centred on 1990). Cyclonic and anticyclonic are denoted by C and A, respectively. The CZD, CMD, OZD, and OMD are represented by blue, green, red, and black lines respectively.

It may be seen that for the W type, there are no particular changes in the correlation with the EOF loading factors. The only exception to this is the decrease in the correlation with PC-OMD, with a minimum (non-significant correlation) at 1967. Over time, however, this correlation increases and is statistically significant for almost the entire period of analysis. In fact, it seems that changes in the intensity (towards positive values) of the OMD are correlated negatively with changes in the frequency of the W type.

For the NW type, there is a striking change in behaviour concerning PC-CZD (PC-OZD) where a positive (negative) correlation may be seen prior to 1976, with a negative (positive) correlation after 1976. Furthermore, the correlation in the final window seems to be more significant, with values greater than 95%. By comparing the NW type (Fig. 6.2) and the CZD in the first few time windows (Fig. 7.6), it may be seen that they are very similar. This could help to explain the significant positive correlation with the frequency of this CWT. Over time, the shift of the CZD towards Europe has a negative influence on the frequency with which this CWT occurs. In the case of the OZD, it seems that there is an increase in the intensity of this mode up to the 1965 alongside with a decrease in the correlation between PC-OZD and the frequency of the NW type. By the time there is a change in the intensity of the OZD (towards more negative values), the correlation between the frequency of the NW type and PC-OZD changes from negative values to positive values. In addition, these (trend) changes in the correlation coefficient are also significant at a 95% level. As we explained for the SW type (but with an opposite behavior in the NW type) it is expectable that, the correlation between PC-OZD and the frequency of NW type increases when the intensity of the OZD mode tends to negative values.

For the cyclonic type, an increase of the anti-correlation (significant in all periods of analysis) with PC-CZD may be observed for the last 15 time windows. This is most probably derived from the eastward shift (especially at that time) of the position of the first mode (Fig. 7.6), blocking the storm track in the region. Furthermore, there is a slight increase in the correlation (always significant) with PC-OZD after 1967. The (significant) anti-correlation between the cyclonic type and PC-OMD shows a slight decrease over the whole period.

Focusing on the correlation between the frequency of anticyclonic type and the EOF loadings, there is a strong resemblance between the correlation for this circulation type and PC-CZD and PC-OZD (but with the opposite sign). With the eastward shift of the CZD centre of action close to the region, its influence increases, not only on the cyclonic type but also on the anticyclonic type, as the results seem to indicate. There is also an interesting result for the CMD mode, with a decreasing correlation with the anticyclonic type (an important decrease in the correlation coefficient significant at a 95% level). It is interesting to note that the curve of correlation between the PC-CMD and the frequency of anticyclonic circulation are alike to the curve of the CMD intensity.

7.6. Summary

The compatibility between hemispheric modes and modes in NAE sector has been described, by using the local circulation regimes of a specific study area, namely those found in the North West Iberian Peninsula for winter months (JFM). Evidence was provided that the modes computed using the SLP field or the H500 field are very alike in this spatial window. The results show that there is a high degree of

coherence between the modes derived from a statistical approach (using PCA) and the real physical circulations (as represented by the CWT). This coherence was obtained not only when we used stationary modes, but also with nonstationary ones. The use of a PCA approach using continuous time windows has enabled us to assess whether changes in the intensity or position of these modes could influence the local circulation. The results confirm that changes in both the position and the intensity of the modes tend to favour the occurrence of some CWT in preference to others. Again, these changes are coherent and consistent.

The most important results are as follows:

- Correlation coefficients obtained between hemispheric modes and the frequencies of 10 CWT during winter show that the NAO pattern yields the greatest correlation with the cyclonic and anticyclonic type, these types being responsible for higher and lower precipitation in the Iberian Peninsula, respectively. The EA pattern has a significantly high correlation with the SW circulation type. The EA/WR pattern shows a significant correlation with the W and the NW types. Finally, the SCA pattern exhibits the opposite behaviour from the NAO, with a negative correlation with the anticyclonic type and a positive correlation with the cyclonic. It is interesting to note that these types occur at a high frequency during winter (more than 60% of the total frequency).
- By studying the compatibility between local circulation type classification and modes in NAE sector, we found that, for the winter months (JMF), the zonal dipoles (Continental and Ocean) have a major influence, not only on the occurrence of the cyclonic and anticyclonic type, but also on the zonal types. As expected, the meridional dipoles influence the CWT that are related to meridional circulations, such as the E and W CWT.

- Changes in the position and intensity of modes over the last 50 years have influenced the local circulation in our study area. There is an increase in the explained variance of the continental zonal dipole from 27% in the first time window to 32% in the final one. There is also an eastward shift in the position of this mode, which is in agreement with the findings of Ulbrich and Christoph, (1999) and Vicente-Serrano and López-Moreno, (2008), along with an increase in its intensity. For the other modes, namely the ocean zonal dipole and the two meridional ones, no obvious shifts in their positions were found.

In summary, relationships between the real physical local circulations (as represented by CWT) and the modes obtained from statistical analysis have been identified. Changes in the positions and intensities of these modes have an impact on the local circulation (here assessed by the CWT) for our target area. The increase in explained variance of the continental zonal dipole and the increasing negative (positive) correlation between this mode and the cyclonic (anticyclonic) type can help to explain the overall decrease of precipitation in winter (Paredes et al., 2006; Trigo et al., 2008) in the study region.

8. Trends in present and future circulation weather type frequency in the northwest Iberian Peninsula

8.1. Introduction

The findings of recent studies have shown that the North Atlantic-European (NAE) sector is characterized by significant climate trends that occur over different timescales (IPCC, 2007; Trigo et al., 2008; Gomez-Gesteira et al., 2011).

As mentioned in the previous chapters, circulation weather types (CWTs) reflect the atmospheric circulation that is specific to a given region. Moreover, changes in the frequency of occurrence of CWTs often result in changes in climatic variables at the earth's surface; variables such as precipitation (e.g., Goodness and Jones, 2002; Hope et al., 2006; Fowler and Kilsby, 2002) or temperature (e.g., Cahynova and Huth, 2009). Furthermore, as studied in chapter 7, the frequency of CWTs is sensitive to the low-frequency variability modes, and vice versa. In this

way, changes in intensity or shifts in the position of the low-frequency variability modes are related to changes in the local circulation, (i.e., the circulation or CWT) (Ramos et al., 2010).

The use of CWTs can also be a useful tool in validating the control simulations of coupled general circulation models (CGCMs), in assessing the accuracy of the CGCMs, and in analyzing changes in CWTs under future climate change scenarios. Despite this, very few studies have compared the ability of GCMs to replicate historical circulation patterns. Hulme et al., (1993) analyzed two CGCM control simulations to evaluate if they were able to reproduce the Lamb, (1972) CWT in the UK. Demuzere et al., (2008a) carried out a similar study to analyze present and future ECHAM5 pressure fields using the Lamb (Lamb, 1972) CWT for Belgium. Using a different approach, Schoof and Pryor, (2006) used the Kirchhofer correlation-based map method to evaluate the ability of two GCMs in reproducing 500-hPa map pattern frequencies over the Midwestern US, for the 1990-2001 period. A similar study was conducted by Anagnostopoulou et al. (2008), in which they evaluated the capability of the HadAM3P to reproduce the mean CWT pattern and frequency over Europe and the Mediterranean region, in terms of the 500 hPa geopotential height fields and the 1000-500 hPa thickness fields. Huth, (2000) tried a different approach, using a modification of the T-mode principal component analysis as a classification method; this classification procedure was applied to reanalyze (Kalnay et al., 1996) daily 500 hPa geopotential height pattern data, and data simulated by the control ECHAM3 GCM runs.

The main purpose of the study described herein was to investigate changes in the frequency of the Lamb circulation weather affecting the northwest (NW) Iberian Peninsula, not only in the present

climate but also in future climate change scenarios; this was achieved using the output from several of the CGCMs used throughout the IPCC Fourth Assessment Report (4AR).

The remainder of this chapter is organized as follows: In section 8.2, a comprehensive description of the methodology is given. In section 8.3, the trends in CWTs over the last 60 years will be studied. In section 8.4 an evaluation of the GCMs for the present climate is made, while in section 8.5 the changes in the frequency of the CWTs in the 21st century are studied. Finally, section 8.6 presents the conclusions.

8.2. Methodology

As mentioned previously, the CWTs used in this work were computed using the procedure specified by Lamb (Lamb, 1972; Jones et al., 1993), in which the method was applied to the NW Iberian Peninsula (Galician area). In this chapter, two different SLP datasets were used to compute the CWT:

- a) The National Center for Environmental Prediction/National Center for Atmospheric Research (NCEP/NCAR) reanalysis data (Kalnay, 1996; chapter 5) ($2.5^{\circ} \times 2.5^{\circ}$ longitude-latitude) of the daily mean SLP for the period January 1948 - December 2008. The use of this period of time not only allowed the study of recent trends in CWTs, but also allowed a comparison with the output of the CGCMs models for the present climate (1961-1999 period); in performing this comparison, we evaluated these models.
- b) The data used were taken from three models that were studied in the IPCC 4AR; these were the IPSL climate system model (IPSL-CM4), the 5th generation of the ECHAM general circulation model (ECHAM5/MPI-OM) and the CCSM3, NCAR Community

Climate System Model 3.0 from the USA (chapter 5). The choice of these models was determined mainly by the availability of daily data, but the use of more than one GCM simulation also conferred greater reliability when the uncertainties were quantified. Daily sea level pressure (SLP) data from the three climate models, and from three different forcing simulations B1, A1B and A2, were obtained from the WCRP CMIP3 multi-model database (<https://esg.llnl.gov>).

The climatological normal period used in the 20th century was the period 1961-1999. For the 21st century, the coincidental temporal resolution availability of daily data for the 3 models allowed us to analyze two periods, the first between 2046 and 2065 and the second between 2081 and 2100.

To compute the CWTs, daily SLP data from a $2.5^{\circ} \times 2.5^{\circ}$ longitude-latitude regular grid was required. The points under consideration were located between $35\text{--}55^{\circ}\text{N}$ and $25^{\circ}\text{W}\text{--}5^{\circ}\text{E}$ (chapter 6). Since the daily SLP data from the CGCMs were on different spatial scales, the SLP fields for the different CGCMs simulations were interpolated (using a bicubic interpolation) to obtain a set of regular $2.5^{\circ} \times 2.5^{\circ}$ grids, which were then used to compute the CWTs for the different CGCMs and the different time periods.

The method used in the work described in this chapter was applied as follows:

- 1) Computation of the CWTs for the NW Iberian Peninsula for the 1948-2008 period, using the NCEP/NCAR reanalysis;
- 2) Evaluation of the GCMs mean seasonal SLP fields, achieved by comparing them with the NCEP/NCAR reanalysis SLP fields for the present climate (1961-1999 period);

3) Objective comparison of the ability of the GCMs simulations to reproduce the mean frequency of the CWTs for the present climate with the results obtained when using the NCEP/NCAR reanalysis.

4) Removal of the systematic seasonal errors that were observed in the SLP mean fields of each model. For this purpose, for each grid point, the seasonal mean bias—i.e., the difference between the mean seasonal SLP values obtained from the CGCMs and those obtained from the NCEP/NCAR data—was computed. The new daily fields of the CGCMs were then computed by removing the corresponding grid point seasonal bias for each model in the daily fields.

5) Computation of the mean CWT frequency using the new CGCM daily adjusted SLP fields for the present climate, and comparison of these results with those obtained using the NCEP/NCAR reanalysis; this comparison showed if there was any improvement in the quality of the GCM SLP fields.

6) Computation of the mean frequency of the CWTs for future CGCM scenarios (in the 2046-2065 and 2081-2100 periods), and comparison with the mean CWT frequency obtained using present CGCM simulations.

The Mann-Kendall trend test (Mann, 1945; Kendall, 1975; Santos and Leite, 2009) was applied to analyze the significance of the trends. This non-parametric test uses a correlation between the ranks of a time series and their time order, and it has been widely applied to the time series of environmental data (Hipel, 2005).

8.3. Trends in circulation weather types in the 20th century

The Jones et al. (1993) procedure was adopted, thereby maintaining the 10 main CWTs (NE, E, SE, S, SW, W, NW, N, anticyclonic (A) and cyclonic (C)) for the NW Iberian Peninsula, relative to the 1948-2008 period, using the NCEP/NCAR reanalysis dataset. The relative frequency of each synoptic CWT for each season is shown in Fig. 6.3.

The mean CWT frequency was computed for each season, for the period 1948-2008. Linear trends were obtained, taking into account not only the entire period of analysis, but also the two sub-periods 1948-1975 and 1976-2008. The year 1975 coincides approximately with a general change in circulation in the Northern Hemisphere (Trenberth, 1990; Karl et al., 2000). The Mann-Kendall test was applied to analyze the significance of the trends.

Only those results that were significant to at least a 95% level are shown in Table 8.1. One can see that for the entire 1948-2008 period, significant trends were only observed in winter and summer. Winter was characterized by a decrease in the frequency of the NW type, whereas in summer there was an increase in the frequency of the SW and C types.

When treated separately, the significant trends in each period were more frequent, particularly in the second period. In summer and autumn, an increase in the N type was observed in the first period (1948-1975), but this trend did not continue into the second period (after 1975).

Table 8.1. Linear trends (percentage/year) for the different circulation weather types computed using the NCEP/NCAR reanalysis SLP field for the three periods studied; only results that were significant (Mann-Kendall rank test) at the **99% or *95% level are shown.

	1948-2008	1948-1975	1976-2008
Winter	NW *-0.059		C *-0.187
			A *0.361
Spring			SW *0.113
			N**-0.154
Summer	SW ** 0.060	N *0.144	
	C *0.083		
Autumn		N **0.114	NE *0.1633

In the first period (1948-1975), no trends were observed for types C and A, but in the second period (1976-2008) there was a clear increase in type A and decrease in type C for the winter months. Analysis of the second period revealed an increase in the frequency of the SW and a decrease in the frequency of the N types in spring. This could be related to the observed upward trend in the maximum and minimum temperatures in this period, especially in spring, where the maximum temperature values increased at an average rate of approximately 1.0°C per decade (Gomez-Gesteira et al., 2011). Finally, an increase in the frequency of the NE type was again observed in autumn in the second period.

8.4. Evaluation of the CGCM models

8.4.1 Evaluation using SLP fields

Before analyzing the changes in the frequency of the CWTs for the 21st century, the mean SLP fields of the three models were evaluated for each season, using the NCEP/NCAR reanalysis data obtained between 1961 and 1999 (DJF, MAM, JJA and SON). Fig. 8.1 shows the seasonal mean SLP fields obtained from the reanalysis data, as well as

the differences between the mean seasonal SLP from the two datasets (reanalysis data and GCMs). It was generally the case that the CCSM3 model produced the highest discrepancy, in all four seasons. This model reproduced SLP values that were too low at high latitudes and too high at mid latitudes, which led to strong modeled westerlies over the North Atlantic. The IPSL reproduced SLP values that were too high in the Mediterranean in winter, spring and autumn, while in the summer there was a high SLP anomaly in the Iceland region. The ECHAM5 model reproduced SLP patterns that were closest to the reanalysed data.

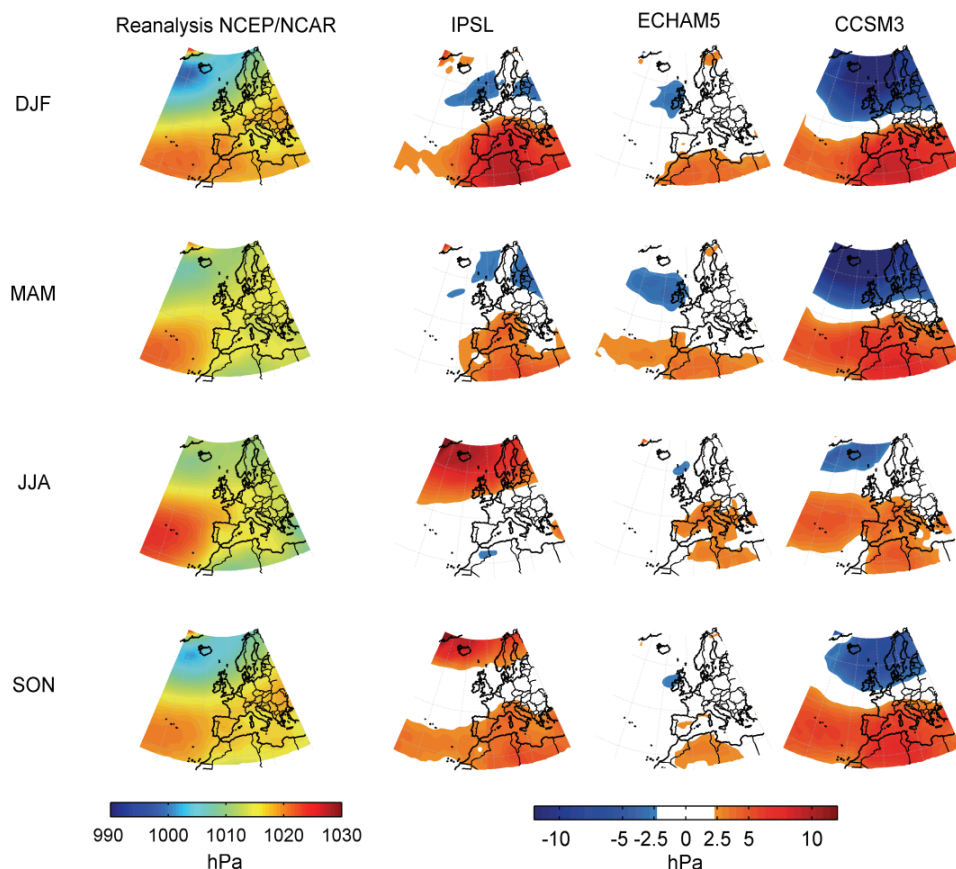


Figure 8.1. Mean seasonal SLP differences for the 1961-1999 period. The first column shows the seasonal mean SLP during the 1961-1999 period, using the NCEP/NCAR reanalysis data. The next columns show the difference between the mean SLP from the three models (IPSL, ECHAM5, CCSM3 respectively) and the mean SLP from the NCEP/NCAR reanalysis during the period 1961-1999.

8.4.2 Evaluation using circulation weather types

After evaluating the mean SLP fields produced by the three models (that used the NCEP/NCAR reanalysis data), the CWTs for the control simulations for the late 20th century and the 21st century were computed, using the three CGCMs, and applying the same methodology as that described in section 6.2.

The frequency of the CWTs in the CGCMs was then compared objectively with the ones obtained previously using the NCEP/NCAR reanalysis data for the 1961-1999 period. As mentioned before, the SLP fields of the CGCMs were interpolated to obtain a set of regular $2.5^\circ \times 2.5^\circ$ grids, which were then used to compute the CWTs. Tables 8.2 to 8.5 (original SLP data columns) show the percentage frequency differences between the results obtained from the CGCMs and those obtained from the NCEP/NCAR reanalysis data, for the different seasons; winter (Table 8.2), spring (Table 8.3), summer (Table 8.4) and autumn (Table 8.5). The differences that were significant at a 5% level—as determined using a Wilcoxon rank sum test—are shown in bold. The results showed that the ECHAM5 model provided the best agreement when compared with the reanalysis data; it showed differences of less than 5% in frequency per type, except in summer, where the model showed a frequency that was higher than the actual one for type A by 10%. This result was not unexpected, because the ECHAM5 model was the one that offered the lowest differences in the mean field (Fig. 8.1).

On the other hand, the CCSM3 model produced the highest frequency bias in the majority of cases, with differences of up to 20% in the frequency of the W type. This disagreement could be explained by the fact that this model overestimates the magnitude of the westerlies at mid-latitudes (vanUlden and van Oldenborgh, 2006 and Fig. 8.2).

The IPSL model showed the greatest differences in summer, when the high positive anomalies in the SLP values at high latitudes led to a decrease in the frequency of type A and an increase in the frequency of type NE over the NW of the Iberian Peninsula. For winter, this model showed a decrease in the frequency of type A, but an increase in the frequency of types SW and W; the reason for this was connected to the SLP anomalies illustrated in Fig. 8.2, in which it is possible to observe an eastward displacement of high and low pressures at high latitudes.

Table 8.2. Differences (%) in the mean frequency of the circulation weather types for each season between the output of the IPSL, ECHAM5 and CCSM3 and the NCEP/NCAR reanalysis data, for the 1961-1999 period, when using the original SLP data and the corrected SLP data. The differences that were significant at a 95% level (Wilcoxon rank sum test) are shown in bold.

Winter	ORIGINAL SLP DATA			CORRECTED SLP DATA		
	IPSL	ECHAM5	CCSM3	IPSL	ECHAM5	CCSM3
WT	-2.71	-1.32	-2.74	-1.38	-0.14	-0.77
NE	-2.36	-1.35	-3.32	-0.69	-0.76	-0.83
E	-2.58	-1.28	-3.17	-1.41	-0.24	-1.68
SE	-1.84	-0.88	-3.53	-0.08	0.21	-1.00
SW	13.25	2.83	3.95	0.94	-0.54	-1.88
W	10.83	5.92	22.10	0.70	-0.27	0.76
NW	-1.20	2.06	1.78	1.41	1.44	3.72
N	-1.63	0.32	-1.47	0.74	1.03	0.91
C	-2.65	3.19	-4.81	0.52	1.90	-1.13
A	-9.12	-9.50	-8.79	-0.75	-2.63	1.90

Table 8.3. The same as Table 8.2, but for spring.

Spring	ORIGINAL SLP DATA			CORRECTED SLP DATA		
	IPSL	ECHAM5	CCSM3	IPSL	ECHAM5	CCSM3
WT	-3.53	-4.63	-6.97	0.44	-1.39	-1.56
NE	-1.63	-2.32	-4.54	0.37	1.05	-0.08
E	-0.13	0.01	-1.74	0.43	0.67	-0.18
SE	-1.37	-1.58	-4.26	-1.17	0.62	-0.80
SW	3.38	5.37	4.11	0.12	1.17	-0.01
W	5.93	8.36	21.15	0.48	-1.49	3.33
NW	-1.07	1.21	1.97	-1.03	-0.62	1.80
N	-0.71	-1.89	-3.88	0.88	-0.97	-1.04
C	-2.13	0.41	-7.76	-1.23	0.56	-0.69
A	1.26	-4.94	1.93	0.70	0.40	-0.77

Table 8.4. The same as Table 8.2, but for summer.

Summer	ORIGINAL SLP DATA			CORRECTED SLP DATA		
	IPSL	ECHAM5	CCSM3	IPSL	ECHAM5	CCSM3
WT	13.32	-6.14	-3.68	1.94	-1.38	-1.92
NE	13.32	-6.14	-3.68	1.94	-1.38	-1.92
E	-2.52	-1.69	-1.31	-2.52	-0.18	-0.05
SE	-0.47	0.76	0.00	-0.31	1.15	0.53
S	-1.40	-0.44	-1.04	-1.24	0.27	-0.19
SW	-2.79	0.13	-2.74	-0.87	-0.52	-1.78
W	-5.29	3.02	0.02	-2.41	-0.46	0.81
NW	-0.27	1.06	1.09	0.45	1.33	1.93
N	11.83	-3.89	-1.69	5.16	-1.63	-0.66
C	3.44	-3.59	-3.36	-0.87	-1.19	0.08
A	-15.86	10.78	12.72	0.68	2.61	1.25

Table 8.5. The same as Table 8.2, but for autumn.

Autumn	ORIGINAL SLP DATA			CORRECTED SLP DATA		
	IPSL	ECHAM5	CCSM3	IPSL	ECHAM5	CCSM3
WT	1.25	-1.39	-2.85	5.21	0.90	0.34
NE	1.25	-1.39	-2.85	5.21	0.90	0.34
E	-1.22	-1.36	-3.16	0.35	-0.21	-0.04
SE	-2.39	-1.67	-2.98	-2.13	-0.83	-1.04
S	-1.95	-0.86	-3.22	-0.70	0.35	0.26
SW	4.99	2.34	2.65	1.23	0.67	1.00
W	7.24	3.09	14.33	0.41	-0.15	-0.81
NW	-0.10	2.05	3.54	-1.54	2.32	1.09
N	0.25	-0.23	-1.50	0.19	0.27	-0.48
C	-1.03	-1.54	-5.82	-3.16	1.78	-1.61
A	-7.04	-0.44	-1.01	0.15	-5.10	1.30

The CWT classification obtained herein, which made use of the Lamb CWT (Jones and Hulme, 1993), was applied to the SLP field. For this purpose, the CWTs—this time without the corresponding systematic seasonal errors that were observed in the SLP field for each model—were computed for each model, following the procedure of Demuzere et al., (2008a), as described in the Methodology section (section 8.2.)

The results obtained using this correction illustrated the improvement that can be achieved using this method. Tables 8.2 to 8.5 (corrected SLP data columns) show the differences in the mean

frequency of the CWTs between the three models and the NCEP/NCAR reanalysis data (for the 1961-1999 period), for each season; the corrected CGCM SLP data used is also shown. A comparison of the results presented in Tables 8.2 to 8.5—that is, the original SLP data vs the corrected SLP data columns—showed that the differences between the CWT frequency obtained for the CGCMs and the reanalysis data were rather lower when the correction was applied, the differences being less than 95% in the majority of cases. The differences that were significant at a 95% level (evaluated using a Wilcoxon rank sum test) are shown in bold. It was therefore possible to conclude that the differences between the CWT frequencies from the models and the NCEP/NCAR reanalysis were mainly due to the seasonal mean bias.

8.5. Changes in the frequency of circulation weather types in the 21st century

The changes in the frequency of the CWTs were computed for each of the three scenarios A1B, B1 and A2, and the differences between the respective control runs and the two periods 2046-2065 and 2081-2100 were determined, using all three models.

For all of the models, the major differences were observed to be between the control run (1961-1999) and the 2081-2100 period. Regarding the 2046-2065 period, there were no differences in the frequency greater than 6%. Because of this, only the second period was analyzed. The differences in the second period (2081-2100) were greater, particularly in scenarios A1B and A2. Figs. 8.2 to 8.4 show the changes in the frequency of the CWTs during the 2081-2100 period compared with those for the 1961-1999 period, for the three different SRES scenarios.

Only those changes that were significant at a 95% level or greater are discussed.

Scenario A1B (Fig. 8.2) led to significant changes in all seasons; in winter, the frequency of type C decreased in the ECHAM5 and CCSM3 models. This would result in a decrease in precipitation in the region, because type C is one of the types most responsible for winter rainfall over the NW of the Iberian Peninsula (Lorenzo et al., 2008; chapter 6). In spring, there was an increase in the frequency of type A in the ECHAM5 and CCSM3 models.

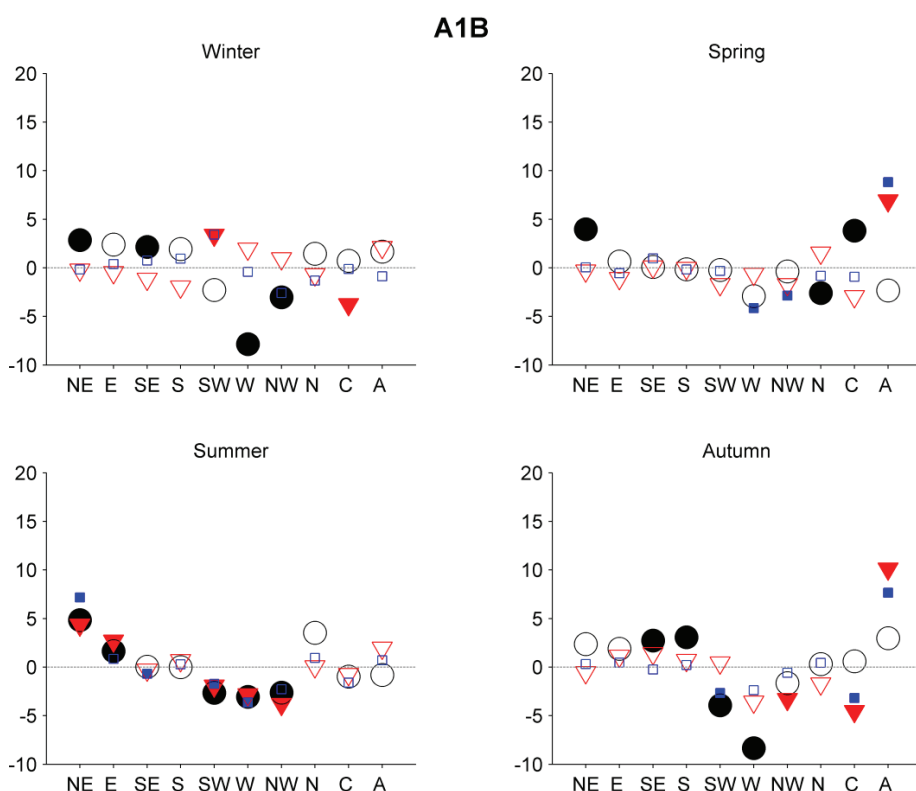


Figure 8.2. Projected seasonal mean frequency of the circulation weather types changes (%) for the late 21st century (2081-2100), in the scenario A1B. The mean frequency of the circulation weather types are shown relative to the 1961-1999 period (IPSL, black circle, ECHAM5, red triangle and CCSM3, blue square). The filled symbols show the differences that were significant at a level of 0.05, as determined using a Wilcoxon rank sum test. The seasons were defined as follows; winter (DJF), spring (MAM), summer (JJA) and autumn (SON).

In summer, all models showed an increase in the frequency of type NE, and a decrease in the frequency of types SW and W. Furthermore, in two out of the three models, an increase in the frequency of type E was observed, along with a decrease in the frequency of the NW types. The picture as a whole showed a general intensification of the easterlies, compared with the westerlies. Finally, under this scenario, the autumn results showed a significant decrease in the frequency of types SW, W and C, and a significant increase in type A; this would result in a decrease in precipitation, because all of these types are linked with precipitation in the region (Gomez-Gesteira et al., 2011).

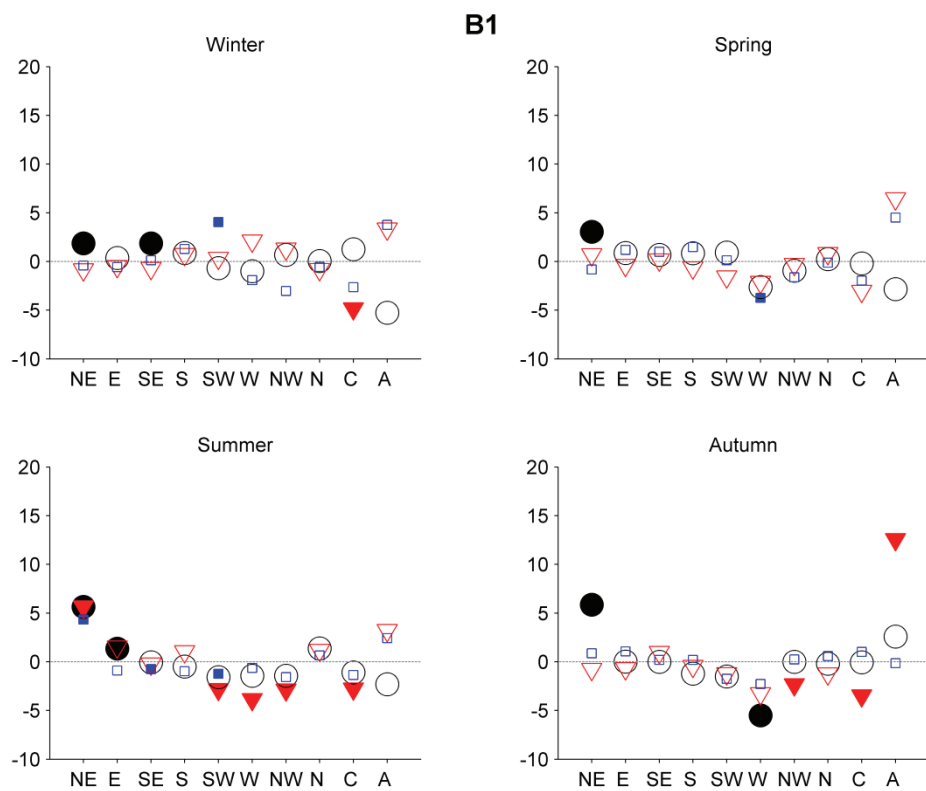


Figure 8.3. The same as Fig. 8.2, but for the SRES B1 scenario.

Under scenario B1 (Fig. 8.3), in general, no significant changes were seen relative to the 1961-1999 period. It was only in summer that we observed a significant change for the three models ($\alpha=0.05$), with an increase in the frequency of the NE types and a decrease in the frequency of the SW types, in both ECHAM5 and CCSM3.

As expected, scenario A2 (Fig. 8.4) was associated with the greatest set of changes. In this case, the models (IPSL in particular) seemed to show different behavior in winter and spring. The CCSM3 and ECHAM5 models showed an increase in the frequency of type A and a decrease in the frequency of type C. The three models were in agreement regarding the projected decrease in type C in spring. In summer, all three models also projected an intensification of the easterlies, with a general increase in the frequency of the NE types and a decrease in the frequency of the SW, W and NW types. Finally, in autumn there was a decrease in the frequency of types W and C and an increase in the frequency of type A, as projected by at least two of the models.

The general trend described a decrease in the C and SE types in spring, summer and autumn. For the autumn, a significant increase in the A type was observed. Furthermore, in summer, the changes in the frequency of different CWTs showed an intensification of the easterlies compared with the westerlies. In winter, the frequency of type C decreased and the frequency of type A increased.

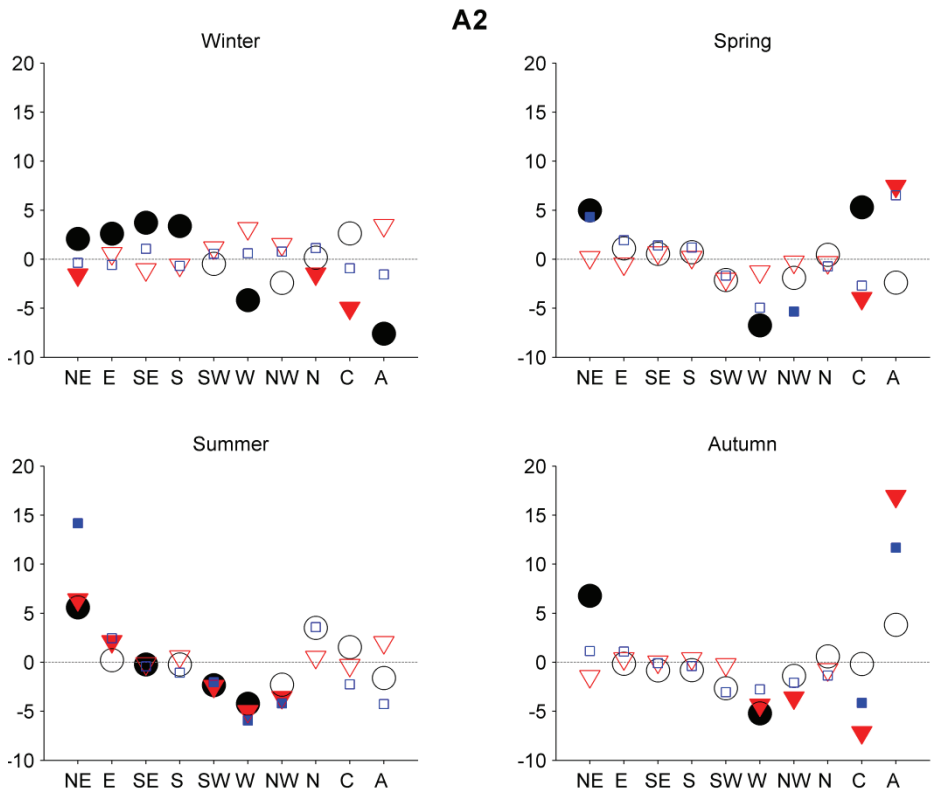


Figure 8.4. The same as Fig. 8.2, but for the SRES A2 scenario.

8.6. Summary

In recent years, few studies have investigated the ability of CGCMs to reproduce circulation weather patterns. In this chapter, CWTs are used to evaluate the ability of CGCMs to reproduce the present mean frequency of the CWT over the NW Iberian Peninsula, and to study projection scenarios to find changes in the CWT variability in the 21st century. The procedure of Demuzere et al., (2008a) was used to compute the CWTs for each of the GCMs; that is, the corresponding systematic seasonal errors observed in the SLP field of each model for the present climate were omitted. The results obtained showed significant improvement when the systematic errors were removed from the SLP fields; the differences between the CWT frequencies from the

models and the reanalysis data were smaller than those in the results with no SLP corrections applied. It was therefore found that, in most cases, the discrepancies between the CWTs from the models and the reanalysis could be explained by the seasonal mean bias. On the other hand, the frequency of different CWTs in a given area gives information valuable for the assessment of climate change.

The most important results were as follows:

- Trends in CWTs in the NW Iberian Peninsula were analyzed for the 20th Century. In the second period (1976-2008) of the analysis, there was a clear increase in type A and decrease in type C for the winter months, suggesting a relationship between the positive phase of the NAO (Lorenzo et al., 2008), and its eastward displacement towards Europe that has taken place over the last 20 years (Ramos et al., 2010; Cassou et al., 2004).
- The CWTs were computed for each model without the corresponding systematic seasonal errors that were observed in the SLP field of each model. The results obtained using this correction showed some improvement, in that the differences between the mean CWT frequencies from the models and the reanalysis data were smaller than in the results in which no SLP correction had been applied.
- The changes in the mean CWT frequency for the 21st century were analyzed. Small changes (most of them less than 6% significant) in the frequency of the types were found for the 2046-2065 period, while the differences in the second period (2081-2100) were greater, particularly in scenarios A1B and A2. In summary, for the second period, results for all scenarios seemed to show a decrease for types Cyclonic, W and SW, in spring and summer. This change was larger for scenario A2. Based on the relationship between the different CWTs and

the precipitation in the Galicia region for the present climate (Gomez-Gesteira et al., 2011; Lorenzo et al., 2008), one can make the assumption that there will be dry conditions in these seasons. These results were in agreement with previous studies of precipitation in future scenarios (Lopez-Moreno et al., 2009; Giorgi and Lionello, 2008). For autumn, we may also assume dryer conditions, based on the expected decrease in types W and Cyclonic, and an increase in the Anticyclonic type. This behavior was in agreement with the expected increase in the NAO index toward the end of the 21st century for those scenarios (Stephenson et al., 2006).

9. A new circulation weather type classification based upon Lagrangian air trajectories

9.1. Introduction

The relationship between circulation weather types (CWT) and surface climate gained a lot of interest in the last decades as mentioned several times during this work and also studied here for the target region.

Traditionally, CWT are specific to a certain region and result from the examination of gridded synoptic weather data - typically based on SLP or geopotential height (usually at 500hPa). Since these types are based on one time instance of SLP or H500, they are called Eulerian classifications.

The analysis of trajectories approaching a target region provides an alternative possibility of studying CWT (e.g., Stohl and Scheifinger, 1994; Jorba et al., 2004; Nyanganyura et al., 2008). For such applications, Lagrangian models are used to divide the atmosphere into a set of air parcels moving according to the three-dimensional winds (Stohl, 1998;

Stohl et al., 2001). The path followed by the air parcels, i.e. the trajectory, accurately characterizes the history of the air streams arriving at a specific site. Trajectory analyses are commonly used in air quality studies and are typically based on cluster analysis for large sets of trajectories (e.g., Dorling et al., 1992a; Riccio et al., 2007). Most of these studies only rely on the position (latitude, longitude and height) of the air parcels. If, in addition considering specific humidity along the trajectories, they can also be used to study atmospheric moisture transport by tracking air parcels moving into a given area (James et al., 2004; Nieto et al., 2006; Gimeno et al., 2010) or to identify moisture sources for precipitation events (Sodemann et al., 2008). Trajectory analysis has also been very fruitful for the examination of meteorological phenomena like warm conveyor belts and tropical moisture export (e.g., Wernli and Davies, 1997; Stohl, 2001; Eckhardt et al., 2004; Knippertz and Wernli, 2010).

In this chapter, a new classification method of the synoptic-scale circulation is presented. It is based on the analysis of backward trajectories (see section 5.6) and determines for each day at 12 UTC the representative flow for the target region (Northwest Iberian Peninsula). The new method is then compared to an automated version of the Eulerian Lamb classification (Lamb, 1972; Jones et al., 1993). Additionally, the relationship between CWT and precipitation is analysed in order to investigate if the new method is able to distinguish different precipitation characteristics. Several case studies (see section 5.7) will be presented in order to illustrate and validate the method. The case studies embrace different synoptic patterns that typically affect the Northwest Iberia Peninsula such as: cold front, cut off low, high precipitation event, coldwave, heatwave and blocking event.

The remainder of this chapter is organized as follows: section 9.2, the new CWT classification based on Lagrangian backward trajectories is described. The usefulness of the proposed methodology is investigated with several case studies in section 9.3 and compared with the Lamb circulation in section 9.4. A climatological assessment of the trajectory types is discussed in section 9.5. Finally, section 9.6 summarises the main results.

9.2. New classification based upon Lagrangian Backward Trajectories

From the global dataset, the particles that arrive in the NW Iberia Peninsula (41°N – 44.5°N and 10°W – 6°W) on a particular day are selected so that the classification will be based on the properties of those selected air particles. In this case, the number of daily trajectories ranges approximately from 50 to 400. The amount of air particles has a seasonal cycle with higher values in winter and lower values in summer.

In a first step we apply a non-hierarchical clustering to normalize the data set, i.e., we make sure that an equal number of representative trajectories characterize the general flow at NW Iberia Peninsula in all seasons. Based on the normalized back-trajectories, the CWT catalogue is built by further classification. Note that stratospheric air parcels are neglected through the exclusion of the clusters whose centroids have a height larger than 14 km. In the following sections the method is described in greater detail.

9.2.1. Clustering of trajectories

Trajectories of air parcels that are in the target domain at the chosen time step were selected and the respective 90-hour backward

trajectories were retrieved from the global dataset (Fig. 9.1). The atmospheric circulation, for each day at 12 UTC, is assumed to be characterized by at most five distinct air streams (trajectory clusters). In a first step, a non-hierarchical clustering algorithm is applied, using the squared Euclidean distance as a similarity measure between the members of the initial set. The aim is to horizontally separate different air streams. It is based on the first part of the method proposed by Dorling et al., (1992a). For a detailed description of the method please refer to sections 2a) to 2c) of Dorling et al., (1992a).

Clusters with less than 10 trajectories are not included in the next clustering step. This is done to only keep the most representative air streams for a given day. The intensity of the remaining air streams can be measured by the number of trajectories in each cluster. An example for a particular day (11/11/1999) is provided in Fig. 9.1 with the color lines showing the trajectories of different clusters and the thick black lines representing the centroid trajectory of each cluster, which is defined at each time as the average of the latitude-longitude coordinates and the meteorological variables (see section 5.6) of the trajectories in that cluster.

In the Dorling method, if less than five centroid trajectories are found, the assumption is made that they are meteorologically different enough from each other. Then, no additional action is required and they remain as separate clusters.

On the other hand, if the number of clusters from the first (horizontal) clustering exceeds five, a further reduction is necessary. This is accomplished with a second (hierarchical) clustering based on the height of the centroid trajectory (H), the distance to the target area (D), specific humidity (Q) and latitude (LAT).

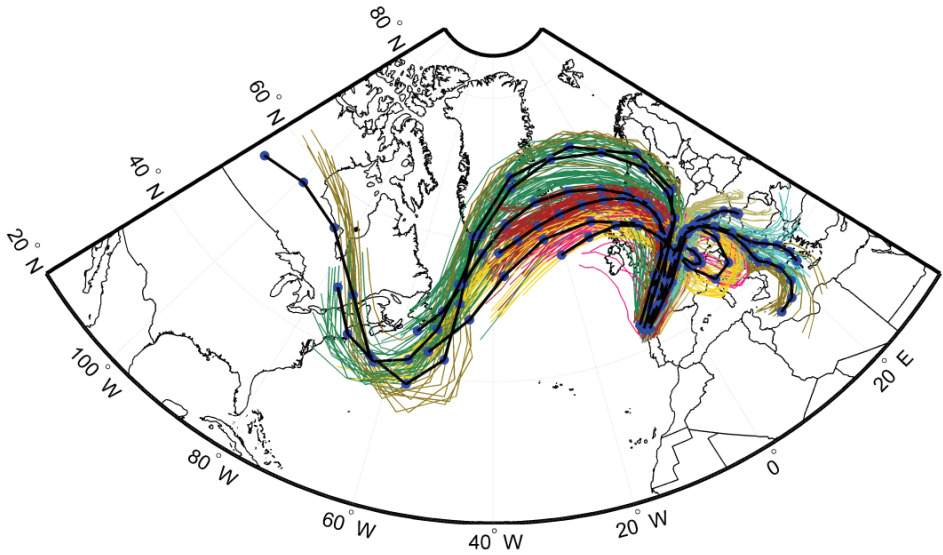


Figure 9.1. Backward trajectories (90h) arriving to the northwest Iberia Peninsula (41°N – 44.5°N and 10°W – 6°W) on a particular day (11/11/1999 - 12 UTC) in color lines and the respective clusters position (blue dots) computed by the Dorling method (dark lines).

Hierarchical clustering constructs a hierarchy of sets of groups, each of which is formed by merging one pair from the collection of previously defined groups. In order to choose which clusters should be combined, a measure of dissimilarity between the different trajectories is used. This is achieved by use of an appropriate metric (a measure of distance between pairs of observations).

In this case, the standardized Euclidean distance is used to compute the pairwise distance between centroid trajectories. Furthermore a linkage criterion which specifies the dissimilarity of the trajectories as a function of the pairwise distances of observations is also used (Wilks, 2006). Here, the dissimilarity of the trajectories is the weighted average distance (Hastie et al., 2009). This process is iterated until the maximum number of clusters in the hierarchical clustering becomes five. The centroids of the hierarchical clustering are computed

with the centroids trajectories taken from the previous clustering (Dorling method) as shown in Fig. 9.2.

At this stage, a maximum of five distinct air stream represent the flow on a particular day, each being characterized by their temporal evolution of latitude, longitude, height, specify humidity and distance to the target region. This was achieved by using the two-step clustering methodology explained above

As an example, the hierarchical clustering for the day shown in Fig. 9.1 is provided in Fig. 9.2 where time evolution of the backtrajectory properties (which correspond to the centroids found in the previous clustering (Dorling method) for each variable used in the clustering is shown.

9.2.2. New characteristics and dynamical classification

For each day, each representative air stream is characterized by four distinct Lagrangian flow properties. This classification enables to attribute to each air stream an 'index' for each of the four studied features. A description of the respective variables and criteria is given now.

Moisture Uptake (MU)

MU describes the moisture uptake of the air stream. It represents the integrated change in specific humidity (ΔQ) of an individual air stream from the initial point (i) to the arrival in the target region (f), computed as:

$$(1) \quad \Delta Q = Q_f - Q_i$$

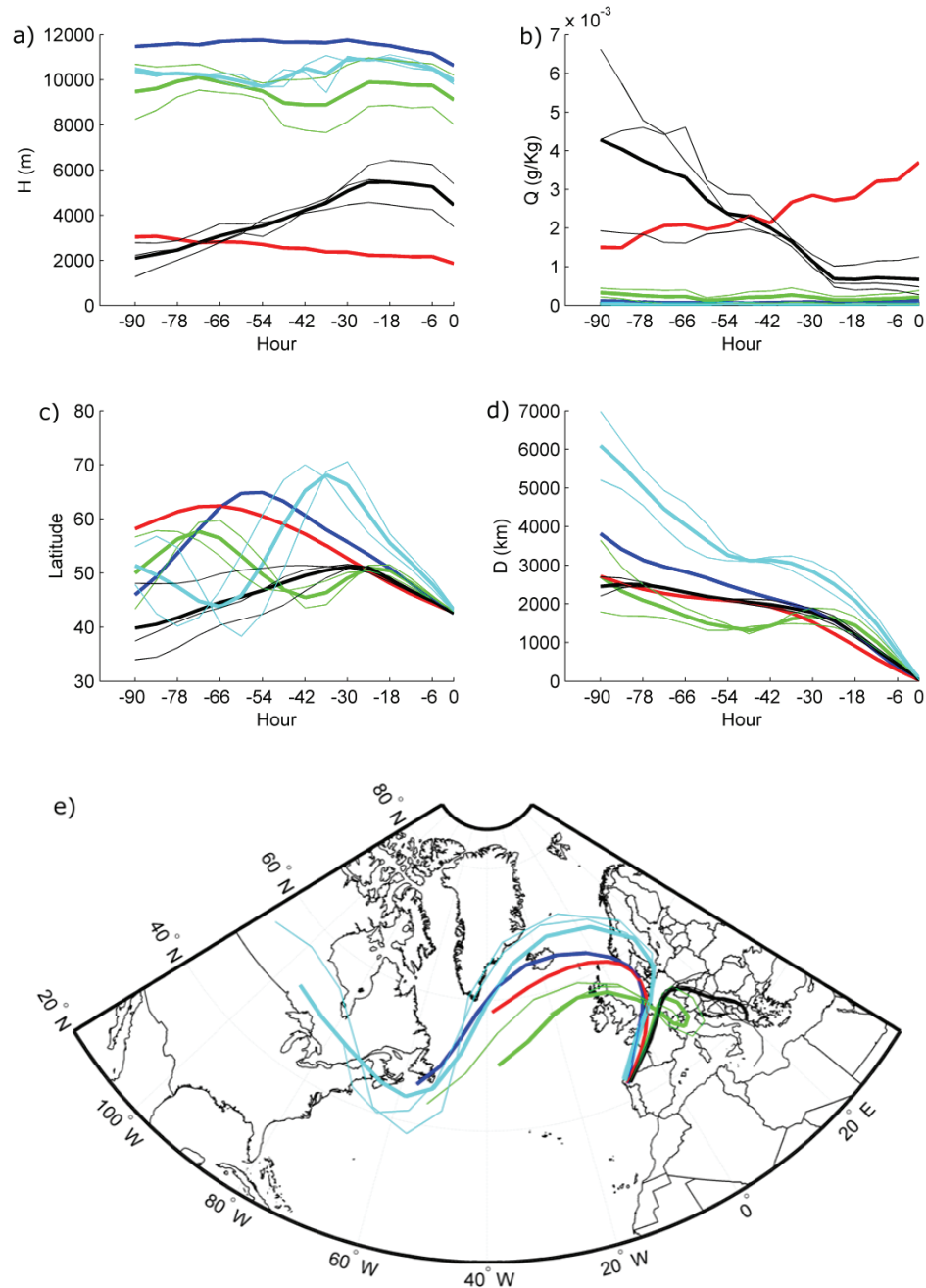


Figure 9.2. Time evolution of the back-trajectory properties for a) height of trajectory (H), b) specific humidity (Q), c) latitude and d) distance to the center (D) shown in Fig. 9.1. The colored thin line corresponds to the centroid trajectories (previous computed with the Dorling method) while the colored thick lines correspond to the final five air streams characterizing the day (see text for details). In e) the final air streams are shown. The color code is the same as in a) to d).

The histogram of ΔQ (Fig. 9.3a) for all air streams resembles a normal distribution and the division is made into 3 classes:

- (Q-) ΔQ in the lower tercile of the distribution; it corresponds to a decrease in humidity along the path;
- (Q+) ΔQ in the upper tercile of the distribution; it corresponds to an increase in humidity along the path.
- (Q0) if ΔQ falls between the two classes mentioned above; it corresponds to small changes (positive or negative) of the humidity along path.

Zonality Index (ZI)

ZI describes the curvature of the path of the air streams (curved or straight). It is computed by integrating the absolute value of the radius of curvature (R) for each sub-section of the air stream:

$$(2) \quad ZI = \sum_{t=i}^{t=f} (|R_t|)$$

It can be seen as a Lagrangian based zonality index – the term ‘zonality’ used in a generalized way where it refers to a weakly-curved flow compared to a strongly undulating flow. The histogram of ZI (Fig. 3d) shows a positively skewed distribution. It is divided into two classes:

- (Z-) ZI below the 50th percentile; it corresponds to a weakly-curved air stream;
- (Z+) ZI above the 50th percentile corresponds to a strongly curved air stream.

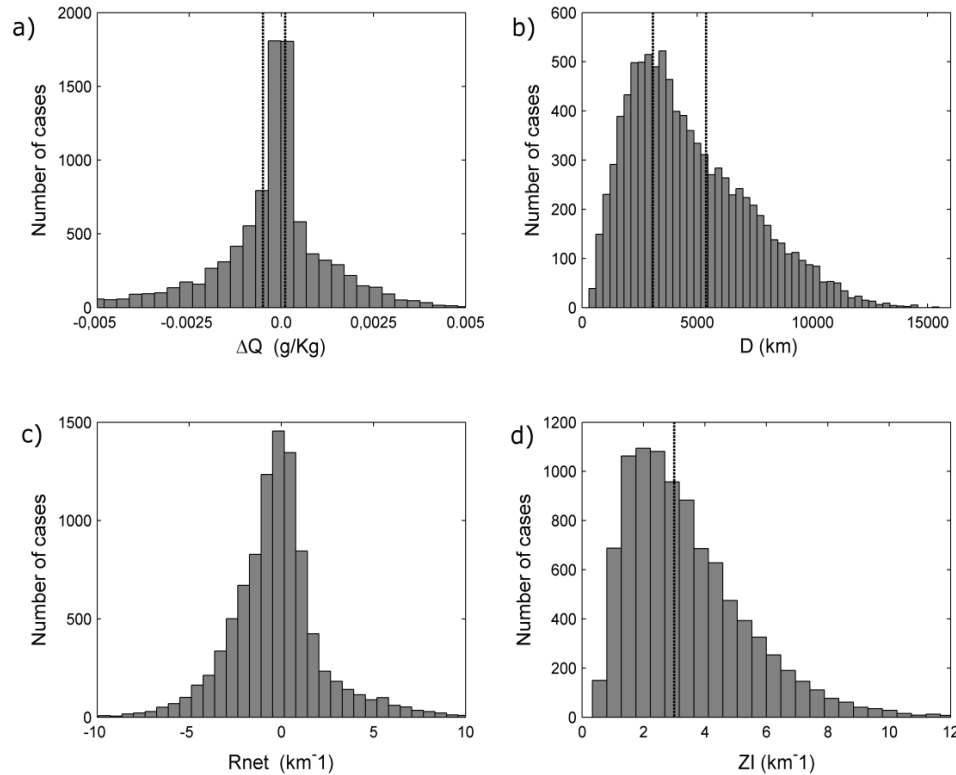


Figure 9.3. Histograms distribution for: a) integrated changes in specific humidity (ΔQ), b) distance “travelled” by the particle (D); c) integrated value of the curvature (R_{net}) and d) integrated absolute value of the curvature (ZI). For ΔQ and D the tercile values are indicated with a dotted black line and for ZI the 50th percentile.

Cyclonicity Index (CI)

This index determines whether the flow is cyclonic or anticyclonic, and to which degree this applies. It is based on the radius of curvature (R) of the air stream and combines three flow features:

(1) RC, the percentage of the air stream with a relatively small cyclonic radius of curvature between 0 km and 1000 km: $RC = \% (0 \text{ km} < R < 1000 \text{ km})$; as an example, if RC is greater than 25%, at least 25% of the air stream has a small cyclonic radius of curvature.

(2) RA, the corresponding percentage with an anticyclonic radius of curvature between 0 km and 1000 km: $RA = \% (-1000 \text{ km} < R < 0 \text{ km})$;

(3) Rnet, the net curvature of the flow (negative for anticyclonic and positive for cyclonic) computed by integrating the value of the curvature along the air stream (the histogram for Rnet is presented in Fig. 9.3c):

$$(3) R_{net} = \sum_{t=i}^{t=f} (R_t)$$

The Cyclonicity Index CI is divided into five classes:

- (Cs) RC > 25% and RA < 25%, the air stream has small cyclonic curvatures during at least 25% of the path; it is strongly affected by meso- and synoptic-scale cyclonic systems (e.g. extra-tropical cyclones)
- (As) RA > 25% and RC < 25%, the air stream has small anticyclonic curvatures during at least 25% of the path;
- (CsAs) RC > 25%, and RA > 25%, during the path the air stream has both small cyclonic and anticyclonic curvatures;
- (Cnet) if the three classes above do not apply, Rnet, is used: Rnet > 0, i.e., on average cyclonic path;
- (Anet) as (Cnet), but for an average anticyclonic path, i.e., Rnet < 0.

Distance and Origin (DO)

This characteristic classifies each air stream both in terms of integrated distance D along the air stream (short (S), medium (M) and long (L) range transport) and its initial position. A four-point compass is centered in the domain allowing 90° per sector (see Fig. 9.4 for details) and the variable O (origin quadrant) therefore can take on four discrete values (NE, SE, SW, and NW). O is determined by the position of the initial point of the air stream.

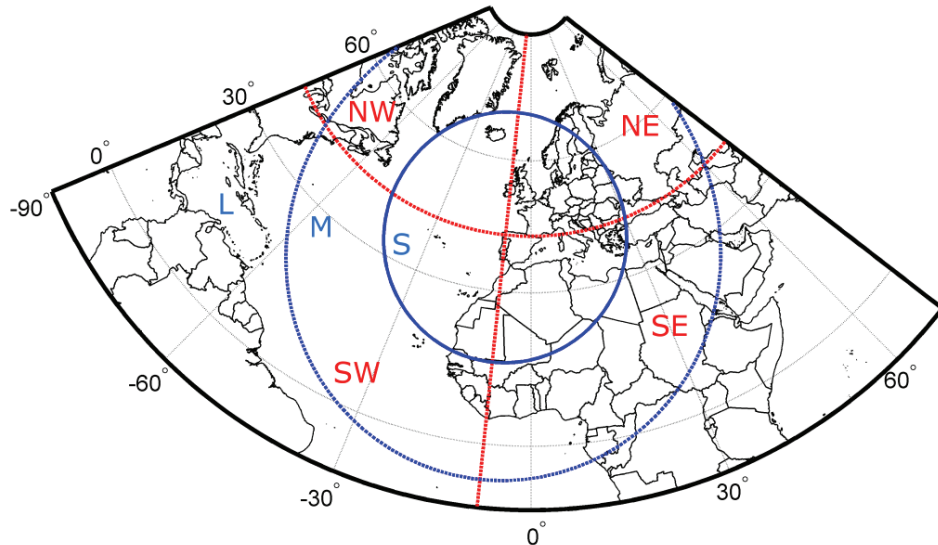


Figure 9.4. Definition for the Distance and Origin (DO) characteristic for the air streams. The circles separate the different distance (D) classes: short range (S), medium range (M) and long range (L). The origin of the air streams is split into the four regions SW, NW, SE and NE. In total, 12 classes result for DO.

The histogram of D is shown in Fig. 9.3b for all air streams, and it is divided into three classes:

- (S) D in the lower tercile of the distribution (less than 3076 km).

It corresponds to short range transport;

- (M) D in the middle tercile of the distribution (greater than 3076 km and less than 5391 km), corresponding to medium range transport;

- (L) D in the upper tercile of the distribution (greater than 5391 km) corresponding to long range transport.

As an example, if an air stream is classified as L-SW in terms of DO it means that it experienced long range transport and its initial point was in the 3rd quadrant (SW).

Final Catalogue

A sample of the catalogue from 01/12/1999 to 18/02/2000 is provided in Fig. 9.5. In synthesis, the final catalogue has for each day a maximum of five air streams (clusters) and each air stream is characterized by the four parameters (MU, ZI, CI and DO) described above. Additionally, one day or multiple days can be characterized by a single string of labels indicating the most frequent classes encountered for each characteristic. For example, if one day or multiple days are classified as [Q-, Z+, Anet, L-SW] – this case corresponds to the first air stream of the first day (01/12/1999) and it is shown in Fig. 9.5. Then the majority of the air streams had respectively: a decrease in humidity during the path, a significantly curved trajectory, a mean anticyclonic path, and a long-distance pathway from the SW quadrant.

9.3. Trajectories types for selected case studies synoptic patterns

The NW Iberia Peninsula is affected by different synoptic weather systems (Gomez-Gesteira et al., 2011). Several case studies will now be analysed in order to validate the Lagrangian classification for different synoptic conditions and to compare it with the Eulerian Lamb CWT for a given case (chapter 6). The corresponding CWT for the NW Iberia Peninsula (Lorenzo et al., 2008; chapter 6) will be given for each case study. Furthermore, the case studies also illustrate different ways how the information in the final catalogue can be presented. It is also important to notice that every trajectory that is represented in the case studies corresponds to the final cluster results and therefore representing the different air streams for each day.

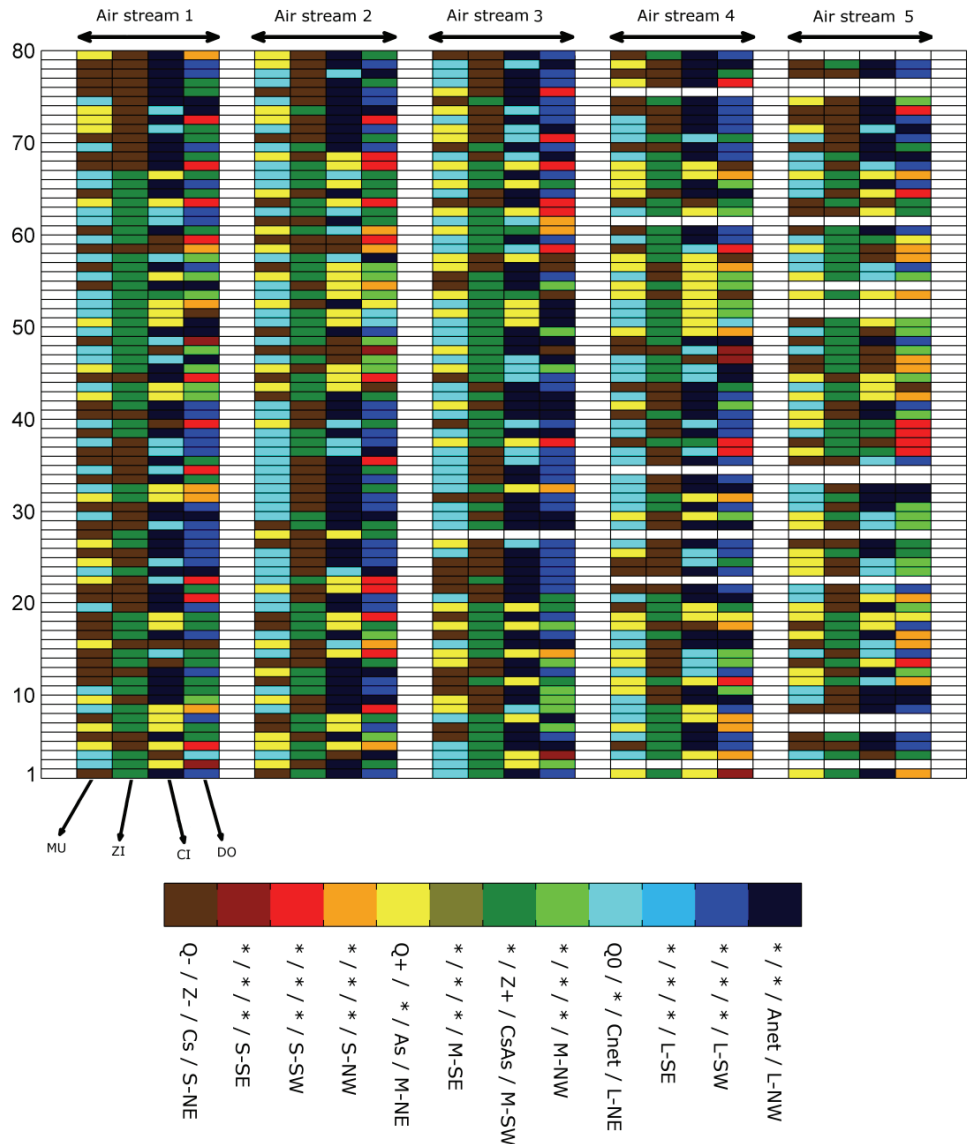


Figure 9.5. Representation of the final catalog for 80 first days (from 01/12/1999 to 18/02/2000). Each day is characterized by at most five air streams and each air stream can be described by four flow properties (MU, ZI, CI and DO), as discussed in section 9.2. The legend should be interpreted like this: for different categories the colors indicates a different class. For example, the first air stream of the first day (01/12/1999) is classified has [Q-, Z-, Anet, L-SW]. The * in the legend indicates that there is no correspondent class.

9.3.1. Cold front - 12/11/2002

The NW Iberia Peninsula is often affected by the passage of cold fronts associated with the storm track in the North Atlantic Ocean and the passage of cyclones that strike directly the region (Trigo, 2006). Therefore, the study of a cold front system is first presented. On the 12th November 2002, a typical cold front associated to a low pressure system located west of the British Isles affected the NW Iberia Peninsula (Fig. 9.6). The corresponding Lamb CWT for that day was a 'W' type. Additional information can be obtained from the Lagrangian-based classification. For this day there are five main airstreams arriving to the region, their characterization given in Fig. 9.6. For example, besides the long range transport, some short range and medium range transport features are also found. All the air streams present on average a cyclonic path (CI), while the majority is only weakly curved (ZI): they are not strongly affected by meso- and synoptic-scale cyclones on their way to NW Iberia Peninsula. With respect to the integrated changes in the specific humidity (MU) the signal is not so clear. There is one air stream with a decrease in humidity, two air streams with an increase in humidity, and two with small humidity changes. In summary, this day can be characterized by the string [Q+/Q0, Z-, Cnet, L-SW], as determined from the predominant characteristics.

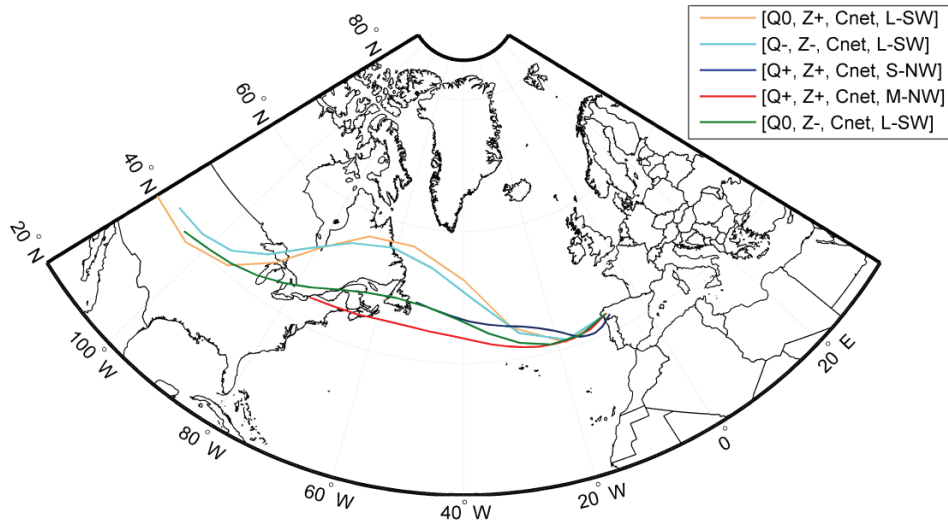


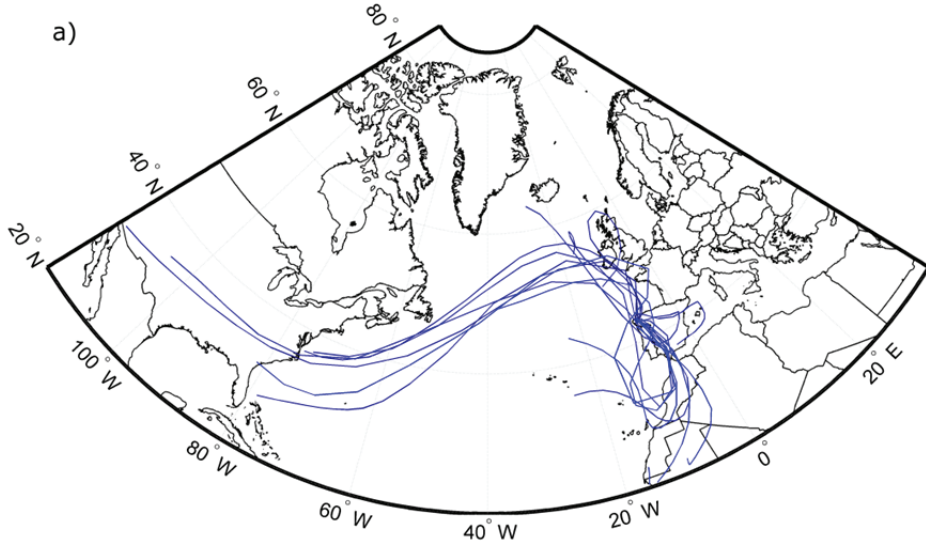
Figure 9.6. Air streams for the cold front case study (12/11/2002). Each color represents a different air stream – see legend.

9.3.2. Cut off low system - 10/10/2001 to 12/10/2001

Cut off low systems (COLS) are very common in the Mediterranean region of the Iberia Peninsula, but not as common in the NW Iberia Peninsula (Nieto et al., 2005). In any case COLS are a very important synoptic weather system to be analyzed since most of the time they are associated with reduced thermodynamic stability beneath, hence enhancing the convection in the region, and they do not necessarily have any signature in the SLP field (Nieto et al., 2005; Nieto et al., 2007a; Ramos et al., 2011). This particular COL became stationary for three days in the Iberia Peninsula between 10/10/2001 and 12/10/2001 (Nieto et al., 2008) and it did not have any particular signature at the surface level. The Lamb CWT for the three days are A, A and S, respectively. These CWT are often associated with low rainfall in the region (Lorenzo et al., 2008), which is not the case for the present case, since a total of 32 mm of precipitation was registered at the Lourizán station.

The total number of air streams for these three days are 15 which makes the pure listing of the characterising strings no longer a reasonable option and therefore a more graphical presentation needed. Fig. 9.7a) presents the air streams for this case while in Fig. 9.7b) the catalogue of the Lagrangian types for these 3 days. This catalogue (Fig. 9.7b) must be carefully read from bottom to top. The air streams are identified and characterized independently for each day: e.g. air stream 2 at day 2 might be the ‘natural continuation’ of air stream 1 at day 1. Therefore, an abrupt change in the air stream characteristics from one day to the next is not necessarily physical relevant.

The new method is able to capture the cyclonic circulation at high levels of the atmosphere. This is clear in CI where the cyclonic classes (Cs and Cnet) dominate. The air streams on these three days are typically strongly curved (Z+). With respect to humidity (MU) the most frequent class corresponds to small changes (positive or negative) followed by the class that corresponds to a decrease in humidity. These three days have the following characterization: [Q0, Z+, Cs, L-SW].



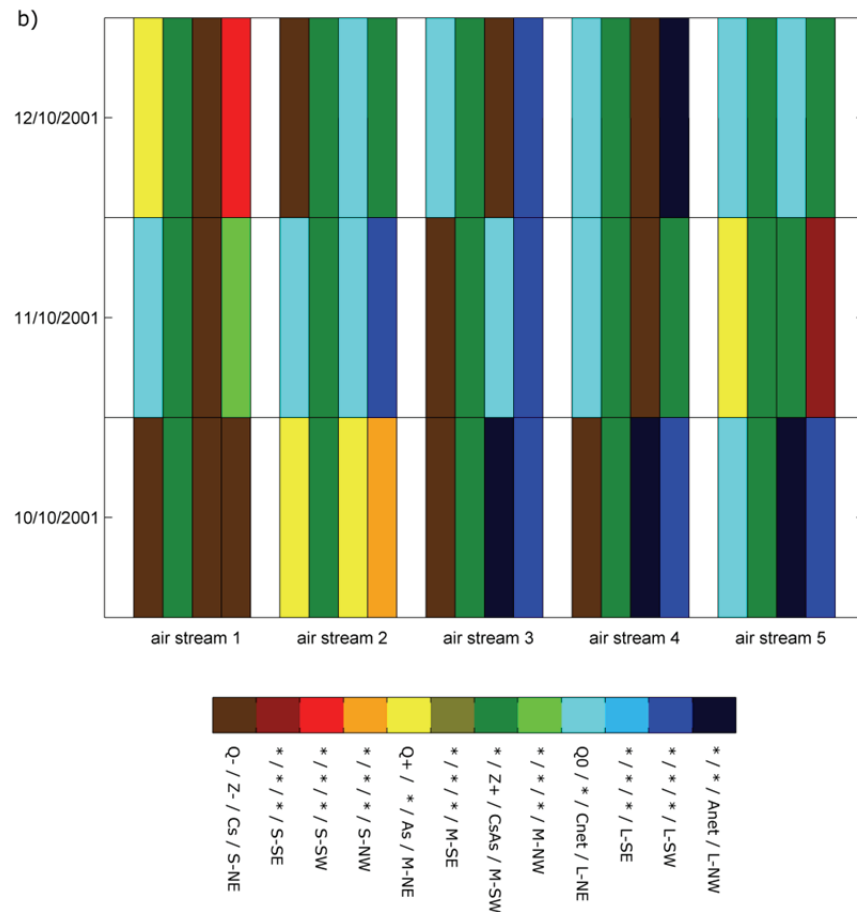


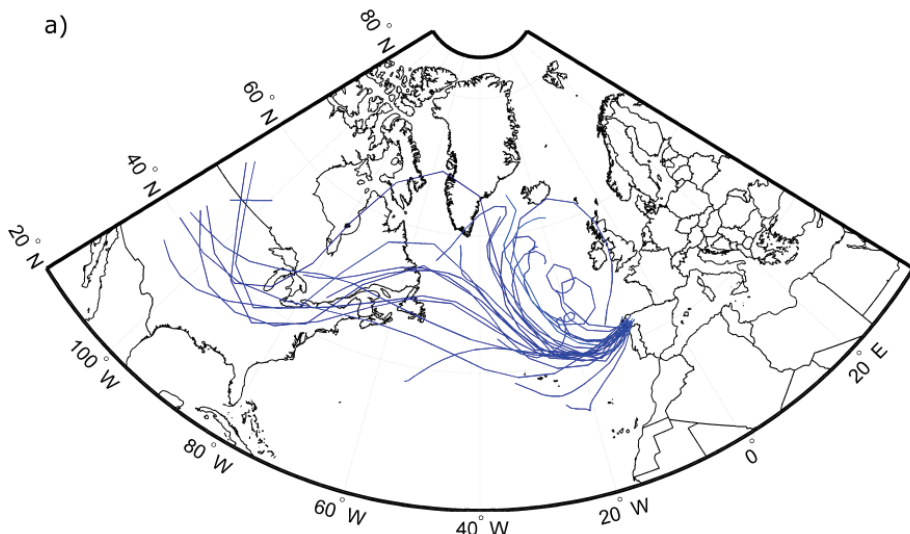
Figure 9.7. a) Air streams and b) final characteristics catalogue of the trajectory types classification for the cut-off low system case study (10/10/2001 - 12/10/2001).

9.3.3. 5-day averaged highest precipitation period - 17/10/2001 to 21/10/2001

Given that the NW Iberia Peninsula is the region with highest annual precipitation in the Iberia Peninsula (Herrera et al., 2010; SIAM, 2002), the next case study focuses on the most intense precipitation period averaged during five days for the region (17/10/2001 to 21/10/2001) with an average amount of 41.9 mm. During these days the NW Iberia Peninsula was under the influence of a stationary extra-tropical cyclone located in the NW Iberia Peninsula with pressure centre

values below 1000 hPa (not shown). The correspondent Lamb CWT for the five days respectively were CSW, SW, C, C, CSW, corresponding to types that often produce precipitation in NW Iberia Peninsula.

Focusing on the Lagrangian types (Fig. 9.8), results confirm a high cyclonic circulation in the region (Cs and Cnet) with more of 80% of the air streams presenting strong curvature (Z+), which is perfect visible when looking at the trajectories of the air masses. Most of the air streams correspond to short or medium range transport. In addition, the string [Q-, Z+, Cs / Cnet, M-NW] summarizes the features for this period.



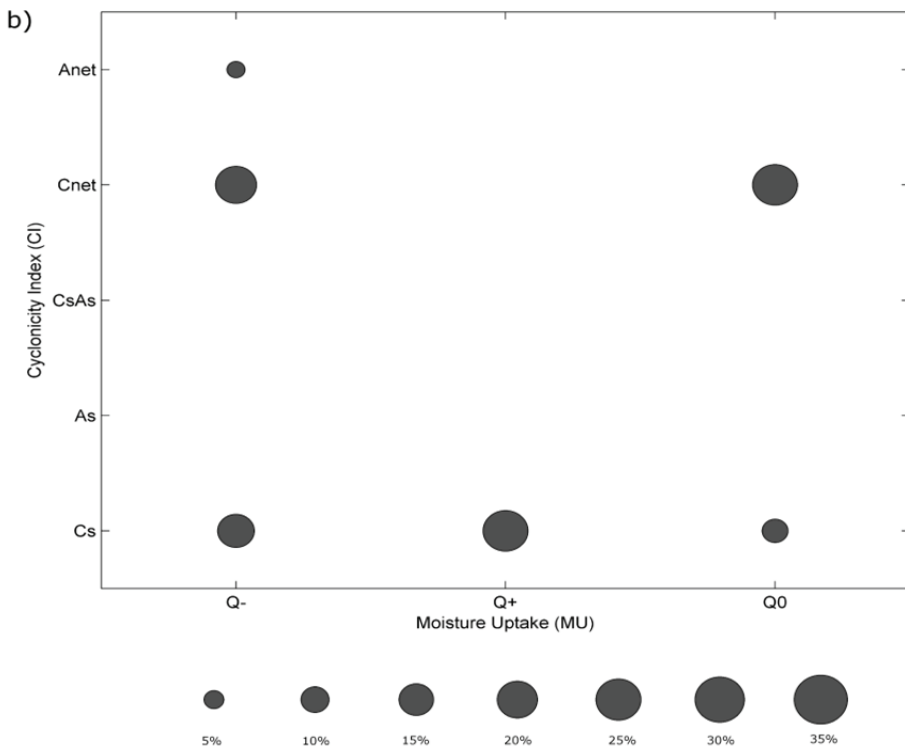
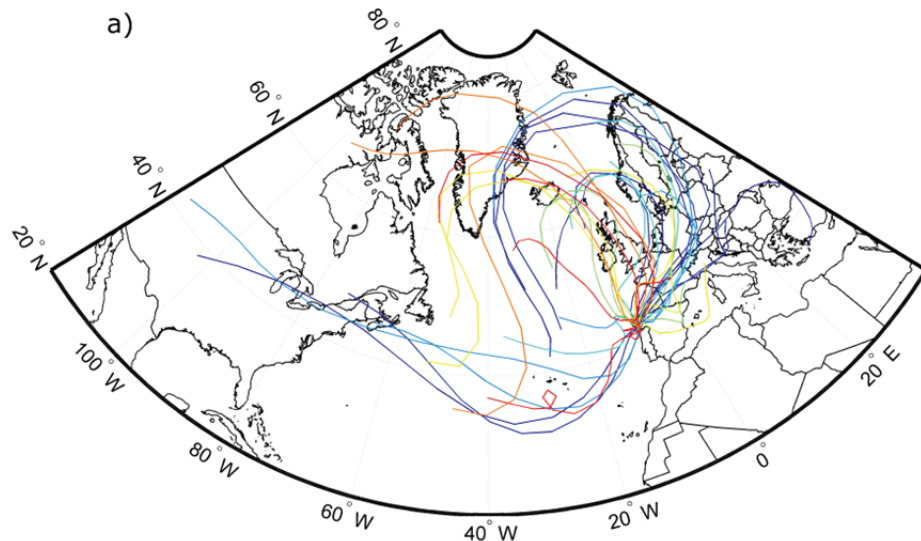


Figure 9.8. a) Air streams for the precipitation period case study (17/10/2001 to 21/10/2001). b) Scatter plot with frequencies of air streams characterized by MU and CI.

9.3.4. Coldwave - 15/12/2001 to 22/12/2001

The December 2001 cold wave stroke not only the NW Iberia Peninsula, with the highest anomalies for minimum temperature in the Lourizán weather station, but also other countries in Europe. In this particular days (15/12/2001 to 22/12/2001), there was an anticyclone located over the British Isles and two low-pressure systems located on the left and right of the anticyclone, usually known as the omega blocking pattern (not shown). In fact, according to the blocking database by Barriopedro et al., (2010), there was a blocking episode in the Atlantic during those days. The Lamb CWT for this period varies from SE, AS and A types.

When looking at the trajectories types (Fig. 9.9) a clear omega pattern emerges with cold air being advected from the North and SE of central Europe to the NW Iberia Peninsula. On the contrary of Catalonia region (where heavy snow occurs), the precipitation in NW Iberia Peninsula (Lorizán Station) in those days was zero. This seems to be confirmed by the analysis of MU, where most of the trajectories present no significant changes in the specific humidity while the circulation is mainly anticyclonic (As and Anet). The distance and origin is distributed approximately to 1/3 in each class. This cold-wave event, in the trajectory types, is categorized as [Q0, Z+, Anet, L-NW].



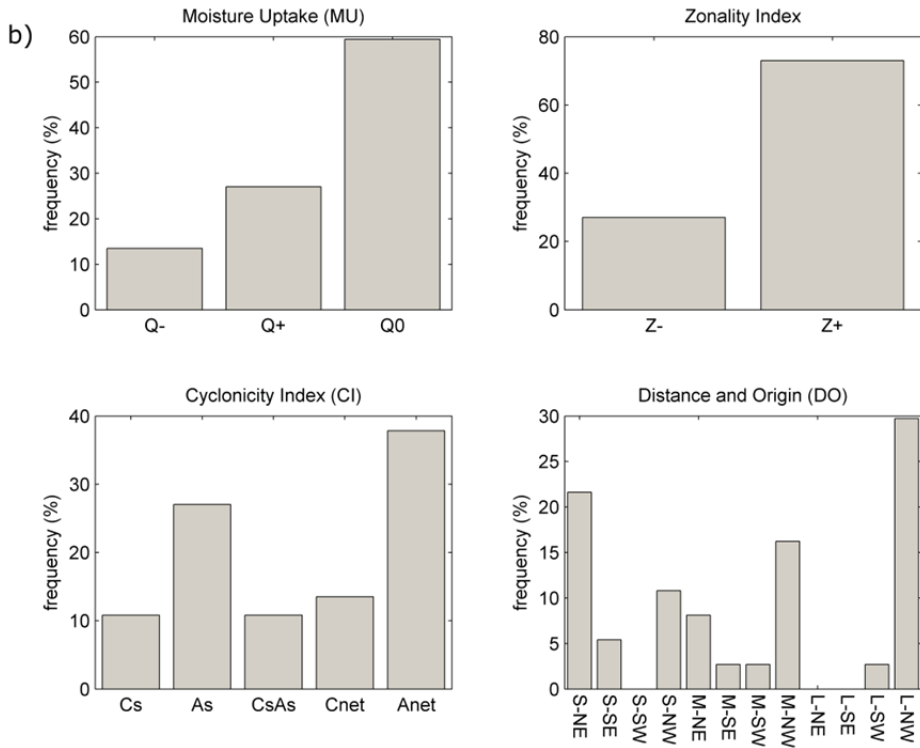


Figure 9.9. a) Air streams (each color represent a different day) and b) characteristics of the trajectory types classification for the coldwave case study (15/12/2001 to 22/12/2001).

9.3.5. Heatwave - 01/08/2003 to 15/08/2003

The heatwave event of 2003 (01/08/2003 to 15/08/2003) stroke not only Central Europe (García-Herrera et al., 2010) but also the NW Iberia Peninsula (Trigo et al., 2009; deCastro et al., 2011). The northward displacement of the North Atlantic Subtropical High is recognized to be the most probable mechanism responsible for the August 2003 heatwave (e.g., Black et al., 2004; deCastro et al., 2011). The correspondent daily Lamb CWT for this period is shown in Table 9.1). Most of the days are A-related types followed by C type. This C type is probably due to the thermal low that frequently develops over the Iberia Peninsula in summer (Hoinka and De Castro, 2003).

Table 9.1. Lamb Circulation weather types for each day of the heatwave (1/8/2003 - 15/8/2003) case study.

Date	WT
1/8/2003	A
2/8/2003	A
3/8/2003	S
4/8/2003	C
5/8/2003	N
6/8/2003	A
7/8/2003	A
8/8/2003	A
9/8/2003	AN
10/8/2003	N
11/8/2003	A
12/8/2003	A
13/8/2003	A
14/8/2003	C
15/8/2003	C

Additional information can be retrieved when analysing the Lagrangian types (Fig. 9.10). Short range transport dominates (almost 2/3 of the air streams). In addition, there is advection of African air to the Iberia Peninsula. Concerning MU, Q+ (increase in specific humidity) is the most frequent class. Regarding CI, the most frequent classes are As (small anticyclonic curvatures) and Cnet (air streams with averaged cyclonic path). This is very interesting because the Lagrangian method is able not only to capture the thermal low, responsible for the re-circulations in the Iberia Peninsula with short range transport, but also the anticyclonic circulation associated with medium and long range transport. This heatwave event, according to the Lagrangian classification, is categorized as [Q+, Z+, As, S-SW].

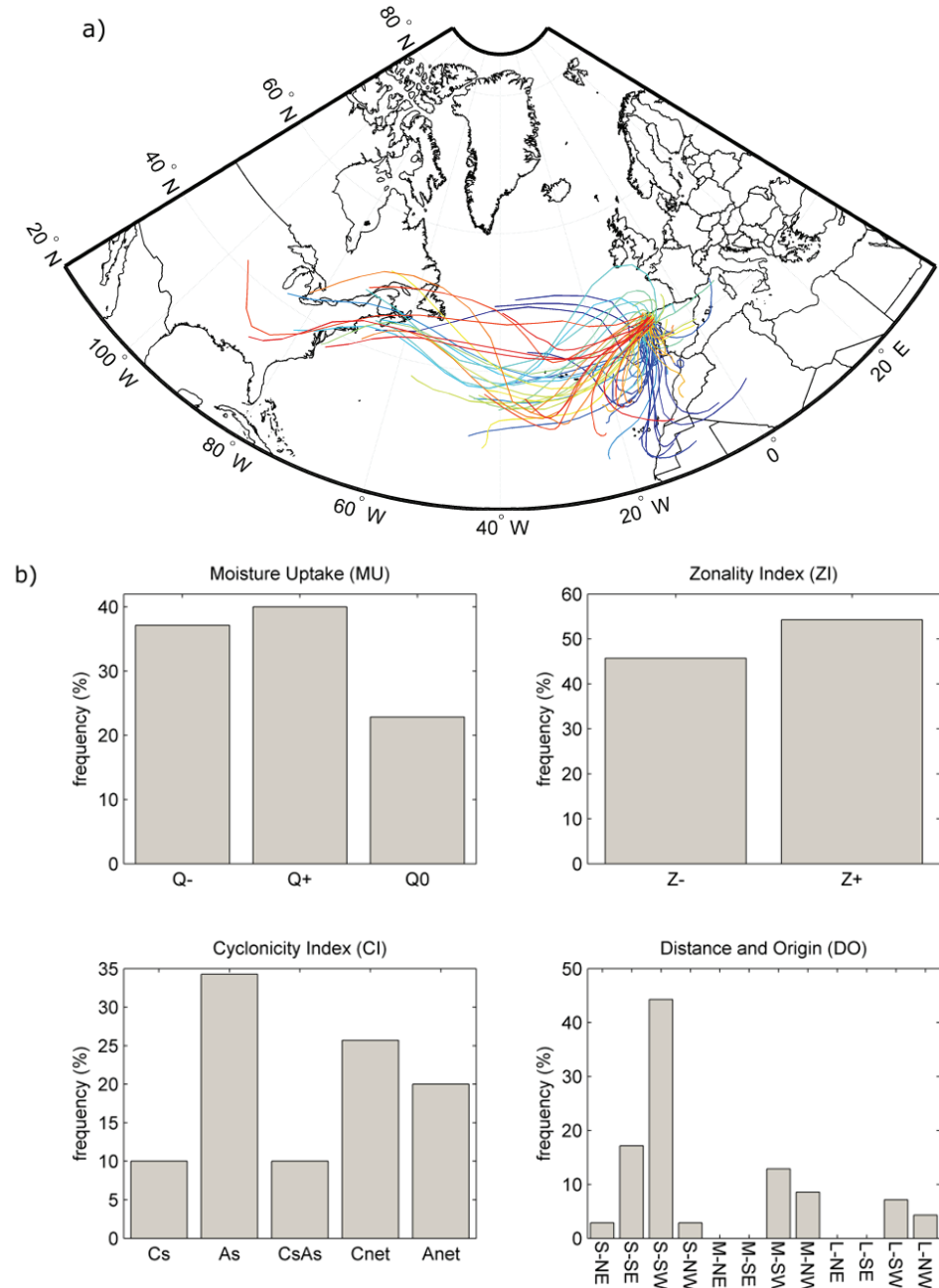


Figure 9.10. a) Air streams (each color represent a different day) and b) characteristics of the trajectory types classification for the heatwave case study (01/08/2003 to 15/08/2003).

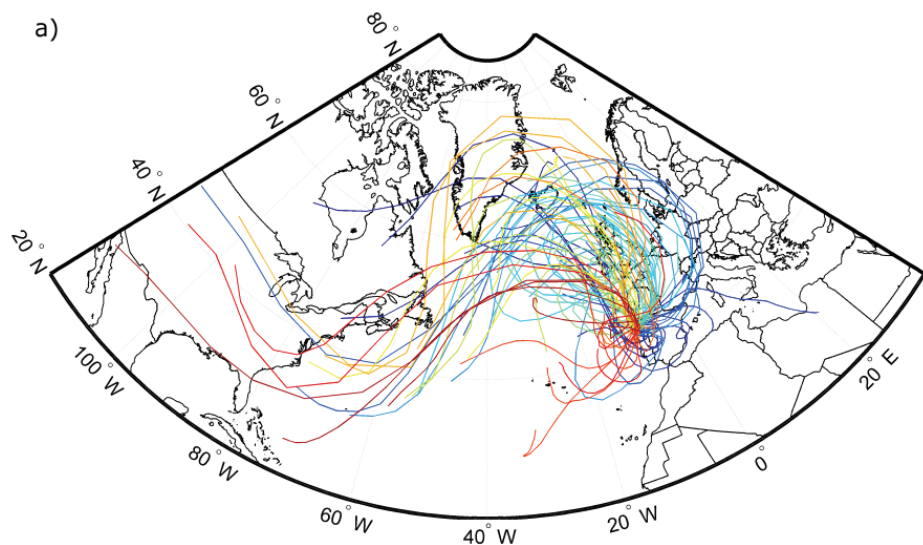
9.3.6. Blocking episode - 14/01/2000 to 29/01/2000

Blocking events are characterised by a large-scale high pressure system with an anticyclonic circulation dominating the troposphere (Rex, 1950). In the target region the blocking events located over the North Atlantic are known to influence the local weather (Barriopedro et al., 2006). The selected event from 14/1/2000 to 29/1/2000 was the most persistent blocking that occurred in the 12/1999 to 11/2004 period in the North Atlantic. Blocking is associated with anomalous weather conditions over long periods of time and large areas of the mid and high latitudes (Barriopedro et al., 2010; García-Herrera et al., 2007; Trigo et al., 2004a). The correspondent daily Lamb circulation circulation type for this period is shown in Table 9.2). Most common for this period are the A and S related types.

A closer look at the Lagrangian classification catalogue (Fig. 9.11) reveals that most of the air streams present an anticyclonic path (As and Anet). In addition more than 3/4 of the air streams are strongly curved (ZI+), while the air streams with no change in humidity are the most common ones (Q0). In terms of integrated length (D), medium and long range transport dominates. This blocking event can be summarized as [Q0, Z+, As, M-NW].

Table 9.2. Lamb Circulation weather types for each day of the blocking (14/1/2000 - 29/1/2000) case study.

Date	WT
14/1/2000	CNE
15/1/2000	E
16/1/2000	S
17/1/2000	S
18/1/2000	AS
19/1/2000	S
20/1/2000	AS
21/1/2000	AE
22/1/2000	ANE
23/1/2000	ANE
24/1/2000	ANE
25/1/2000	S
26/1/2000	SE
27/1/2000	SE
28/1/2000	A
29/1/2000	AW



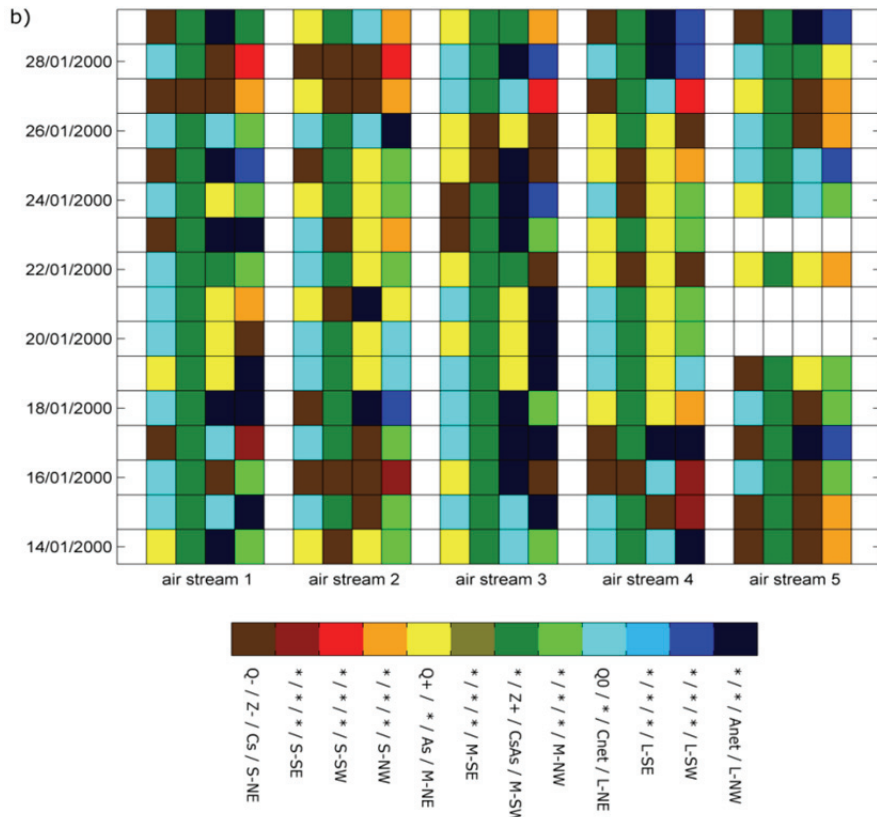


Figure 9.11. a) Air streams and b) final characteristics catalogue of the trajectory types classification for the blocking event case study (14/01/2000 to 29/01/2000).

9.4. Comparison between Lamb circulation weather types and trajectory types

In this section the relationship between the Lamb CWT and each characteristic of the new Lagrangian classification is studied, in order to check for coherence and consistence. The frequency of each Lamb CWT is shown in Table 9.3. Circulation type A is the most frequent one with almost 25% of the days followed by the SW and W type. Since the HC and HA circulation types are a mixture of all the hybrid directional types, the following discussion is only focused on the pure types.

Table 9.3. Frequency (%) of occurrence of Lamb circulation weather types during the 1/12/1999 - 30/11/2004 period.

Circulation type	Number of days (%)
NE	4.3
E	2.5
SE	1.8
S	2.4
SW	10.2
W	10.5
NW	5.7
N	2.6
C	7.2
A	25.9
HC	7.6
HA	19.4

For each day with a certain Lamb CWT the frequency of the Lagrangian classes is analysed. For MU (Fig. 9.12), there is a clear difference between the frequency of Q- when comparing the easterly with the westerly types. In general, easterly types are characterized by small changes in humidity along the path, while the westerlies are characterized by a decrease in the humidity. The difference between the C and A type is also prominent, higher frequencies are found for Q+ in the case of C type and Q0 in the case of the A type.

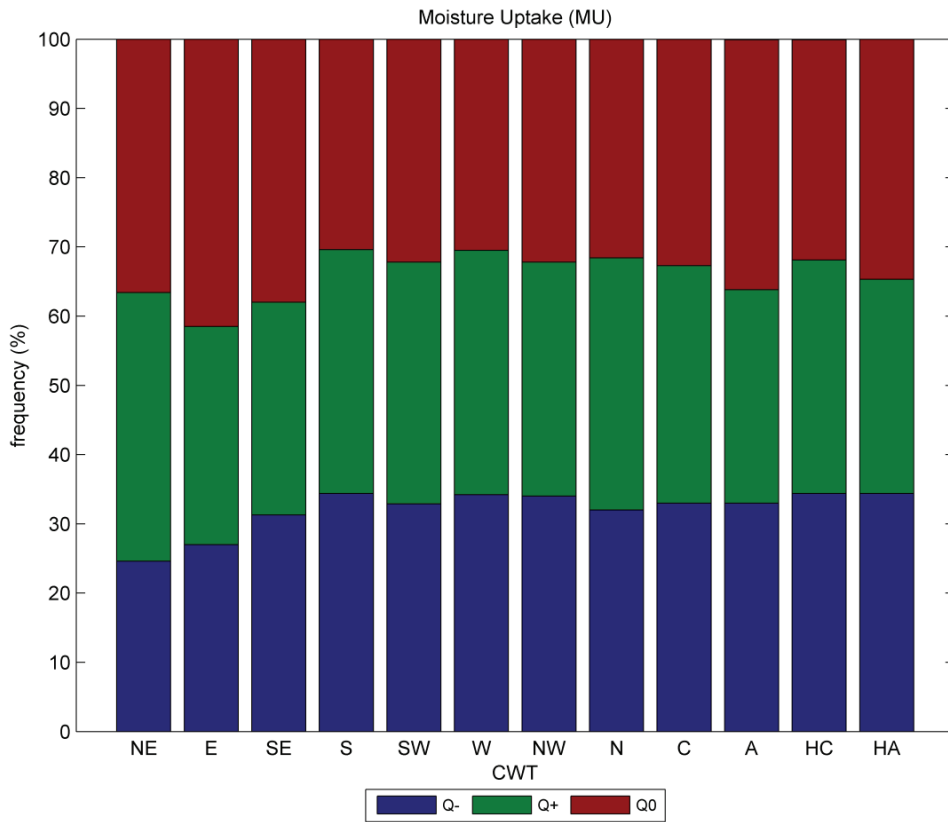


Figure 9.12. Relationship between Lamb circulation weather types and the Lagrangian flow property MU. For each circulation weather type the frequency of each MU class is presented.

For the zonal index (ZI) (Fig. 9.13), a marked difference between easterly and westerly types is observed. The easterlies are characterised by more frequently curved trajectories (Z+) while the opposite occurs for the westerlies (less curved trajectories). The difference between the C type and the A types is also noticeable with the trajectories being frequently more curved in the C type than in the A type.

Results for the cyclonicity index (CI) (Fig. 9.14) show a good differentiation between the frequencies of the five classes when comparing different CWT. For example, in the C types the frequency of the air streams which have Cs (small cyclonic curvatures) and Cnet (averaged cyclonic trajectory) is very high, 40% and 37.5%, respectively.

On the contrary, the A type presents higher frequencies for class As (small anticyclonic curvatures) and Anet (averaged anticyclonic curvatures). For the NW and W types also the Anet class is more frequent while for the SW types the Cnet class is more frequent.

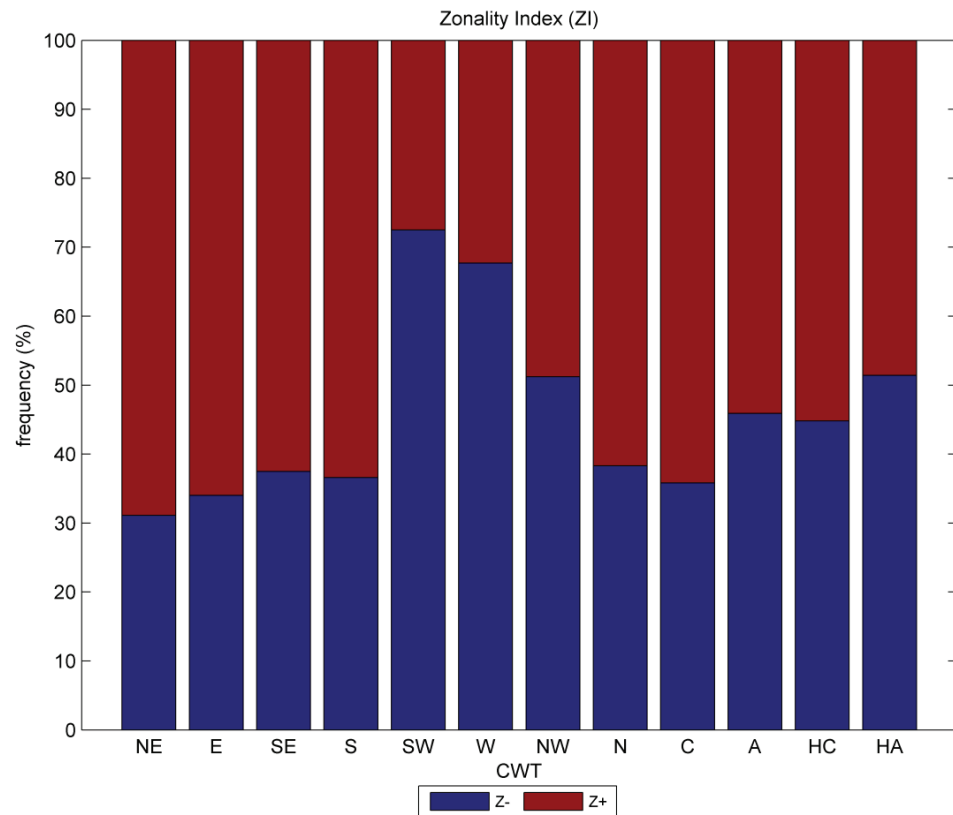


Figure 9.13. Relationship between Lamb circulation weather types and the Lagrangian flow property ZI. For each circulation weather type the frequency of each ZI class is presented.

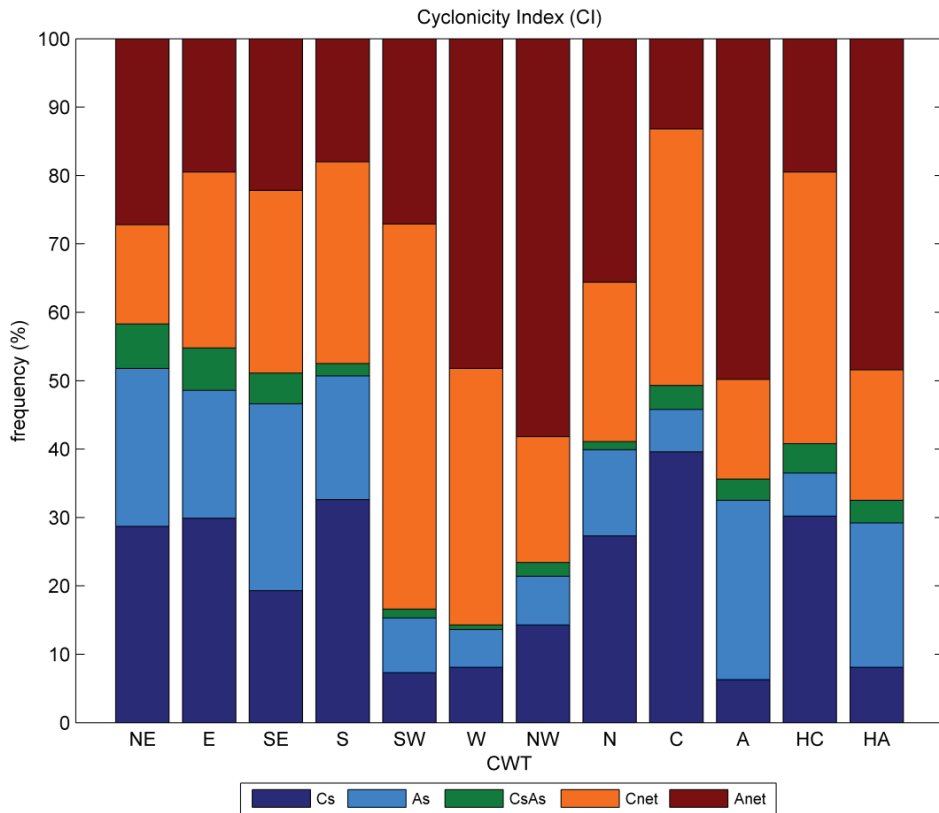


Figure 9.14. Relationship between Lamb circulation weather types and the Lagrangian flow property CI. For each circulation weather type the frequency of each CI class is presented.

Regarding the distance characteristic (D) (Fig. 9.15), the frequencies of the different classes are expected to differ between the Lamb CWT. For the NE, E, SE and S types nearly 45% of the air streams show short range transport, while the SW, W and NW types are typically characterized by medium and long transport.

The origin characteristic (O) (Fig. 9.16), is going to be analysed. As expected, when an S/SW/W/NW CWT occurs, the air streams for these days have their origin points mainly in the SW/NW quadrants. Concerning the NE/E/SE CWT days, results show that despite an increase in the air streams coming from the NE and SE quadrants (regarding the O characteristic) the majority of the air streams are

classified as coming from the SW and NW. This can be explained because the Lamb CWT are based on the surface level, while the trajectory types are taking into account the 3-D structure of the atmospheric motion. For this reason the signature of the jet stream (air streams where its initial point is in the NW and SW quadrant) is present in the majority of the analysed days.

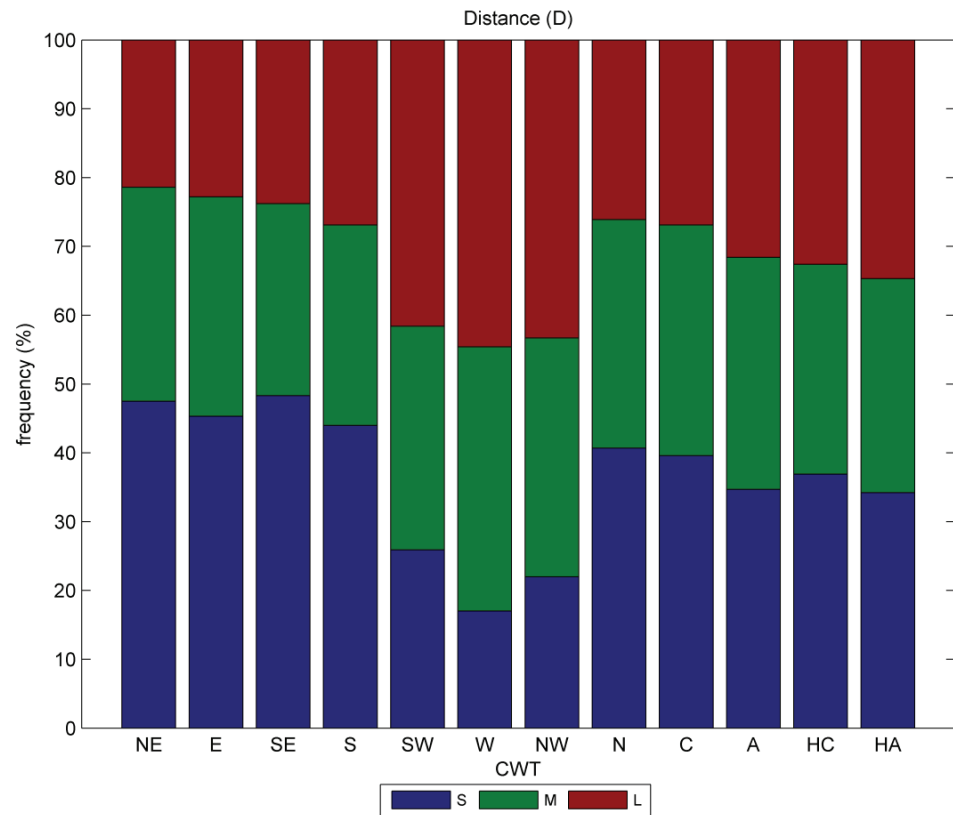


Figure 9.15. Relationship between Lamb circulation weather types and the Lagrangian flow property D . For each circulation weather type the frequency of each D class is presented.

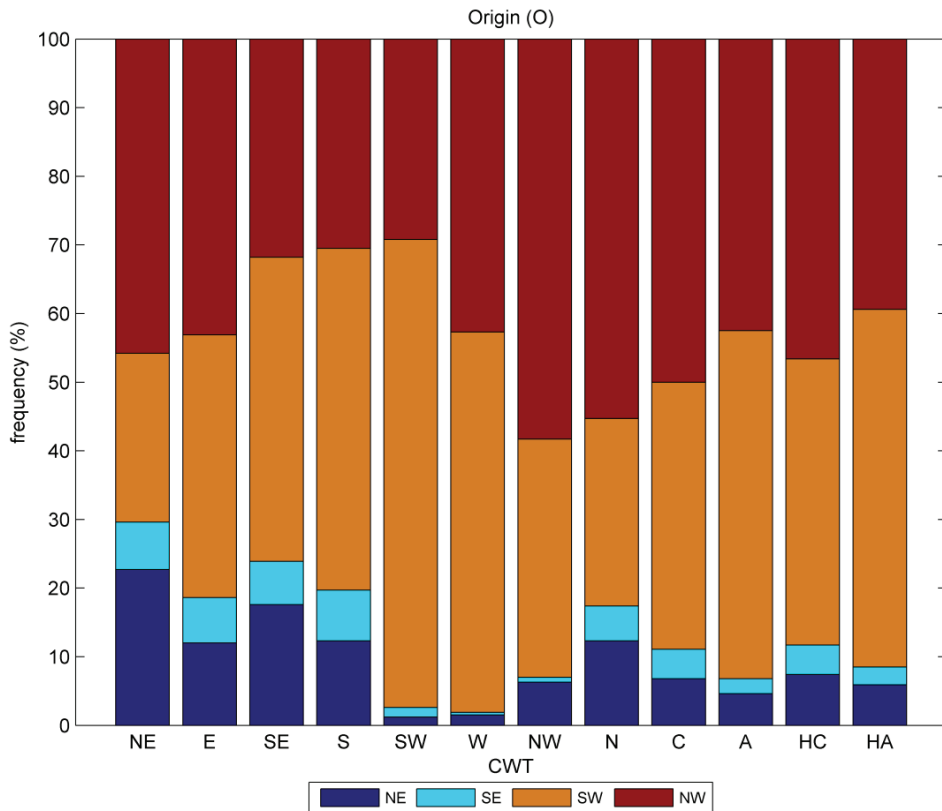


Figure 9.16. Relationship between Lamb circulation weather types and the Lagrangian flow property O . For each circulation weather type the frequency of each O class is presented.

9.5. Climatological assessment of Lagrangian circulation type classification

9.5.1. Intra-seasonal variability of individual characteristics

In this section we analyse if the new method presented in section 9.2 is able to distinguish the intra-seasonal circulation variability in the region (Lorenzo et al., 2008; Gomez-Gesteira et al., 2011), and to this end the mean frequency of the different characteristics of air streams is examined for all seasons: winter (DJF), spring (MAM), summer (JJA) and autumn (SON). In addition the respective seasonal standard

deviation was also computed in order to have an insight of the inter-annual variability.

The analysis first focuses on the DO characteristic (Distance and Origin) (Table 9.4). Results show that the western quadrants (S-SW, S-NW, M-SW, M-NW, L-SW, L-NW) are found more frequently than the eastern ones (S-SE, S-NE, M-SE, M-NE, L-SE, L-NE) for all seasons, which reflects the fact that most of the time the domain is under the influence of the westerlies (Peixoto and Oort, 1992). A remarkable difference between winter and summer occurs for the transport distance. Short transport classes are more frequent in summer (almost 43%) while the frequency of long range transport is larger in winter (nearly 45%). This is in line with the intensification of the Northern Hemisphere jet stream in winter compared to summer. In addition, there is a shift of about 10° latitude in the belt of the westerlies towards the pole in summer (Peixoto and Oort, 1992). The atmospheric circulation in summer in the Iberia Peninsula is most of the time, under the influence of a thermal low (Hoinka and De Castro, 2003). This thermal low is responsible for local range transport and re-circulations in the region. Finally, differences between spring and autumn are small. The highest standard deviation are in general found for spring and autumn season which are transition seasons and therefore have higher variability than the other seasons.

Table 9.4. Mean frequencies (%) of occurrence of the different classes for category Distance and Origin (DO) and the respective standard deviation (%) in brackets. They are shown during winter (DJF), spring (MAM), summer (JJA) and autumn (SON) seasons in the 1/12/1999 - 30/11/2004 period and disaggregated by (a) short, (b) medium and (c) long range transport.

a)

Short (S)	NE	SE	SW	NW	Total
Winter	4.0 (1.4)	2.1 (1.6)	10.4 (3.3)	7.6 (1.7)	24.1
Spring	7.0 (3.5)	2.9 (0.9)	12.2 (4.6)	11.2 (1.0)	33.4
Summer	3.6 (1.8)	2.3 (1.8)	19.1 (2.0)	17.9 (1.7)	42.9
Autumn	3.6 (2.4)	2.5 (1.3)	14.1 (3.4)	12.8 (2.4)	33.1

b)

Medium (M)	NE	SE	SW	NW	Total
Winter	1.7 (0.9)	0.2 (0.2)	15.5 (1.7)	13.2 (2.8)	30.6
Spring	1.2 (0.6)	0.3 (0.2)	14.7 (3.5)	17.3 (2.0)	33.4
Summer	0.5 (0.3)	0.0 (0.0)	16.8 (2.1)	17.3 (1.1)	34.7
Autumn	1.4 (0.8)	0.1 (0.2)	13.4 (1.9)	18.0 (1.5)	32.9

c)

Long (L)	NE	SE	SW	NW	Total
Winter	0.4 (0.3)	0.0 (0.0)	30.9 (4.3)	14.0 (1.7)	45.3
Spring	0.2 (0.2)	0.0 (0.1)	20.7 (5.1)	12.2 (2.0)	33.2
Summer	0.0 (0.1)	0.0 (0.0)	8.9 (1.3)	13.4 (1.7)	22.4
Autumn	0.0 (0.1)	0.0 (0.1)	18.1 (2.9)	15.8 (1.6)	34.0

Focusing on the MU parameter (Moisture Uptake), Fig. 9.17 shows that Q0 dominates in winter and spring, i.e. only small changes (positive or negative) of the humidity are found along the air streams. In contrast, Q+ is the most frequent class in summer corresponding to an increase of humidity along the path. This fact can be associated with high values of sea level temperature (SST) of the Atlantic Ocean and Mediterranean Sea, favouring evaporation in summer. In autumn, Q- is the most frequent class, associated with a loss of humidity due to precipitation along the air stream. The seasonal variability (standard deviation) is relatively low for the MU parameter.

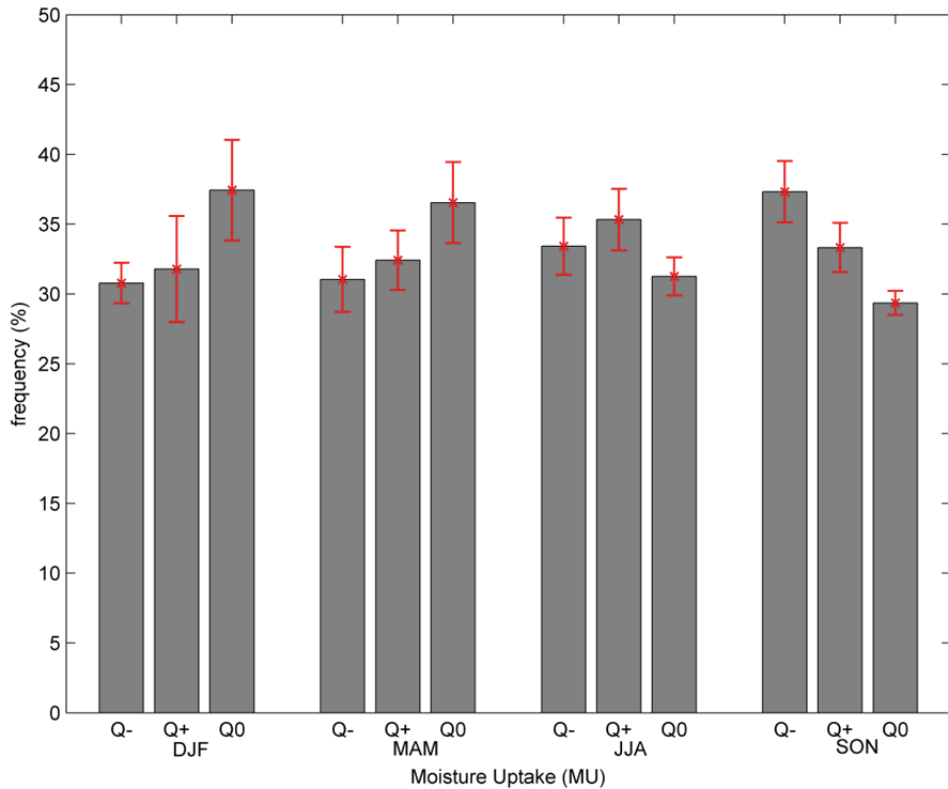


Figure 9.17. Frequencies (%) of occurrence of the Moisture Uptake (MU) during winter (DJF), spring (MAM), summer (JJA) and autumn (SON) seasons in the 1/12/1999 - 30/11/2004 period. The respective seasonal standard deviation is also shown (red lines).

With respect to ZI (Zonality Index) (Fig. 9.18), Z+ is the most frequent class during the transition seasons spring and autumn, i.e. strongly curved air streams predominate. The frequencies of the classes differ clearly in winter and summer. In summer, Z- is more frequent than Z+, while in winter both classes have similar frequencies. In summer, as shown before, short transport classes are more frequent (almost 43%) when compared with winter. This is in line with the intensification of the Northern Hemisphere jet stream in winter compared to summer, which produces strongly curved air stream in winter, and weakly curved air streams in summer.

Again, the highest standard deviations are found for spring and autumn. In summer and winter, the standard deviations are relatively low, despite being higher for winter than for summer.

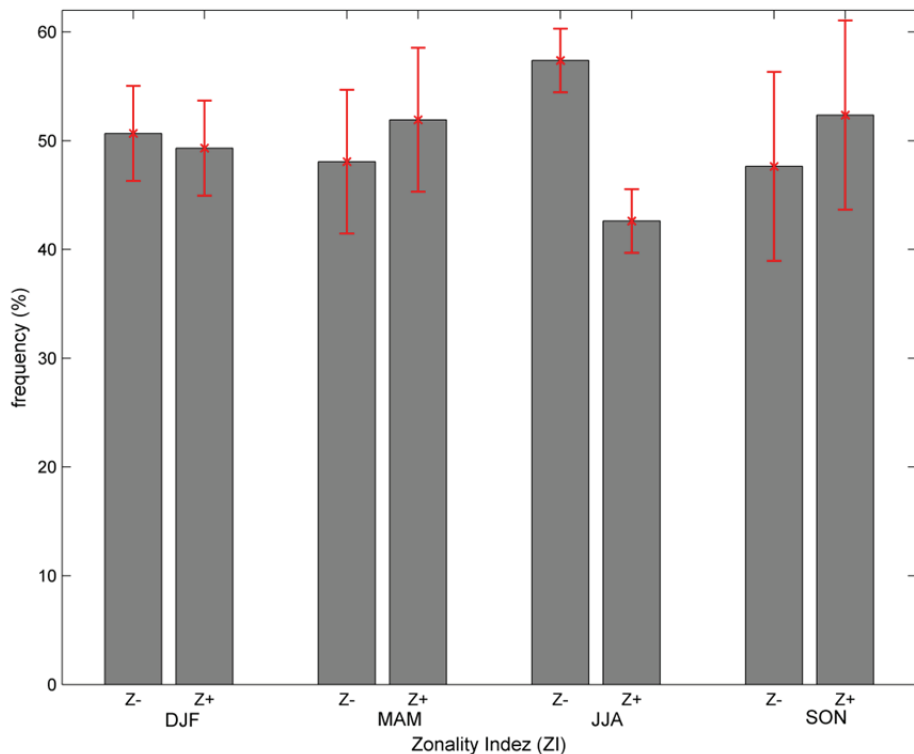


Figure 9.18. Frequencies (%) of occurrence of the Zonality Index (ZI) during winter (DJF), spring (MAM), summer (JJA) and autumn (SON) seasons in the 1/12/1999 - 30/11/2004 period. The respective seasonal standard deviation is also shown (red lines).

The frequency distribution for CI (Cyclonicity Index) (Fig. 9.19) is again similar for the different classes during spring and autumn, with Anet being the most frequent class. In winter the most frequent class is Anet with 45% of the cases followed by the averaged cyclonic class (Cnet) with a frequency near 25%. For summer the averaged anticyclonic and cyclonic classes (Anet and Cnet) have similar frequencies (near 32%) and also the classes with small anticyclonic (As) and cyclonic curvature (Cs) exhibit similar frequencies (near 14%). In

winter, as discussed above, most of the transport is long range and from the western quadrants. In the selected domain, these quadrants correspond to the North Atlantic domain frequently associated with a high frequency of the anticyclonic CI. As mentioned before, in summer, it is interesting to note that most of the time the Iberia Peninsula is under the influence of a thermal low (Hoinka and De Castro, 2003) and the method is able to identify this cyclonic feature in the region by an increase of the frequency of the cyclonic CI class. In this case, the standard deviations are relatively high compared to the other characteristics (MU, ZI and DO). In any case these standard deviations are less than 6% in the cases of spring, summer and autumn. In winter, the intra-types variability is high specially in the As and Cnet classes.

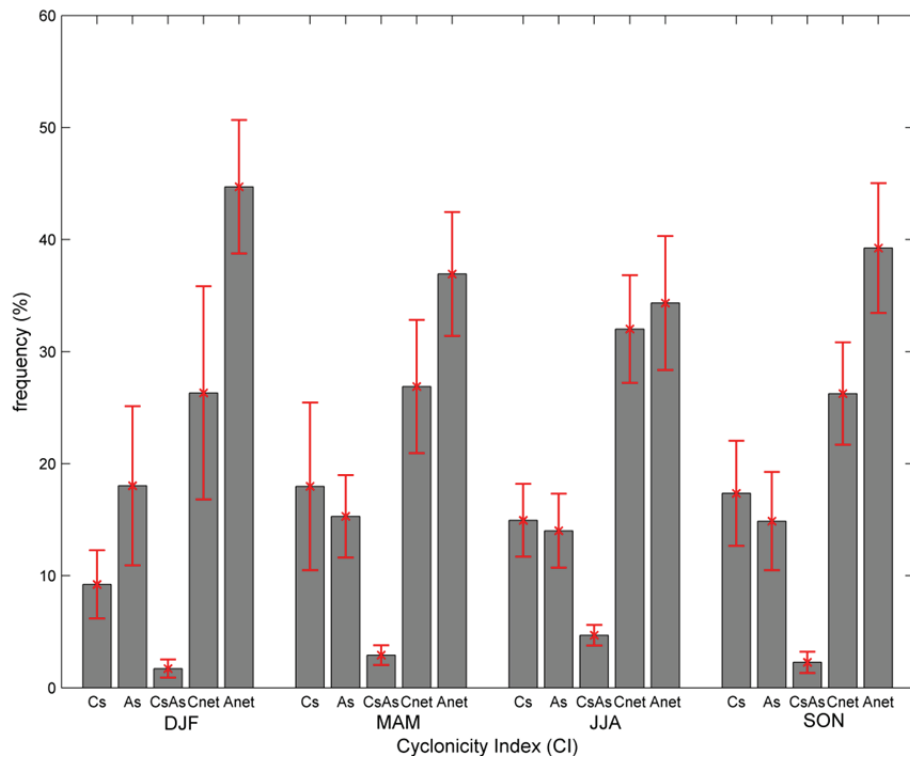


Figure 9.19. Frequencies (%) of occurrence of the Cyclonicity Index (CI) during winter (DJF), spring (MAM), summer (JJA) and autumn (SON) seasons in the 1/12/1999 - 30/11/2004 period. The respective seasonal standard deviation is also shown (red lines).

9.5.2. Combined characteristics

In this section, the combination of the different characteristics is considered, separately for summer and winter. The characteristics MU, ZI, CI and DO span a 4d phase space, with in total $3 \times 2 \times 5 \times 12$ discrete "boxes" according to the number of classes for each characteristic - 3 for MU; 2 for ZI; 3 for CI and 12 for DO (which in this section is divided into 3 (D) \times 4(O) characteristics. But due to physical constraints some combinations are evidently rather unlikely. For instance, air streams that are classified as long-range transport for the east quadrants are very rare due to the typical westerlies in the target region.

In order to look to this phase space a multi panel plot is shown in Fig. 9.20 with a total of 5×5 panels for each characteristic for both summer and winter. Each panel consists of a small matrix with the frequency of occurrence between the correspondent characteristic, e.g. the panel in row 1 and column 2 (MU vs ZI) is a 2×3 matrix according to the classes Z- and Z+ and Q-, Q+, Q0. For instance, in the MU vs ZI panel for summer and winter, it is shown that the most common combination for the Q- class is the Z- class. In each panel the circles of different sizes indicate the frequency with which a specific combination is found, i.e. the radius of the circles is proportional to this frequency. In addition, for each panel, the combination with highest frequency is marked with a red dot.

For summer the most frequent air stream is [Q-, Z-, Anet, M-SW], while for winter it is [Q-, Z-, Anet, L-SW]. It is interesting to note that the most frequent air streams for summer and winter are almost the same; the only change is found for the DO characteristic (M-SW vs L-SW). This air streams corresponds to a decrease in humidity along the path within a mainly zonal and anticyclonically curved flow. This

means that some of the humidity that is advected, e.g. from the Gulf of Mexico, across the North Atlantic is lost during the transport.

Since an exhaustive description of Fig. 9.20 is neither practical nor simple, the most common combinations are marked (red dot) and will be further discussed for summer and winter. For MU, the most frequent classes (of the other characteristics) that occur in an air stream classified as Q- are: Z-, Anet and M-SW in summer and L-SW in winter, respectively. The latter is the most frequent combination in the entire catalogue as mentioned before. For Q+ the most frequent combination is Z-, Cnet (for winter and summer) and S-NW in summer and L-NW in winter, respectively. This corresponds to air streams that have a mean cyclonic trajectory and an increase of humidity along their path. Gimeno et al., (2010) found that during wintertime the tropic-subtropical North Atlantic corridor is the main supply of moisture to the NW Iberia Peninsula, consistent with the above finding.

Regarding the Z- of the ZI characteristic the most frequent combination is Q-, Cnet and M-SW in summer, and Q+, Anet and L-SW in winter. For Z+, results show that the preferred combination is Q+, Cs and S-SW in summer and Q0, Anet and L-SW in winter. In summer this most frequent combination is associated with air streams that come from the SW, experience short range transport and an increase in humidity along their path. In winter, the more meridional circulation (Z+) is often related with mean anticyclonic circulation that can be associated to blocking events (see section 9.3).

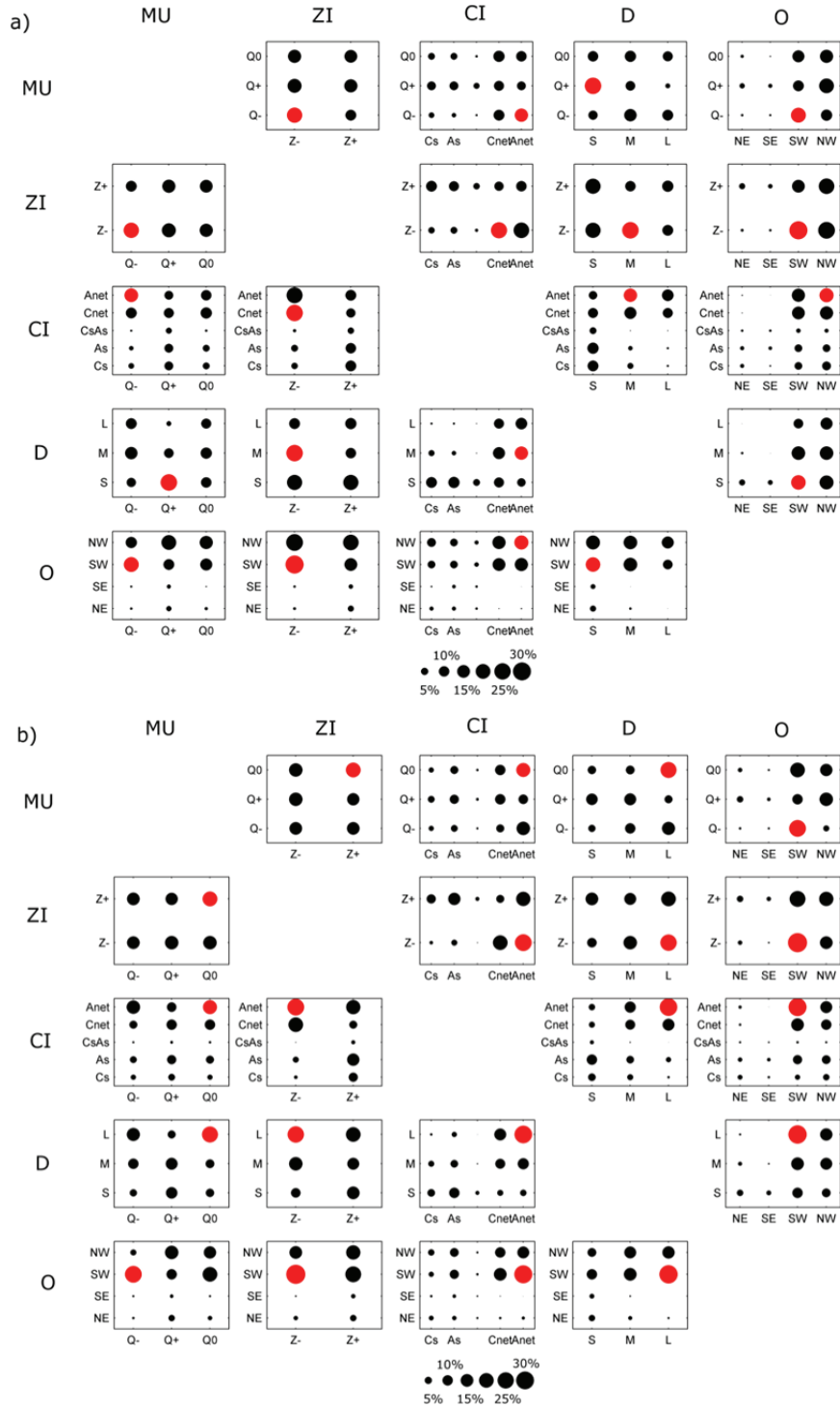


Figure 9.20. Multi-dimensional catalogue frequencies for (a) summer and (b) winter. Each panel correspond the frequency of one characteristics compared with other. For each panel the combination with highest frequency is marked with a red dot.

The last characteristic discussed here is CI. There are no particular differences in the three classes that corresponds to small-radius circulation (Cs, As and CsAs), we therefore focus on the Cnet and Anet classes. The most probable combination with Cnet in summer is Q0, Z- and M-NW and in winter Q+, Z- and L-SW, respectively. It is interesting to note that for summer Cnet is associated with Q0 while in winter it is more frequently associated with Q+. Regarding Anet, results for ZI, D and O are very similar to the ones found for Cnet. The main difference occurs for MU with the most frequent class being Q- in summer and Q0 in winter.

With this multi panel plot it is possible to see the combinations shift from summer to winter, especially for the CI, D and O characteristics.

9.5.3. Precipitation associated with trajectory weather types

CWT are often reflected in several surface climate variables (Goodess and Jones, 2002; Hope et al., 2006; Lorenzo et al., 2008). In the Iberia Peninsula, the relationship is particularly strong for precipitation, therefore many studies investigated the impact of CWT on precipitation (Trigo and DaCamara, 2000; Lorenzo et al., 2008; Gomez-Gesteira et al., 2011). The most prominent differences occur between summer and winter (see section 9.5.1) and therefore results are only shown for these two seasons.

For each season, the average rainfall associated with each class and its inter-annual variability has been computed. To do so, only the days with at least two air streams with the same class were chosen. This is done in order to choose only the days where a dominant class occur. For instance, when computing the average rainfall related to the class Q-

of the characteristic MU, only days with at least two air streams classified as a Q- were chosen.

First of all, as expected, the average rainfall is higher in winter than in summer (Fig. 9.21). For MU, there is no difference in the average rainfall for the different classes during summer, while in winter a considerably higher average rainfall is found for Q+ than for the other classes. Moreover as mentioned before, there is long range transport mainly from the western quadrants for this season. On the contrary the lowest average rainfall is found for the Q0 (small changes in humidity).

For the ZI characteristic, again there is no particular difference in precipitation for summer, while during winter higher values of average rainfall are found for the less curved trajectories (Z-). In the NW Iberia Peninsula, most of the precipitation in winter is associated with the extra-tropical cyclones within the storm track (Trigo, 2006), mainly via frontal systems passing over the region (Lorenzo et al., 2008). These frontal systems, as shown in section 9.3, are typically characterized by rather straight air streams. The case study for a blocking event (section 9.3), which typically is not associated to high values of precipitation in the domain (Barriopedro et al., 2006) was characterized by rather curved trajectories.

The CI characteristic is particularly interesting in terms of the associated average rainfall. The cyclonic classes (Cs and Cnet) present the highest values of average rainfall and the anticyclonic classes (As and Anet) the lowest values. This result confirms the findings by Lorenzo et al., (2008) who showed that the cyclonic types are most prominent in situations with rainfall in the NW Iberia Peninsula.

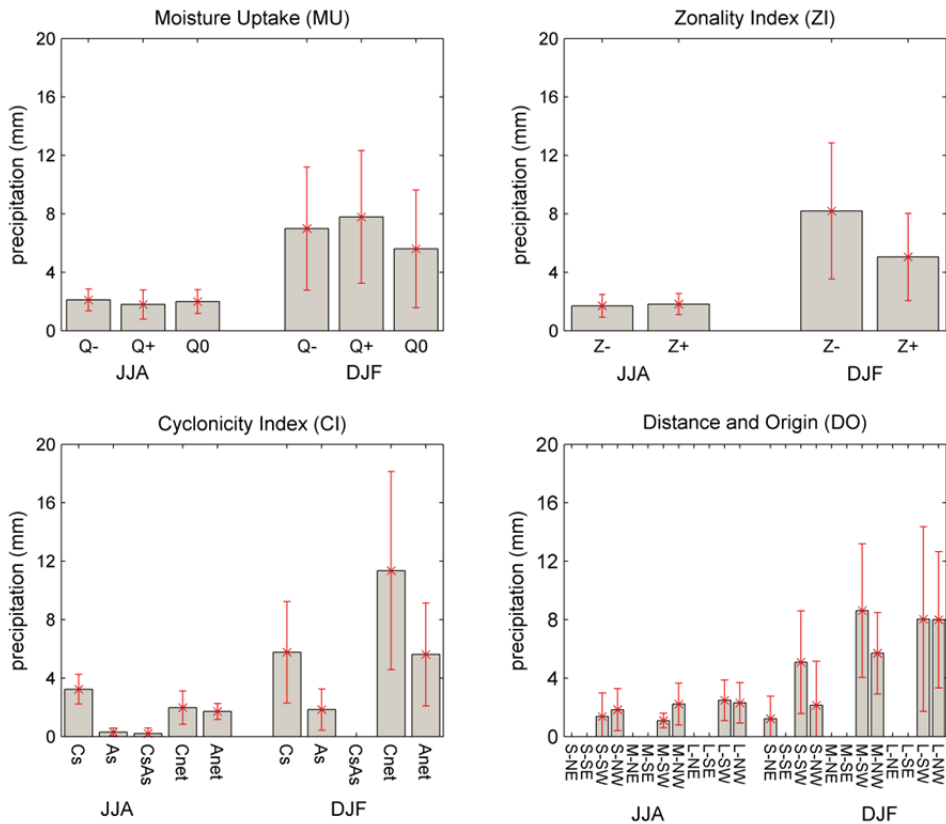


Figure 9.21. Seasonal average precipitation (mm) and the corresponding inter-annual variability (red lines) attributed to the Lagrangian.

Finally the DO characteristic presents high variability of average rainfall for each class. In winter, it is found that the air streams that come mainly from the western quadrant (S-SW, S-NW, M-SW, M-NW, L-SW, L-NW) are associated with the highest values of average rainfall. For these air streams from the western quadrants, the highest precipitation values occur for the medium and long range transport, in agreement with the results by Gimeno et al., (2010).

As a final investigation, five classes of rainfall magnitude are defined: no rain, light rain, moderate, intense and very intense following the method adopted in previous studies (Osborn et al., 2000; Lorenzo et

al., 2008). The definition of the rainfall magnitude classes for summer and winter can be found in Table 9.5 and results are shown in Fig. 9.22.

Table 9.5. Definition of each category of precipitation for winter (DJF) and summer (JJA) seasons. Values are given in mm.

Period	Light	Moderate	Intense	Very intense
Winter	$0 < DP \leq 3$	$3 < DP \leq 9$	$9 < DP \leq 21$	$DP > 21$
Summer	$0 < DP \leq 1.5$	$1.5 < DP \leq 4$	$4 < DP \leq 10$	$DP > 10$

In general, the highest values of average rainfall (Fig. 9.21) correspond to the highest values of days with intense and very intense rainfall (Fig. 9.22). The most interesting case is perhaps related to CI where the cyclonic class (Cnet) has almost 50% of the cases considered as intense or very intense precipitation days. Conversely, for the anti-cyclonic class (As and Anet) most of the days (almost 80% and 70%, respectively) correspond to no precipitation or light precipitation class.

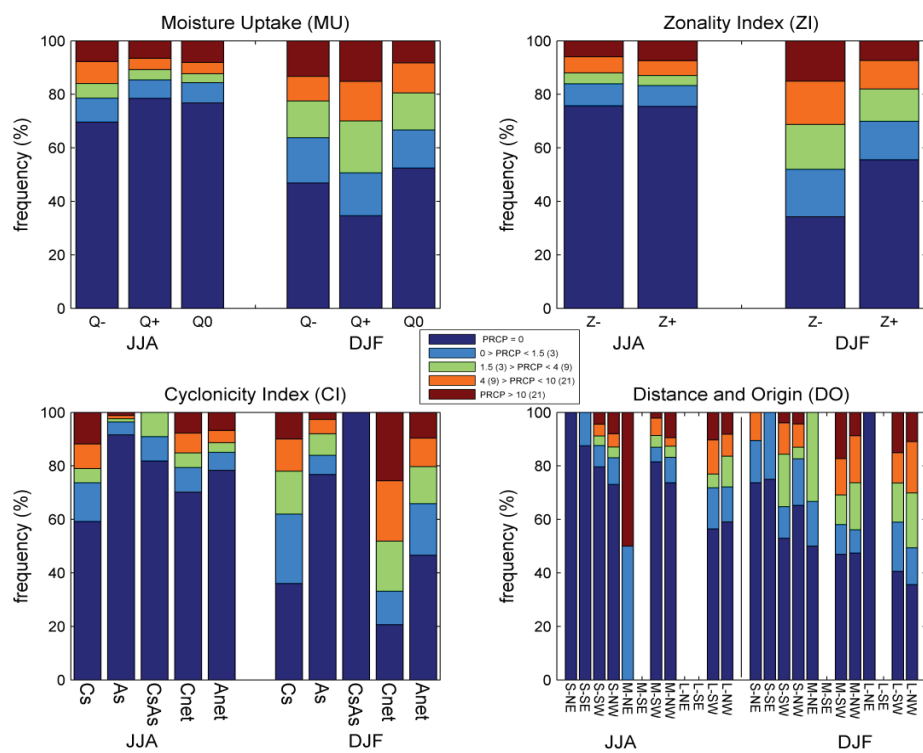


Figure 9.22. Contribution of each Lagrangian type (in %) to five different categories of precipitation. The definitions of each category of precipitation are shown for summer (winter) in the legend and are summarized in Table 9.5.

9.6. Summary

A new classification method of CWT, based on the analysis of backward trajectories, is presented in this work. A representative air stream was determined for each day (at 12 UTC) for the target region in the Northwest Iberian Peninsula.

Air parcels that are in the target domain (NW Iberia Peninsula) at the chosen time steps were selected and the corresponding 90-hour backward trajectories were then retrieved. The inherent time scale of 90 hours was chosen in order to focus the study not only the local circulation but also to include the main synoptic features that often affect the target area. In a first step, a clustering algorithm was applied allowing a horizontally separation of the different air streams. Secondly, if the number of clusters from the first (horizontal) clustering exceeded five, a further reduction was accomplished with a secondary clustering based on the height of the trajectory (H), the distance to the target area (D), specific humidity (Q) and latitude (LAT). When the main representative air streams are finally found, each air stream is characterized by four distinct flow properties: 1) Moisture Uptake (MU) represents the integrated change in specific humidity; 2) Zonality Index (ZI) represents the curvature of the path; 3) Cyclonicity Index (CI) represents the cyclonicity of the flow; and 4) Distance and Origin (DO) classifies the air stream in terms of distance and initial position. The final catalogue has for each time step a maximum of five air streams, each being characterized by the four characteristics described above. This method is able in reducing the large amount of information in a comprehensive trajectory data set into a small number of distinct air streams, which capture the essential dynamics of the meso- and synoptic-scale flow situation.

The method describes the three-dimensional complexity of the atmospheric circulation. Moreover it provides time-integrated physical information on the development of the systems (Lagrangian perspective), which goes beyond the traditional description of the instantaneous synoptic situation (Eulerian perspective). For example, the Lagrangian classification allows capturing changes in moisture along the flow due to evaporation and precipitation.

The climatological assessment of this new classification indicates that the method is able to capture with good accuracy the main features of the seasonality of regional climate. It allows for a proper distinction of processes between seasons and helps determining aspects of the intra-seasonal variability. For example, the short transport classes are most frequent in summer (43%) while the frequency of long range transport is largest in winter (45%).

Besides characterizing aspects of the annual cycle, the method is able to identify distinct dynamical structures. The case studies illustrate the Lagrangian categorization of intense precipitation events, heat waves, cold fronts, blocking systems, cut off lows and extra-tropical cyclones. For example, for the 2003 heatwave in the Iberia Peninsula, the method captures the short range transport associated with the thermal low, advection of African air streams, and the medium and long range transport associated with the anticyclonic circulation. As a further example, the cut-off low systems with its high-altitude depression is picked up by the new method, whereas the Eulerian Lamb classification is only able to pick up surface characteristics of the flow. In this sense, the method goes a step further in adding valuable information to the classification of a particular atmospheric flow situation. Indeed, a comparison between this method and an automated version of the Lamb

CWT classification for the Iberia Peninsula is shown in section 9.4 and illustrates the general agreement while providing important additional information.

In summary, the key advantages of the new method are:

1) it is able to summarize the complexity of the atmospheric circulation by a string of five labels denoting, for each of the considered flow characteristics, the class populated by the largest number of air streams;

2) in contrast to the Eulerian CWT classification it takes into account the history of the flow reaching a certain area. It better captures both local and large-scale characteristics of the meteorological situation and incorporates important information about the dynamic and thermodynamic processes associated with the flow situation;

3) it captures aspects of the three-dimensional structure of the atmosphere since the backward trajectories entering the flow classification scheme are calculated on several tropospheric levels.

4) it is able to pinpoint synoptic situations, like cut-off low pressure systems, that may not have a clear signature at lower atmospheric levels and would be missed by classification based upon the SLP field only.

Some disadvantages of using the new trajectory-based method can also be found. First, the novel classification method is computationally more demanding than traditional Eulerian ones. In addition, if the target domain is increased, the number of trajectory whiting a day also increases and therefore computation takes longer. Furthermore, the novel method characterizes the complexity of the atmospheric circulation by a set of five parameters. Clearly, this multi-

dimensional approach results in a more challenging daily catalogue compared to the classical CWT classifications.

The novel approach, developed here for the region of the Iberian Peninsula, should be general enough to be suitable for the classification of air streams over other regions on the globe.

10. Summary, concluding remarks and future work

This PhD thesis presented an assessment of the use of circulation weather types in different climatological contexts. A pure methodological essay was also presented, in which a new circulation weather type's classification is based on Lagrangian air trajectories. This thesis focused on the northwestern Iberia Peninsula, but all of the procedures and methodologies studied here could be easily applied to other regions of the world.

As mentioned before, the objectives of this work were divided into three parts:

- 1) In part one, the relationship between surface climate variables and circulation weather types was studied (chapter 6);
- 2) In part two, the relationship between circulation weather types and climate variability was examined (chapter 7 and chapter 8).
- 3) In part three, a new circulation weather type classification scheme based on Lagrangian air trajectories was presented (chapter 9).

A brief summary of each part is presented below.

In the first part, the relationships between the circulation weather types and the precipitation, temperature and lightning activity

(cloud-ground discharges) in the northwestern Iberian Peninsula were studied, as was the seasonal variability of these relationships (chapter 6). The results showed a clear difference between the occurrence of a particular circulation weather type and the average precipitation and temperature produced by it.

The relationship between the circulation weather types and lightning activity also allowed us to distinguish which types were frequently associated with lightning episodes, and which types were favourable for severe lightning episodes (in which a very high number of cloud-ground discharges occurred per event). For the summer months (which showed the highest lightning discharge frequency), the northeasterly type showed by far the most prominent association with thunderstorms over the northwestern Iberian Peninsula, with a high lightning days ratio (45.7). Other circulation weather types such as the anticyclonic type presented lower lightning days ratios (7.1) but high cloud-ground discharge values.

In the second part, the compatibility between hemispheric modes and low frequency variability modes in the North Atlantic European sector was analyzed (chapter 7), using the circulation weather types for the winter months in the northwestern Iberian Peninsula (January, February and March). Evidence was provided that the low frequency variability modes computed using the sea level pressure field and those computed using the geopotential height at 500hPa fields were very alike in this spatial window. The results showed that there was a high degree of coherence between the frequency variability modes derived using a statistical approach (using principal component analysis) and the real physical circulations (as represented by the circulation weather types).

This coherence was obtained not only for stationary modes, but also for non-stationary ones. The use of a principal component analysis approach that used continuous time windows enabled us to assess whether changes in the intensity or position of these modes could influence the local circulation.

The circulation weather types were used to evaluate the ability of the coupled general circulation models to reproduce the present mean frequency of the circulation weather types over the northwestern Iberian Peninsula, and to study projection scenarios to find changes in the circulation weather type variability in the 21st century (chapter 8). For the present climate, a significant improvement was observed when the systematic errors were removed from the sea level pressure fields, since the differences between the circulation weather type frequencies from the models and the reanalysis data were smaller than those found in the results obtained without any sea level pressure corrections. It was therefore found that in most cases, the discrepancies in the circulation weather types between the models and the reanalysis data could be explained by the seasonal mean bias.

The changes in the mean circulation type frequency were also analyzed for the 21st century. Small changes (most of them less than 6% significant) were found in the frequency of the types for the 2046-2065 period, while the differences in the second period (2081-2100) were larger. The results showed that for the second period, there was a decrease in the cyclonic, western, and southwestern types in spring and summer, in all scenarios. This change was larger for the A2 scenario. For autumn, there was a projected decrease in the western and cyclonic types, and an increase in the anticyclonic type.

The last part of this work presented a new method for the classification of circulation weather types, which was based on the analysis of backward trajectories (chapter 9). A two-step clustering algorithm was applied to the backward trajectories arriving at the northwestern Iberia Peninsula; this algorithm assumed that the grouping of trajectories was established by taking into account not only a horizontal separation of the different air particles, but also the meteorological properties of each air particle. The final catalogue has, for each time step, a maximum of five air streams, each being characterized by the four characteristics described in chapter 9. This new method was able to reduce the large amount of information in a comprehensive trajectory dataset into a small number of distinct air streams that captured the essential dynamics of the meso- and synoptic-scale flow.

In the first part of this chapter, a small summary describing the main results of the PhD thesis has been presented; in the following section, the main conclusions of this PhD thesis are listed:

- 1) The cyclonic, western and southwestern types were the synoptic patterns that produced the highest levels of precipitation, while on anticyclonic-type days there was virtually no precipitation in the northwestern Iberian Peninsula. Regarding the maximum temperature, the highest values were generally found for the southeast, south and southwestern types, while the lowest values were found for the western, northwestern and northern types.
- 2) It was observed that for different seasons, there were different mechanisms associated with the triggering of

- lightning activity in the northwestern Iberian Peninsula. These mechanisms were often related to atmospheric features that did not have a clear signature at lower atmospheric levels, (e.g. sea level pressure fields); the circulation weather types alone could not fully explain the mechanisms in all cases.
- 3) Changes in the position and the intensity of the low frequency variability modes in the North Atlantic European sector tended to favour the occurrence of some circulation weather types, in preference to others. The increase in the explained variance of the continental zonal dipole, and the increasing negative (positive) correlation between this mode and the cyclonic (anticyclonic) type, helped to explain the overall decrease in winter precipitation in the region studied.
 - 4) The study of atmospheric local circulation using circulation weather types can give valuable information when assessing future climate change scenarios. Moreover, they are easy to compute, which is an advantage over other methods (e.g., downscaling methods)
 - 5) Based on the relationship between different circulation weather types and the precipitation in the northwestern Iberian Peninsula for present climate, one can make the assumption that there will be dry conditions in summer and spring. For autumn we may also assume dryer conditions, based on the expected decrease in the western and cyclonic types, and an increase in the anticyclonic type. This behavior is in accordance with the increase in the NAO index that is expected to occur toward the end of the 21st century.

- 6) The novel trajectory-type method developed in this PhD thesis is able to describe the three-dimensional complexity of atmospheric circulation. Moreover, it provides time-integrated physical information on the development of the systems (from a Lagrangian perspective); this goes beyond the traditional description of the instantaneous synoptic situation (Eulerian perspective).
- 7) The new trajectory types capture aspects of the three-dimensional structure of the atmosphere that allow synoptic situations to be pinpointed—for example, cut-off low pressure systems—that may not have a clear signature at lower atmospheric levels, and would be missed by classification methods based only on the sea level pressure field.

The findings of this PhD thesis provide some insights for future research. The use of circulation weather types to study surface climate variability can be extended to other meteorological variables (e.g., relative humidity or wind speed). The use of wind speed at different heights and different spatial locations and its relationship with circulation weather types can be used by wind power generation companies to decide on a first-guess location for their wind farms (Carro-Calvo et al., 2011).

Regarding numerical weather prediction models, much could be accomplished in the future. The implementation of a forecast system based on circulation weather types could be easily applied for different operational forecast models (e.g. MM5, WRF, ALADIN, GFS or ECMWF), since the methodology used in this work (Lamb circulation

weather types) requires only the forecast sea level pressure field; in addition, the computation is extremely fast, and uses very few computing resources. This tool could help forecasters to improve the prediction of weather, because of the prior knowledge of the relationship between circulation weather types and the surface climate.

As mentioned before in section 9.6, there are some disadvantages associated with this novel trajectory-based method. First, the novel classification method is more computationally demanding than traditional Eulerian ones. In addition, if the target domain is increased, it is expected that the number of trajectory per day also increases, and computation therefore takes longer. Furthermore, this novel method characterizes the complexity of the atmospheric circulation using a set of five parameters. Clearly, this multi-dimensional approach results in a more challenging daily catalogue, compared with classical circulation weather type classifications.

Taking into account these disadvantages, some improvements are planned as future work:

- 1) Adapt the subroutine for the new trajectory types (which was initially developed for Matlab) for the C++ language, so that the subroutine can be used in a computational cluster, reducing the time needed for the calculation of the trajectory types. This will allow the method to be applied not only for larger areas, but also for longer time periods, as seen below. This software, when finished, will be available for free on the webpage of the Ephyslab research group.
- 2) Use a 20 year (1980-2000) global Flexpart experimental run (using ECMWF reanalysis data) that was simulated in the computational cluster of the Ephyslab group. In addition, with

this 20-year data, new comparisons could be made between the trajectory types and other circulation weather type methods. This was not possible in this work, since the COST 733 circulation weather type catalogue uses ERA40 data as an input, which only spans to 2001. As proven before, there is a high degree of coherence between the low frequency variability modes and the circulation weather types. The use of 20 years of data would also allow the detailed study of the relationship between the low frequency variability modes and the trajectory types.

This method can also be applied in other regions of the world. It was shown that this method described the three-dimensional complexity of the atmospheric circulation, capturing the dynamics of the meso- and synoptic-scale flow. This method can therefore be applied in cases where one would like to study the atmospheric weather circulation. A modified version of the trajectory types method is currently being applied to study the summer transport of air masses in the North American monsoon (Durán-Quesada et al., 2012).

The novel trajectory type method could also be applied in the evaluation of extra-tropical cyclones in mid-latitude climates, improving the knowledge of their structure and their role in moisture transport.

The method could also be applied in studies focusing on the transport of pollutants (or dust intrusions), or even sources of local atmospheric contamination; this would help to increase knowledge of this topic, since most of these studies are currently based on the analysis of the latitude, longitude and height of the trajectories.

Bibliography

Alonso-Pérez S, Cuevas E, Querol X (2011) Objective identification of synoptic meteorological patterns favouring African dust intrusions into the marine boundary layer of the subtropical eastern north Atlantic region. *Meteorology and Atmospheric Physics*. doi: 10.1007/s00703-011-0150-z.

Anagnostopoulou C, Tolika K, Maher P, Kuti H, Flocas H (2008) Performance of the General Circulation HadAM3P Model in simulating circulation types over the Mediterranean region. *International Journal of Climatology*, 28:185-203.

Aran M, Pena JC, Tora M (2011) Atmospheric circulation patterns associated with hail events in Lleida (Catalonia). *Atmospheric Research*. doi: 10.1016/j.atmosres.2010.10.029.

Azorín C, Chen D, Baldi M (2009) A multi-year study of sea breeze in Mediterranean coastal site: Alicante (Spain). *International Journal of Climatology*, 31:468-486. doi: 10.1002/joc.2064.

Barnston AG, Livezey RE (1987) Classification, seasonality and persistence of low-frequency atmospheric circulation patterns. *Monthly Weather Review*, 115:1083-1126.

Barriopedro D, García-Herrera R, Lupo A, Hernández E (2006) A Climatology of Northern Hemisphere Blocking. *Journal of Climate*, 19: 1042-1063.

Barriopedro D, García-Herrera R, Trigo RM (2010) Application of blocking diagnosis methods to General Circulation Models. Part I: A

Bibliography

novel detection scheme. *Climate Dynamics*, 35:1373-1391. doi: 10.1007/s00382-010-0767-5.

Barry RG, Chorley RJ (2003) *Atmosphere, weather and climate* (eighth edition). London, UK ISBN: 0 415 27171 1.

Baur F (1931) Die Formen der atmospharischen Zirculation in der gemassigten Zone. *Beiträge zur Geophysik*, 34, 264-309.

Beranová R, Huth R (2007) Time variations of the relationships between the North Atlantic Oscillation and European winter temperature and precipitation. *Studia Geophysica et Geodaetica*, 51:575-590.

Beranová R and Huth R (2008) Time variations of the effects of circulation variability modes on European temperature and precipitation in winter. *International Journal of Climatology*, 28:139–158. doi: 10.1002/joc.1516.

Bermejo M and Ancell R (2009) Observed changes in extreme temperatures over Spain during 1957-2002 using Weather Types. *Revista de Climatología*, 9:45-61.

Black E, Blackburn M, Harrison G, Hoskins B, Methven J (2004) Factors contributing to the summer 2003 European heat wave. *Weather*, 59:217-223.

Blackburn M, Hoskins BJ (2001) The UK record-breaking wet autumn 2000. *UGAMP Newsletter*, 24:38-40.

Bojariu R, Gimeno L (2003) Modelling and predictability of the North Atlantic Oscillation. *Earth-Science Reviews*, 63:145-168.

Cahynová M, Huth R (2009) Changes of atmospheric circulation in central Europe and their influence on climatic trends in the Czech Republic. *Theoretical and Applied Climatology*, 96: 57–68.

Cammas JP, Brioude J, Chaboureau, JP, Duron J, Mari C, Mascart P, Nédélec P, Smit H, Pätz HW, Volz-Thomas A, Stohl A, Fromm M (2009) Injection in the lower stratosphere of biomass fire emissions followed by long-range transport: a MOZAIC case study. *Atmospheric Chemistry and Physics*, 9:5829-5846. doi: 10.5194/acp-9-5829-2009.

- Carro-Calvo L, Salcedo-Sanz S, Kirchner-Bossi N, Portilla-Figueras A, Prieto L, Garcia-Herrera R, Hernández-Martín E (2011) Extraction of synoptic pressure patterns for long-term wind speed estimation in wind farms using evolutionary computing. *Energy*, 36:1571–1581.
- Casado MJ, Pastor MA, Doblas-Reyes FJ (2010) Links between circulation types and precipitation over Spain. *Physics and Chemistry of the Earth*, 35:437–447.
- Cassano EN, Cassano JJ, Nolan M (2011) Synoptic weather pattern controls on temperature in Alaska. *Journal Geophysical Research*, 116:D11108. doi: 10.1029/2010JD015341.
- Cassou C, Laurent T, Hurrell JW, Deser C (2004) North Atlantic Winter climate regimes: spatial asymmetry, stationarity with time and oceanic forcing. *Journal Climate*, 17:1055–1068.
- Cavazos T (1997) Downscaling large-scale circulation to local winter rainfall in northeastern Mexico. *International Journal of Climatology*, 17:1069–1082.
- Chen D (2000) A monthly circulation climatology for Sweden and its application to a winter temperature case study. *International Journal of Climatology*, 20:1067–1076.
- Cheng X, Wallace JM (1993) Cluster analysis of the Northern Hemisphere wintertime 500-hPa height field: Spatial patterns. *Journal of the Atmospheric Sciences*, 50:2674–2696.
- Chung C, Nigam S (1999) Weighting of geophysical data in Principal Component Analysis. *Journal Geophysical Research*, 104:16925–16928.
- Collier CG, Krzysztofowicz R (2000) Quantitative precipitation forecasting. *Journal of Hydrology*, 239:1–2.
- Conway D, Wilby RL, Jones PD (1996) Precipitation and air flow indices over the British Isles. *Climate Research*, 7:169–183.
- Corte-Real J, Qian B, Xu H (1998) Regional climate change in Portugal: precipitation variability associated with large-scale atmospheric circulation. *International Journal of Climatology*, 18:619–635.

Bibliography

- Corte-Real J, Qian B, Xu H (1999) Circulation patterns, daily precipitation in Portugal and implications for climate change simulated by the second Hadley Centre GCM. *Climate Dynamics*, 15:921-935.
- Corte-Real J, Zhang X, Wang X (1995) Downscaling GCM information to regional scales: a non-parametric multivariate regression approach. *Climate Dynamics*, 11:413-424.
- Corti S, Molteni F, Palmer T (1999) Signature of recent climate change in frequencies of natural atmospheric circulation regimes. *Nature*, 398: 799–802.
- Croci-Maspoli M, Schwierz C, Davies HC (2007) A multifaceted climatology of atmospheric blocking and its recent linear trend. *Journal of Climate*, 20:633–649.
- Ćurić M, Janc D, Vučović D, Vučković V (2003) The effects of a river valley on an isolated cumulonimbus cloud development. *Atmospheric Research*, 66:123–139.
- de Pablo F, Tomás C, Rivas Soriano L, Diego L (2009) Winter circulation weather types and hospital admissions for cardiovascular, respiratory and digestive diseases in Salamanca, Spain. *International Journal of Climatology*, 29:1692–1703. doi: 10.1002/joc.1802.
- deCastro M, Gomez-Gesteira M, Álvarez I, Lorenzo MN, Cabanas JM, Prego R, Crespo AJC (2008a) Characterization of fall-winter upwelling recurrence along the Galician western coast (NW Spain) from 2000 to 2005: Dependence on Atmospheric forcing. *Journal of Marine Systems*, 72:145–158.
- deCastro M, Gomez-Gesteira M, Lorenzo MN, Álvarez I, Crespo AJC (2008b) Influence of atmospheric modes on coastal upwelling along the western coast of the Iberian Peninsula, 1985 to 2005. *Climate Research*, 36:169–179.
- deCastro M, Gomez-Gesteira M, Ramos AM, Álvarez I, deCastro P (2011) Effects of heat waves on human mortality, Galicia, Spain. *Climate Research*, 48:333–341. doi: 10.3354/cr00988.
- deCastro M, Lorenzo MN, Taboada JJ, Sarmiento M, Alvarez I, Gomez-Gesteira M (2006) Influence of teleconnection patterns on precipitation

variability and on river flow regimes in the Miño River basin (NW Iberian Peninsula). *Climate Research*, 32:63–73.

Demuzere M, Werner M, van Lipzig NPM, Roeckner E (2008a) An analysis of present and future ECHAM5 pressure fields using a classification of circulation patterns. *International Journal of Climatology*, 29:1796–1810.

Demuzere M, Trigo RM, Vila-Guerau de Arellano J, van Lipzig NPM (2008b) The impact of weather and atmospheric circulation on O₃ and PM10 levels at a mid-latitude site. *Atmospheric Chemistry and Physics*, 8:21037–21088.

Dittmann E, Barth S, Lang J, Müller-Westermeier G (1995) Objektive Wetterlagenklassifikation (Objective weather type classification). Ber. Dt. Wetterd. 197, Offenbach a. M., Germany (in German).

Dorling SR, Davies TD, Pierce CE (1992a) Cluster analysis: a technique for estimating the synoptic meteorological controls on air and precipitation chemistry method and applications. *Atmospheric Environment*, 26:2575–2581.

Dorling SR, Davies TD, Pierce CE (1992b) Cluster analysis: A technique for estimating the synoptic meteorological controls on air and precipitation chemistry—Results from Eskdalemuir, South Scotland. *Atmospheric Environment*, 26:2583–2602.

Dunkeloh A, Jacobbeit J (2003) Circulation Dynamics of Mediterranean precipitation variability 1948–98. *International Journal of Climatology*, 23:1843–1866.

Durán-Quesada AM, Ramos AM, Gimeno L, Dominguez F (2012) Local and remote sources of moisture for the development and maintenance of the North American Monsoon. (in preparation).

Eckhardt S, Stohl A, Wernli H, James P, Forster C, Spichtinger N (2004) A 15-Year Climatology of Warm Conveyor Belts. *Journal of Climate*, 17:218–237.

Enke W, Spekat A (1997) Downscaling climate model outputs into local and regional weather elements by classification and regression. *Climate Research*, 8:195–207.

Bibliography

- Esteban P, Jones PD, Martin-Vide J, Mases M (2005) Atmospheric circulation patterns related to heavy snowfall day in Andorra, Pyrenees. *International Journal of Climatology*, 25:319–329.
- Esteban P, Martin-Vide J, Mases M (2006) Daily atmospheric circulation catalogue for Western Europe using multivariate techniques. *International Journal of Climatology*, 26:1501–1515.
- Esteban P, Ninyerola M, Prohom M (2009) Spatial modeling of air temperature and precipitation for Andorra (Pyrenees) from daily circulation patterns. *Theoretical and Applied Climatology*, 96:43–56.
- Fernández-Montes S, Rodrigo FS, Seubert S, Hertig E, Philipp A (2010) Circulation types classification for the Iberian Peninsula and relationships with observed relative extreme values of temperature and precipitation. 10th EMS Annual Meeting, 10th European Conference on Applications of Meteorology (ECAM) Abstract id.EMS2010-573, held Sept. 13-17, 2010 in Zürich, Switzerland.
- Fowler HJ, Kilsby CG (2002) A weather-type approach to analysing water resource drought in the Yorkshire region from 1881 to 1998. *Journal of Hydrology*, 262:177–192.
- Fragoso M, Tildes PG (2008) Classification of daily abundant rainfall patterns and associated large-scale atmospheric circulation types in Southern Portugal. *International Journal of Climatology*, 28:537–544. doi: 10.1002/joc.1564.
- Frias T, Trigo RM, Garreaud R (2009) Weather Type classification over Chile; patterns, trends, and impact in precipitation and temperature. EGU Annual General Assembly 2009, held 19-24 April, 2009 in Vienna, Austria <http://meetings.copernicus.org/egu2009>, p.8432.
- Gallego MC, García JA, Vaquero JM, Mateos VL (2006) Changes in frequency and intensity of daily precipitation over the Iberian Peninsula. *Journal of Geophysical Research*, 111:D24105.
- Garcia-Herrera R, Diaz J, Trigo RM, Luterbacher J, Fischer, EM (2010) A review of the European Summer Heat Wave of 2003. *Critical Reviews in Environmental Science and Technology*, 40:267-306.

García-Herrera R, Paredes D, Trigo RM, Trigo IF, Hernández E, Barriopedro D, Mendes MA (2007) The Outstanding 2004-05 Drought in the Iberian Peninsula: Associated Atmospheric Circulation. *Journal of Hydrometeorology*, 8:469-482.

Garcia-Serrano J, Rodriguez-Fonseca B, Blade I, Zurita-Gotor P, de la Camara A (2010) Rotational atmospheric circulation during north Atlantic-European winter: the influence of ENSO. *Climate Dynamics*, 37:1727-1743. doi: 10.1007/s00382-010-0968-y.

Gimeno L, de la Torre L, Nieto R, García-Herrera G, Hernández E, Ribera P (2003) Changes in the relationship NAO-Northern hemisphere temperature due to solar activity. *Earth and Planetary Science Letters*, 206:15-20.

Gimeno L, Nieto R, Trigo R, Vicente S, Lopez-Moreno JI (2010) Where does the Iberian Peninsula moisture come from? An answer based on a Lagrangian approach. *Journal of Hydrometeorology*, 11:421-436. doi: 10.1175/2009JHM1182.1.

Giorgi F, Lionello P (2008) Climate change projections for the Mediterranean region. *Global Planet Change*, 63:90-104.

Glowienka-Henze R (1990) The North Atlantic Oscillation in the Atlantic-European SLP. *Tellus*, 42:497-507.

Gomez-Gesteira M, Gimeno L, deCastro M, Lorenzo MN, Alvarez I, Nieto R, Crespo AJC, Ramos AM, Taboada JJ, Santo FE, Barriopedro D, Trigo IF (2011) The state of climate in NW Iberia. *Climate Research*, 48:109-144.

Gong X, Richman MB (1995) On the application of cluster analysis to growing season precipitation data in North America east of the Rockies. *Journal of Climate*, 8:897-931.

Goodess CM, Jones PD (2002) Links between circulation and changes in the characteristics of Iberian rainfall. *International Journal of Climatology*, 22:1593-1615.

Goodess CM, Palutikof JP (1998) Development of daily rainfall scenarios for southeast Spain using a circulation-type approach to downscaling. *International Journal of Climatology*, 18:1051-1083.

Bibliography

Hanssen-Bauer I, Førland EJ (2000) Temperature and precipitation variations in Norway 1900-1994 and their links to atmospheric circulation. *International Journal of Climatology*, 20:1693–1708.

Hartigan JA (1975) Clustering Algorithms. Wiley Series in Probability and Mathematical Statistics. New York. 351 pp.

Hastie T, Tibshirani R, Jerome F (2009) The Elements of Statistical Learning: Data Mining, Inference, and Prediction. Second Edition (Springer Series in Statistics). New York, 763pp.

Herrera S, Gutiérrez JM, Ancell R, Pons MR, Frías MD, Fernández J (2010) Development and analysis of a 50-year high-resolution daily gridded precipitation dataset over Spain (Spain02). *International Journal of Climatology*, 32:74–85. doi: 10.1002/joc.2256.

Hess P, Brezowsky H (1952) Katalog der Großwetterlagen Europas. Berichte des Deutschen Wetterdienst in der US-Zone 33.

Hipel KW, McLeod AI (2005) Time Series Modelling of Water Resources and Environmental Systems. Electronic reprint of our book originally published in 1994. <http://www.stats.uwo.ca/faculty/aim/1994Book/>.

Hoinka KP, de Castro M (2003) The Iberian Peninsula thermal low. *Quarterly Journal of the Royal Meteorological Society*, 129:1491–1511.

Hope PK, Drosdowsky W, Nicholls N (2006) Shifts in the synoptic systems influencing southwest Western Australia. *Climate Dynamics*, 26:751–764.

Hulme M, Briffa KR, Jones PD, Senior CA (1993) Validation of GCM control simulations using indices of daily airflow types over the British Isles. *Climate Dynamics*, 9:95–105.

Hurrell JW (1995) Influence of Variations in Extratropical Wintertime Teleconnections on Northern Hemisphere Temperatures. *Geophysical Research Letters*, 23:665–668.

Hurrell JW, Kushnir Y, Visbeck M, Ottersen G (2003) An Overview of the North Atlantic Oscillation, in The North Atlantic Oscillation: Climate Significance and Environmental Impact. Geophysical Monograph, vol 134 edit by J.W. Hurrell, Y. Kushnir et al., pp1-36, AGU, Washington, D.C.

Hurrell JW, van Loon H (1997) Decadal Variations associated with the North Atlantic Oscillation. *Climate Change*, 36:301-326.

Huth R (1993) An example of using obliquely rotated principal components to detect circulation types over Europe. *Meteorologische Zeitschrift*, 2:285–293.

Huth R (2000) A circulation classification scheme applicable in GCM studies. *Theoretical and Applied Climatology*, 67:1–18.

Huth R (2001) Disaggregating climatic trends by classification of circulation patterns. *International Journal of Climatology*, 21:135–153.

Huth R (2006) The effect of various methodological options on the detection of leading modes of sea level pressure variability. *Tellus*, 58A:121-130.

Huth R, Beck C, Philipp A, Demuzere M, Ustrnul Z, Cahynová M, Kyselý J, Tveito OE (2008) Classifications of Atmospheric Circulation Patterns. *Annals of the New York Academy of Sciences*, 1146:105–152. doi: 10.1196/annals.1446.019.

IPCC, 2007: Climate Change 2007: The Physical Science Basis. Contribution of Working Group I to the Fourth Assessment Report of the Intergovernmental Panel on Climate Change [Solomon, S., D. Qin, M. Manning, Z. Chen, M. Marquis, K.B. Averyt, M. Tignor and H.L. Miller (eds.)]. Cambridge University Press, Cambridge, United Kingdom and New York, NY, USA, 996 pp.

James PM (2007) An objective classification for Hess and Brezowsky Grosswetterlagen over Europe. *Theoretical and Applied Climatology*, 88: 17–42.

James PM (2008) The use of synoptic regime classifications in medium- and extended-range ensemble forecasting. Available online at: http://www.ecmwf.int/newsevents/meetings/forecast_products_user/Presentations2008/James.pdf. Last access: June 2011.

James P, Stohl A, Spichtinger N, Eckhardt S, Forster C (2004) Climatological aspects of the extreme European rainfall of August 2002 and a trajectory method for estimating the associated evaporative source regions. *Natural Hazards and Earth System Sciences*, 4:733-746.

Bibliography

James R, Bonazzola M, Legras B, Surbled K, Fueglister S (2008) Water vapor transport and dehydration above convective outflow during Asian monsoon. *Geophysical Research Letters*, 35:L20810. doi: 10.1029/2008GL035441.

Jenkinson AF, Collison FP (1977) An initial climatology of gales over the North Sea. *Synoptic Climatology Branch Memorandum No. 62*, Meteorological Office, Bracknell.

Jerauld J, Rakov VA, Uman MA, Rambo KJ, Jordan DM, Cummins KL, Cramer JA (2005) An evaluation of the performance characteristics of the U. S. National Lightning Detection Network in Florida using rocket-triggered lightning. *Journal of Geophysical Research*, 110:D19106. doi: 10.1029/2005jd005924.

Jolliffe IT (1990) Principal component analysis: A beginner's Guide. Part I: Introduction and application. *Weather*, 45:375-382.

Jolliffe IT (2002) Principal Component Analysis. Springer-Verlag, 2nd Edition, 487pp, New York.

Jones PD, Hulme M, Briffa KR (1993) A comparison of Lamb circulation types with an objective classification scheme. *International Journal of Climatology*, 13:655-663.

Jones PD, Osborn TJ, Briffa KR (2003) Pressure-based measures of the North Atlantic Oscillation (NAO): A comparison and an assessment of changes in the strength of the NAO and in its influence on surface climate parameters, in *The North Atlantic Oscillation: Climate Significance and Environmental Impact*. Geophysical Monograph, vol. 134, edited by J.W. Hurrel et al., pp 51-62, AGU, Washington, DC.

Jorba O, Pérez C, Rocadenbosch F, Baldasano JM (2004) Cluster Analysis of 4-Day Back Trajectories Arriving in the Barcelona Area, Spain, from 1997 to 2002. *Journal of Applied Meteorology*, 43:887-901.

Jung T, Hilmer M, Ruprecht E, Kleppuk S, Gulev SK, Zolina O (2003) Characteristics of the recent eastward shift of interannual NAO variability. *Journal of Climate*, 16:3371-3382.

Kalnay E, Kanamitsu M, Kistler R, Collins W, Deaven D, Gandin L, Iredell M, Saha S, White G, Woollen J, Zhu Y, Leetmaa A, Reynolds B,

- Chelliah M, Ebisuzaki W, Higgins W, Janowiak W, Mo KC, Ropelewski C, Wang J, Jenne R, Joseph D (1996) The NCEP/NCAR 40-Year Reanalysis Project. *Bulletin of the American Meteorological Society*, 77:437-472.
- Karl TR, Knight RW, Baker B (2000) The record breaking global temperature of 1997 and 1998: evidence for an increase in rate of global warming? *Geophysical Research Letters*, 27:719-722.
- Kassomenos P (2010) Synoptic circulation control on wild fire occurrence. *Physics and Chemistry of the Earth*, 35:544-552.
- Kendall MG (1975) Rank Correlation Methods. Griffin, London. 272pp.
- Kiehl J, Trenberth K (1997) Earth's annual global mean energy budget. *Bulletin of the American Meteorological Society*, 78:197-2006.
- Kimoto M, Ghil M (1993) Multiple flow regimes in the Northern Hemisphere winter. Part I: Methodology and hemispheric regimes. *Journal of the Atmospheric Sciences*, 50:2625-2643.
- Kirchhofer W (1974) Classification of European 500 mb patterns. *Arbeitsbericht der Schweizerischen Meteorologischen Zentralanstalt*, vol. 43. Zurich, Switzerland, pp. 1-16.
- Knippertz P, Wernli H (2010) A Lagrangian Climatology of Tropical Moisture Exports to the Northern Hemispheric Extratropics. *Journal of Climate*, 23:987-1003.
- Kohonen T (1982) Self-organized formation of topologically correct feature maps. *Biological Cybernetics*, 43:59-69.
- Krichak S, Alpert P (2005) Decadal trends in the East Atlantic/West Russia pattern and the Mediterranean precipitation. *International Journal of Climatology*, 25:183-192.
- Kruizinga S (1979) Objective classification of daily 500 mbar patterns. *Preprints Sixth Conference on Probability and Statistics in Atmospheric Sciences*, Banff, Alberta. American Meteorological Society, Boston, MA, pp. 126-129.

Bibliography

Lamb HH (1972) British Isles Weather types and a register of daily sequence of circulation patterns, 1861-1971. Geophysical Memoir 116, HMSO, London, 85pp.

Lauscher F (1985) Klimatologische Synoptik Österreichs mittels der ostalpinen Wetterlagenklassifikation (Synoptic Climatology of Austria based on the Eastern- Alpine Weather Type Classification). Arbeiten aus der Zentralanstalt für Meteorologie und Geodynamik, Publikation Nr. 302, Heft 64, Austria (in German).

Lechuga A (2006) Where freak waves involved in the sinking of the Tanker "Prestige"? Natural Hazards and Earth System Sciences, 6:973-978.

Leśniok M, Małarzewski L, Niedźwiedź T (2010) Classification of circulation types for Southern Poland with an application to air pollution concentration in Upper Silesia. Physics and Chemistry of the Earth, 30:516-522.

Lityński J (1969) A numerical classification of circulation patterns and weather types in Poland. Prace Państwowego Instytutu Hydrologiczno-Meteorologicznego, 97:3-15 (in Polish).

Longshore D (2000) Encyclopedia of hurricanes, typhoons, and cyclones. Checkmark Books, New York, NY. 384pp.

López-Moreno JL, Serrano-Vicente SM (2006) Atmospheric circulation influence on the interannual variability of snowpack in the Spanish Pyrenees during the second half of the twentieth century. Nordic Hydrology, 38:38-44.

López-Moreno JL, Serrano-Vicente SM, Gimeno L, Nieto R (2009) Stability of the seasonal distribution of precipitation in the Mediterranean region: Observations since 1950 and projections for the 21st century. Geophysical Research Letters, 36:L10703.

Lorenzo MN, Ramos AM, Taboada JJ, Gimeno L (2011) Changes in present and future circulation types frequency in northwest Iberian Peninsula. PLoS ONE, 6:e16201. doi: 10.1371/journal.pone.0016201.

- Lorenzo MN, Taboada JJ (2005) Influences of atmospheric variability on freshwater input in Galician Rías in winter. *Journal of Atmospheric and Ocean Science*, 10:377-387.
- Lorenzo MN, Taboada JJ, Gimeno L (2007) Links between circulation weather types and teleconnection patterns and their influence on precipitation patterns in Galicia (NW Spain). *International Journal of Climatology*, 28:1493-1505. doi: 10.1002/joc.1646.
- Lu J, Greatbatch RJ (2002) The changing relationship between the NAO and northern hemisphere climate variability. *Geophysical Research Letters*, 29:1148. doi: 10.1029/2001GL014052.
- Lund IA (1963) Map-pattern classification by statistical methods. *Journal of Applied Meteorology*, 2:56-65.
- Mann HB (1945) Nonparametric tests against trend. *Econometrica*, 13: 245-259.
- Martín ML, Luna MY, Morata A, Valero F (2004) North Atlantic teleconnection patterns of low-frequency variability and their links with springtime precipitation in the western Mediterranean. *International Journal of Climatology*, 24:213-230.
- Martin-Vide J (2002) Aplicación de la clasificación sinóptica automática de Jenkinson y Collison a días de precipitación torrencial en el este de España. In: La información climática como herramienta de gestión ambiental. Universidad de Zaragoza. Zaragoza. 123-127.
- Michaelides SC, Liassidou F, Schizas CN (2007) Synoptic classification and establishment of analogues with artificial neural networks. *Pure and Applied Geophysics*, 164:1347-1364.
- Monahan AH, Fyfe J, Pandolfo L (2003) The Vertical Structure of Wintertime Climate Regimes of the Northern Hemisphere Extratropical Atmosphere. *Journal of Climate*, 16:2005-2021.
- Nakicenovic N, and Intergovernmental Panel on Climate Change. Working Group III. (2000) Special report on emissions scenarios : a special report of Working Group III of the Intergovernmental Panel on Climate Change, 599 pp., Cambridge University Press, Cambridge ; New York.

Bibliography

Namias J (1950) The index cycle and its role in the general circulation. *Journal of Meteorology*, 7:130–139.

Nieto R, Gimeno L, de la Torre L, Ribera P, Gallego D, García-Herrera R, García JA, Nuñez M, Redaño A, Lorente J (2005) Climatological features of cut-off low systems in the Northern Hemisphere. *Journal of Climate*, 18:3085–3103.

Nieto R, Gimeno L, de la Torre L, Ribera P, Barriopedro D, García-Herrera R, Serrano A, Gordillo A, Redano A, Lorente J (2007a) Interannual variability of Cut-off-low systems over the European sector: The role of blocking and the Northern Hemisphere circulation modes. *Meteorology and Atmospheric Physics*, 96:85–101.

Nieto R, Gimeno L, Añel JA, de la Torre L, Gallego D, Barriopedro D, Gallego D, Gordillo A, Redaño A, Delgado G (2007b) Analysis of the precipitation and cloudiness associated with COLs occurrence in the Iberian Peninsula. *Meteorology and Atmospheric Physics*, 96:103–119.

Nieto R, Gimeno L, Trigo RM (2006) A Lagrangian identification of major sources of Sahel moisture. *Geophysical Research Letters*, 33:L18707. doi: 10.1029/2006GL027232.

Nieto R, Sprenger M, Wernli H, Trigo RM, Gimeno L (2008) Identification and Climatology of Cut-off Lows near the Tropopause. *Annals of the New York Academy of Sciences*, 1146:256–290.

Ninyerola M, Pons X, Roure JM (2005) Digital Climatic Atlas of the Iberian Peninsula. Anman Gràfiques del Valles, Barcelona, Spain.

Nyanganyura D, Makarau A, Mathuthu M, Meixner FX (2008) A five-day back trajectory climatology for Rukomechi research station (northern Zimbabwe) and the impact of large-scale atmospheric flows on concentrations of airborne coarse and fine particulate mass. *South African Journal of Science*, 104:43–52.

Osborn TJ, Hulme M (2002) Evidence for trends in heavy rainfall events over the United Kingdom. *Philosophical Transactions of the Royal Society London series A*, 360:1313–1325. doi: 10.1098/rsta.2002.1002.

Osborn TJ, Hulme M, Jones PD, Basnett TA (2000) Observed trends in the daily intensity of United Kingdom precipitation. *International Journal of Climatology*, 20:347–364.

Palau JL, Pérez-Landa G, Millán MM (2009) Transitional dispersive scenarios driven by mesoscale flows on complex terrain under strong dry convective conditions. *Atmospheric Chemistry and Physics*, 9:119-130. doi: 10.5194/acp-9-119-2009.

Pandolfo, L (1993) Observational aspects of the low-frequency intraseasonal variability of the atmosphere in middle latitudes. *Advances in Geophysics*, 34:93-174.

Paredes D, Trigo RM, Garcia-Herrera R, Trigo, IF (2006) Understanding precipitation changes in Iberia in early Spring: weather typing and storm-tracking approaches. *Journal of Hydrometeorology*, 7:101-113.

Paris JD, Stohl A, Ciais P, Nédélec P, Belan BD, Arshinov MYu, Ramonet M (2010) Source-receptor relationships for airborne measurements of CO₂, CO and O₃ above Siberia: a cluster-based approach. *Atmospheric Chemistry and Physics*, 10:1671-1687.

Peixoto JP, Oort AH (1992) Physics of Climate. Springer-Verlag New York, Inc., ISBN 0-88318-712-4.

Pereira, MG, Trigo RM, da Camara CC, Pereira JMC, Leite SM (2005) Synoptic patterns associated with large summer forest fires in Portugal. *Agricultural and Forest Meteorology*, 129:11-25.

Perlitz J, Graf HF (1995) The statistical connection between tropospheric and stratospheric circulation of the Northern Hemisphere in winter. *Journal of Climate*, 8:2281-2295.

Peterson KA, Lu J, Greatbatch RJ (2003) Evidence of nonlinear dynamics in the eastward shift of the NAO. *Geophysical Research Letters*, 30:1030. doi: 10.1029/2002GL015585.

Philipp A (2008) Comparison of principal component and cluster analysis for classifying circulation pattern sequences for the European domain. *Theoretical and Applied Climatology*, 96:31-41. doi: 10.1007/s00704-008-0037-1.

Philipp A, Bartholy J, Beck C, Erpicum M, Esteban P, Fettweis X, Huth R, James P, Jourdain S, Kreienkamp F, Krennert T, Lykoudis S, Michalides SC, Pianko-Kluczynska K, Post P, Rasilla Alvarez D, Schiemann R, Spekat A, Tymvios FS (2010) Cost733cat – a database of

Bibliography

weather and circulation type classifications. Physics and Chemistry of the Earth, 35:360–373.

Philipp A, Della-Marta PM, Jacobbeit J, Fereday DR, Jones PD, Moberg A, Wanner H (2007) Long term variability of daily North Atlantic European pressure patterns since 1850 classified by simulated annealing clustering. Journal of Climate, 20:4065–4095.

Pineda N, Esteban P, Trapero L, Soler X, Beck C (2010) Circulation types related to lightning activity over Catalonia and the Principality of Andorra. Physics and Chemistry of the Earth, 35:469–476.

Pozo-Vázquez D, Gámiz-Fortis SR, Tovar-Pescador J, Esteban-Parra MJ, Castro-Díez Y (2005) El Niño–Southern Oscillation events and associated European winter precipitation anomalies. International Journal of Climatology, 25:17–31.

Prudhomme C, Genevier M (2011) Can atmospheric circulation be linked to flooding in Europe? Hydrological Processes, 25:1180–1190. doi: 10.1002/hyp.7879.

Quadrelli R, Wallace JM (2004) A Simplified Linear Framework for Interpreting Patterns of Northern Hemisphere Wintertime Climate Variability. Journal of Climate, 17:3728–3744.

Ramos AM, Lorenzo MN, Gimeno L (2010) Compatibility between modes of low frequency variability and Circulation Types: a case study of the North West Iberian Peninsula. Journal of Geophysical Research, 115:D02113. doi: 10.1029/2009JD012194.

Ramos AM, Ramos R, Sousa P, Trigo RM, Janeira M, Prior V (2011) Cloud to ground lightning activity over Portugal and its association with Circulation Weather Types. Atmospheric Research, 101:84–101. doi: 10.1016/j.atmosres.2011.01.014.

Rasilla DF, García Codrán JC (2010) Circulation patterns and wave climate along the coast of the Iberian Peninsula. 10th EMS Annual Meeting, 10th European Conference on Applications of Meteorology (ECAM) Abstract id.EMS2010-381, held Sept. 13-17, 2010 in Zürich, Switzerland.

Rasilla DF, Garcia-Codron JC, Carracedo V, Diego C (2010) Circulation patterns, wildfire risk and wildfire occurrence in continental Spain. *Physics and Chemistry of the Earth*, 35:553–560.

Rasilla DF, Garcia-Codron JC, Garmendia C (2002) Los temporales de viento: propuesta metodológica para el análisis de un fenómeno infravalorado. In: La información climática como herramienta de gestión ambiental. Universidad de Zaragoza, 129-136.

Rasmusson EM, Wallace JM (1983) Meteorological aspects of El Niño / Southern Oscillation. *Science*, 222:1195-1202.

Rex DF (1950) Blocking action in the middle troposphere and its effect upon regional climate. Part II: The climatology of blocking action. *Tellus*, 2:275–301.

Riccio A, Giunta G, Chianese E (2007) The application of a trajectory classification procedure to interpret air pollution measurements in the urban area of Naples (Southern Italy). *Science of the Total Environment*, 376:198-214.

Richman MB (1981) Obliquely rotated principal components: an improved meteorological map typing technique? *Journal of Applied Meteorology*, 20:1145–1159.

Richman MB (1986) Rotation of principal components. *Journal of Climatology*, 6:293–335.

Rivas Soriano L, de Pablo F, Tomas C (2005) Ten-year study of cloud-to-ground lightning activity in the Iberian Peninsula. *Journal of Atmospheric and Solar-Terrestrial Physic*, 67:1632-1639.

Rodó X, Baert E, Comin FA (1997) Variations in seasonal rainfall in southern Europe during the present century: relationships with the North Atlantic Oscillation and the El Niño-Southern Oscillation. *Climate Dynamics*, 13:275–284.

Rodrigo FS, Trigo RM (2007) Trends in daily rainfall in the Iberian Peninsula from 1951 to 2002. *International Journal of Climatology*, 27: 513-529. doi: 10.1002/joc.1409.

Rodrigues RB, Mendes VMF, Catalao JPS, Correia S, Prior V, Aguado M (2008) An Investigation over the Lightning Location System in Portugal

Bibliography

for Wind Turbine Protection Development. Power and Energy Society General Meeting - Conversion and Delivery of Electrical Energy in the 21st Century, 2008:2324-2331.

Rodríguez-Fonseca B, Rodríguez-Puebla C (2010) Teleconexiones climáticas en el entorno de la Península Ibérica. Predictabilidad y cambios esperados. Clima en España: Pasado, presente y futuro. Informe de Evaluación del Cambio Climático Regional. Red temática Clivar-España, 53-68.

Rodríguez-Fonseca B, Serrano E (2002) Winter 10-Day Coupled Patterns between Geopotential Height and Iberian Peninsula Rainfall Using the ECMWF Precipitation Reanalysis. *Journal of Climate*, 15: 1309–1321.

Rodríguez-Puebla C, Encinas AH, García-Casado LA, Nieto S (2009) Trends in warm days and cold nights over the Iberian Peninsula: relationships to large-scale variables. *Climatic Change*, 100:667–684. doi: 10.1007/s10584-009-9721-0.

Rodríguez-Puebla C, Encinas AH, Nieto S, Garmendia J (1998) Spatial and temporal patterns of annual precipitation variability over the Iberian Peninsula. *International Journal of Climatology*, 18:299–316.

Romero R, Sumner G, Ramis C, Genoves A (1999) A classification of the atmospheric circulation patterns producing significant daily rainfall in the Spanish Mediterranean area. *International Journal of Climatology*, 19:765–785.

Saenz J, Rodriguez-Puebla C, Fernández J, Zubillaga J (2001) Interpretation of interannual winter temperature variations over southwestern Europe. *Journal of Geophysical Research*, 106:20641-20651.

Sanchez Lorenzo A, Calbó J, Brunetti M, Deser C (2009) Dimming/brightening over the Iberian Peninsula: Trends in sunshine duration and cloud cover and their relations with atmospheric circulation. *Journal of Geophysical Research*, 114:D00D09.

Santos JA, Corte-Real J, Leite S (2005) Weather regimes and their connection to the winter rainfall in Portugal. *International Journal of Climatology*, 25:33-50. doi: 10.1002/joc.1101.

Santos JA, Leite S (2009) Long-term variability of the temperature time series recorded at Lisbon. *Journal of Applied Statistics*, 36: 323–337. doi: 10.1080/02664760802449159.

SIAM, 2002: Santos FD, Forbes K, Moita R (eds) (2002) Climate change in Portugal: scenarios, impacts and adaptation measures. Gradiva, Lisboa, Portugal.

SIAM, 2006: Santos FD, Miranda P (eds) (2006) Alterações climáticas em Portugal: cenários, impactos e medidas de adaptação. Gradiva, Lisboa, Portugal.

Schoof JT, Pryor SC (2003) Evaluation of the NCEP-NCAR reanalysis in terms of synoptic-scale phenomena: a case study from the Midwestern USA. *International Journal of Climatology*, 23:1725–41.

Sepp M, Jaagus J (2002) Frequency of circulation patterns and air temperature variations in Europe. *Boreal Environment Research*, 7:273–279.

Sheridan SC (2002) The Redevelopment of a Weather-Type Classification Scheme for North America. *International Journal of Climatology*, 22:51–68.

Serra C, Fernàndez-Mills G, Periago M, Lana X (1999) Winter synoptic weather types in Catalonia (NE Spain) and their linkage with minimum temperature anomalies. *International Journal of Climatology*, 19:1675–1695.

Serrano A, García JA, Mateos VL, Cancillo ML, Garrido J (1999) Monthly modes of variation of precipitation over the Iberian peninsula. *Journal of Climate*, 12:2894–2919.

Slonosky VC, Jones PD, Davies TD (2001) Atmospheric circulation and surface temperature in Europe from the 18th century to 1995. *International Journal of Climatology*, 21:63–75.

Smyth P, Ide K, Ghil M (1999) Multiple regimes in Northern Hemisphere height fields via mixture model clustering. *Journal of the Atmospheric Sciences*, 56:3704–3723.

Bibliography

- Sodemann H, Schwierz C, Wernli H (2008) Inter-annual variability of Greenland winter precipitation sources. Lagrangian moisture diagnostic and North Atlantic Oscillation influence. *Journal Geophysical Research*, 113:D03107. doi: 10.1029/2007JD008503.
- Soriano LR, de Pablo F, Tomas C (2005) Ten-year study of cloud-to-ground lightning activity in the Iberian Peninsula. *Journal of Atmospheric and Solar-Terrestrial Physics*, 67:1632-1639.
- Spellman G (2000) The application of an objective weather-typing system to the Iberian peninsula. *Weather*, 55:375-385.
- Stephenson DB, Pavan V, Collins M, Junge MM, Quadrelli R and Participating CMIP2 Modelling Groups (2006) North Atlantic Oscillation Response to Transient Greenhouse Gas Forcing and the Impact on European Winter Climate: A CMIP2 multi-model assessment. *Climate Dynamics*, 27:401-420.
- Stohl A (1998) Computation, accuracy and applications of trajectories a review and bibliography. *Atmospheric Environment*, 32:947-966.
- Stohl A, Forster C, Frank A, Seibert P, Wotawa G (2005) Technical note: The Lagrangian particle dispersion model FLEXPART version 6.2. *Atmospheric Chemistry and Physics*, 5:2461-2474.
- Stohl A, Haimberger L, Scheele MP, Wernli H (2001) An intercomparison of three trajectory models. *Meteorological Applications*, 8:127-135.
- Stohl, A, Scheifinger, H (1994) A weather pattern classification by trajectory clustering. *Meteorologische Zeitschrift*, 6:333-336.
- Stohl A, Sodemann H (2010) Characteristics of atmospheric transport into the Antarctic troposphere. *Journal of Geophysical Research*, 115: D02305. doi: 10.1029/2009JD012536.
- Sutera A (1986) Probability density distribution of large-scale atmospheric flow. *Advances in Geophysics*, 29:227-249.
- Tomás C, de Pablo F, Rivas Soriano L (2004) Circulation weather types and cloud-to-ground flash density over the Iberian Peninsula. *International Journal of Climatology*, 24:109-123. doi: 10.1002/joc.917.

Trenberth KE (1990) Recent observed interdecadal climate changes in the Northern Hemisphere. *Bulletin of the American Meteorological Society*, 71:988–993.

Trigo IF (2006) Climatology and interannual variability of storm-tracks in the Euro-Atlantic sector: a comparison between ERA-40 and NCEP/NCAR reanalyses. *Climate Dynamics*, 26:127–143.

Trigo RM, DaCamara CC (2000) Circulation weather types and their influence on the precipitation regime in Portugal. *International Journal of Climatology*, 20:1559–1581.

Trigo RM, Osborn TJ, Corte-Real JM (2002) The North Atlantic Oscillation influence on Europe: climate impacts and associated physical mechanisms. *Climate Research*, 20:9–17.

Trigo RM, Palutikof JP (2001) Precipitation scenarios over Iberia: a comparison between direct GCM output and different downscaling techniques. *Journal of Climate*, 14:4422–4446.

Trigo RM, Trigo IF, DaCamara CC, Osborn TJ (2004a) Climate impact of the European winter blocking episodes from the NCEP/NCAR reanalyses. *Climate Dynamics*, 23:17–28.

Trigo RM, Pozo-Vazquez D, Osborn TJ, Castro-Diez Y, Gamiz-Fortis S, Esteban-Parra MJ (2004b) North Atlantic Oscillation influence on precipitation, river flow and water resources in the Iberian Peninsula. *International Journal of Climatology*, 24:925–944.

Trigo RM, Ramos AM, Nogueira P, Santos FD, Garcia-Herrera R, Gouveia C, Santo FE (2009) Evaluating the impact of extreme temperature based indices in the 2003 heatwave excessive mortality in Portugal. *Environmental Science & Policy*, 12:844–854.

Trigo RM, Valente MA, Trigo IF, Miranda PMA, Ramos AM, Paredes D, García-Herrera R (2008) The impact of North Atlantic wind and cyclone trends on European precipitation and significant wave height in the Atlantic. *Annals of the New York Academy of Sciences*, 1146:212–234.

Tveito OE (2010) An assessment of circulation type classifications for precipitation distribution in Norway. *Physics and Chemistry of the Earth*, 35:395–402.

Bibliography

- Ulbrich U, Christoph M (1999) A shift of the NAO and increasing storm track activity over Europe due to anthropogenic greenhouse gas forcing. *Climate Dynamics*, 15:551-559.
- Valero F, Martín ML, Sotillo MG, Morata A, Luna MY (2009) Characterization of the autumn Iberian precipitation from long-term datasets: comparison between observed and hindcasted data. *International Journal of Climatology*, 29:527-541.
- vanUlden AP, van Oldenborgh GJ (2006) Large-scale atmospheric circulation biases and changes in global climate model simulations and their importance for climate change in Central Europe. *Atmospheric Chemistry and Physics*, 6:863-881.
- Vicente-Serrano SM, López-Moreno JI (2006) The influence of atmospheric circulation at different spatial scales on winter drought variability through a semi-arid climatic gradient in Northeast Spain. *International Journal of Climatology*, 26:1427-1453.
- Vicente-Serrano SM, López-Moreno JI (2008) Nonstationary influence of the North Atlantic Oscillation on European precipitation. *Journal of Geophysical Research*, 113:D20120. doi: 10.1029/2008JD010382.
- Vicente-Serrano SM, Trigo RM, Liberato MLR, López-Moreno JI, Lorenzo-Lacruz J, Beguería S, Morán-Tejeda H, El Kenawy A (2011) Extreme winter precipitation in the Iberian Peninsula, 2010: anomalies, driving mechanisms and future projections. *Climate Research*, 46:51-65. doi: 10.3354/cr00977.
- Wallace JM, Gutzler DS (1981) Teleconnections in the geopotential height field during the Northern hemisphere Winter. *Monthly Weather Review*, 109:784-812.
- Wallace JM, Hobbs PV (2006) Atmospheric science: an introductory survey, 2nd ed., xvi, 483 pp., Elsevier Academic Press, Amsterdam; Boston.
- Wallace JM, Smith C, Bretherton CS (1992) Singular value decomposition of wintertime sea surface temperature and 500-mb height anomalies. *Journal of Climate*, 5:561-576.

- Walter K, Graf HF (2002) On the changing nature of the regional connection between the North Atlantic Oscillation and sea surface temperature. *Journal of Geophysical Research*, 107:4338. doi: 10.1029/2001JD000850.
- Wernli H, Davies, HC (1997) A Lagrangian-based analysis of extratropical cyclones. I: The method and some applications. *Quarterly Journal of the Royal Meteorological Society*, 123:467-489.
- Wibig J (1999) Precipitation in Europe in relation to circulation patterns at the 500 hpa level. *International Journal of Climatology*, 19:253–269.
- Wilks DS (2006) Statistical Methods in the Atmospheric Sciences. 2d ed. International Geophysics Series, Vol. 91, Academic Press, 627 pp.
- Wolter K, Timlin MS (1998) Measuring the strength of ENSO - how does 1997/98 rank? *Weather*, 53:315-324.
- Zhang X, Wang XL, Corte-Real J (1997) On the relationships between daily circulation patterns and precipitation in Portugal. *Journal of Geophysical Research*, 102:13495–13507.
- Zvereva II (2006) Seasonally varying modes in long-term variability of European precipitation during the 20th century. *Journal of Geophysical Research*, 111:D21116.

List of Acronyms

- A: anticyclonic
- AEMET: Agencia Estatal de Meteorología
- C: cyclonic
- CAPE: convective available potential energy
- CG: cloud-ground
- CGCMs: coupled general circulation models
- CMD: continental meridional dipole
- COLs: Cut off lows
- GPCP: global precipitation climatology project
- CWT: circulation weather types
- CZD: continental zonal dipole
- DJF: December, January, February months
- E: easterly
- EA: East Atlantic Pattern
- EA/WR: East Atlantic / Western Russia Pattern
- ENSO: El Niño-Southern Oscillation
- EOF: empirical orthogonal function (EOF)
- F: total flow
- G: Xures/Geres

List of Acronyms

- H1000 / H 950 / H500: geopotential height at level 1000hPa / 950hPa / 500hPa
- IM: Instituto de Meteorologia
- JFM: January, February, March months
- JJA: June, July, August months
- LD: total lightning days
- LI: lifted index
- M: Marão
- MA: Manzaneda
- MAM: March, April, May months
- MDF: magnetic direction finding
- N: north
- NAE: North Atlantic European
- NAO: North Atlantic Oscillation
- NE: northeasterly
- NW: northwesterly
- OMD: ocean meridional dipole
- OZD: ocean zonal dipole
- PC: principal components
- PCA: principal component Analysis
- PDF: probability density function
- PW: precipitable water
- rLD: lightning days ratio
- RPCA: rotated principal component analysis
- S: south
- SCA: Scandinavian Pattern
- SE: southeasterly
- SET: Serra Estrela

- SLP: sea level pressure
- SF: southerly flow
- SON: September, October, November months
- SSTs: sea surface temperatures
- SW: southwesterly
- Tmax: maximum temperature
- Tmin: minimum temperature
- TOA: time of arrival
- U: zonal wind component
- V: meridional wind component
- W: west
- WF: westerly flow
- Z: total shear vorticity
- ZS: southerly shear vorticity
- ZW: westerly shear vorticity

List of Figures

Figure 1.1. Schematic view of the components of the climate system, and their processes and interactions. Source: IPCC, 2007. **2**

Figure 1.2. Estimate of the Earth's annual and global mean energy balance. Source: Kiehl and Trenberth, 1997. **3**

Figure 1.3. Spatial patterns of the main teleconnections over the Atlantic Northern Hemisphere. The figures represent the temporal correlation between monthly standardized height anomalies at each grid point, and the monthly teleconnection pattern time series from 1950-2005. (Adapted from Lorenzo et al., 2008). **6**

Figure 2.1. Example of the objectivized Hess and Brezowsky (GWLs). Climatological composites of GWLs 1–15 (out of 29) for the winter half-year, showing H500 (color-filled field) and SLP (black contours) (source: James, 2007). **18**

Figure 2.2. An example of circulation weather types generated using T-mode PCA. Mean H500 patterns of circulation weather types over Europe, found for the observed data (left column), and their projections onto the UKHI global climate model (right column). Each type is represented by its number, and its frequency of occurrence (adapted from: Huth, 2008). **20**

Figure 2.3. An example of circulation weather types in Central and Western Europe, generated using CKMEANS (source: Enke and Spekat, 1997). Composite images of 1000 hPa geopotential height charts for summer (JJA) in Central and Western Europe are shown. The percentage values at the top right of each graph indicate the frequency of the respective circulation weather type. **22**

Figure 2.4. Results of a trajectory cluster analysis showing nine clusters that were identified with their trajectory members (originally presented by Dorling et al., 1992a). The work is based on trajectories arriving at Eskdalemuir (south Scotland) in the period February-July, 1981-1984.

28

Figure 3.1. Location of the area studied, enclosed by the red rectangle. 31

Figure 3.2. Orography of the Iberian Peninsula. The topologic names mentioned throughout the chapter are also included in the figure. 32

Figure 3.3. Spatial distribution of (a) the mean annual maximum air temperature (b) the mean annual minimum air temperature in the Iberian Peninsula, during the 1951-1999 period (source: Ninyerola et al., 2005).

34

Figure 3.4. Spatial distribution of the mean annual accumulated precipitation, during the 1951-1999 period (source: Ninyerola et al., 2005).

35

Figure 3.5. Seasonal spatial distribution of the mean maximum air temperature ($^{\circ}\text{C}$) for the 1961-2006 period, in winter (DJF), spring (MAM), summer (JJA) and autumn (SON) (source: Gomez-Gesteira et al., 2011).

36

Figure 3.6. Seasonal spatial distribution of the mean minimum air temperature ($^{\circ}\text{C}$) for the 1961-2006 period, in winter (DJF), spring (MAM), summer (JJA) and autumn (SON) (source: Gomez-Gesteira et al., 2011).

37

Figure 3.7. Seasonal spatial distribution of the mean accumulated precipitation (mm) for the 1961-2006 period, in winter (DJF), spring (MAM), summer (JJA) and autumn (SON) (source: Gomez-Gesteira et al., 2011).

38

Figure 3.8. Annual spatial density distribution of CG discharges (colored contours). Values are given as number of discharges/km 2 per year, over a regular $0.2^{\circ} \times 0.2^{\circ}$ grid. All CG discharges for each year are represented by grey dots. The percentage of CGs per year is also shown.

41

Figure 3.9. Seasonal spatial density distribution of CG discharges (colored contours). Values are given as the number of discharges/km² per season, over a regular 0.2° x 0.2° grid. All CG discharges for each season are represented by grey dots. The percentage of CGs per season is also shown.

42

Figure 3.10. Seasonal a) mean sea level pressure (hPa) and b) geopotential height (m), during the 1961-1999 period, using the NCEP/NCAR reanalysis data.

43

Figure 3.11. Seasonal spatial distribution of the positions where lows reach their minimum central pressure, using the 6-hourly database of the ERA-40 reanalysis and the cyclone tracking method of Trigo et al., 1999. The values correspond to the average number of events detected per 1.125° × 1.125° grid box (source: adapted from Gomez-Gesteira et al., 2011).

45

Figure 3.12. Total seasonal frequency of blocking centre positions for the 55-yr period 1948-2002; (a) spring, (b) summer, (c) autumn and (d) winter. Blocking centre positions were calculated using the NCEP/NCAR reanalysis dataset (source: adapted from Barriopedro et al., 2006).

46

Figure 3.13. Spatial annual distribution of the cut off low systems, created using NCEP/NCAR reanalysis. The values correspond to the average number of events detected per 2.5° × 2.5° grid box (source: adapted from Nieto et al., 2008).

47

Figure 3.14. Values showing correlation between monthly European precipitation (CRU data set) and the corresponding monthly NAO index, for the 1960-2000 period (source: adapted from Trigo et al., 2008).

49

Figure 5.1. The locations of the nine (four in Portugal and five in Spain) Lightning Location System detectors are indicated with capital letters. The Portuguese regions referred to in the text are also identified in the figure.

59

Figure 5.2. Location of each weather station. The ID numbers correspond to the ones in Table 5.3.

61

225

List of Figures

Figure 6.1. Pressure grid points used to compute the Lamb weather types for the NW Iberian Peninsula.	70
Figure 6.2. Annual average composite SLP field of the 10 pure circulation weather types, for the period 1948-2008.	73
Figure 6.3. Mean frequency (%) of circulation weather types in winter (DJF), spring (MAM), summer (JJA) and autumn (SON). These frequencies were computed using the NCEP/NCAR reanalysis SLP fields for the period 1948-2008.	74
Figure 6.4. Values for the correlation between the monthly precipitation data of the Lourizán station in Galicia and the monthly precipitation data of the GPCP, during the 1979-2004 period.	76
Figure 6.5. Average precipitation explained by each weather type, at annual and seasonal scales. The seasonal division is the same as that used in Fig. 6.3.	78
Figure 6.6. Contribution of the CWT to the different categories of annual precipitation.	80
Figure 6.7. Same as Fig.6.6, but showing seasonal data.	80
Figure 6.8. Average annual and seasonal maximum and minimum temperature for each pure circulation weather type.	82
Figure 6.9. Composites of days in winter with the NE circulation weather type, for a) stable days and b) unstable days, for mean daily fields of CAPE (J/kg), H1000 (m), and RH (%) and H500 (m).	89
Figure 7.1. Frequency (%) of circulation weather types in winter months (JFM).	100
Figure 7.2. The first four leading EOF patterns for the winter months (JFM) for the SLP field together with the respective variance (%) explained by each.	102
Figure 7.3. The first four leading EOF patterns for the winter months (JFM) for the H500 field together with the respective variance (%) explained by each.	102

Figure 7.4. Distribution of the four corresponding PC indices for each circulation weather type. The boxes represent the lower, median, and upper quartile values. The whisker lines are drawn at a scale of 1.5 times the inter-quartile range.

108

Figure 7.5. Variance explained by each EOF over time. The first analysis window is 1948-1977 (centred on 1962) and the last is 1976-2005 (centred on 1990). The CZD, CMD, OZD, and OMD are represented by the blue, green, red, and black lines, respectively.

111

Figure 7.6. The first four leading EOF patterns for the winter months (JFM) obtained using a PCA on the SLP field using a 30-year moving window.

112

Figure 7.7. Intensity of the modes given by doing the seasonal average (JFM) of the daily PCs of the modes represented in Fig. 7.2 30-year moving average is also represented (black lines).

113

Figure 7.8. Correlation between the four principal loading factors and the winter frequency of the circulation weather types. The significance at the 95% level is also shown (dotted lines). The first analysis window is set as 1948-1977 (centred on 1962) and the last window is 1976-2005 (centred on 1990). Cyclonic and anticyclonic are denoted by C and A, respectively. The CZD, CMD, OZD, and OMD are represented by blue, green, red, and black lines respectively.

115

Figure 8.1. Mean seasonal SLP differences for the 1961-1999 period. The first column shows the seasonal mean SLP during the 1961-1999 period, using the NCEP/NCAR reanalysis data. The next columns show the difference between the mean SLP from the three models (IPSL, ECHAM5, CCSM3 respectively) and the mean SLP from the NCEP/NCAR reanalysis during the period 1961-1999.

128

Figure 8.2. Projected seasonal mean frequency of the circulation weather types changes (%) for the late 21st century (2081-2100), in the scenario A1B. The mean frequency of the circulation weather types are shown relative to the 1961-1999 period (IPSL, black circle, ECHAM5, red triangle and CCSM3, blue square). The filled symbols show the differences that were significant at a level of 0.05, as determined using a Wilcoxon rank sum test. The seasons were defined as follows; winter (DJF), spring (MAM), summer (JJA) and autumn (SON).

133

227

Figure 8.3. The same as Fig. 8.2, but for the SRES B1 scenario. **134**

Figure 8.4. The same as Fig. 8.2, but for the SRES A2 scenario. **136**

Figure 9.1. Backward trajectories (90h) arriving to the northwest Iberia Peninsula (41°N – 44.5°N and 10°W – 6°W) on a particular day (11/11/1999 - 12 UTC) in color lines and the respective clusters position (blue dots) computed by the Dorling method (dark lines). **143**

Figure 9.2. Time evolution of the back-trajectory properties for a) height of trajectory (H), b) specific humidity (Q), c) latitude and d) distance to the center (D) shown in Fig.9.1. The colored thin line corresponds to the centroid trajectories (previous computed with the Dorling method) while the colored thick lines correspond to the final five air streams characterizing the day (see text for details). In e) the final air streams are shown. The color code is the same as in a) to d). **145**

Figure 9.3. Histograms distribution for: a) integrated changes in specific humidity (ΔQ), b) distance “travelled” by the particle (D); c) integrated value of the curvature (R_{net}) and d) integrated absolute value of the curvature (ZI). For ΔQ and D the tercile values are indicated with a dotted black line and for ZI the 50th percentile. **147**

Figure 9.4. Definition for the Distance and Origin (DO) characteristic for the air streams. The circles separate the different distance (D) classes: short range (S), medium range (M) and long range (L). The origin of the air streams is split into the four regions SW, NW, SE and NE. In total, 12 classes result for DO. **149**

Figure 9.5. Representation of the final catalog for 80 first days (from 01/12/1999 to 18/02/2000). Each day is characterized by at most five air streams and each air stream can be described by four flow properties (MU, ZI, CI and DO), as discussed in section 9.2. The legend should be interpreted like this: for different categories the colors indicates a different class. For example, the first air stream of the first day (01/12/1999) is classified has [Q-, Z+, Anet, L-SW]. The * in the legend indicates that there is no correspondent class. **151**

Figure 9.6. Air streams for the cold front case study (12/11/2002). Each color represents a different air stream – see legend. **153**

Figure 9.7. a) Air streams and b) final characteristics catalogue of the trajectory types classification for the cut-off low system case study (10/10/2001 - 12/10/2001). **155**

Figure 9.8. a) Air streams for the precipitation period case study (17/10/2001 to 21/10/2001). b) Scatter plot with frequencies of air streams characterized by MU and CI. **157**

Figure 9.9. a) Air streams (each color represent a different day) and b) characteristics of the trajectory types classification for the coldwave case study (15/12/2001 to 22/12/2001). **159**

Figure 9.10. a) Air streams (each color represent a different day) and b) characteristics of the trajectory types classification for the heatwave case study (01/08/2003 to 15/08/2003). **161**

Figure 9.11. a) Air streams and b) final characteristics catalogue of the trajectory types classification for the blocking event case study (14/01/2000 to 29/01/2000). **164**

Figure 9.12. Relationship between Lamb circulation weather types and the Lagrangian flow property MU. For each circulation weather type the frequency of each MU class is presented. **166**

Figure 9.13. Relationship between Lamb circulation weather types and the Lagrangian flow property ZI. For each circulation weather type the frequency of each ZI class is presented. **167**

Figure 9.14. Relationship between Lamb circulation weather types and the Lagrangian flow property CI. For each circulation weather type the frequency of each CI class is presented. **168**

Figure 9.15. Relationship between Lamb circulation weather types and the Lagrangian flow property D. For each circulation weather type the frequency of each D class is presented. **169**

Figure 9.16. Relationship between Lamb circulation weather types and the Lagrangian flow property O. For each circulation weather type the frequency of each O class is presented. **170**

Figure 9.17. Frequencies (%) of occurrence of the Moisture Uptake (MU) during winter (DJF), spring (MAM), summer (JJA) and autumn (SON) seasons in the 1/12/1999 - 30/11/2004 period. The respective seasonal standard deviation is also shown (red lines). **173**

Figure 9.18. Frequencies (%) of occurrence of the Zonality Index (ZI) during winter (DJF), spring (MAM), summer (JJA) and autumn (SON) seasons in the 1/12/1999 - 30/11/2004 period. The respective seasonal standard deviation is also shown (red lines). **174**

Figure 9.19. Frequencies (%) of occurrence of the Cyclonicity Index (CI) during winter (DJF), spring (MAM), summer (JJA) and autumn (SON) seasons in the 1/12/1999 - 30/11/2004 period. The respective seasonal standard deviation is also shown (red lines). **175**

Figure 9.20. Multi-dimensional catalogue frequencies for (a) summer and (b) winter. Each panel correspond the frequency of one characteristics compared with other. For each panel the combination with highest frequency is marked with a red dot. **178**

Figure 9.21. Seasonal average precipitation (mm) and the corresponding inter-annual variability (red lines) attributed to the Lagrangian. **181**

Figure 9.22. Contribution of each Lagrangian type (in %) to five different categories of precipitation. The definitions of each category of precipitation are shown for summer (winter) in the legend and are summarized in Table 9.5. **182**

List of Tables

Table 2.1. Overview of the different circulation weather type classification methods. The Lamb circulation weather type is highlighted in bold. The abbreviations are defined as follows: variables used for classification (SLP: sea level pressure; H: geopotential height; U/V: zonal and meridional wind; PW: precipitable water).	16
Table 2.2. Example of studies of the Iberian Peninsula that use classification methods other than the Lamb circulation weather type.	26
Table 5.1. Variables for the NCEP/NCAR reanalysis data used in this work.	55
Table 5.2. Variables for the NCEP Final Analyses of the Global Tropospheric Analyses reanalysis data used in this work.	56
Table 5.3. Characteristics of the weather stations used in this work. Additionally, the type of climate variable used, the climate variables (temperature (Temp) or/and precipitation (Prec)), the period and the respective source are shown.	61
Table 5.4. Different case studies analyzed to validate the trajectory method.	64
Table 6.1 Definition of each category of precipitation (P) in mm for winter (DJF), spring (MAM), summer (JJA) and autumn (SON) seasons, and for annual cycles.	79

Table 6.2. Circulation weather type frequency, lightning days ratio (rLD), total lightning days (LD) and cloud-ground discharge (CG) frequency, on an annual basis. (Bold values represent the three dominant situations).	85
Table 6.3. Same as Table 6.2, but for seasonal data.	86
Table 7.1. Correlation between the times series of both EOFs fields (SLP vs H500) computed for the region of study is shown (values in bold represent correlations that are statistically significant at the 99% level).	103
Table 7.2. Correlation between the hemispheric modes time series and the time series of the EOF computed a) for the SLP field and b) for the H500 field (values in bold represent correlations that are statistically significant at the 99% level).	103
Table 7.3. Correlation between the hemispheric modes time series and the frequency of the synoptic circulation weather types in winter (values in bold represent correlations that are statistically significant at the 99% level). The cyclonic and anticyclonic circulation weather types are referred to as C and A, respectively.	107
Table 8.1. Linear trends (percentage/year) for the different circulation weather types computed using the NCEP/NCAR reanalysis SLP field for the three periods studied; only results that were significant (Mann-Kendall rank test) at the **99% or *95% level are shown.	127
Table 8.2. Differences (%) in the mean frequency of the circulation weather types for each season between the output of the IPSL, ECHAM5 and CCSM3 and the NCEP/NCAR reanalysis data, for the 1961-1999 period, when using the original SLP data and the corrected SLP data. The differences that were significant at a 95% level (Wilcoxon rank sum test) are shown in bold.	130
Table 8.3. The same as Table 8.2, but for spring.	130
Table 8.4. The same as Table 8.2, but for summer.	131
Table 8.5. The same as Table 8.2, but for autumn.	131

Table 9.1. Lamb Circulation weather types for each day of the heatwave (1/8/2003 - 15/8/2003) case study. **160**

Table 9.2. Lamb Circulation weather types for each day of the blocking (14/1/2000 - 29/1/2000) case study. **163**

Table 9.3. Frequency (%) of occurrence of Lamb circulation weather types during the 1/12/1999 - 30/11/2004 period. **165**

Table 9.4. Mean frequencies (%) of occurrence of the different classes for category Distance and Origin (DO) and the respective standard deviation (%) in brackets. They are shown during winter (DJF), spring (MAM), summer (JJA) and autumn (SON) seasons in the 1/12/1999 - 30/11/2004 period and disaggregated by (a) short, (b) medium and (c) long range transport. **172**

Table 9.5. Definition of each category of precipitation for winter (DJF) and summer (JJA) seasons. Values are given in mm. **182**

List of Publications

- [16] Durán-Quesada AM, **Ramos AM**, Gimeno L (2012) Application of a Lagrangian method for the analysis of the sensitivity of precipitation in southern Central America to the transport of moisture. Submitted to Geophysical Monograph Series.
- [15] Liberato MLR, Durán-Quesada AM, **Ramos AM**, Nieto R, Trigo IF, Gimeno L, Trigo RM (2012) Lagrangian Perspective of a North Atlantic Extra-tropical Cyclone and Associated Flash Flood Event. Submitted to Geophysical Monograph Series.
- [14] Santo FE, **Ramos AM**, de Lima MIP, Trigo RM (2012) Seasonal changes in daily precipitation extremes in mainland Portugal from 1941 to 2007. Submitted to Regional Environmental Change.
- [13] de Lima MIP, Santo FE, **Ramos AM**, de Lima JLMP (2012) Recent changes in daily precipitation and surface air temperature extremes in mainland Portugal, in the period 1941-2007. Submitted to Atmospheric Research.

- [12] **Ramos AM**, Sprenger M, Wernli H, Durán-Quesada AM, Lorenzo MN, Gimeno L (2012) A new circulation type classification based upon Lagrangian air trajectories. Submitted to Quarterly Journal of the Royal Meteorological Society.
- [11] Gouveia C, Liberato MLR, DaCamara CC, Trigo RM, **Ramos AM** (2011) Modelling past and future wine production in the Portuguese Douro Valley. *Climate Research*, 48:349–362. doi:10.3354/cr01006.
- [10] **Ramos AM**, Ramos R, Sousa P, Trigo RM, Janeira M, Prior V (2011) Cloud to ground lightning activity over Portugal and its association with Circulation Weather Types. *Atmospheric Research*, 101:84-101. doi: 10.1016/j.atmosres.2011.01.
- [9] deCastro M, Gomez-Gesteira M, **Ramos AM**, Álvarez I, deCastro P (2011) Effects of heat waves on human mortality, Galicia, Spain. *Climate Research*, 48:333–341. doi:10.3354/cr00988.
- [8] Lorenzo MN, **Ramos AM**, Tabuada JJ, Gimeno L (2011) Changes in present and future circulation types frequency in northwest Iberian Peninsula. *PLoS ONE*, 6:e16201. doi:10.1371/journal.pone.0016201.
- [7] Gomez-Gesteira M, Gimeno L, deCastro M, Lorenzo MN, Alvarez I, Nieto R, Crespo AJC, **Ramos AM**, Taboada JJ, Santo FE, Barriopedro D, Trigo IF (2011) The state of climate in NW Iberia. *Climate Research*, 48:109–144.

- [6] **Ramos AM**, Trigo RM, Santo FE (2011) Evolution of extreme temperatures over Portugal: recent changes and future scenarios. *Climate Research*, 48:177–192. doi:10.3354/cr00934.
- [5] **Ramos AM**, Lorenzo MN, Gimeno L (2010) Compatibility between modes of low frequency variability and Circulation Types: a case study of the North West Iberian Peninsula. *Journal of Geophysical Research*, 115:D02113. doi:10.1029/2009JD012194.
- [4] Trigo RM, **Ramos AM**, Nogueira P, Santos FD, Garcia-Herrera R, Gouveia C and Santo FE (2009) Evaluating the impact of extreme temperature based indices in the 2003 heatwave excessive mortality in Portugal. *Environmental science & policy*, 12:844-854. doi:10.1016/j.envsci.2009.07.007.
- [3] Trigo RM, Valente MA, Trigo IF, Miranda PM, **Ramos AM**, Paredes D, García-Herrera R (2008) North Atlantic wind and cyclone trends and their impact in the European precipitation and Atlantic significant wave height. *Annals of the New York Academy of Sciences*, Volume 1146, Issue Trends and Directions in Climate Research, Pages 212-234.
- [2] Andrade, C, Freitas MC, Trigo RM, Gallego MC, Borges P, **Ramos AM** (2008) Comparing Historic Records of Storm frequency and the North Atlantic Oscillation (NAO) chronology for the Azores region. *The Holocene*, 18:745-754.

List of Publications

- [1] Trigo, RM, Garcia-Herrera R, Paredes D, **Ramos A** (2007) Iberia, in State of the Climate in 2006. Arguez, A., ed. Bulletin of the American Meteorological Society, 88:S106-S107.